Design of Energy Efficient Snubber Circuits for Protection of Switching Devices in High Power Applications

Submitted in fulfilment of the requirements for
the degree of Doctor of Philosophy

by
Satyanand Mohanram

Department of Electronics and Computer Engineering,
College of Engineering, Design and Physical Sciences
Brunel University,
London, UK

January, 2021

Abstract

Semiconductor devices are subjected to elevated levels of dv/dt and di/dt when used at high voltage high current and elevated temperature applications. To reduce the stress from semiconductor switches, turn-on snubber circuits are used during the turn on time and turn-off snubber circuits during the turn-off time. In low power applications where the switching losses is not significant these can be ignored. Over the last few years, Voltage Controlled Voltage Source (VCVS) applications in High Voltage Direct Current (HVDC) has increased particularly with the use of Multilevel Converters (MLCs). Switching Losses in such high power applications now needs to be considered as it is no longer insignificant. Energy efficient snubber circuits (EESCs) became available only for low power applications according to the literature review.

The research dealt with the design of EESCs in high power cascaded H-bridge MLCs. The main contributions made were: - (1) A critical review of present snubber circuits. (2) Design of energy efficient snubber circuits. (3) Design of Safe Operating Area (SOA) was possible by application of COMSOL thermal simulation for the power switch used in MLCs. (4) A reduction in switching power loss of 1782 MWh before EESC and 1379 MWh after the EESC (22.6%), which is an annual reduction of 403MWh, which impacts on the reduction in Global Warming. (5) Significant annual cost benefits from £125,000 to £68,612 (55%) in the reduction of wasted switching dissipated energy. (6) Additional benefit in the connection of inductors in the EESCs, resulted in a reduction of harmonic levels of 6% at V_3 down to 1.5% at V_7.

Optimisation methods, like Particle Swarm Optimisation (PSO) and Graduated Reduction Gradient (GRG) were used to evaluate individual components in the proposed EESCs. Use of COMSOL thermal simulation software was critical in the design of the power IGBT SOA.

A case study of 250 kW station, a reduced scale of a typical HVDC station of 2000 MW (for example Sellindge HVDC station), based on 7-level MLC used Isolated Gate Bipolar Transistors (IGBTs) to evaluate the annual reduction in power losses and reduction in cost. If an upward trajectory is computed, based on the number of UK HVDC Converter stations, enormous economic and energy recovery can result with significant impact towards a decrease in global warming. The results obtained validated the research goals and identified a high potential for the application of EESCs in HVDC.

Declaration of Authorship

I Satyanand V. S. Mohanram declare that this thesis is original and prepared by myself. It has not been submitted to any other Academic Intitution for award or degree.

Satyanand V.S. Mohanram

January 2021

Dedication

With sincere humility and love, I present this thesis to my late parents Mrs Sarju Devi Mohanram (Mishra) and Mr Bachoo Mohanram.

Thanks to my children, Vidyanand (Vid), Kavita Banga (Kavi), and their respective spouses, Lisa and Rajesh (Lach), Vishnu and Vivekanand (Anand).

Thanks to my son Vid with a Ph.D and a JD, and to my daughter Kavi who multi-tasked with her fulltime secondary school teaching job and her MA study in Education, you were both superb examples of commitment for me to follow.

Thanks to Lach for his constant positive attitude and advice to maintain focus on my work.

Thanks to Vishnu and Anand for their continued support and encouragement.

Thanks to my two amazing grandsons, Dhruv Banga and Kishan Banga, for brighting up my days with your refereshing video messages.

Most importantly, thanks to my wife Vejai, who has always encouraged me to keep on working, but whose company I have missed for the last four plus years.

Acknowledgement

Massive thanks to my Senior Supervisor Dr. Mohamed Darwish, who has always been available 24/7. He was instrumental in reaching this final stage due to his Effort, Support, Patience, Guidance and Knowledge.

Many thanks to Dr. Ahmed Zobaa, Dr. Maysam Abbod and Professor Hamed Al-Raweshidy for my successful passage through the 18, 30 and 42 months Progression Reviews, without which I could not have advanced to the PhD research stage.

Many thanks to Dr. Zobaa for his recommendation to use SMARTDRAW which resulted in professional looking diagrams and avoided the constant crashing of other Drawing Applications.

Many thanks to Professor Hamed Al-Raweshidy, for his advice to investigate Optimisation methods.

Many thanks to Dr. Maysam for the valuable introduction to PSO, which awakened a desire to further investigate Optimisation and AI applications.

Thanks to Dr. Yang Yang, who provided COMSOL Simulation results from data I provided for the IGBT Power module.

Thanks to all my sisters and spouces, Lalita Arya, Saeeda and Dr. Asghar Malik, Sharada Bhajan, Chrisnadat and Shanta Sawh, and Amrita Rameshaur, also brothers and spouces, Vivekanand and Vishwani Mohanram, Yoganand and Fareeda Mohanram. For encouraging support from all my nieces, especiaslly Swasti, and nephews around the world, thank you.

Particular thanks to Shahid Malik and Shakti Clark for portraying me as an inspiration for the younger generation.

Thanks to my sister L (Lalita Arya), for hints in writing dedications, to my brother Vivekanand, for his patience in the long hours of discussions on my research. Thanks to my brother Yoganand for his proactive, stimulating and constructive ideas.

Jazāk Allāhu Khayran to my nephew Shahzad Malik, for all the Applications updating for my computer, which were critically important to my research,.

Appreciation and thanks to my retired BSI colleagues, Alan Christopher, and David Charleston, for their responses to the many research discussions during my four years of research.

TABLE OF CONTENTS

LIST OF ABBREVIATIONS

ANSI	American National Standards Institute
AVC	Automatic Voltage Control
BIL	Basic Insulation Level
BJT	Bipolar Junction Transistor
BSI	British Standard Institution
CB	Circuit Breaker
Cr	Capacitor Resistor
CHBMLC	Cascaded H-Bridge Multilevel Converter
CHB7LC	Cascaded H-Bridge 7- Level Converter
EESC	Energy Efficiency SC
EMC	Electromagnetic Compatibility
EMI	Electromagnetic Interference
ERU	Energy Recovery Unit
F/W	Free Wheel
GA	Genetic Algorithm
GaN	Gallium Nitride
GRG	Generalised Reduction Gradient (Solver)
GTO	Gate Turn Off Thyristor
HF	High Frequency
HFT	High Frequency Transient
HP	High Power
HV	High Voltage
HVCB	High Voltage Circuit Breaker
IEC	International Electrotechnical Commission
IEEE	Institute of Electrical and Electronics Engineers
IGBT	Insulated-Gate Bipolar Transistor
IGCT	Integrated Gate-Commutated Thyristor
IRMS	Root-mean-square value of current
MOSFET	Metal Oxide Field Effect Transistor
NP	No Protection
NR	Newton Raphson
PDSC	Passive Dissipative Snubber Circuit
PE	Power Electronics
PER	Period
ph-to gr	Phase to Ground
ph-to-ph	Phase to Phase
PSO	Particle Swarm Optimisation

PSs	Passive Snubbers
PU	Per Unit
PW	Pulse Width
PWM	Pulse Width Modulation
RFI	Radio Frequency Interference
RSC	Resonant SC
SC	Snubber Capacitor
SW	Switch
SA	Surge Arresters
SBR	Super Barrier Rectifier
SC	Snubber Circuit or Surge Capacitor
SCR	Silicon Controlled Rectifier
SD	Switching Devices
SF	Softness Factor
Si	Silicon
SiC	Silicon Carbide
SOA	Safe Operating Area
SSSD	Solid State Switching Device
τ	Time Constant
t_D	Time Delay
t_{on}	Switch Turn-On Transition Period
t_{off}	Switch Turn-Off Transition Period
WGMs	Wideband Gap Materials
ZC	Zero Crossing
ZCD	Zero Cross Detector
ZCS	Zero Current Switching
ZVS	Zero Voltage Switching

LIST OF TABLES

LIST OF FIGURES

Chapter 1 Introduction

1.1 Research Motivation and Research Background

The main motivation to engage in this research occurred at retirement in 2006, after a mentally engaging and stimulating period of 15 years as secretary to technical committees at BSI, European Committee for Electrotechnical Standardisation (CENELEC) and IEC. A vacuum was created, with a desire to pursue knowledge and self-betterment. Subsequently, the title of the research resulted from the gap (Figure 3-14) uncovered from articles reviewed.

Switching actions in semiconductor devices generate switching losses and RFI. If the voltage or current is switched before zero crossing (hard switching), there will be *dv/dt* and *di/dt* across and through the switch respectively, the products of which is the source of the switching losses. High voltage and current oscillations due to stored energy within the switch during the turn-on and turn-off times, giving rise to loss as heat and possible irreparable damage to the expensive switching devices. To avoid this problem, passive and active snubber circuit are used to transfer the switching loss energy from the expensive and delicate switches and dissipate it in a resistor as heat. These types of snubber circuits are called dissipative snubber circuits because they do not save power but mainly remove the switching stress from semiconductor devices. These types of dissipative snubber circuits are acceptable for low power applications where the emphasis is on the protection of the semiconductor devices. When the efficiency of the circuit has a high priority, then other types of snubber circuits are used, and they are called energy efficient snubber circuits (EESC). While types of dissipative snubber circuits (DSC) are well known [1] and they can be used for variety of applications, EESC needs to be designed specifically for each application.

The research carried out in the area of EESC is limited to low power applications [2], as for high power applications the heat generated from the switches is either wasted in resistors or water cooling techniques used to remove the heating losses for domestic applications within the local area of the HVDC installation [3]. According to the literature survey carried out in this research work there is no reference of EESC in high power applications. As mentioned before EESC cannot be duplicated from low power circuits like DC/DC converters and applied to high power applications like HVDC converters. For this reason, survey was carried out which resulted in a gap to design of EESC for high power applications and specifically for Multilevel-VCVS used in HVDC stations.

1.2 Research Aim and Objectives

1.2.1 Research Aim

To design Energy Efficient Snubber Circuits (EESC) for Multilevel VCVS converter with optimum parameters to reduce the wasted energy using the switching period only.

1.2.2 Objectives

- To critically review current articles on passive and active snubber circuits including dissipative and Energy Efficient Snubber Circuits (EESCs).
- To design an EESC with the task of optimising the components used.
- To apply COMSOL thermal simulation with the task of determining the Safe Operating Area (SOA) of the power switching module.
- To test the proposed design on a cascaded 7-level MLC case study

1.3 Thesis Contributions/Findings

The major contributions of this thesis are:

- It critically investigates the characteristics of dissipative and energy efficient snubber circuits.
- It presents a design and development of EESC suitable for high power Cascaded H-Bridge MLCs.
- It evaluates the characteristics power range against junction temperature of power switching modules used in H-Bridge MLC using COMSOL thermal simulation software.
- It presents a case study to show that EESC can contribute significantly to the reduction of dissipated energy when used in conjunction with the current water cooling methods.
- Using current energy tariffs (£/kWh), to reveal that annual cost reduction is possible in wasted dissipated energy.
- It presents the possibility of scaling up the designed EESC for higher power applications.

1.3.1 Publications

The following articles were published during the PhD study period.

- *Sat Mohanram, M. Darwish, CC Marouchos, "Optimisation and Simulation of RC Time Constants in Snubber Circuits", University Power Engineering Conference (UPEC), September 2018.*

- *Sat Mohanram, M. Darwish, CC Marouchos, "Power Switching Device Losses – Simulation and Non-Simulation Methods of Calculations", University Power Engineering Conference (UPEC), September 2018.*

The following paper has been submitted for publication:

- *Sat Mohanram, Maysam Abbod and M. Darwish, "Application of PSO in Calculating the Optimum Snubber Circuit Parameters for Minimum Switching Energy".*

1.4 Time Constant with Constraint at Low Power Level

At low power levels, analysis revealed [4] that for minimum switching energy the Turn-Off snubber circuit capacitor resistor time constant (RC) need to be less than the turn-off switching period with no snubber circuit connected. However, the above strategy was subjected to an important design constraint for the Turn-Off EESC, i.e., to determine the capacitor value at IGBT turn-off which reduced the current to zero and increase the IGBT voltage to supply level at the same time. i.e.,

$$Constraint\ for\ optimum\ 'C', \qquad (t_{fall} = t_{rise})$$

1.4.1 Optimisation and Simulation

Subsequent analysis to minimise IGBT switching energy resulted in objective functions with single and multiple variables. These objective functions were analysed applying Generalised Reduction Gradient (GRG) Solver, Graphical, and PSO Optimisation techniques in the determination of optimal component values for the energy efficient snubber circuits. The optimum component values were then validated by means of PSpice Simulations. The most efficient evaluation method was the GRG solver, in reducing the IGBT switching energy to a minimum off 0.052 µJ and at the highest efficiency of 99.92%.

1.4.2 Least square Analysis to Linearise Step current wave

In the case study the input voltage and load current levels for the Cascaded H-Bridge Multi Level Converter (CHBMLC) were set to 1.65 kV and 150 Amps, respectively. Least Square analysis was used to approximate the IGBT turn-on step-rise current to a linear rise. This enabled a common Turn-On EESC Inductor for each of the three bridges to be determined and connected to the IGBTs. This strategy removed the complex analysis required for each bridge, to determine individual Turn-On Inductors for each step rise in the current.

1.4.3 Application of COMSOL Multiphysics Simulation

Another valuable tool was the use of COMSOL Multiphysics Thermal Simulation. It resulted in an input Power kW versus $T_{Jmax}{}^{0}C$ benchmark Safe Operating Area (SOA) characteristic, to design the EESCs guaranteeing the IGBTs T_{Jmax} parameter not exceeding the data sheet SOA. The CHBMLC in a HVDC Transmission sub-stations was used in the analysis.

1.5 Research Organisation

This thesis is organised in eight chapters.

Chapter 1 Presented the Introduction.

The review chapters were split into two (2 & 3) since they cover switching devices and switching power losses and passive and active SCs.

Chapter 2, presented the review of switching devices and switching power losses.

Chapter 3, presented the review of passive and active SCs.

Chapter 4, presented the optimisation of Passive SC.

Chapter 5, presented the use of Solvers, Optimisers, and PSpice Paramatisation to determine the optimum SC parameters to minimise switching energy.

Chapter 6, Application of COMSOL Multiphysics Thermal Simulation to determine the SOA and T_{Jmax} for the high-power switching device.

Chapter 7, presented a case study of EESCs connected to a CHBMLC for HVDC Converter Stations.

Chapter 8, discussed the conclusions and suggested areas for future work.

Figure 1-1, shows the structure of the thesis with the Chapters and Titles and Figure 1-2, presents a micro view and summary of the research.

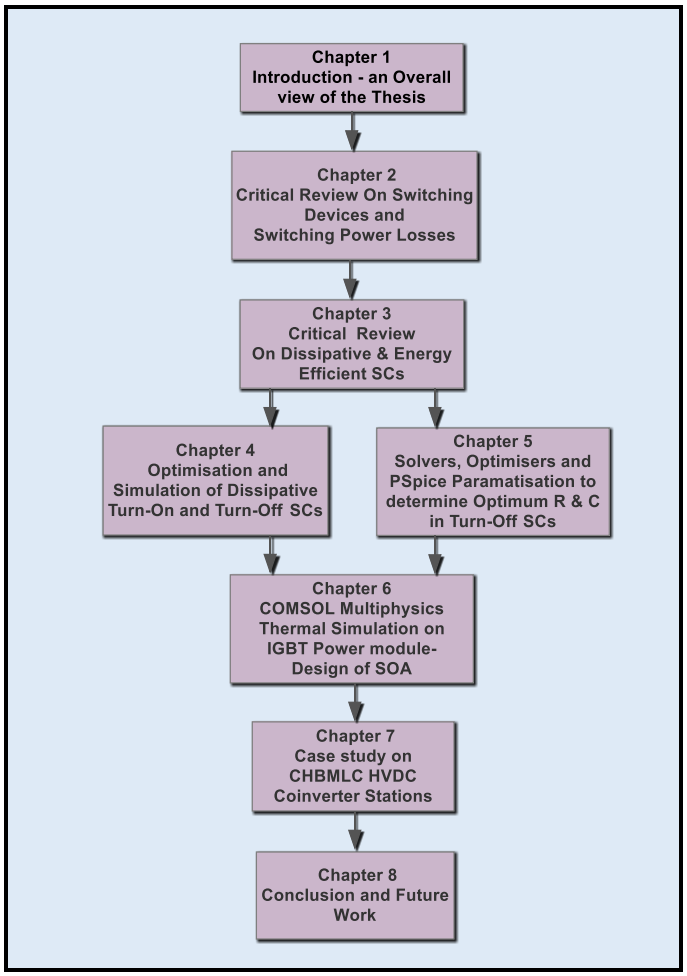

Figure 1-1 Thesis Research Structure

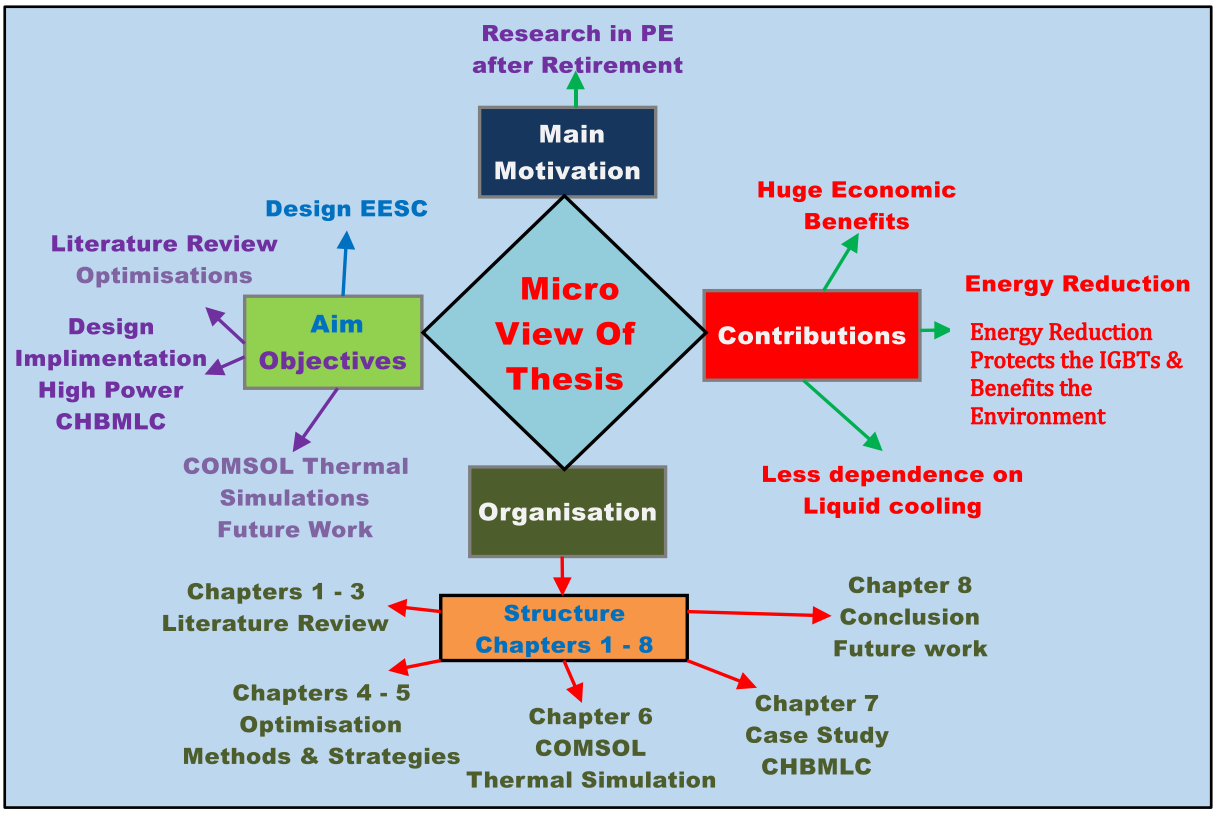

Figure 1-2 Micro View and Summary of Thesis Research

In Figure 1-2, Main Motivation, Aim and Objectives and parts of Organisation have been covered in Chapter 1. The analysis of Articles in the Literature Review now follows in Chapters 2 and 3.

Chapter 2 Literature Review – Switching Devices and Losses

2.1 Introduction

The Review is divided in two parts.

Part 1 presents historical changes in Switching Devices. Their development was influenced by demand for faster switching times, higher power, and reduction of losses. This was delayed due to lack of modelling software and dependent on experimentation. Due to progress in modern technologies and new materials, IGBTs and MOSFET were being manufactured. New materials, such as the Wideband Gap (WBG) were investigated to further enhance the power capacity and elevated temperature applications.

Part 2, presents the power losses during the switching transitions and on/off periods.

2.2 Solid State Switching Devices, Encapsulation, Evolution, and their Future.

To guarantee the safe operation of Solid State Switching Devices (SSSDs), some switching devices included built-in SC. To reduce design cost, and project times, encapsulated switching device were chosen. Figure 2-1 shows a built-in RC snubber (control) circuit across a Triac device.

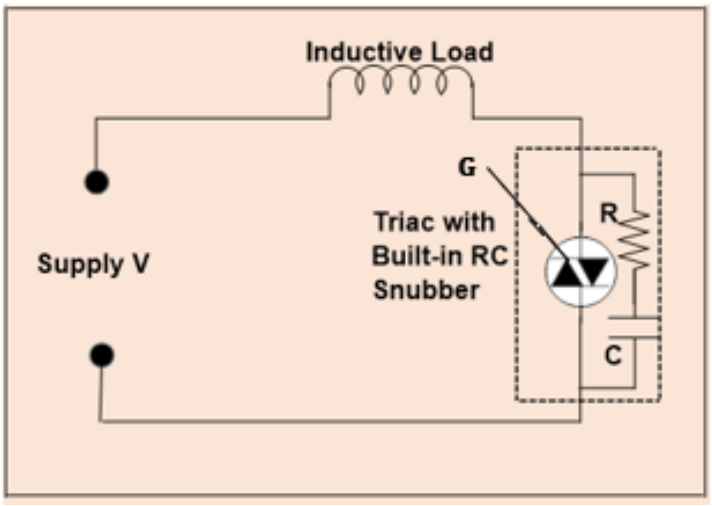

Figure 2-1 Triac device with a built-in RC SC

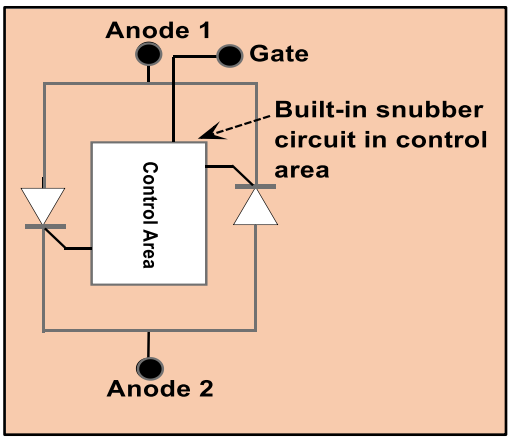

Figure 2-2 Triac with built-in SC within its package

Figure 2-2 shows the SC in Figure 2-1 within the package which includes the gate control signal [5].

Due to the need for flexibility in circuits design, snubbers circuits are designed as external circuits for connection to the main switching device. This allows for design characteristics to be achieved such as, zero volts switching (ZVS), zero current switching (ZCS), hard and soft switching and not limited to fixed characteristic with built-in SC.

A chronology of the development and inventions of switching devices is presented in Figure 2-3 [6]. Non-mechanical switching devices appeared during the years 1930 to1934, when mercury-arc rectifier was used in DC-DC converters. From 1948 to 1996, the transistor was invented followed by power switching devices. Bell laboratories started the solid-state revolution in 1948, and the General Electric Company was the contributor for introducing switching components. During those early years, there were periods of delays between inventions and developments. Today, the use of modelling and simulation has accelerated the research time scales for new materials to enhance the applications of new power solid-state devices and to enable rapid progress in Power Electronics. The next section looks into the progress and development into the materials used in the switching devices.

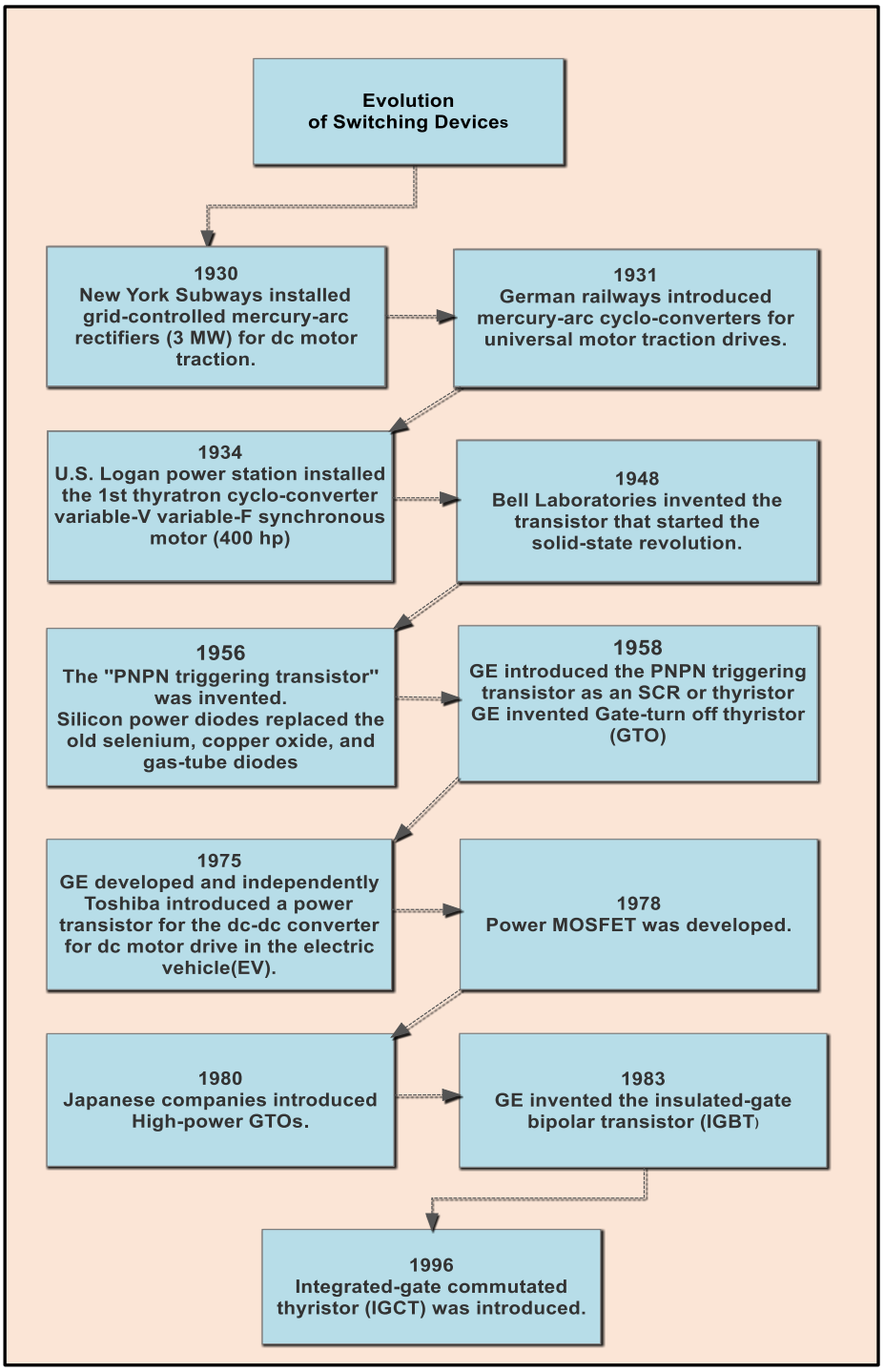

Figure 2-3 Evolution of Switching Devices

2.3 Future Trends in Switching Devices

Figure 2-4 traces the changes that occurred in silicon switching devices and their future development using wideband gap materials.

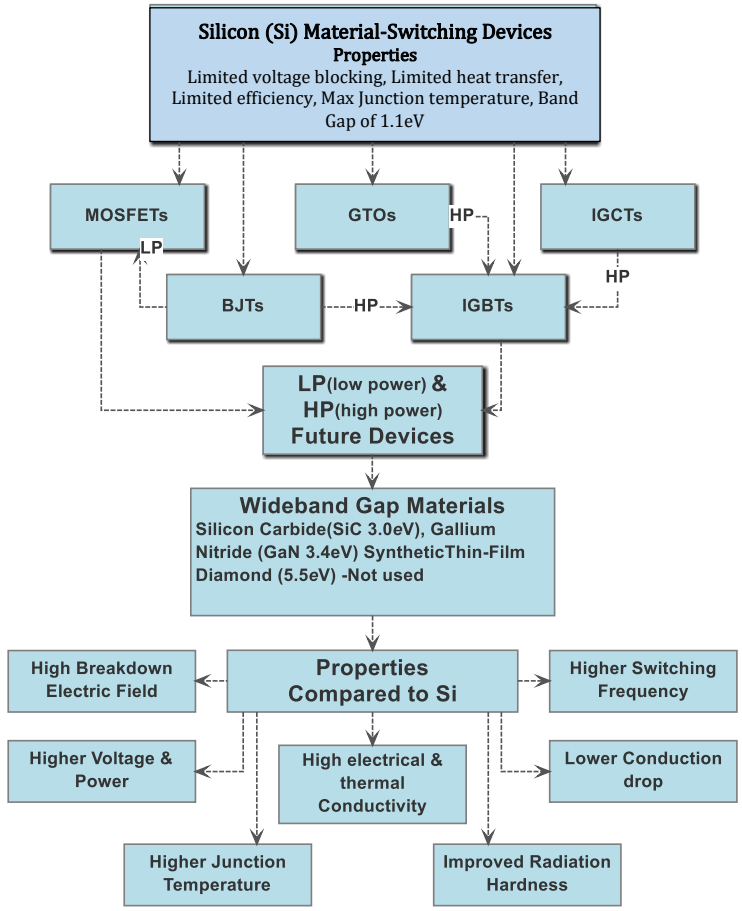

Figure 2-4 LP & HP Si-SDs replaced with WGM SDs.

Silicon has been the basic raw material for power semiconductor devices. Their use and applications were well established. But the range of applications were limited due to a low bandgap of 1.1eV, limited voltage blocking, low efficiency, low operating temperature, and low heat transfer. Due to these limitations, switching devices were replaced with, MOSFETS and IGBTs in both low and high-power applications. Further development to find higher specifications for switching devices, resulted in materials, such as Silicon Carbide (SiC) (3.0 eV), Gallium Nitride (GaN) (3.4eV) and synthetic thin-film diamond (5.5 eV). These were known as wideband gap materials. Due to manufacturing regulations in using diamond, only SiC and GaN materials are used [7]. Such materials when used in converters will improve overall efficiency and require less cooling due to their high operating temperature. These New Switching Devices will create new opportunities in the design of SC to operate in elevated temperature, high Voltage and Power applications.

2.4 Wide Band Gap (WBG) Materials Contribute to Cost Reduction.

2.4.1 Thermal Management

Thermal management is important in IT and consumers equipment, Industrial and in EV. In alternative drive, hybrid and electric vehicle are increasing with the batteries presenting heat dissipation challenges. Refrigerants and water-cooling systems regulate the temperature to increase safety and extend battery life. The excessive costs of these cooling systems can be minimised by using elevated temperature WBG switching devices. This change has the additional benefit of reducing the drive volume, and hence the losses [8].

Power electronics is of paramount importance to improve EV efficiency, reduce weight and size of the power management control and motor drive. SiC MOSFETs bring significant benefits compared to standard IGBTs silicon technology, in both efficiency and reduction of the ratio of volume to dimensions (form factor). However, the use of silicon has reached its maximum application limits of high power and temperature (150^0C - 200^0C). To extend this temperature limitation (300^0C +), semiconductor components, especially switching devices made from these advance materials can make this possible.

2.4.2 Identification of Switching Parameters impacting on Losses and Costs

Examples of two simulations were conducted, [9] one using a Si-IGBT and the other using a SiC–MOSFET, on a 60 kW inverter to power an EV motor drive, with the main parameters of Vdc (900 V) and switching frequency (20 KHz). The measured results are presented in Table 2-1.

Table 2-1 Loss Comparison between Si-IGBT and SiC – WBG switching device

Parameters	Si-IGBT	SiC-MOSFET	MOSFET Losses as a % of IGBT losses	Benefits
Total chip area per switch - mm^2	300	168	n/a	Reduced footprint/volume
Conduction losses - W	125	55	44	Smaller or no heat-sinks
Turn-on losses - W	280	90	32	Allows for higher switching frequency
Turn-off losses - W	246	40	16.3	Small Snubber Dissipation resistor
Body diode conduction losses – W	n/a	12.3	n/a	No change
Diode conduction losses – W	5	n/a	n/a	No change
Diode Q_{rr} losses – W	260	5.3	2	Faster switching frequencies
Total Losses (Column addition)	1216	370.6	30.5	Comparative % Reduction in total MOSFET Losses

Table 2-1, shows a distinct advantage in using MOSFET switching devices made from WBG materials. The percentage loss is a good indicator of the reduction in lower operating temperature, increasing efficiency, reducing volume, and lowering costs of power electronic

devices made from WBG materials. Figure 2-5 and Figure 2-6 were plotted from Table 2-1, to present a visual benefits of WBG materials.

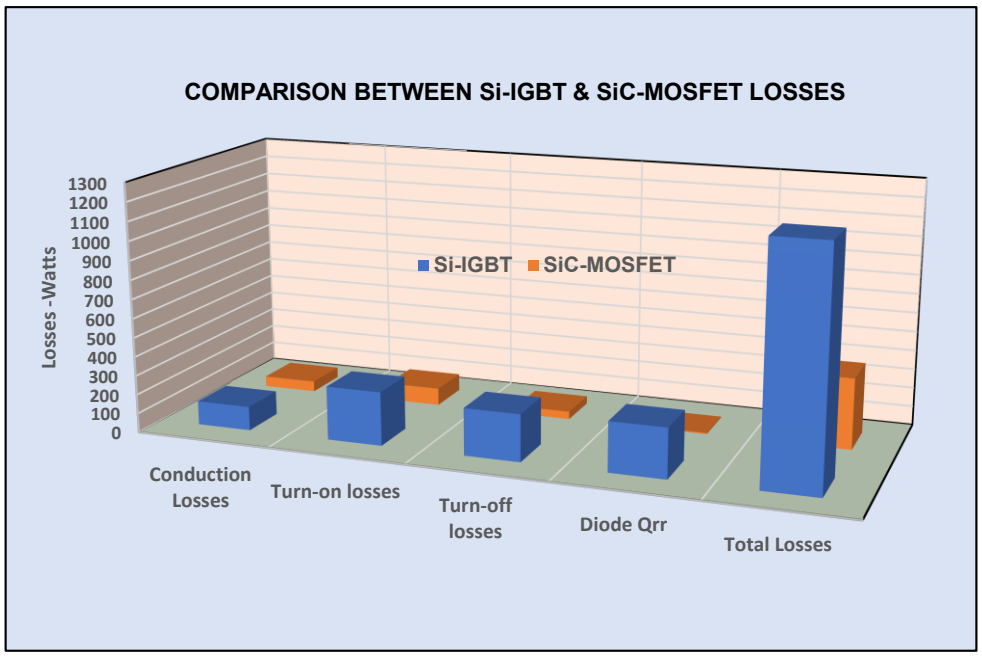

Figure 2-5 Comparison of losses between Si-IGBT and SiC-MOSFET SDs

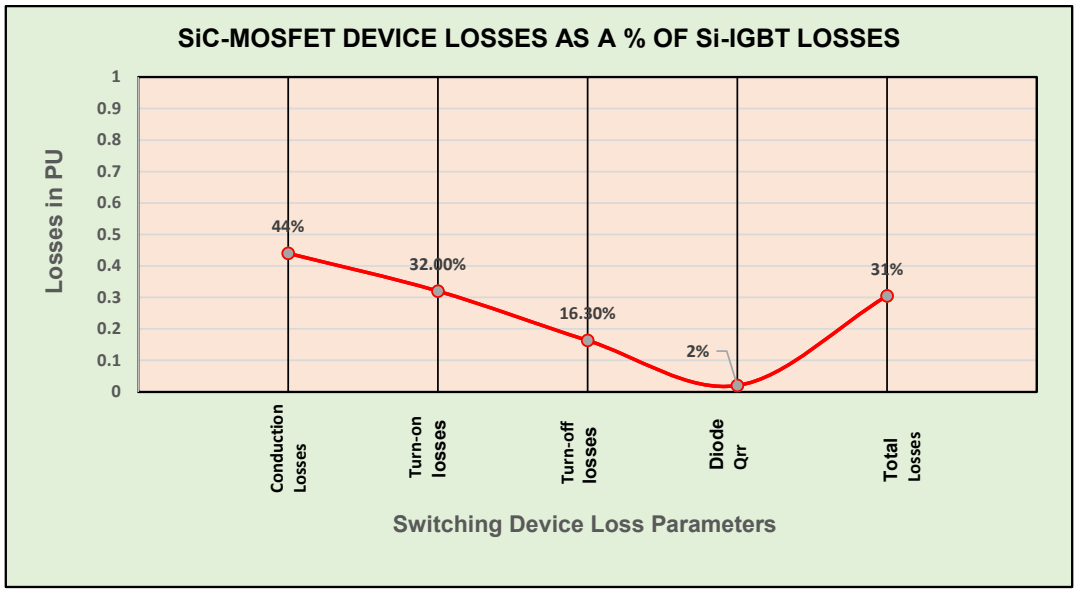

Figure 2-6 WBG MOSFET Losses as a % of Si-IGBT Losses

Figure 2-5 shows WBG MOSFET switching device has much lower parameter losses compared to a SI-IGBT device and contributes to the advance performance. Figure 2-6 presents the comparison in percentages and identifies that the lowest loss is with the diode reverse recovery loss. It enables faster switching times since the short recovery time quickly

restore its forward bias state ready for the next operation. Article [9] also gave useful figures for thermal conductivity and the eV-bandgap for Si, Gan (Gallium nitride) and 4H-SIC (Polytype crystal structure with a double twist), which are listed in

Table 2-2.

Table 2-2 Comparison of Si and
WBG Thermal and Band Gap properties [9]

Materials	Thermal Conductivity K (W/cmk)	Band Gap eV (electron volts)
Si	1.5	1.1
Gan - WBG	1.7	3.4
4H-SiC - WBG	5	3.3

The switching devices made from the Sic WBG material would have the highest heat dissipation rate, which would reduce the need for heat sink and operate at a high switching frequency. The benefit of a high eV band, also permits for elevated temperature (300^0C – 600^0C) environment and increases the device voltage rating to high kV levels.

2.4.3 Multiple SiC Switching Devices Connected in Series for High kV Rating.

Stand-alone high power and elevated temperature WBG switching devices are still being developed. Currently, there is no high voltage SiC device available at voltages higher than 1.7 kV. A research in power switch development [10], combined twelve smaller SiC power devices in series to achieve a high-power rating of 15 kV and 40 A. It required one gate signal to turn it on and off, making it simple to implement and less complicated than IGBT series connection-based solutions. It can operate over a wide range of temperatures and frequencies due to its efficiency in heat dissipation, a critical factor in power devices. Pending the manufacture of stand-alone high kV devices, this series circuit solution opens the way for power switches to be developed in combined quantities with breakdown voltages from 2.4 kV to 15 kV to fill current demands [10].

2.4.4 Applications Of SiC on Power Electronics Development.

The IT/consumer and industry sections are expected to develop power electronics systems to satisfy the growing demands to reduce costs, using WBG materials. Figure 2-7, identifies the areas where WBG SiC materials can replace similar equipment made from Si materials. The automotive section is worldwide engaged in the development of EV for ground, air, and military applications, to replace the environment polluting diesel, petrol, and gas fuel types of drives. The HV, high power DC-DC converters and Cascaded H-Bridge Multi level Converters (CHBMLC), will also be in very hostile elevated temperature environments. These conditions

can only be safely and economically met using WBG materials due to their advantages mentioned above. The switching devices being the main component used in those equipment will need reliable protection to ensure safe and long-life operation, by using SC. These circuits will have energy efficient recovery circuits, to minimise losses, reduce costs and achieve high switching efficiency, which is the main contribution in this research [11]

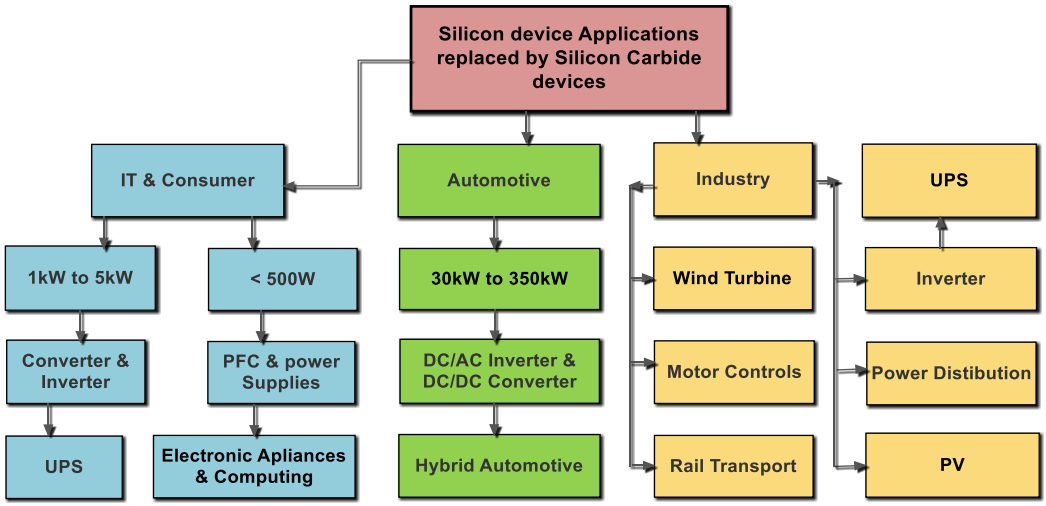

Figure 2-7 HP & HT Applications of Silicon Carbide -WBG components

2.4.5 Parameters that directly affects cost reduction.

WBG wafers manufactured in a dedicated foundry can be at a high unaffordable cost of $100M-$200M (£71M-£142M) and would prevent wider research by the private developers. A proposal to use existing Silicon (Si) foundry, resulted in new companies immediately launching a product with as little as $1M-$2M (£0.71M-£1.42M) [12]. Dedicated foundries now produce Silicon Carbide (SiC) devices (1200V, 20A, SiC MOSFET) at roughly 54¢/A - cents/Amp (38p/A -pence/Amp)) or five times the cost of silicon devices at 10¢/A (7.1p/A). With high volume production the cost could reduce to 7.4¢/A (5.3p/A). Because WBG semiconductors are inherently more efficient than silicon, less energy is expended as heat, resulting in smaller system sizes and material costs. Through technological innovations and the shift from 6” to 8” wafers, the cost of a SiC-MOSFET could be competitive to present cost of silicon devices in five years [12].

The cost reduction of future development of DC-DC converters, DC-AC inverters, and other PE equipment, due to WBG components can be expected to be radically reduced due to the criteria: -

- Higher power density results in smaller volume, higher switching frequencies and operational temperatures.
- The higher switching frequencies allows for smaller inductors and capacitors.
- None or smaller heat sinks are required due to high working temperature of WBG materials.

The above advantages would impact on huge future cost savings. In addition, weight, and volume of power electronic drives, EV drives, DC-DC converters, and DC-AC inverters, decrease as the switching frequency increases. There is an optimum size, weight, volume, and cost of WBG power equipment due to the maximum switching frequency limit, imposed by the shortest switching transition time of the switching device.

2.5 Losses in Switching Devices due to Hard Switching

Hard switching occurs when the solid state switching device (SSSD) is switched-on before the voltage or current passes through zero level. This type of switching causes an intersection between the gradients of *dv/dt* and *di/dt* as shown in Figure 2-8. The shaded area under these gradients represents the energy wasted in the switch. Oscillation due to stray C & L in the switching device is an additional source of wasted energy. These switching gradients generates EMI radiation and high frequency losses. In an RCD turn-off SC, the loss energy in the switch is transferred to the capacitor as $\frac{1}{2}CV^2$ Joules, which is dissipated as heat in the snubber resistor R [13] [14].

Soft switching can be applied to the switching device at ZVS or at ZCS resulting in no *dv/dt* or *di/dt* gradients, hence no switching losses [2] [15]. Hard switching, if not controlled by use of soft switching (also referred to as passive soft switching PSS), the switching loss can eventually degrade the life of the switch and can result in irreparable damage. There are cost implications due to down time in repairing or replacing expensive equipment. The cost increases proportionally as the scale of power rating goes up, a serious economic concern for power supply authorities and consumers [16] [17].

The *dv/dt* and *di/dt* gradients can also be reduced, by a reduction in the switching frequency [18]. If hard switching cannot be avoided, then a balance between switching frequency and EMI radiation will be required to minimize losses.

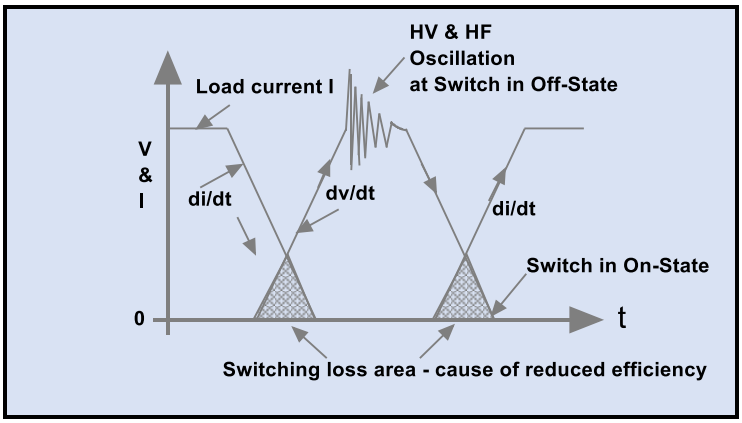

Figure 2-8 Hard voltage and current switching [19]

2.6 Methods to Determine SSSD Power Losses

In the design and manufacture of power supplies and converters, commercial factors demand high efficiency figures. Potential loss areas in the circuits are identified to achieve minimum losses. One of the main component contributing to losses in converters is the switching device [20] [21]. Figure 2-9 presents the main methods, to determine the loss in switching devices. The main losses are, switching loss, losses due to the high peak voltage and *dv/dt* oscillations generated across the switch. Optimised time constant in RC Turn-Off SC are effective in reducing these losses [19].

The switching loss methods are complex and involves several interrelated parameters [22] [23]. Depending on the design limitations, a balance between these parameters will be decided. This balance is achieved by considering the parameters for the IGBT/MOSFET, switching frequency, parasitic capacitances, and size. Furthermore, losses due to device structure impacts on design efficiency, conduction and switching losses [4].

The switching losses, will give the engineer the flexibility of choosing the method suitable for the design application under consideration [24] [25]. The benefits will also contribute to achieving critical decisions between inflated costs with enhanced performance and lesser cost at the expense of lower performance.

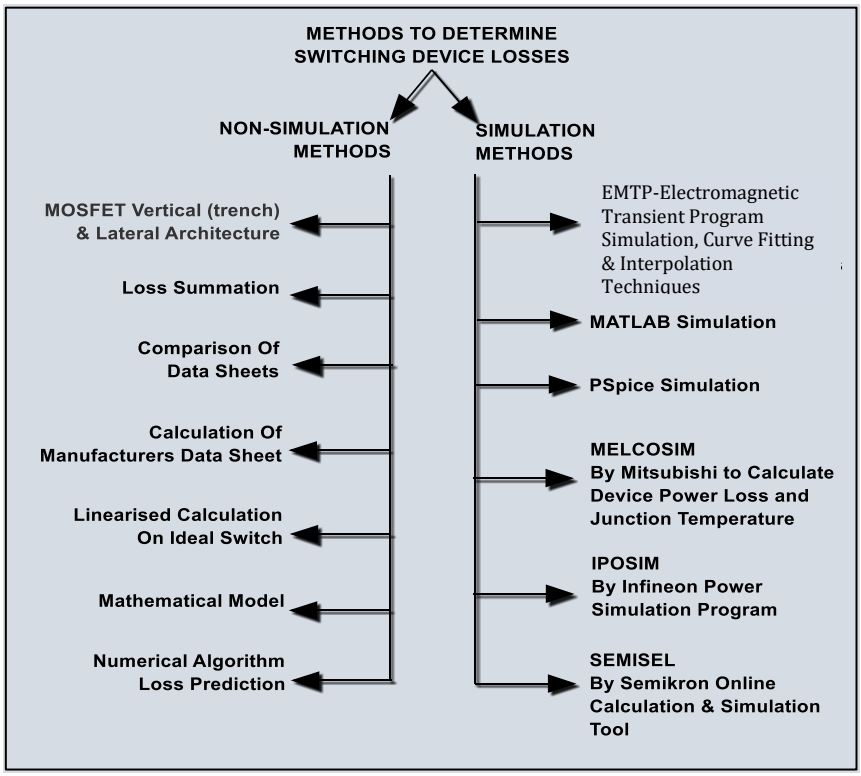

Figure 2-9 Methods to Determine Switching Loss [19]

Figure 2-9, presents the current methods, which are divided into seven Non-Simulation and six Simulation methods. The popular methods used are PSpice and MATLAB.

2.7 SSSD Losses – Non-Simulation methods – Linear calculation

Figure 2-10 shows a solid-state switch in series with an inductive load with a free wheel diode D1, and an RCD snubber circuit connected across it. The circuit will be used to explain the current and voltage waveforms and the switch losses during the on/off transitions and the on and off periods of the switching.

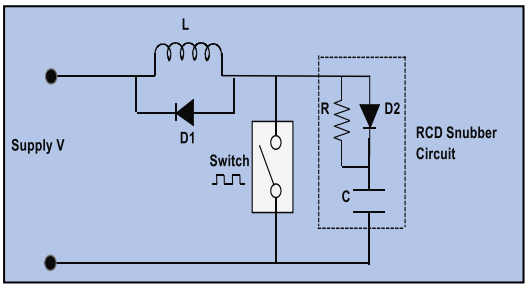

Figure 2-10 Ideal switch with Inductive load and Turn-Off SC

Figure 2-11, Section (A), shows the control signal, with the on and off periods that closes and opens the switch. Section (B), shows the waveforms for the load current I_L and the switch voltage V_{SW} and Section (C), shows the power waveform for the losses in the switch [19].

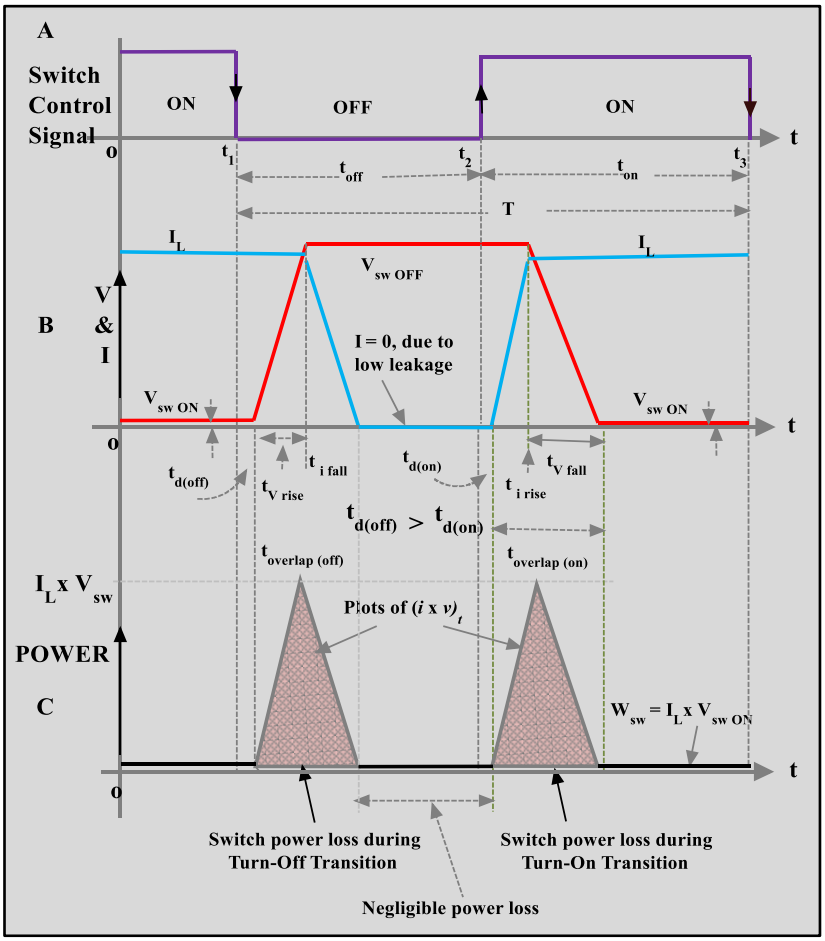

Figure 2-11 Losses in ideal switch based on linear approximation of V & I waveform [19]

Figure 2-11 (A), shows the switch control signal, with period, T = (t_{off} + t_{on}) and frequency f = 1/T Hz.

2.7.1 Control Signal - Explanation

2.7.1.1 Control Signal On

Figure 2-11 (B), shows that the switch is initially ON, with a load current I_L and a low '$V_{sw\ ON}$' voltage drop across it. At 't_1' the control signal switches to the OFF state. The switch voltage remains at '$V_{sw\ ON}$' and starts to increase after a delay of '$t_{d(off)}$' from 't_1'. After a further delay of '$t_{V\ rise}$' the switch voltage increases to '$V_{sw\ OFF}$' (equal to the supply voltage) at a voltage gradient of,

$$+\frac{dv}{dt} = \frac{V_{SW\ off}}{t_{V\ rise}} \tag{2.1}$$

2.7.1.2 Control Signal Off

At 't_2' the control signal switches to the OFF state, but the switch voltage remains at the 'Vsw OFF' level. If the load were purely resistive, the voltage across it would be instantly zero and the voltage across the switch equal to the supply voltage without any delay. Since the load is inductive, due to the collapse of the magnetic field there is a delay for the growth of the -Ldi/dt voltage, whilst the diode D1 in Figure 2-10 remains forward biased due to 'Vsw OFF' during the 't1 to t2' Off period and maintains a connection between the top end of the switch and the supply voltage (equal to Vsw OFF). When the -Ldi/dt voltage is equal to the supply voltage, D1 is reversed biased and the switch voltage drops at a negative gradient of,

$$-\frac{dv}{dt} = \frac{V_{SW\ off}}{t_{V\ fall}} \tag{2.2}$$

to a low value of '$V_{sw\ ON}$' volts. This cycle is repeated during the frequency of the control signal.

2.7.2 Current Wave-Form Cycle - Explanation

Figure 2-11 (B), shows the switch is initially ON, with a load current I_L flowing through it.

2.7.2.1 Control Signal Off

At 't_1' the control signal switches to the OFF state, but the load current I_L is maintained due to the load inductance and starts to decrease (when the switch voltage is at the open circuit level of '$V_{sw\ OFF}$') at a negative gradient of,

$$-\frac{di}{dt} = \frac{I_L}{t_{i\ fall}} \tag{2.3}$$

and continues until (near) zero level is reached.

2.7.2.2 Control Signal On

At 't_2', I_L remains at the low level and begins to rise after a delay of *'$t_{d(on)}$'* at a gradient of,

$$+\frac{di}{dt} = \frac{I_L}{t_{i\ rise}} \tag{2.4}$$

and reaches full load current of I_L and remains at this level for the duration of the on period of the control signal.

2.7.3 Switch Losses – During Transition, Open & Closed States

Figure 2-11 (C), shows the power loss wave-form due to the product of I_L and V_{SW} in Figure 2-11 (B). The shaded areas represent the power loss, due to its linearity, it can be estimated by using the formula for the area of a triangle. See equations (2.8) and (2.9).

Table 2-3 Equations derived from Figure 2.11 [19]

A	Control signal period	$T = (t_{on} + t_{off}) = 1/f$ Hz		(2.5)
B	Overlap (off) period,	$t_{OL\ off} = t_{V\ rise} + t_{i\ fall}$		(2.6)
	Overlap (on) period	$t_{OL\ on} = t_{i\ rise} + t_{V\ fall}$		(2.7)
C	Energy dissipated during Turn-Off Transition	$W_{PLoff} = ½ \times (t_{OLoff}) \times (I_L V_{SW})$	Joules	(2.8)
	Energy dissipated during Turn-On Transition	$W_{PLon} = ½ \times (t_{OLon}) \times (I_L V_{SW})$	Joules	(2.9)
	Power loss in the switch/cycle	Power = {(2.8) + (2.9)} x f	Watts	
		$= ½\ I_L\ V_{sw}\ (t_{OLoff} + t_{OLon})\ f$	Watts	(2.10)
	Switch loss per switch cycle	$\frac{1}{2} I_L V_{SW} x \frac{(t_{Olon} + t_{Oloff})}{(t_{on} + t_{off})}$	Watts	(2.11)
	and it is deduced that,	Power loss $\propto$ f, (t_{OLon}) and (t_{OLoff})	Watts	(2.12)
	Turn-Off loss (Negligible, due to low leakage current)	$W_{sw} = V_{sw\ off} \times I_L$	Joules	(2.13)
	Turn-On loss,	$W_{sw} = V_{sw\ on} \times I_L$	Joules	(2.14)
	and the average Power during the on state,	$W_{SW} = I_L \times (V_{sw\ on}) \times (t_{on}/T)$	Joules	(2.15)
	Equations' key - (OL = Overlap); (PL = Power loss); (SW = Switch)			

2.7.4 Summary

This Part 1 of the Literature review presented the historical evolution of the switching devices from the early 1930, 1931, when Mercury-arc-Rectifiers were used. The other main mile-stone years were, 1934 which saw the introduction of the thyratron, cyclo-converters, and in 1948,1956,1958, the invention of the PNPN transistor, and gas-tube diodes were replaced by silicon diodes. GE introduced the SCR, GTO, Power transistor for EV and competition to produce power switches saw in 1980, the Japanese High-Power GTO and finally in 1983 to 1996 GE produced the IGBT and IGCT.

Present day use of MOSFET and the IGBT are the main switching components in Power electronics. WBG materials which impact on losses, cost reduction and improvement of thermal management due to their high eV. Analysis on the percentage loss was a good indicator of the reduction in operating temperature, increasing efficiency, reducing volume, and lowering costs of Power Electronic Devices made from WBG materials. In the concluding section a detail analysis on the energy losses due to the -di/dt and dv/dt by hard switching. It also produced useful equations for the losses in the switching cycle which was followed up by identifying different methods using Simulation to calculate the switching losses. The next section continues with Part 2 of the Literature Review on the Dissipative and Energy Efficient snubber circuit.

Chapter 3 Review On Dissipative and Energy Efficient SC

3.1 Introduction

Figure 3-1 shows a snubber circuit (SC) connected in series or in parallel with a switching device.

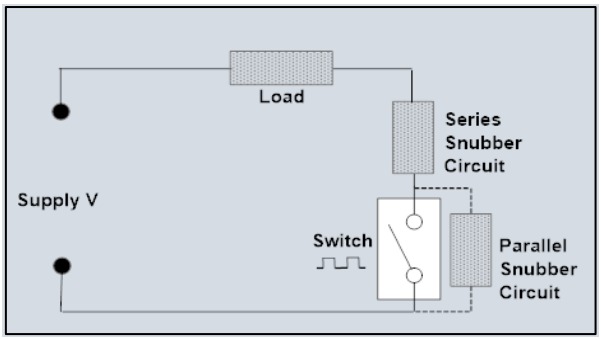

Figure 3-1 Block diagram of a series parallel SC

SC can be of the passive/active dissipative type or the energy efficient type. The Passive/Active type transfers the switch energy into a resistor and is dissipated as heat loss. The energy efficient snubber will take the switch energy and feed it either into the load or return it back to the supply. The objective of the SC is to protect the switch by removing its switching losses.

The series (turn-on) SC will reduce the in-rush current through the switch when it closes, and the parallel (turn-off) SC will suppress voltage spikes, and ringing oscillations that occurs across the switch when it opens and diverts the load current into a capacitor [26]. SC are therefore essential in reducing failures, losses and costly down-time and increase the switching efficiency of the switching device. With energy efficient SC, the recovered switching losses are returned to the supply, reducing the switch junction temperature (T_J) within its datasheet limits and maintain the switching device within its Safe Operating Area (SOA).

3.2 The need for SCs

In the mid1920s, DC to DC converters were designed using solenoid switches and for the conversion process, thermionic rectifying valves. Voltage spikes/surges were due to "switch bounce", i.e., the switches were not opening and closing instantaneously. In normal digital systems time scale, switches make and break in one action [27]. The technology was not

developed to filter the interference. Hence, a single capacitor SC was connected to remove the voltage surges and radio frequency, radiation/noise produced from mechanical vibrating switches [28]. An example in Figure 3-2 DC–DC converter 1920s–1930s, Mallory Handbook 1947 shows the DC input being switched via a vibrating contact to produce DC pulses. In further development of switching circuits, when the switch opened, a spring-operated part "snapped" away from the fixed contact to achieve a fast opening time. This action reduced the time taken for the current to fully establish an arc. Many years later, Solid State Switches were developed to replace those mechanical ones in the design of DC-DC converters, inverters, DC transmission links, controlled rectification, and other DC systems.

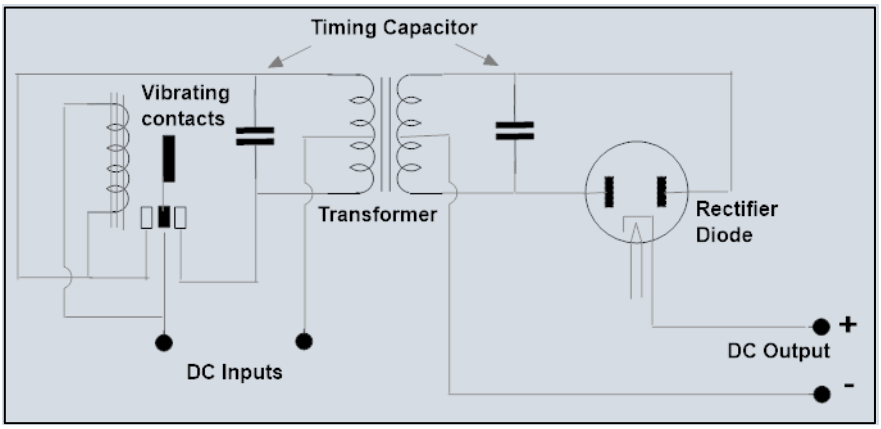

Figure 3-2 DC–DC converter 1920s–1930s, Mallory Handbook 1947

3.3 Classification of Dissipative SCs

Figure 3-3, presents five classifications of SC based on: -

1 Functions, which presents four types of SC together with functional parameters.

2 Power factor control and regulations by the energy suppliers

3 Power range, which is application driven with the main power components of Resistor and Capacitor.

4 Component configurations, which is subdivided into the six possible combinations of diode, resistor, capacitor, and Inductor. A detail discussion on each classification with their subdivisions are presented.

5 Efficiency of SC

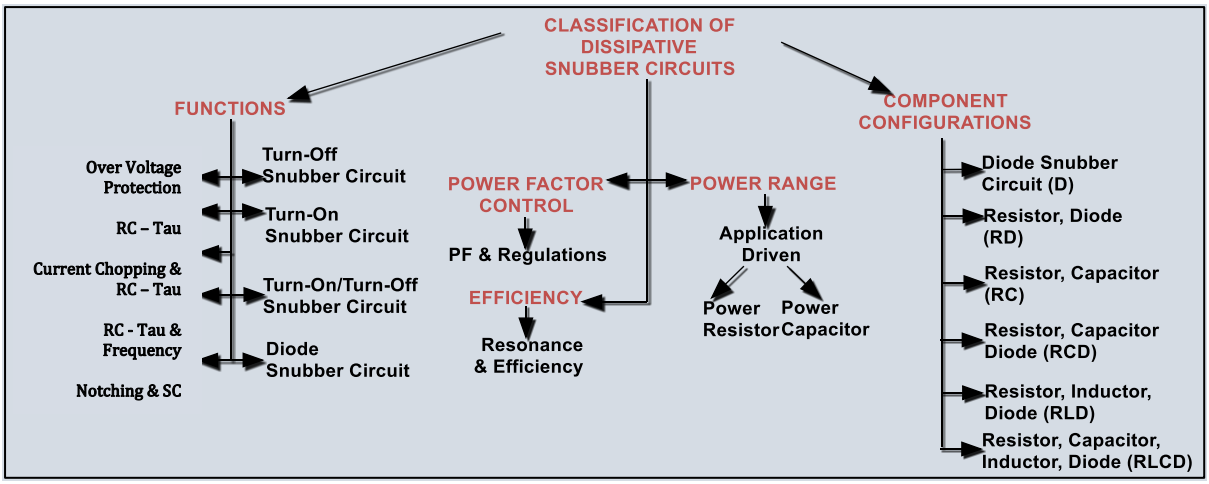

Figure 3-3 Classification of Dissipative SC

3.3.1 Classification of SC According to Function

3.3.1.1 Overvoltage Protection

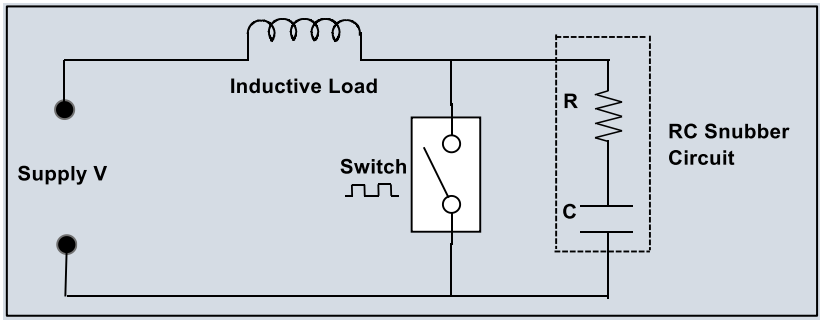

Figure 3-4 RC SC connected across a switching device.

Figure 3-4, is an example of an SC comprising of an 'R' and 'C' connected in series and across the switch providing over-voltage protection. When the switch opens, the magnetic field in the inductive load collapses and a high over voltage spike with modulated ringing appears across the switch due to the inductive voltage *-Ldi/dt*, and charges C via R. When the switch is closed, a series circuit is formed with R, C and the switch, and the capacitor's energy $\frac{1}{2} CV^2$ is dissipated in the resistor R as heat loss.

3.3.1.2 RC Time Constant

An important parameter is the RC time constant τ. The values of 'R' and 'C' should be chosen to be less than or equal to the switching/transition turn-off period of the switching device [2]. τ will allow the capacitor to discharge and charge completely for each on/off cycle.

To calculate the values for R and C, consider the following switching wave form shown in Figure 3-5.

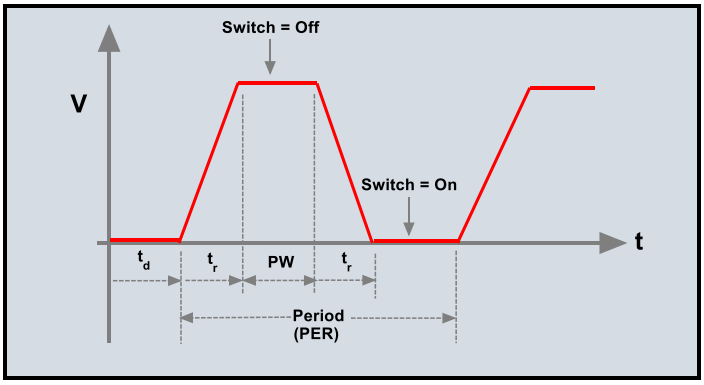

Figure 3-5 Switching Waveform.

Parameters for Figure 3-5

Assumptions for calculating tau

$t_d = 0$, $t_r = t_f = 1\mu s$ (symmetrical pulse);

Switching period, PER = 10ms;

Pulse width, PW = Toff;

Toff + Ton = PER $-t_f - t_r$ = 10ms $-2\mu s \approx$ 10ms, (ignoring t_f and t_r);

PW ≈ 5ms

Calculation of RC time constant τ (with examples of practical parameters). In Figure 3-4, during the OFF period (5ms) the capacitor is required to capture the stress energy from the switch and discharge it during the ON period (5ms) via R. i.e., RC = PW at a switching frequency of 1/10ms = 100Hz.

$$\tau = \mathrm{PW} = \frac{\mathrm{PER}}{2}\ \mathrm{S} \tag{3.1}$$

Therefore, RC = 5 ms

Choose, R = 1000 Ω,

and C = 0.005/1000 = 0.000005 F = 5 μF

Since there is no capacitor energy to discharge through 'R', from which it can be determined, a value is chosen to enable the calculation for 'C'.

Hence, the RC snubber components are, R = 1KΩ, and C = 5μF. With a calculated time-constant RC and a fast-acting diode, the switching frequency can be increased, adjusted, or optimised [15]. Alternative low-loss active SC using energy recovery units (ERU's) are used to prevent such losses to occur with high efficiency in the main circuit. However, the main disadvantage of active SC is that ERUs adds to the cost and complexity of the design. Compared to active snubbers, passive dissipative SC are simpler to design, cost less, and is more reliable, since there are no additional active switches. However, assuming a fixed turn-

off transition period of the switch, the switching losses will be constant with a fixed frequency. Hence, the losses dissipated in the RC SC will increase as the frequency increases [29].

3.3.1.3 RC Time Constant and Current Chopping (CC)

The interruption of a current at an amplitude before natural zero current crossing is referred to as the "current chopping level", (can be compared to hard switching). The chopped current will generate a magnetic energy in the inductances on the load side of the switching device circuit breaker (CB). This will cause an oscillatory current between capacitances and inductances on the load side of the CB which can generate a transient over voltage [30] See Figure 3-6.

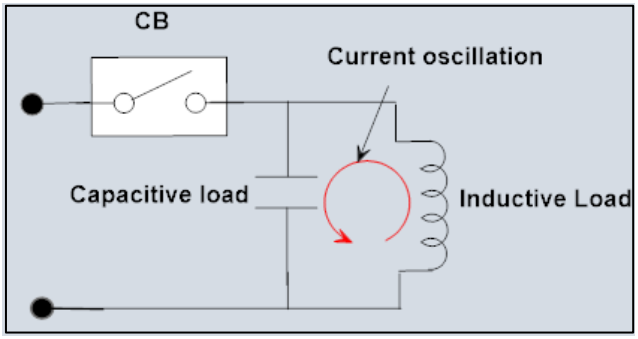

Figure 3-6 Current oscillation between load L&C when CB is opened

To determine the RC snubber components to protect a circuit under current chopping conditions, an analysis of the inductive and capacitive energies is presented in Table 3-1. Hence the transient voltage gradient is related to the peak over voltage and the transient frequency. To enable complete charge of the snubber capacitor in the first half of the transient cycle and complete discharge in the second half and to repeat the charge/discharge in the next cycle, the time constant τ of the RC SC cannot be greater than the period T of the transient voltage.

i.e., the time constant, $\tau = T/k$ Where $k \geq 1$

Table 3-1 Determination of *dv/dt* parameters

Description	Equations	Equations No.
From Figure 3-6 equating the electric & magnetic energies	$^1/_2 L_{load} i^2 = {}^1/_2 C_{load} v^2$	(3.1)
Gives an expression for the over voltage	$V_{over\ voltage} = i\sqrt{\frac{L_{load}}{C_{load}}}$	(3.2)
Equating the reactances in resonance	$2\pi f L_{load} = 1/2\pi f C_{load}$	(3.3)
Gives an expression for the frequency	$f = \frac{1}{2\pi\sqrt{L_{load}\, C_{load}}}$	(3.4)
Assuming a sinusoidal input voltage	$V_{over\ voltage} = V(sin2\pi ft)$ $(\omega = 2\pi f)$	(3.5)
Rate of rise of $\frac{dv}{dt}$ is proportional to ω and V with the relationship	$\frac{dv}{dt} \approx 2\pi f.V(cos2\pi ft)$	(3.6)
At $t = 0$ (when CB operates)	$\frac{dv}{dt} \approx \omega.V$	(3.7)

From equation (3.7) in Table 3-1, Figure 3-7 was drawn to show the relationship between the change in dv/dt, peak overvoltage and transient frequency.

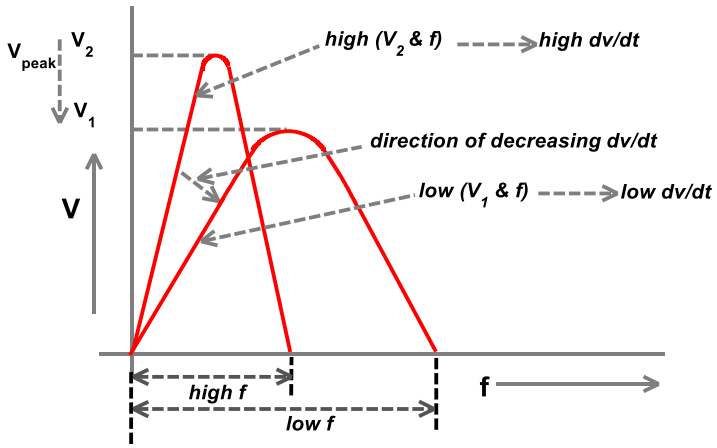

Figure 3-7-Relationship between, high & low *dv/dt*, V peak & frequency

An effective time constant for a RC SC will reduce the high dv/dt, the peak voltage and the frequency of the transient voltage, as shown in Figure 3-7.

3.3.1.4 The Turn-Off Characteristics of Power Diode

Since the power diode plays an important part in the operation of SC, it is important to review its characteristics. Figure 3-8 shows the Turn-Off characteristics of the diode. In section (a) the diode current $\mathbf{I_f}$ flows until it is zero at $\mathbf{t_a}$ and continues to conduct in the negative direction for the period of $\mathbf{t_a}$ due to the presence of stored charge. This current continues to flow during the reverse recovery time $\mathbf{T_{rr}}$ until the total charge (shaded area) is removed.

T_{rr} = 25% of the total time for reverse recovery to be established.

$T_{rr} = t_a + t_b$

t_a = time to remove the charge from the depletion layer

t_b = time to remove the charge from the semiconductor layer

Figure 3-8(b) shows the diode with a negative voltage gradient for the period t_b with a decaying oscillation as the stored charge is removed. Figure 3-8(c), shaded area is the diode power loss due to $V_f \times I_f$

Manufacturers have graded diodes by defining a Softness Factor SF [31] [32].

$SF = + t_b / t_a$

SF = 1, diode with low oscillatory reverse recovery voltage, (soft recovery).

SF < 1, diode with high oscillatory reverse recovery voltage, (fast recovery).

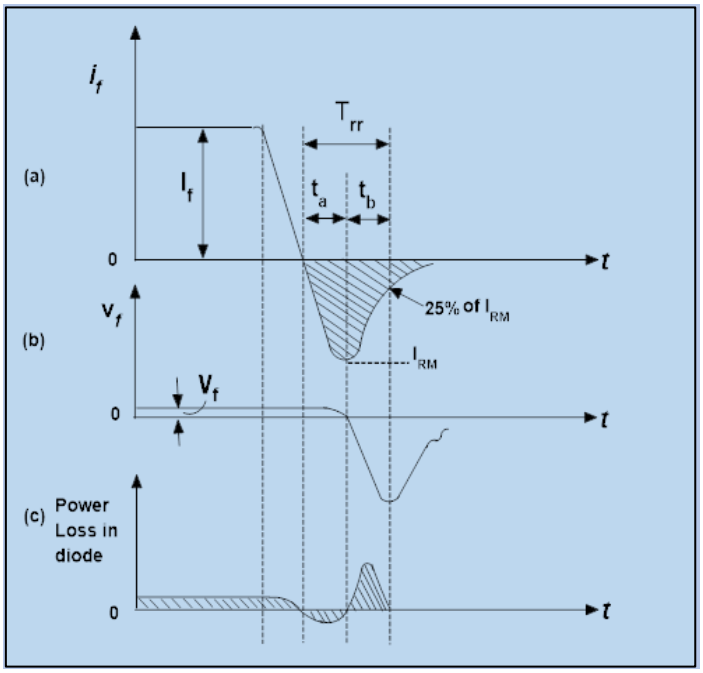

Figure 3-8 Turn-Off Characteristics of Power Diode,
a) Variations of Forward Current I_f,
b) Variations of Forward Voltage v_f,
c) Variation of Power Loss [32]

The two main characteristics of the power diode are: -

Time to achieve reverse recovery voltage – T_{rr}, and softness factor – SF

3.3.2 Turn-Off SC action at ON/OFF transitions of the switch

Figure 3-9, is an example of the diode in the RCD Turn-Off SC which is connected across the switch.

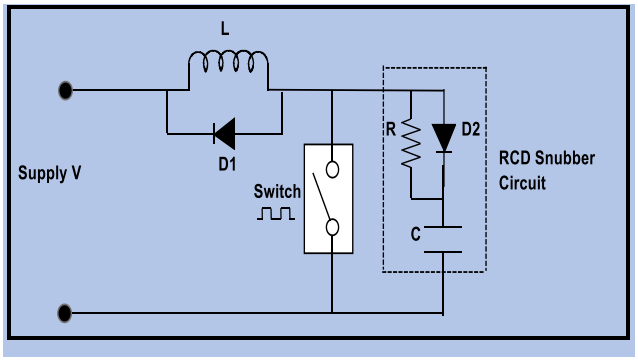

Figure 3-9 RCD Turn-Off Snubber, D1 in F/W mode,
D2 in Voltage diverter mode

Referring to Figure 3-9

Transition 1, Switch – ON

At steady state current flows through the inductor load and the switch. A magnetic field develops in the inductor.

Transition 2, Switch – OFF

The magnetic field collapses and generates a $\left[-L\frac{di}{dt}\right]$ voltage. D1 provides a freewheel path for the current through the inductor. The current continues to circulate until the inductive energy $\left[\frac{1}{2}Li^2\right]$ is dissipated in the diode and the inductor resistance. The $\left[-L\frac{di}{dt}\right]$ voltage also appears at the top of the switch and the SC. Via D2, the capacitor C appears as a short-circuit and removes the voltage spike due to $\left[-L\frac{di}{dt}\right]$ from the switch and charges with a stored energy of $\left[\frac{1}{2}CV^2\right]$ [33].

Transition 3, Switch - ON

A closed circuit is made between the switch, C and R. C discharges its stored energy as heat loss $\left[\frac{1}{2}CV^2\right]$ in the resistor R [34].

The Turn-Off snubber therefore protects the switch during turn-off by dampening the overshoot and oscillatory voltages and transfers the energy from the switch to the dissipative resistor.

3.3.3 RLD Turn–On SC

The two main functions of Turn-On SC are: -

1 - to protect switching devices from high in-rush current during turn-on,

2 - to modify voltage-current waveforms and reduce power loss in the switch during the turn-on transition. Figure 3-10 shows a common Turn-On dissipative SC.

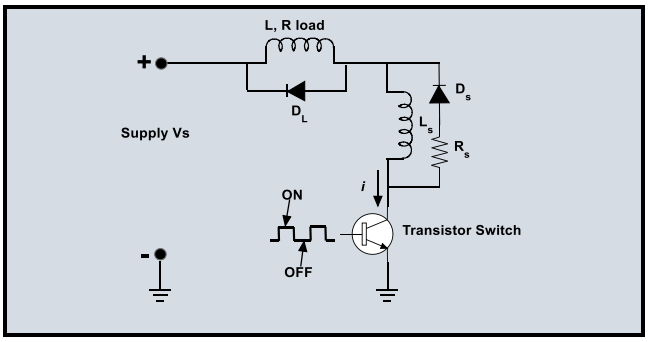

Figure 3-10 Transistor Turn-On Dissipative SC

The Turn-On and Turn-Off stages achieve the above snubber requirements, which ideally is zero voltage across the transistor.

During Turn-On

In Figure 3-10, D_S is OFF while D_L is ON, since D_L is discharging the stored energy in Load L. D_L connects L_S to the supply V_S. Choosing a value for L_S so that,

$$-L_S \times \frac{di}{dt} = V_S \tag{3.8}$$

and there will be zero voltage across the transistor with no in-rush current and reduced power loss in the switch.

During Turn-Off

The rise in voltage across the switch forward biases D_S which transfers the stored energy in L_S (during turn-on) to the resistor R_S as heat loss. The decaying snubber current reduces to a level for the SC to be ready for the next Turn-Off period of the switch. In practice, to reduce the voltage power across the switch [35] [36] the value for time constant for L_S/R_S is based on:,

$$T_{off} > \frac{3L_S}{R_S}$$

and

$$\frac{L_S}{R_S} = \frac{T_{off}}{3} \tag{3.9}$$

Hence, for the Turn-On SC the Ratio, Ls/Rs = 1/3 x T_{off}

3.3.4 Turn-On/Turn-Off SC

By combining the Turn-Off snubber of Figure 3-9 with the Turn-On SC of Figure 3-10, a Turn-On & Off snubber is formed. The snubber component values can be reduced without change in the two modes of protection. The combined and simplified circuits are shown in Figure 3-11.

3.3.4.1 Circuit Operation

In Figure 3-11, (simplified circuit) with the correct value chosen for L_s at turn-on, the induced voltage will be equal and opposite to Vs, resulting with zero voltage across the switch, hence no high inrush damaging current through the switch. The L_s discharge current will circulate via D_s and R_s. At turn-off, the high kV spike and HF transients appearing across the switch are clamped by C_s via D_s. At the next turn-on cycle, D_s blocks C_s from discharging through the switch and C_s discharges its stored energy through R_s. The value for R_s must be adequate to dissipate both the L_s and C_s stored charges. Since R_s is common to both L_s and C_s, values will be chosen and possibly adjusted at testing stage to ensure minimum stress in the switch [37].

The main disadvantage of the Turn-On/Turn-Off snubber is the power loss in R_s. To utilize this loss energy, the dotted circuit can be connected as shown. The diode will transfer the charge from C_s for each Off cycle into a storage capacitor [38]. The accumulated charge will be fed into the load thereby reducing the input supply current. R_s will now only dissipate L_s stored energy. However, R_s can be replaced by providing another auxiliary circuit to transfer the energy from L_s into the load, which would be an auxiliary circuit in an active snubber circuit

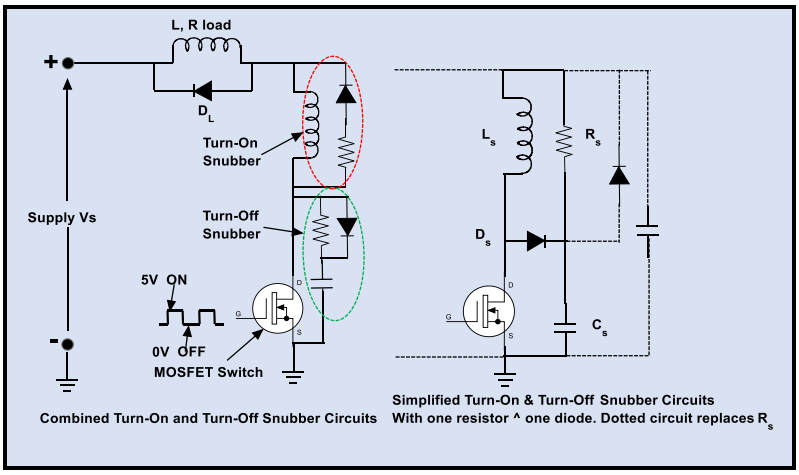

Figure 3-11 RCDL, Turn-On/Turn-Off SC

3.4 Classification of SC According to Configurations

Figure 3-12 shows the configuration of SC divided into six known types with component combinations of, D, RD, RC, RCD, RLD & RCLD. The component characteristics are used to define the type of SC, to achieve the desired function [1].

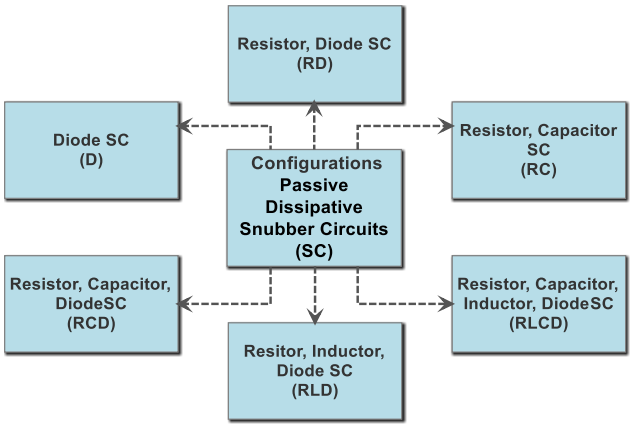

Figure 3-12 SC – configurations

3.4.1 Fast-Recovery Diode

Under diode configuration, there is the fast-recovery diode to ensure all the stored energy in the switch is removed if the switching frequency (on/off transition times) is high. Other special diodes like the super barrier rectifiers (SBR) [39], or switching semiconductor devices (transistors, MOSFETS etc.), may be chosen with built-in fast-acting diodes as shown in Figure 3-13 [18]. Alternatively, to increase the speed of the diode, some manufacturers connect a built-in capacitor across the diode [40].

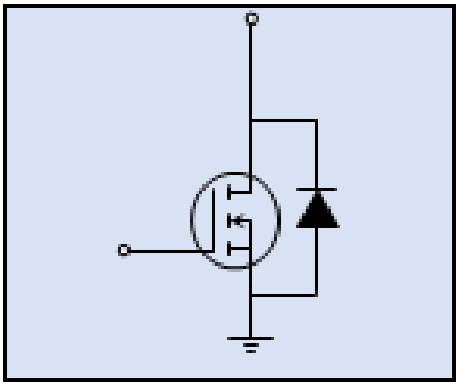

Figure 3-13 MOSFET with built-in Fast-Body diode

3.5 Classification of SC According to Power Rating

3.5.1 Power rating - Application driven

In the review, no power classification for SC have been found. Instead, they are used in various levels of power applications. Consequently, this identified a gap in snubber circuit design which led to the research question [41]. In practice, for power transformer or heavy inductance loads, the switching device can be a MV/HV CB and in LV applications solid-state switches. These switches are used in converters, control circuits for the protection of household electrical appliances and personal computers etc. For these power applications, it is important to ensure that switching devices operate within safe operating area [29] [42]. LV, MV and HV

CBs fitted with SC with adequate power ratings [43] provide such protection. They are installed in proximity to minimize effects of cable inductance and capacitance leakage and can be installed together in one large power panel [44] [45].

3.5.1.1 Gap in Research

The previous analysis, in principle applies to all low voltage electronic circuits, but special designs for protection of the switching devices are required when applied to HV and high power systems. Based on the research carried out for this thesis, there was no work carried out (gap in existing technology) for EESC for high power applications [41], presentation in Figure 3-14. The reason for the lack of research in this area may be due to the limitation of PE in the early years of high power converters and especially in the installation of HVDC stations. However, with the expansion of DC transmission and distribution and with the urgent need to reduce the carbon emission there is a need to focus the research in this direction.

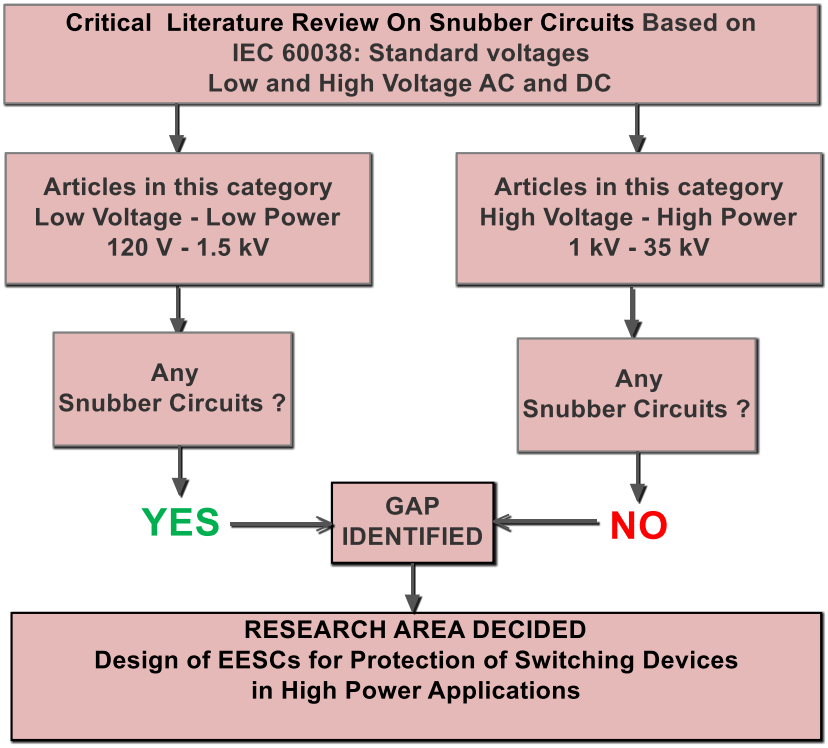

Figure 3-14 Gap in EESCs between Low power and High power Applications

3.5.1.2 Grading Power Resistors and Capacitors

In MV snubber designs where the switching device is an SCR, with a lower voltage rating than the MV supply, the SCRs are connected in series to increase the combined voltage rating to that or more than the supply voltage. To share the voltage equally across each phase, grading resistors are connected across each SCR in addition to the SC. For fast dissipation of the heat generated in the snubber resistor, wire wound resistors are used [46]. An example of the connections in one phase for grading resistor and SC are given in Figure 3-15.

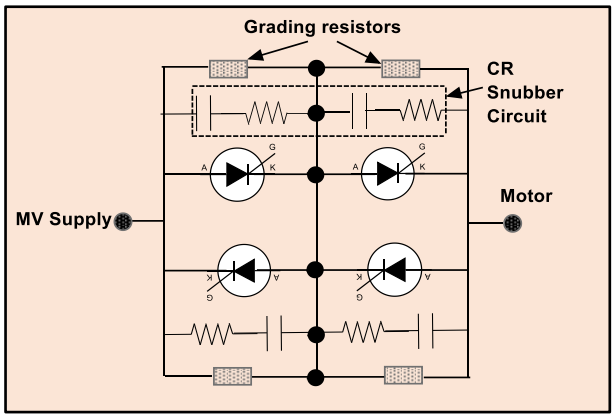

Figure 3-15 Grading resistors & RCSC for SCR application in motor control

For MV and HV Power levels, where the switching devises includes GTOs, capacitors with special ratings are used in the SC. Such capacitors are manufactured with low series resistance and high pulse strength and with very good self-healing characteristics without loss of capacitance [47]. Typical manufactures' capacitor ratings are given in Table 3-2 [48].

Table 3-2 Power Capacitor for High Voltage applications

Properties	Data/Specification
Main Ratings Capacitance	1 μF to 250 μF
Voltage rating	**2300 V – 5000 V DC**
Standards	IEC 61071 *(optional IEC 61881)
Can	Plastic (UL94: VO), 90mm to 140mm diameter (flame retardant plastic)
Insulation Strength	C x R 5000 s
Reference Service Life	100,000 Hours at HOTSPOT ≤ 70° C
**IEC 61071: Capacitors for power electronics applications,* gives the following additional information: - The operating frequency for the systems where these snubber capacitors are used can be up to 15KHz. The pulse/transient frequency can be 5 to 10 times the operating frequency (75kHz – 150kHz). Provides information for capacitor application for Overvoltage Protection, Switching Circuits, Energy Storage, DC/AC Filtering and Auxiliary Inverters. IEC 61881, provides information on Capacitors under Power Electronics for railway traction.	

3.6 Classification of SC According to Regulations for PFC.

3.6.1 Power Factor and Regulations

Power factor correction (PFC) and its benefits are well established. International standard IEC 61000-3-2, which is used by all IEC member countries to ensure common testing requirements are carried out, sets acceptable limits for harmonic levels to avoid pollution to other equipment/operating system connected to the same supply [49]. Power supply authorities penalize consumers whose equipment generates high VARs load demands. To reduce high annual costs, consumers and manufacturers need to provide PFC to their equipment connected to the AC mains supply.

When switching devices in converters employ hard switching to interrupt load currents and voltage before reaching a zero-crossing point, high frequency voltage and current oscillations are generated across the switch resulting in progressive damage to the switch due to heat losses. Snubber circuits are used to provide low *dv/dt* stress and minimum losses.

3.7 Classification of SC According to Efficiency

3.7.1 Resonance SC

Figure 3-16, sections A and B show an AC to DC power supply in the fly back topology mode. section A, shows a Turn-Off Dissipative SC, and section B, a Non-Dissipative Resonant SC.

Section A, Operation - The Turn-Off Dissipative SC functions similarly to the common Turn-Off SC.
At MOSFET Turn-Off, the energy from T1 is transferred to the C4.
At MOSFET Turn-On, D1 is reversed biased and the charge in C4 is dissipated in R1 as wasted heat. This wasted heat can reduce the efficiency of the supply especially at low power levels.

Section B, Operation **-** The Turn-Off SC is replaced with the resonant SC, D1, D2, Cr & Lr.
At MOSFET Turn-Off, the leakage inductance energy from T1 is transferred to Cr and the rate of rise dv/dt of the MOSFET drain voltage is reduced.
At MOSFET Turn-On, Cr discharges into Lr, due to the resonance circuit formed by Cr & Lr.
At the next MOSFET Turn-Off, the energy in Lr is transferred to the bulk capacitor C3 via the series diodes D1 and D2, which improves the overall efficiency of the converter. The resonant snubber circuit functioning without an expensive Active Control Unit (as in Regenerative snubber circuit), is a less expensive alternative for increasing the efficiency of such converters. Results of comparative load testing with efficiency curves of the Turn-Off Snubber and the Resonant Snubber are reproduced below [50]. For simplicity, the manufacturer's control unit NCP1027 [51] was replaced by a MOSFET switching device.

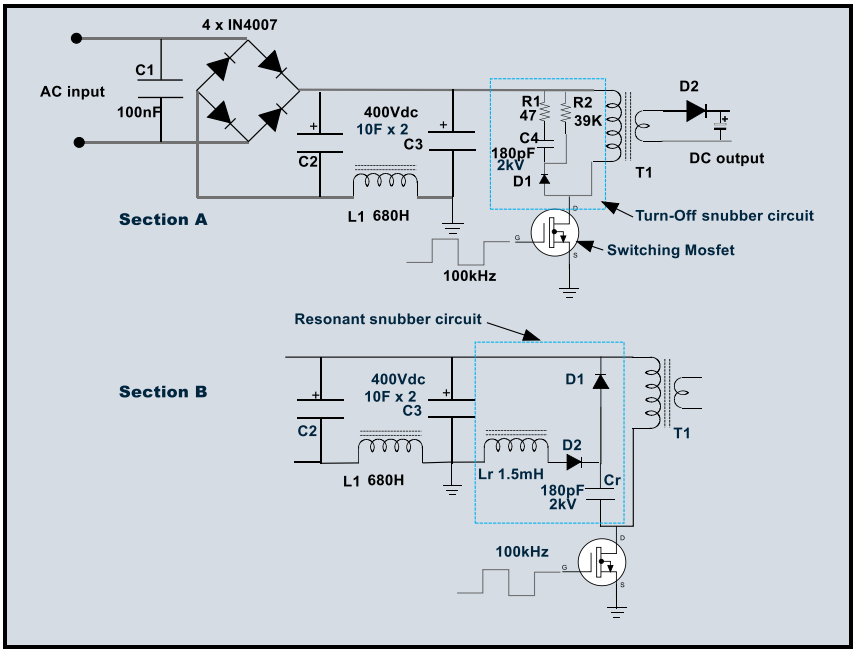

Figure 3-16 Turn-Off SC (A) & Resonant SC (B)

Brief Circuit Specification

Input voltage 120 to 230 (AC) Volts

Output voltage 12 volts

Output current 1.3 A

Output power 16 W

Efficiency – Resonant snubber 81%

Topology – Flyback

3.7.2 Test values and efficiency curves

Table 3-3, for the RCD snubber, shows the calculated efficiency values of loads from 25% to 100% full load [50]. These values were plotted in Figure 3-17, for comparison of efficiencies at 120Vac and 230Vac. Except at lower values of the supply voltages (120Vac & 230Vac) the efficiency increases with increase of the voltage and load. This is an expected result which is consistent with the efficiency equation: -

$$\eta = \left(1 - \frac{\text{Losses}}{\text{Vac} * \text{Iac}}\right) \times 100\% \qquad (3.10)$$

In equation (3.10), as *Vac* increases,$(Losses/(Vac * Iac))$ decreases and η increases.

The RCD SC average efficiency values comply with the Energy Star minimum efficiency requirement at both supply voltages.

For the Resonant snubber, Table 3-3 shows the calculated efficiency values for loads from 25% to 100% full load. These were then plotted in Figure 3-18 to compare efficiencies at 120Vac and 230Vac. The trend of the curves compare to those of the RCD snubber curves, except at lower loads the efficiency is about 2% higher and at higher loads by 1%. At higher

loads, the dissipative loss in the RCD snubber would be a small fraction of the output power, and in comparison, to the resonant snubber the difference in efficiency would be small in the range from 50% to 100% load at both 120Vac and 230Vac. The Resonant SC would be more effective at achieving higher efficiencies when designed in low power converters.

Table 3-3 Comparison of Efficiencies between RCD SC and Non-Dissipative Resonant SC

	Traditional RCD SC at 25^{0}C		Non-Dissipative Resonant SC	
Load %	η @ 120 Vac	η @ 230Vac	η @ 120 Vac (%)	η @ 230Vac
25	74	73	76.2	74.4
50	77	78.2	79	79.8
75	77.6	80	79	80.5
100	76.8	80.6	78.2	81
Average Efficiency	76.4	78	78.1	78.9
Minimum Efficiency as per *Energy Star (ES) formula:	74	74	74	74

Note: *ENERGY STAR is a US Environment Protection Agency voluntary program that helps businesses and individuals save money and protect the climate through superior energy efficiency. (https://www.energystar.gov).

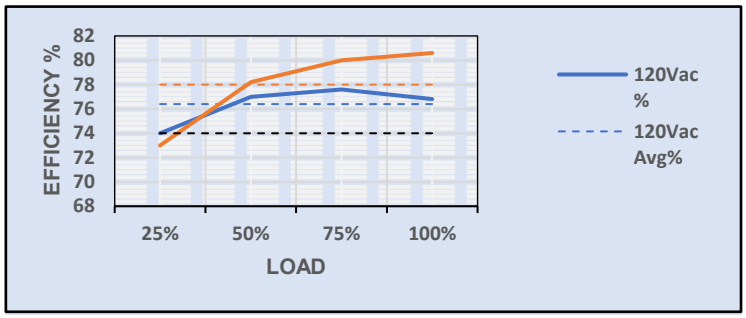

Figure 3-17 Comparison of RCD SC Efficiency Curves at 120Vac & 230Vac

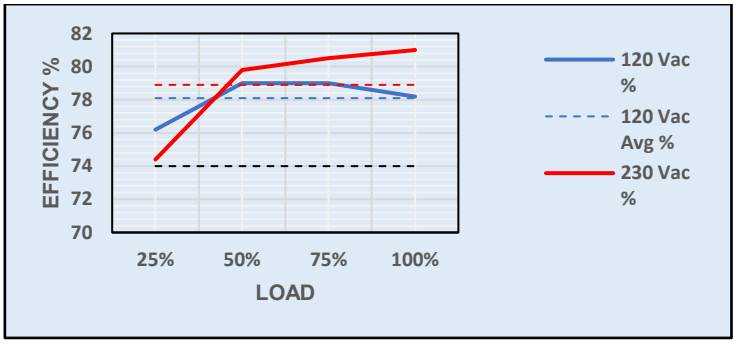

Figure 3-18 Comparison of Resonant SC Efficiency Curves at 120Vac & 230Vac

3.7.3 Types of Resonant SC

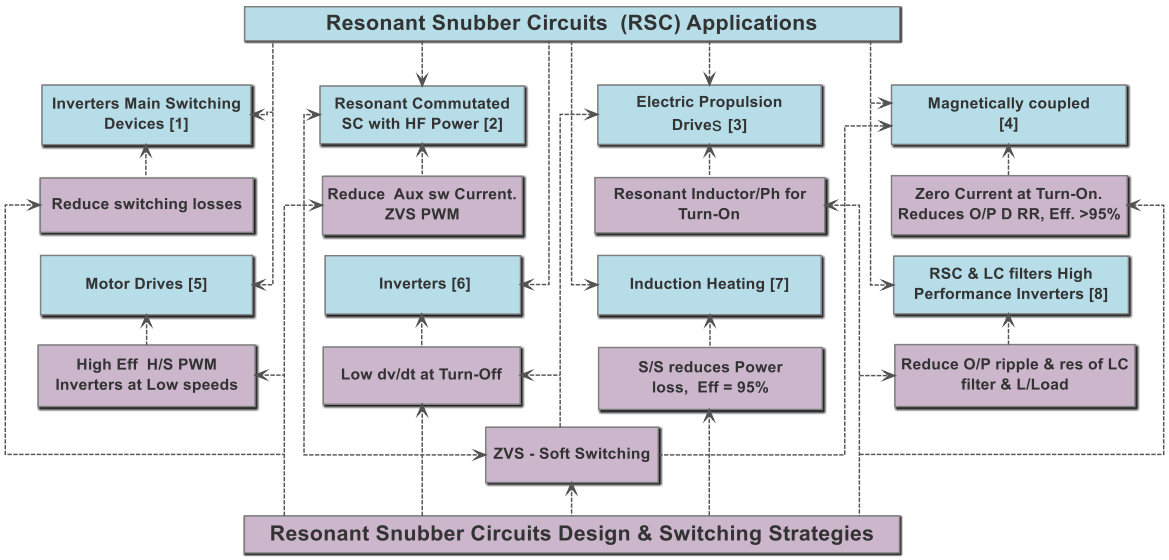

Figure 3-19 Applications of Resonant SCs, with corresponding Design Strategies

Many Applications of RSC are available in the design of DC-DC converters, DC-AC Inverters, and Induction Heating. Eight main applications are presented in Figure 3-19. Each Application (blue block) points to their switching functions and design strategies (mauve block). The majority of RSCs have similar switching and design strategies to reduce losses, either in the main switching devices, or in the auxiliary (e.g., PWM) control switches that provide the gate signals to the main switches. Other common strategies reduce the dv/dt at Turn-Off and zero current at Turn-On. There are others which increase the supply efficiency by using Passive Non-Dissipative RSC. Citations for the applications of RSC in Figure 3-19 are shown in Table 3-4 as it would be difficult to cross refer in the reference list.

Table 3-4 Citation for RSC Application Blocks

Blocks	Citation	Resonant SC – Applications - Strategies
1	[52]	RSC for Inverters Main Switching Devices – Reduce switching Losses
2	[53]	Resonant Commutated SC with HF transformer Power Regeneration – ZVS (soft Switching), Reduce current rating for Auxiliary switching, ZVS transition PWM of which there are four types, Resonant Commutated Arm Link, Resonant AC Link, Resonant DC Link and Resonant Switching Block Link
3	[54]	RSC for Electric Propulsion Drives – ZVS (soft Switching), Resonant Inductor/Ph for Turn-On.
4	[55]	Magnetically coupled RSC – ZVS (soft Switching), Zero Current at Turn-On, Reduces output diode RR, for wide load efficiency greater than 95%.
5	[56].	RSC for Motor Drives – High frequency improvement over Hard Switching PWM Inverters at Low Speeds
6	[57].	RSC for inverters – Low dv/dt at Turn-Off
7	[58].	RSC for Induction Heating – Soft Switching reduces Power loss at High Efficiency, Power regulation of 0.25KW to 2.84KW at a Duty Factor of 0.08 to 0.3, Power conversion Efficiency of 95%
8	[59].	RSC and LC filter in High Performance Inverters – Reduce Output Ripple and resonance of LC filter with Load Inductance

3.7.4 Comparison of Protection Levels of Snubber and other Protection circuits

A manufacturer's HV test, consisted of a three phase supply connected to a three phase transformer via a circuit breaker (CB). The test required to measure the voltage spikes generated across the lines and earth and across the three phase lines when the CB was switch off. The measurements were made without and with surge arresters, RC snubber circuits and their combinations connected to the three phase lines and repeated with the surge arresters, RC snubber circuits and their combinations connected in star with the star point connected to earth. It was required to determine the effectiveness of the surge arresters compared to the snubber circuit and their combinations in reducing the voltage spikes at the terminals of the three phase transformer. Table 3-5 presents the main test conditions.

Table 3-5 High Voltage Test Values

Inductive load	Half the power rating of a HV transformer - dry-type, Resibloc transformer, rated 20 kV/690 V, 900 kVA, Dyn11) [60] [61]
Connection	5mtr cable connection to a HV CB (without RC SC protection)
Switching type	The CB operated at Hard switching
HV Spike	99kV to ground
Transformer Interwinding oscillation	168kV greater than the Basic Insulation Level (BIL)125kV of the transformer [30]

Test Results

The test waveforms contained very high frequency and high kV negative over-voltage transients, predominantly in the red phase with lower high frequency transients in the blue and green phases. The no protection high kV peaks and transients were compared with test results of RC SC, surge arresters, and their combinations, when connected on the 3-phase lines between the CB and Transformer. The various configurations of protection circuits are given in Figure 3-20, Figure 3-21, Figure 3-22 and Figure 3-23.

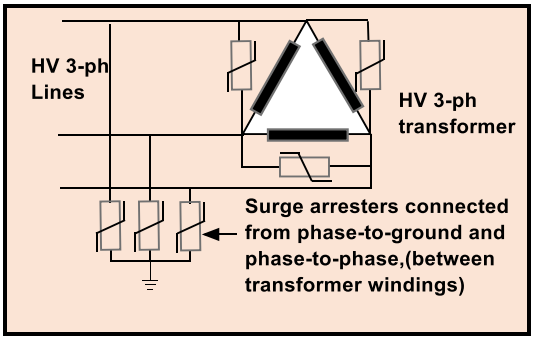

Figure 3-20 Protection by Surge Arrester

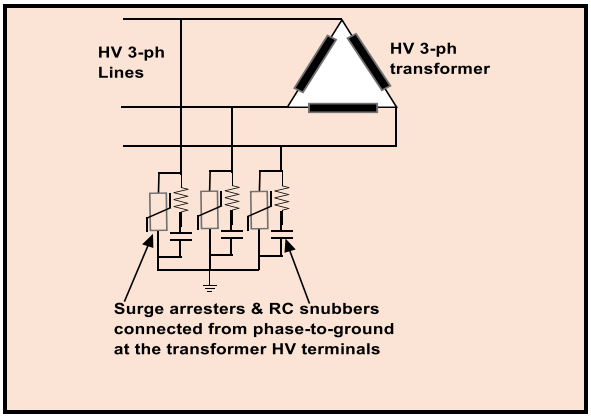

Figure 3-21 Protection by Surge arresters and RC SC

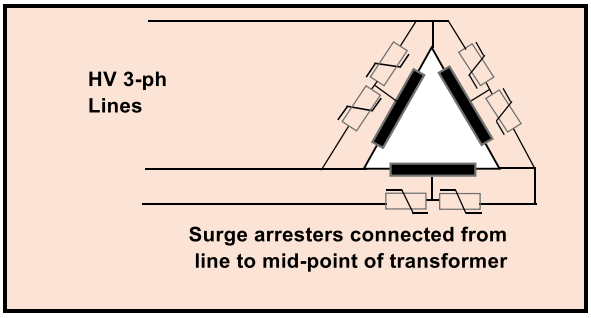

Figure 3-22 Protection by Surge Arresters connected
to mid-points of transformer windings

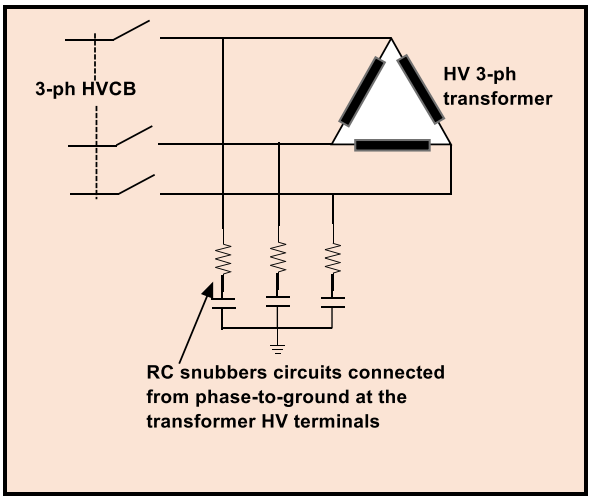

Figure 3-23 Protection by RC SC
connected at transformer HV terminals.

For each protection circuit, the measured maximum kV values are tabulated in Table 3-6 [30]. The following figures generated on the data given are based on the system specifications to determine the protection levels of the surge arresters compared to the protection levels of snubber circuit and their combinations in reducing the voltage spikes at the terminals of the three phase transformer.

Table 3-6 Max kV across transformer windings
by different protection circuits

Protection	Voltage [kV] @ 50% load	High freq transient @ 50% load	Voltage [kV] @ 100% load	High freq transient @ 100% load
Surge arresters (SA) ph-to-ph & ph-to-gr	40-45	65	47	65
Resistor Capacitor Snubber (RCS) & SA ph-to-gr	84	-	88	-
(RCS)	87	-	107	-
SA ph-to-gr	90	95	-	-
Surge capacitor (SC) & (SA) ph-to-gr	90	-	-	-
No protection (NP)	168	-	-	-

From Table 3-6, Figure 3-24 was plotted showing the kV levels of each protection circuit relative to the No-Protection kV level. Figures generated on the data given are based on the system specifications to determine the protection levels of the surge arresters compared to the protection levels of snubber circuit and their combinations in reducing the voltage spikes at the terminals of the three phase transformer.

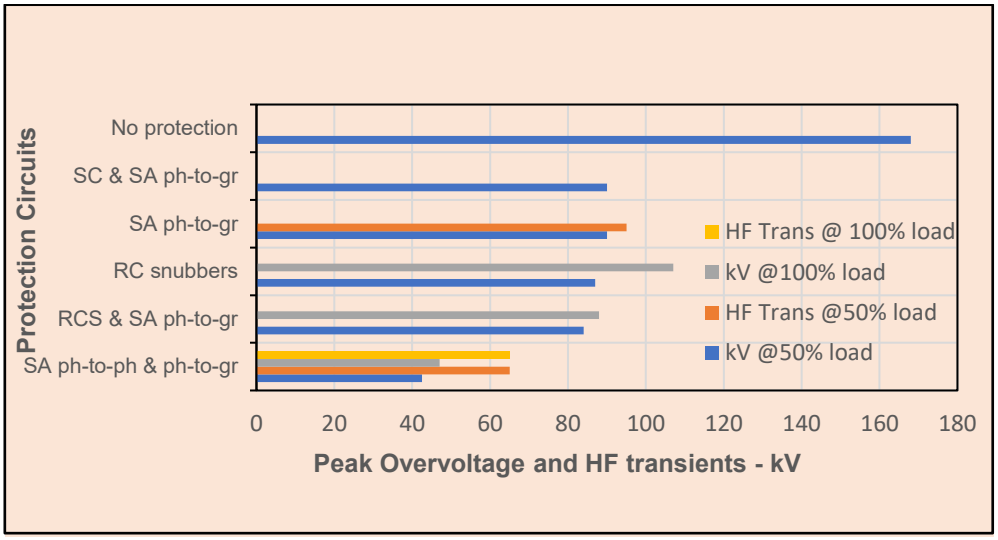

Figure 3-24 Protection circuits kV levels, Compared to kV level without protection [30]

Figure 3-24, shows that the protection circuits have progressively reduced both the high kV and transient kV values, with the lowest reduction by the surge arrester circuit. This is not a surprised result as surge arresters are commonly used to protect installations from high surges due to lightning strikes. Hence, Surge Arresters are very effective in reducing the kV peak transient levels due to their inverse V/R characteristics. However, they are not effective in reducing the high dv/dt gradients [62]. The energy removed from the CB at switch-off by the

different protective circuits, is related to the reduction of over voltage and the high frequency transients in each test case.

3.7.4.1 RC Time constant (τ) and pulse width (PW)

The transient waveform was expanded to enable accurate measurements with the following results shown in Table 3-7.

Table 3-7 RC time constant derived from HVCB test result in Section 3.7.4

Parameters	Values
Maximum kV spike	168kV
Pulse width (PW) of Maximum kV spike	0.049ms
Frequency (1/T = 1/(2xPW) = 1/(2x0.049) ms	10kHz
RC time constant (τ) (R = 30Ω and C = 130nF)	0.0039x10^{-3} s
Ratio of τ/PW (0.0039ms/0.049ms)	1/12.5 ≈ 1/13

From Table 3-7, at a high kV frequency of 10 kHz, due to CB switching, for RC snubbers connected across the three phase lines, the time constant $\tau \approx$ PW/13, i.e.,

$$\tau_{RC} = \frac{\text{Pulse Width}}{13}, \quad \text{for RC SC connected across 3-phase lines} \qquad (3.11)$$

The results show that Surge Arresters are very effective in reducing the kV peak transient levels due to their inverse V/R characteristics. However, they are not effective in reducing the high dv/dt gradients. Further analysis regarding losses continues in the following section.

3.7.5 Relationship between Circuit Breaker (CB) Over-voltage, dv/dt and losses

To establish a link between losses, efficiency, the reduction of over voltage and the high frequency values in each of the above test case, the kV values in Table 3-6 were reproduced in PU values and rearranged in Table 3-8. From this table, Figure 3-25 was plotted to show from the No Protection (1PU kV) level with progressive reductions by the different protection circuits. This graph (Figure 3-25) identifies the protection circuit that is most effective in reducing the CB over voltage and high frequency transients, and hence the reduction of CB losses and increase in efficiency.

Table 3-8 High frequency and overvoltage PU values

Protection circuits	NP @ 50% load	RCS 100% load	SC & SA p/g 50% load	SA p/g 50% load	SC & SA p/g 50% load	RCS & SA p/g 100% load	RCS 50% load	RCS & SA p/g 50% load	SA p/p & p/g HFT@ 100%	SA p/p & p/g HFT@ 50%	SA p/p & p/g 100% load	SA p/p & p/g 50% load	SA p/p & p/g 50% load
kV	168	107	95	90	90	88	87	84	65	65	47	45	40
PU	1.0	0.63	0.56	0.53	0.53	0.52	0.51	0.5	0.39	0.39	0.28	0.27	0.24

Key **Table 3-8**	
NP No Protection	SC Surge Capacitor
Load (3-Ph Transformer - 20 kV/690 V, 900 kVA)	p/g Phase-to-Ground
RCS Resistor Capacitor Snubber	p/p Phase-to-Phase
SA Surge Arrester	HFT High Frequency Transient

Results from, Figure 3-25 for full load and half load were entered in Table 3-9.

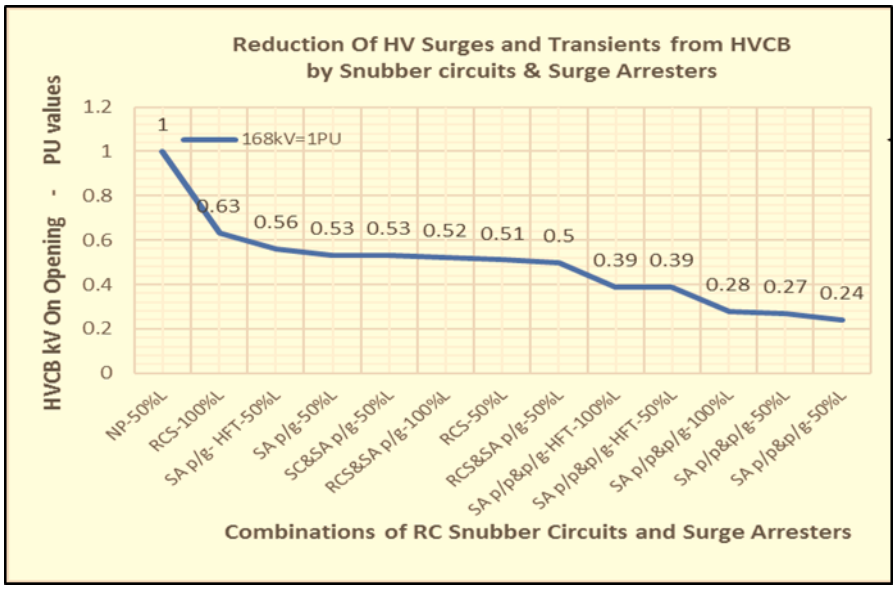

Figure 3-25 Effect of different protection circuits on CB OV & HF levels

Table 3-9 Protection Circuits Average % HV Reduction and Efficiency

Protection Circuit	**Reduction from No Protection level and Efficiency**	
	Average % Reduction values	**Corresponding Average % Efficiency**
Snubber Capacitor & Surge Arresters	52	48
RC SC	51	49
Surge Arresters & RC SC	50	50
Surge Arresters	31	69

The application of surge arresters is known for the protection of buildings from lightning strikes [63]. It is not surprising that in this high voltage CB/transformer test, surge arresters were most effective in reducing the over voltage and high frequency transient levels by 31%.

3.7.6 Comparison of dv/dt Values for Protection Circuits

The snubber circuit values of R (30Ω) and C (130nF) in the HVCB transformer test, were intended to reduce the *dv/dt* gradient of the transient voltages. The *dv/dt* data for each protection circuit was not available. To justify the effectiveness of this RC time constant *dv/dt* data were extracted from the transient waveforms associated with Figure 3-20, Figure 3-21,

Figure 3-22 and Figure 3-23. The kV peak values and transient pulse width where the peak occurred were measured. These enabled the calculation of the *dv/dt*, kV/ms/ph and entered in Table 3-10 in a descending order to enable a sequential comparison. The unbalanced dv/dt shown in the Red, Green and Blue Phases were due to unbalanced load/phase.

Table 3-10 dv/dt per phase for each protection circuit

Protection Type	(dv/dt) / phase - kV/ms					
	Red Phase		Green Phase		Blue Phase	
	-kV/ms	+kV/ms	-kV/ms	+kV/ms	-kV/ms	+kV/ms
No Protection	-3009	+701	-1046	+1989	-1071	+1861
Surge Arresters (SA)	-626	+279	-167	+857	-564	+543
SA across transformer winding L3	-320	+223	-0.0	+0.0	-267	+231
SA & RC SC	-82	+61	-30	+65	-57	+62
RC SC	-27	+32	-58	+55	-26	+30

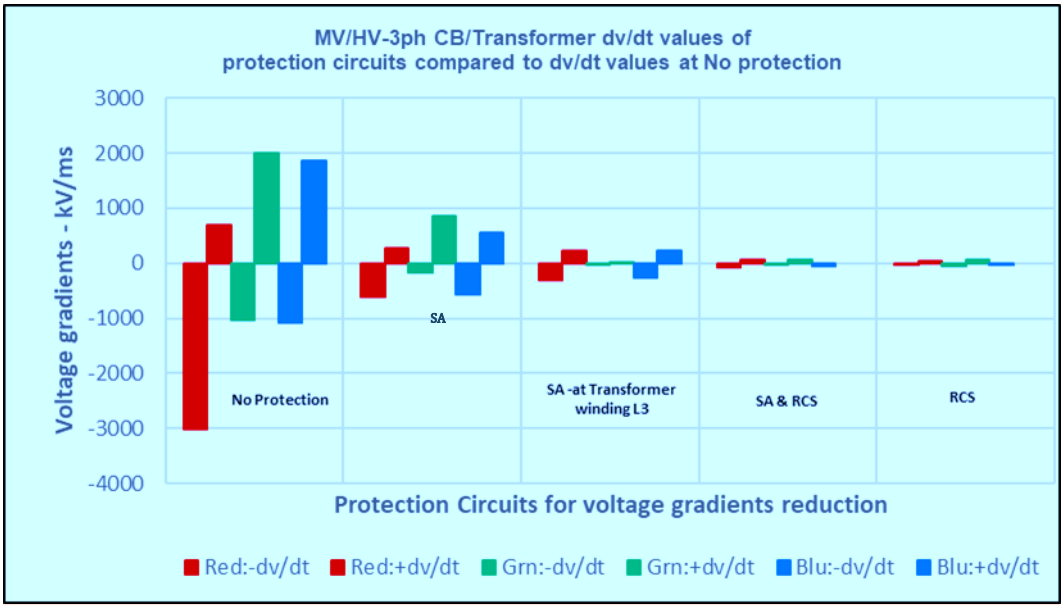

Figure 3-26 Comparison of dv/dt without Protection to dv/dt with Protection circuits

Figure 3-26 was plotted to offer a visual comparison of the data given in Table 3-10. It shows that each protection circuit progressively reduced the dv/dt gradients and confirms that the R&C values (R=30Ω & C =130nF) reduced the No Protection dv/dt value to the lowest level. Hence, with an effective RC time constant (calculated or by experimentation), the RC snubber circuit proved to be most responsive in reducing the dv/dt than the Surge Arrester (SA) circuit. SA is represented by its (V x I) characteristics and its main function is to reduce Voltage Surges but has no effect on the rate of rise (dv/dt [64]. A proposal for future designs of protection

circuits could consider a parallel combination of SA & RCS for the simultaneous reduction of over voltage and dv/dt, as these combinations have also shown to be effective.

RC SC with (R = 30Ω & C = 130nF) are most effective in reducing the dv/dt than Surge arresters and other combinations of protection circuits. The application of a parallel combination of SA & RCS for the simultaneous reduction of high kV over voltage and dv/dt voltage gradients is also effective.

3.8 Passive Energy Efficient SC

3.8.1 Definition

Following the rules of IEC standards for definitions [65], passive energy efficient circuit may be defined as: -

'*a circuit without the use of an auxiliary switch that transfers a switching device loss energy back to the supply*'

The turn-on and turn-off switching losses in the switching device, are reduced by using large L and C components and dissipating the energy as heat loss in a resistor. This is at the cost of reducing the efficiency. If this loss could be reused instead of wasting it as heat by returning it back to the supply, it would increase the efficiency of the circuit. This is the aim of passive Energy Efficient SC. The use of zero volts switching, and zero current switching techniques contribute to energy recovery in these circuits [66].

3.8.2 Energy Efficient Turn-Off SC

Figure 3-27 section A, shows a dissipative Turn-Off SC and section B shows an energy efficient Turn-Off snubber circuit..

3.8.2.1 Operation of the Energy Efficient Turn-Off SC.

In section A when the switch is opened the capacitor is charged via D2. When the switch in closed the stored energy is dissipated in the resistor 'R' since D2 is reversed biased. In section B the discharge 'R' is removed, and a DC-DC converter is connected across the capacitor. When the switch is turned on the charge stored in the capacitor during the turn-off period of the switch is transferred to the input of the DC-DC converter, since the diode D2 is reversed biased. The output of the DC-DC converter transfers the captured energy to the supply, thereby increasing the efficiency of the circuit as there is no heat loss.

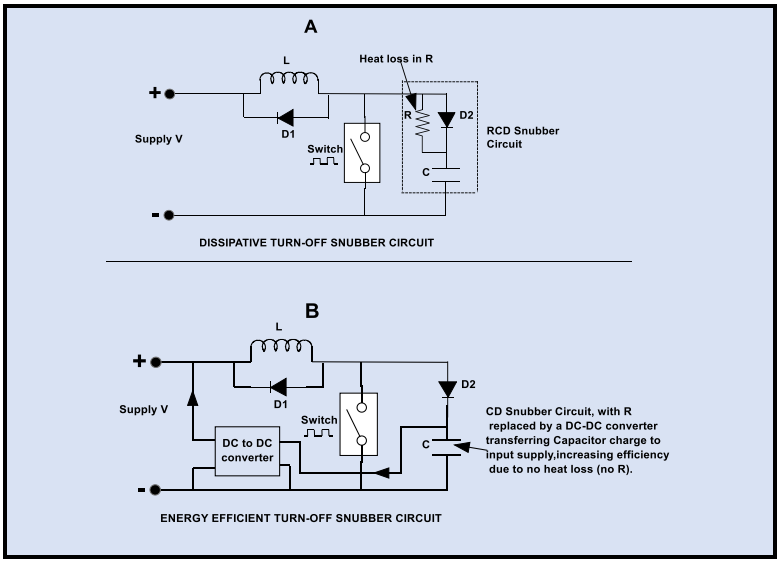

Figure 3-27 Dissipative (A) and Energy Efficient (B)Turn-off SC

3.8.3 Energy Efficient Turn-On SC

Figure 3-28, section A, shows a dissipative Turn-On RLD snubber circuit and section B shows an energy efficient Turn-On snubber circuit.

3.8.3.1 Operation of the Energy Efficient Turn-On SC.

In section A, when the switch closed the voltage developed across ‘L’ reduced the inrush current to the switch since the diode ‘D’ is reversed biased. When the switch is opened the stored energy in ‘L’ is dissipated in the resistor ‘R’ via ‘D’.

In section B, the resistor, inductor, and diode are replaced by a snubber inductor with a primary and secondary winding and a diode connected as shown.

This inductor limits the turn-on current to the switch, and at turn-off the decaying inductor energy in the primary coil is discharged to the secondary via diode ‘D’ and is fed back to the load and the supply [17]. There is no heat loss since the resistor has been removed and the efficiency of the circuit is increased. Since there is no additional switching component, the circuit is a passive energy efficient circuit. If the Converter has a switching component, then the circuit would be an active energy efficient circuit discussed in the next section.

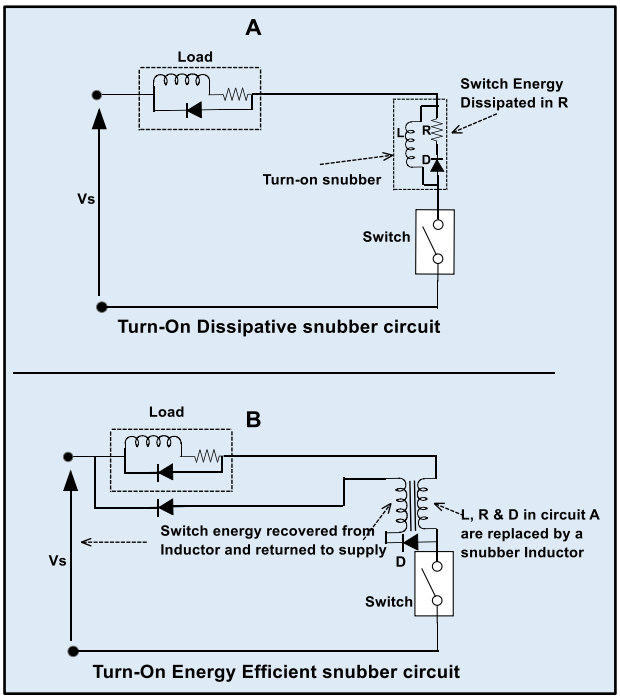

Figure 3-28 Dissipative (A) and Energy Efficient (B)Turn-On SC

3.9 Active Energy Efficient SC

Following the IEC rules for definitions [65], an Active EESC may be defined as: -

'a circuit with the use of an auxiliary switch that transfers a switching device loss energy back to the supply or to the load'

These circuits remove the turn-on and turn-off losses in the switching device, using L, C and diode components and additional switching auxiliary device(s) as defined. Since the snubber is energy efficient there is no energy dissipated but recovered and fed-back to the supply or load. This type of snubber circuit is covered in detail in Chapter 7 which discusses the CHBMLC.

3.10 Summary

This section discussed five classifications of snubber circuit: - Functions, Configurations, Power rating, Power factor enhancement and Efficiency. Some of the key features were, over-voltage protection, the importance of correct RC time constant to minimise switching device loss energy.

Description of Turn-On and Turn-Off passive SC followed, and their combination Turn-On/Off and the resonant snubber. The power rating of SC was found to be application driven, and dependent on the high-power ratings of capacitors, diodes, resistors, and inductors.

In the articles reviewed there was no reference of snubber circuit used in High Power and High Temperature Applications, which ***revealed a Gap for this research****.*

The Review revealed that IEC 61000-3-2, was a useful International Standard that set limits for harmonic, THD and EMI levels.

Classification according to efficiency, identified the main switching strategies required to minimise the loss in switching devices. Application of (ZVS, ZCS) ensured no loss in the switch and impacts on increase in efficiency.

The comparison of different protection circuits to a three phase HVCB connected to a power transformer, identified the use and effectiveness of surge arresters which reduced the kV overshoot compared to SC in the reduction of *dv/dt* and minimisation of switching losses. It was also shown that in some applications, the combination of surge arresters and SC could cover a wider range of protection for switching devices.

The future development of snubber circuits, depended on the use of advance materials e.g., wideband gap, which will accelerate their applications into areas of high power and elevated temperatures, being the object and main contribution of this research. In the next section different methods are investigated in the optimisation of the snubber circuit components to achieve minimum switching losses and validated by PSpice simulation.

A gap was found in the review of Articles – With the aid of IEC 60038 – Standard voltages, no data was found in the articles reviewed on high voltage, high power, and elevated temperature application of snubber circuits on the protection of switching devices. This gap revealed that there is a need to develop snubber circuits to protect expensive power switching devices at the higher power levels. Power switches manufactured with wideband gap materials will accelerate this development.

Chapter 4 Optimisation of Dissipative Turn-On & Turn-Off SC.

4.1 Introduction

In high power converter installations, losses are generated during the switching periods of the IGBTs and also manufacturing down time and cost of equipment replacement. It is therefore necessary to protect the switches with snubber circuits designed with optimum components to ensure minimisation of switching loss and that the switches function within their safe operating area (SOA) [30].

In the Turn-On and Turn-Off SCs, the time constant is a critical fraction of the switch turn-on (t_{on}), and turn-off period (t_{off}), which enables the inductor in the Turn-On SC and the capacitor in the Turn-Off SC to divert optimum switch energy. The inductor and capacitor energies are ½ LI^2 and ½ CV^2 Joules respectively and dissipate the stored energies in the discharge resistors or in the case of EESC, the input supply can accept the return energy for efficiency enhancement [63].

Methods to determine time constants are complex. Most articles recommended R and C values based on practice, which removes most of the switch energy at switch-off transition [12]. Other methods, employ various optimisation procedures, followed by simulations, and most require programs (MATLAB) to execute them [64]. Example of inputs for these optimisation methods and programs are, variables with minimum and maximum limits for R, C, voltage across the switch, load current, switching frequency and switching losses. The latter in most cases being the minimum value of an objective or cost function. The result of the optimisation outputs are e.g., minimum switch loss, optimum values for R and C and ideal switching frequency. The final output depends on several iterations, until the output matches the set target. It will result in the optimum design parameters for the protection circuit. Figure 4-1, gives an example of the optimisation and simulation.

Various methods of optimisation are shown in Figure 4-2. After the optimisation process, the effectiveness of the snubber optimum values found, will be tested using PSpice simulation. The limit of switching frequency is based on the value of (toff) and (ton). These results will enhance the design of over voltage protection and SC [27] to protect the switching device selected and extend its operating life [12] [27] [30] [63] [64].

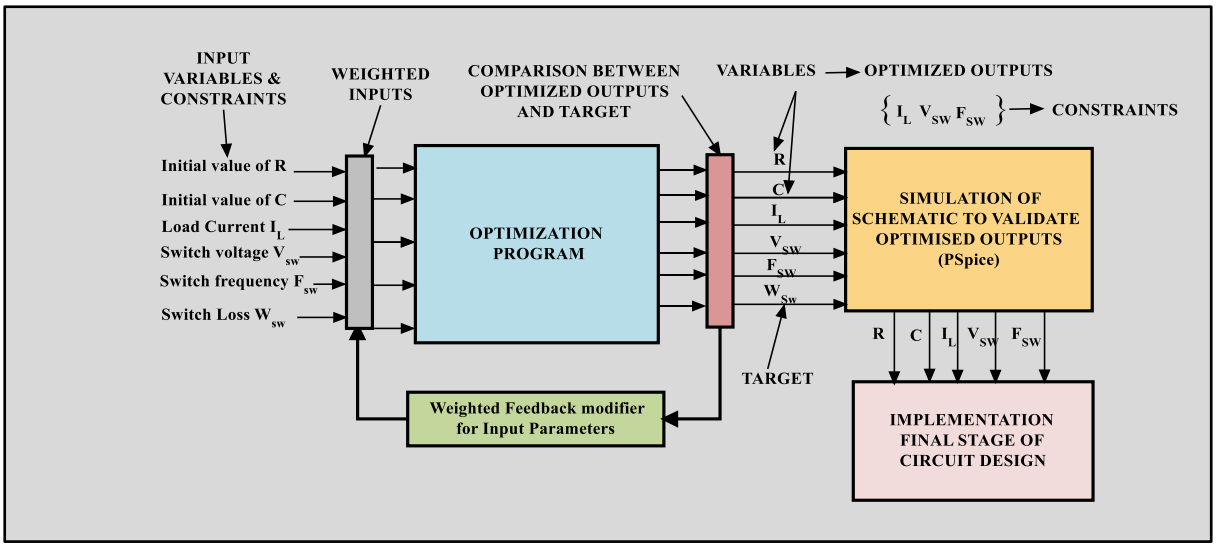

Figure 4-1 Simplified RC Time Constant Optimisation and Simulation process

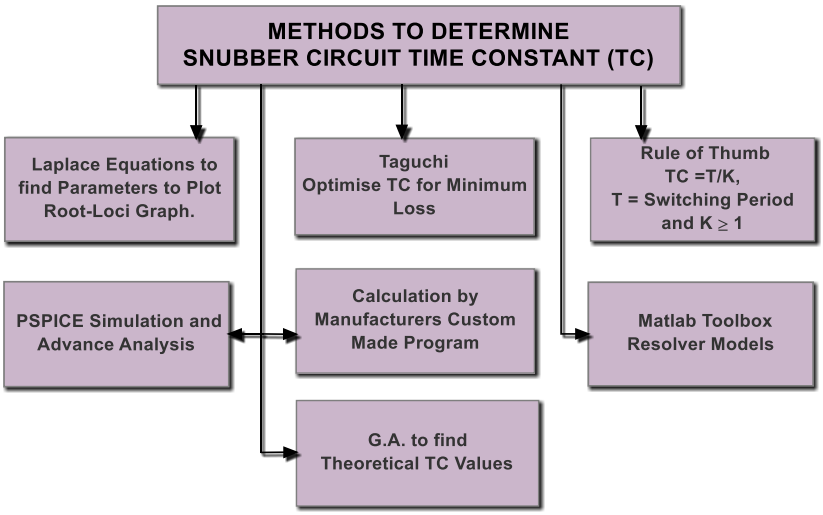

Figure 4-2 Methods to Determine RC Time Constants

Determination of the optimum values of R and C for the snubber circuit is a contribution towards answering the research question for the protection of switching devices for high power applications.

4.1.1 Hard Switching and IGBT Switching Signal

Figure 4-3, presents an example of hard switching during switch turn-on and turn-off, which produces wasted energy due to the overlap of dv/dt and di/dt. HF oscillations also occur due to switch leakage inductance and capacitance. Methods are discussed to minimise this energy, to prevent expensive switch damage by overheating and high dv/dt oscillations. Figure 4-3, also shows a standard voltage pulse switching waveform, defining the timing parameters to drive the IGBT/MOSFET device in the test circuits which follow.

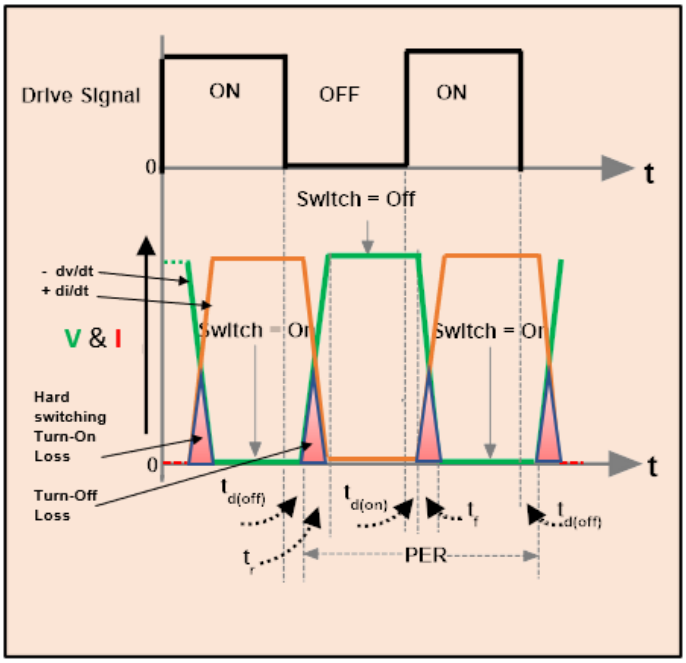

Figure 4-3 Hard Switching of Voltage and current Waveforms

Figure 4-4, shows an RC Turn-Off snubber circuit connected across a switching device. ESR (r1), is the capacitor equivalent series resistance.

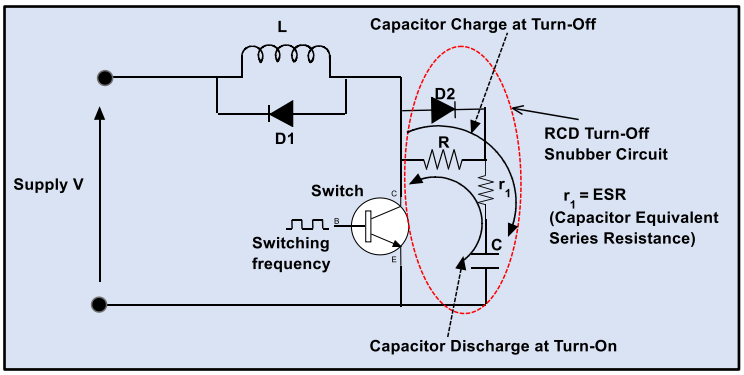

Figure 4-4 Capacitor Charge/Discharge in SC

In Figure 4-4, during the turn-off transition, the capacitor via D2 and r1 diverts the switch current, and reduces the switch terminal voltage, ideally to zero volts. At turn-on, C, r1, R and

the switch forms a series circuit and dissipates the capacitor stored energy in R. The charge time for the capacitor will be less than or equal to the turn-off period toff, to be discussed in the next section.

4.2 Optimisation Methods to Determine Snubber Circuit Time Constants

Various methods to determine the time constants are presented and validated by the application of PSpice simulations.

4.2.1 Manual methods

Manual methods are usually time consuming as it requires an estimation of R & C and tested in a simulation for each RC combination, until the switch loss is reduced to a minimum value. Other methods as in Figure 4-2 Taguchi, GA and Root-Loci and the use of Laplace equations (occasionally), involve circuit analysis to determine the R and C values [30].

In most power electronics research, the popular method used is MATLAB programs to execute the optimisation process followed by PSpice (or other) Simulation programs to validate the results.

4.2.1.1 A Novel method to determine R & C by "Perimeter" minimisation.

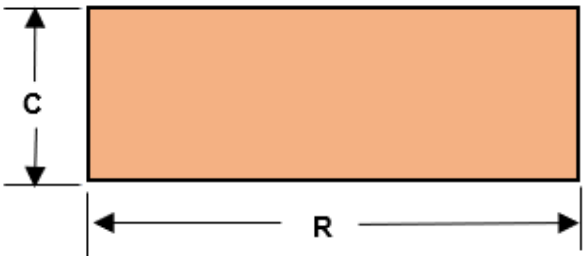

Figure 4-5 RC represented by a rectangle.

In Figure 4-5, the RC product is in units of time and can be represented by the area of a rectangle [67]. The idea originated from the construction industry, where it is required the build the maximum number of 'rooms' given a piece of real estate. The target is to determine the optimum room size for the materials given. Hence, the 'best' combination of the length and width of the room is determined to achieve the desired room size and the, correlation of R and C, with L and W was made. The object is to find the minimum values of R and C for a given area "A".

The Steps in the procedure: -

Step-1,	Area A	=	C x R	
Step-2,	Perimeter P	=	2C + 2R	(4.1)
Condition - Reduce P for a minimum A				
Step-3,	Let minimum area,	=	X	

Step-4,	C x R	=	X	
Step-5,	Substitute for C,	=	X/R	(4.2)
Step-6,	(4.2) in (4.1), P	=	$2(X/R) + 2R$	
Step 7,	Write in the form	=	$2R + 2XR^{-1}$	(4.3)
Step-8,	Derivative of (4.3),	=	$2 - 2XR^{-2}$	with respect to R
		=	$(2R^2 - 2X) / R^2$	(4.4)

In (4.4) are two roots, one in $(2R^2 - 2X)$ and the other in $1/R^2$. The root in $R^2 = 0$, is not practical and is discarded. Hence, the critical value for R, will be found in,

Step-9,	0	=	$2R^2 - 2X$
Step-10,	R^2	=	X
Step-11,	R	=	$\sqrt{x}$
and	C x R	=	X
Step-12,	C	=	$\sqrt{x}$
proof,	$(\sqrt{x} * \sqrt{x})$	=	X

The above 13-steps may be expressed in the form of an algorithm/program for ease of calculating R and C. However, the values of R and C will always be, $\sqrt{x}$ where 'X' is the selected target. This method can be used to find the minimum values of two parameters.

4.2.1.2 Determination of switch energy without SC

To validate the above method, the PSpice schematic in Figure 4-6 was simulated to determine the switch power during the transition turn-off period t_{off}. The current was measured by the red probe, the power by the blue probe and the voltage by the green probe.

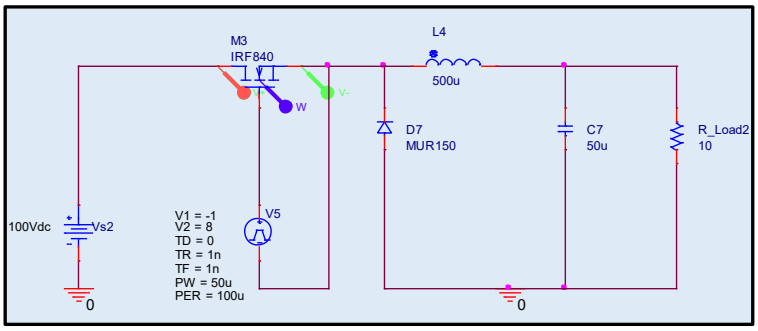

Figure 4-6 Buck Boost converter without SC

The result of the simulation is shown in Figure 4-7 with the voltage, current and power traces.

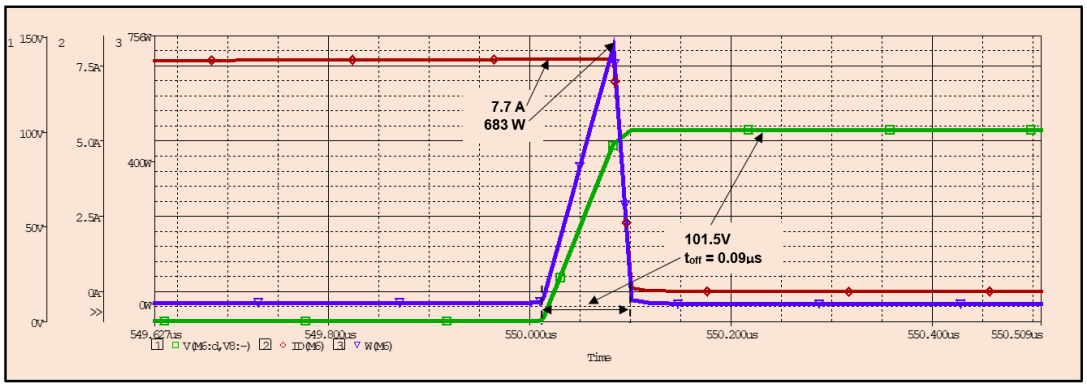

Figure 4-7 PSpice Turn-Off simulation without snubber

The t_{off} switching energy without SC is,

$$\text{Switching Energy, E} = 683\ \text{W} \times \frac{0.09\ \mu\text{s}}{2} = 30.7\ \mu\text{J}$$

The t_{off} period of 0.09µs is used to calculate R and C using the result in the above method. For optimum switching, $V_{SW} = V_C = V_S$ for the t_{off} period [4]. In Figure 4-7, the t_{off} = 0.09 µs. Thus, the RC time constant = 0.09 µs and from Section 4.2.1.1,

$$\text{CR} = \text{X} = 0.09\ \mu\text{s}$$

and C is,

$$\text{C} = \sqrt{0.09} = 0.3\ \mu\text{F}$$

with R having the same value,

$$\text{R} = 0.3\ \Omega$$

The R and C component values were entered in the test Buck converter PSpice schematic in Figure 4-8. The current was measured by the red probe, the power by the blue probe and the voltage by the green probe.

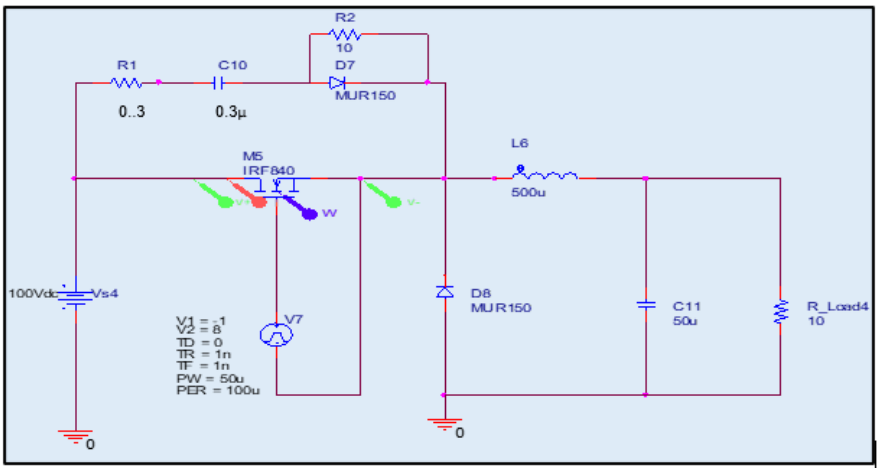

Figure 4-8 Turn-Off SC R & C by perimeter method.

Figure 4-9 shows the result of the PSpice simulation, with a peak power of 2.2 W (with snubber), and a t_{off} of 4.2 µs compared to high-power level of 683W (Figure 4-7 without snubber).

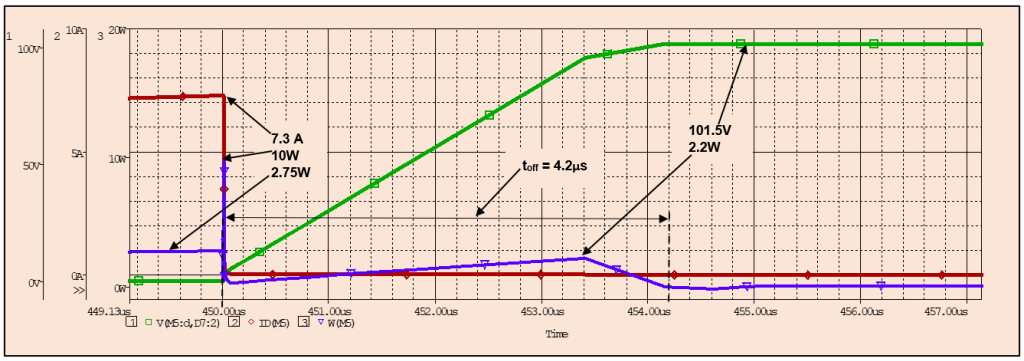

Figure 4-9 PSpice Simulation with Turn-Off SC R & C by perimeter method

The switch energy during the transition period is determined during t_{off} of 2.4 µs. Hence, the peak power of 10 W during the transition of current from the Turn-On value of 7.3 A to zero, is not included as it is the instant change of current at the end of the Turn-On period. The switch energy E_{SW} is: -

$$\text{Switch energy, } E_{SW} = 2.2\text{W} \times \frac{4.2\mu\text{s}}{2} = 4.62\mu\text{J}$$

The switch energy without SC was 30.7 µJ due to the SC is,

$$\%\ \text{Reduction, } E_{SW} = \frac{(30.7 - 4.62)\mu\text{J}}{30.7} \times 100\% = 85\%$$

The reduction of 85%, confirmed the R and C values calculated by the above 'AREA' method, were effective in reducing the switch power loss. However, the critical condition was in choosing the right minimisation target, which in this case was t_{off}. The values of C10 = 0.3µF and R9 = 0.3**Ω**, in the Turn-Off SC, found by this method were very effective in reducing the switch energy, by 85%.

4.2.3 Trial and Error method in Reduction of switch energy

Figure 4-10, shows a Buck converter circuit with a Turn-Off SC connected across the switch. The values of C8 =100n and R6 = 0.2**Ω**, were determined after several simulation runs with combinations of C8 and R6, with a fixed time constant of 20ns. Voltage differential probes (green), current probe (red) and power probe (blue), required separate simulation runs using PSpice. These simulations are shown in Figure 4-11.

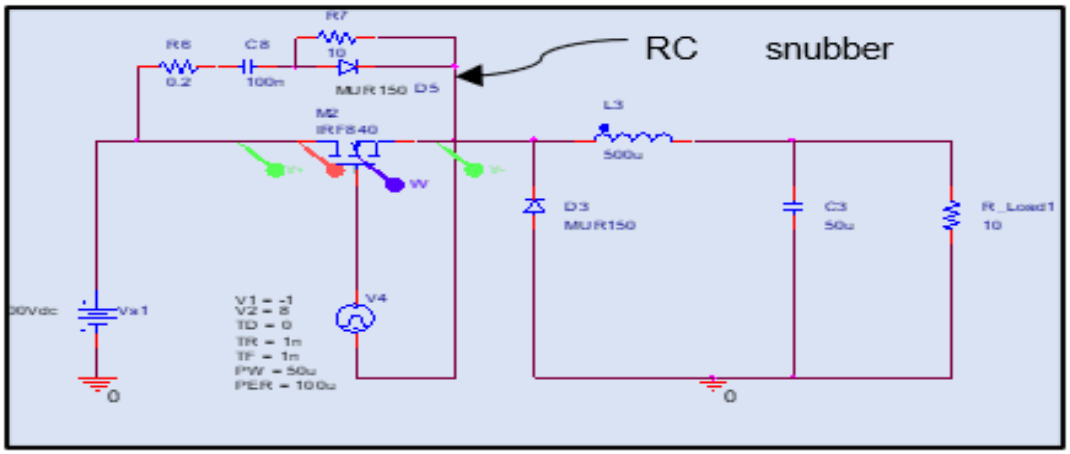

Figure 4-10 Buck Converter with a Turn-Off SC R & C by trial and error method

Table 4-1 Buck converter MOSFET switching waveform parameters

Parameter		Value
Turn On delay	TD	0s
Voltage Rise time	TR	1ns
Voltage Fall time	TF	1ns
Pulse width	PW	50µs
Period	PER	100µs

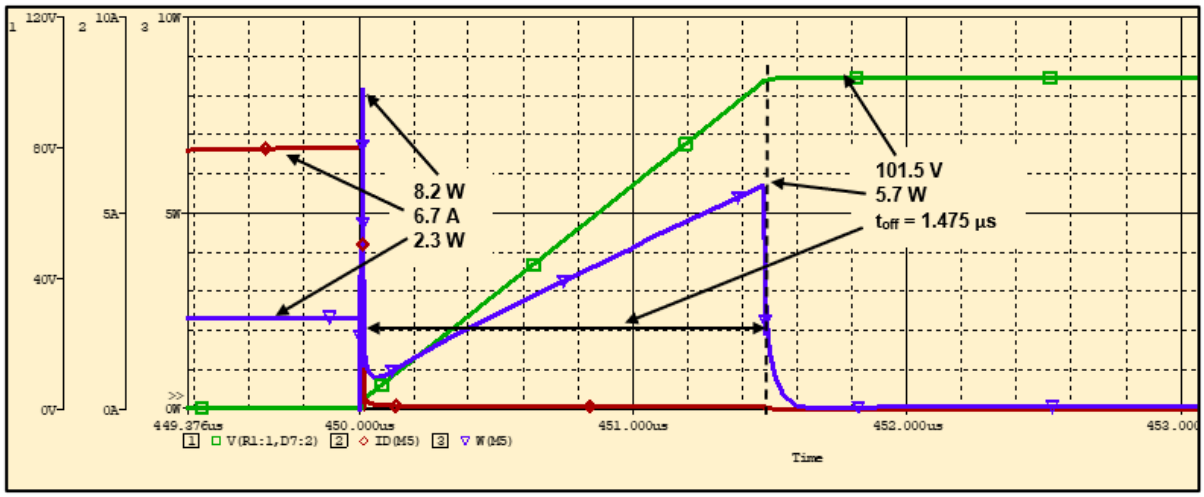

Figure 4-11 Trial and error method Turn-Off Waveforms with snubber circuit

From Figure 4-11, assuming a linear power trace, the switch energy E_{SW} during the t_{off} period with snubber circuit connected is: -

$$E_{SW} = 5.7W \times \frac{1.475\mu s}{2} = 4.2\mu J$$

In section 4.2.1.2, the switch energy E_{SW} without snubber circuit was 30.7 µJ. The reduction in switch energy due to the SC is: -

$$\%\ \text{Reduction, } E_{SW} = \frac{(30.7 - 4.2)\mu J}{30.7} \times 100\% = 86.3\%$$

In this Trial and Error Method although very time consuming, the values of C8 = 100n and R6 = 0.2**Ω**, determined for the Turn-Off snubber circuit were also effective in reducing the switch energy by 86.3%.

4.2.4 Switching Power levels at turn-on and turn-off

The Schematic in Figure 4-6 Buck Boost converter without SC was used in the following simulation. The result of this simulation will be useful for later SC analysis, as it gives the basic power levels at switch Turn-On and Turn-Off without any SC connected across the switch. Figure 4-12, (similar to Figure 4-7) and Figure 4-13 show, the voltage, current and power traces for the Turn-Off and Turn-On periods. Due to the load current the power at Turn-On period (t_{on}), is much greater (3.25 kW) than the power (0.683 kW) at Turn-Off period (t_{off}) since at Turn-Off the load current is decreasing to zero. The only power at Turn-Off is due to the -di/dt decay and dv/dt rise across the switch (hard switching). In Figure 4-13 the Turn-On current of 2 A rises to the level of 7.7 A shown in Figure 4-12.

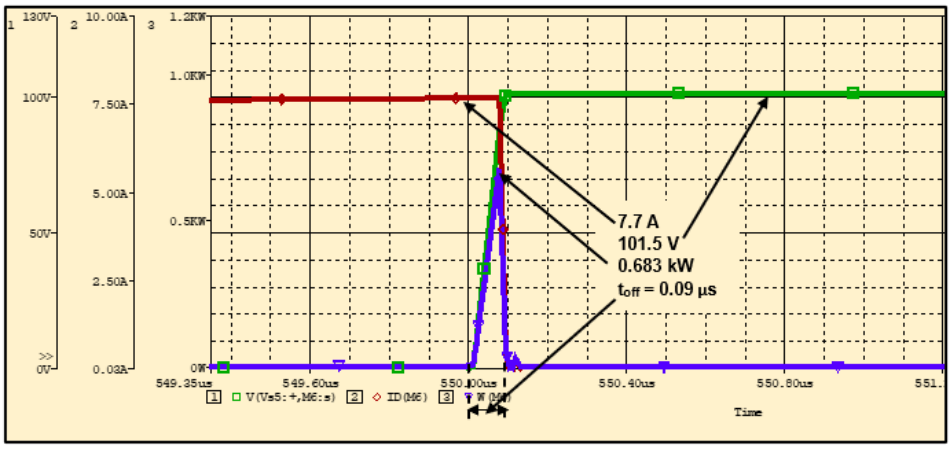

Figure 4-12 Waveforms for Turn-Off period t_{off} of switch without SC

The turn-off E_{SW} for Figure 4-12 was 30.7 µJ calculated under Figure 4-7.

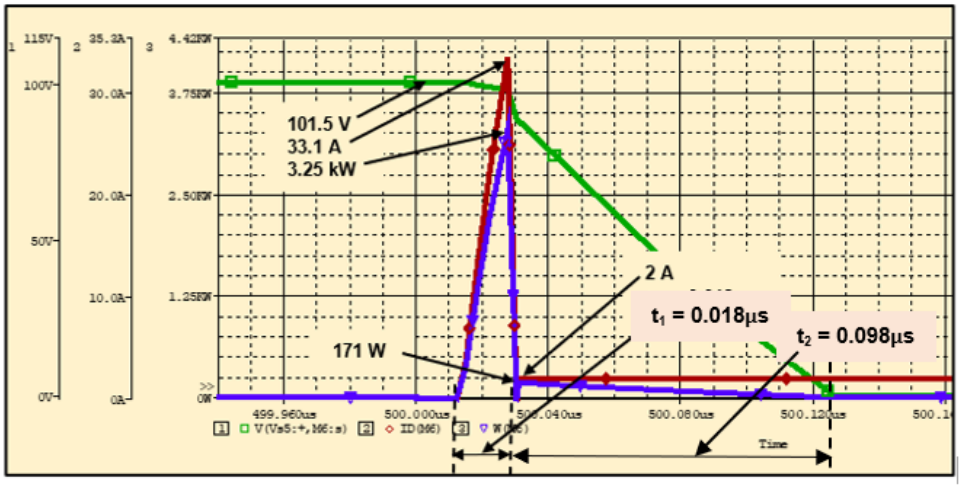

Figure 4-13 Waveforms for Turn-On period t_{on} of switch without SC

The t_{on} for Figure 4-13 is,

$$t_{on} = (t_1 + t_2)\mu s$$

$$t_{on} = (0.018 + 0.098)\mu s$$

$$t_{on} = 0.116\mu s$$

Figure 4-13 the turn-on E_{SW} without SC is,

$$E_{SW} = \sum (E_1 + E_2)\ \text{Joules}$$

$$= 3250\ \text{W} \times \frac{0.018\ \mu s}{2} + 171\ \text{W} \times \frac{0.098\ \mu s}{2} = (29.25 + 8.38)\mu\text{J}$$

$$= 37.63\mu\text{J}$$

The turn-on E_{SW} without SC is, 37.63µJ

4.2.5 Determination of t_{off} period and relationship of Tau/t_{off}

From Figure 4-10, the RC time constant, τ = 20 ns and in Figure 4-11, the measured value of t_{off} = 1.475 µs. The ratio of τ/t_{off} is,

$$\frac{\tau}{t_{off}} = \frac{20\ ns}{1.475\ \mu s} = 13.6 \times 10^{-3}$$

and,

$$\tau \approx 14 \times 10^{-3} \times t_{off}$$

This time constant (RC = 0.014 x 10^{-3} t_{off}) is useful in later designs of RC Turn-Off SC with (R = 0.2 Ω & C = 100 nF) operating at a switching frequency of 10 kHz.

4.2.6 Ratio of tau to turn-off period

In Figure 4-10, RC time constant, τ = 0.2**Ω** x 100nF = 20ns

The turn-off period, T/2 = 50µs

and the ratio, τ/Turn-off is,

$$\frac{\tau}{\text{Turn}-\text{off}} = \frac{20\text{ns}}{50\mu\text{s}} = \frac{2}{5} \times 10^{-3}$$

and,

$$\tau = \frac{2}{5} \times 10^{-3} \times \text{Turn} - \text{Off period}$$

This time constant result (τ = (2/5 x 10^{-3}) x Turn-Off period) is useful in the later designs of RC Turn-Off snubber circuit operating at a switching frequency of 10kHZ.

4.2.7 Calculation of Discharge Resistor R7

In Figure 4-10, during turn-on, C8 dissipates its energy through (R6 + R7) as D5 is reversed bias and be ready to charge again at the next turn-off state. Let the time constant τ for the discharge period, $t_{on} < \tau <$ turn-on where,

$$\tau = \text{C8 x (R6 + R7)} \tag{4.5}$$

R6 with a value of 0.2**Ω**, will be ignored as the dissipation is mainly in R7.

Let the time constant τ << turn-on period (50 μs), i.e., $\tau = 1\ \mu\text{s}$

$$\tau = \text{C8} \times \text{R7} = 1\mu\text{s}$$

Let C8 = 100nF, and the time constant,

$$100\text{nF} \times \text{R7} = 1\mu\text{s}$$

and

$$\text{R7} = \frac{1\mu\text{s}}{100\text{nF}} = 10\Omega$$

$$\text{R7} = 10\Omega$$

The Turn-Off SC discharge resistor R7 = 10Ω, which will dissipate the capacitor energy of ½ CV^2 Joules.

4.2.8 Summary of Dissipative Turn-Off SC

The simulation results are entered in Table 4-2.

Table 4-2 Tabulation of Turn-Off SCs simulation results

Method	R - Ω	C - μF	t_{off} - μs	P_{Power} - W	E_{SW} - μJ	η - %
No SC	-	-	0.09	683	30.7	-
Perimeter	0.3	0.3	4.2	2.2	4.62	85
Trial & Error	0.2	0.1	1.475	5.7	4.2	86.5
V & I for both schematics with and without SC, V = 101.5 volts, I =7.7 A						

4.3 Methods to determine L & R for the dissipative Turn-On SC

Various methods to determine the time constants are presented and validated by the application of PSpice simulations.

4.3.1 Method 1- Determination of Ls & Rs applying equation, - L_S * di/dt = V_S.

To reduce the inrush current to the switching device, let the voltage across L_S equal to the supply voltage Vs, i.e. – *Ls di/dt = Vs*

$$V_{LS} = L_S \frac{di}{dt} = V_S \quad \text{volts} \tag{4.6}$$

and

$$L_S = V_S \times \frac{1}{\frac{di}{dt}} \quad \text{H} \tag{4.7}$$

Substituting in (4.7), the gradient, $di/dt = I_S/t_{on}$

$$L_S = V_S \times \frac{t_{on}}{I_S} \quad \text{H} \tag{4.8}$$

The switch power,

$$P_{SW} = VI \times \frac{t_{on}}{2T} \quad \text{watts} \tag{4.9}$$

From Figure 4-13 substituting the values in (4.8)

$$L_S = 101.5 \times \frac{0.018\mu s}{33.1} \tag{4.10}$$

And the Turn-On Inductor,

$$L_S = 0.055\mu H$$

Let the time constant for the snubber,

$$\frac{L_S}{R_S} = t_{on} \tag{4.11}$$

and

$$\frac{L_S}{t_{on}} = R_S \tag{4.12}$$

For t_{on} = 0.018 µs, the inductor discharge resistor

$$R_S = \frac{0.055\ \mu H}{0.018\ \mu s} = 3\Omega$$

Hence, for the Turn-on snubber circuit, L = 0.055 µH and R = 3Ω.

Figure 4-14, shows the Turn-On snubber circuit connected in series with the IGBT and the supply. The result of the simulation is shown in Figure 4-15.

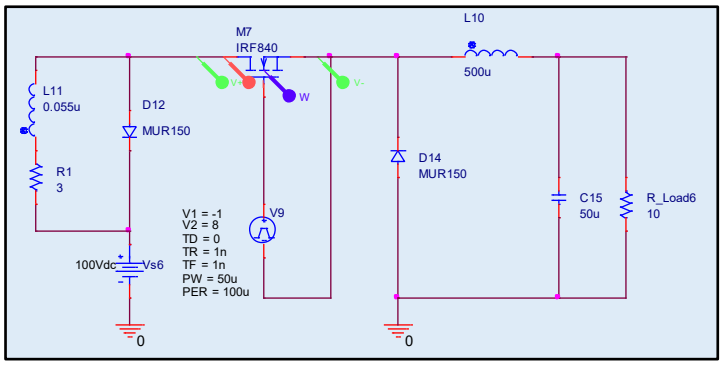

Figure 4-14 Turn-On SC in series with the IGBT switching Device

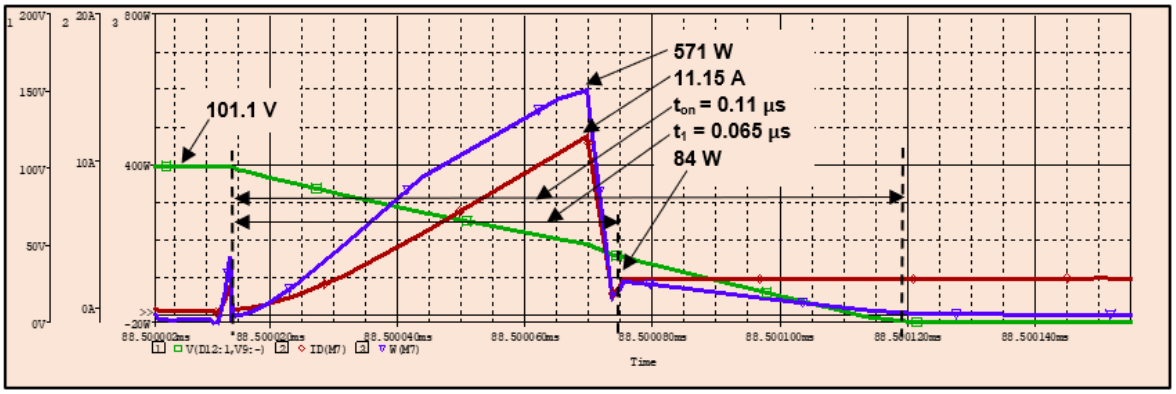

Figure 4-15 Turn-On SC Simulation for L = 0.055µH and R = 3Ω

Calculation of the switch energy E_{SW}, assuming linear power traces,

In Figure 4-15, the switch energy,

$$E_{SW} = \sum E_1 + E_2 \qquad \text{Joules}$$

$$E_{SW} = \left(\frac{571}{2} \times 0.065\ \mu s\right) + \left(\frac{84\ W}{2} \times (0.11\mu s - 0.065\ \mu s\right) \text{ Joules}$$

$$E_{SW} = (18.56 + 1.89)\ \mu J$$

And with snubber circuit $E_{SW} = 20.45\ \mu J$

In section 4.2.4, the switch energy E_{SW} without snubber circuit was 37.63 µJ. The reduction in switch energy due to the SC is: -

$$\%\ \text{Reduction}, E_{SW} = \frac{(37.63 - 20.45)\mu J}{37.63} \times 100\% = 45.7\%$$

In this Method (– *Ls di/dt* = *Vs*), the values of L = 0.055 µH and R= 3**Ω**, determined for the Turn-On snubber circuit reduced the switch energy by 45.7%.

4.3.2 Method 2- Trial and Error to Determine Ls and Rs for the Turn-On SC

The same schematic was used, as in Figure 4-14, except that L = 1μH and R = 0.19**Ω**, which was found after several simulation attempts to determine minimum switch loss.

The time constant, L/R = 5.26μs > 0.116 μs for no snubber, but much less than the Turn-On period of T/2 = 50μs. Figure 4-16, shows the traces for V (green), I (red) and P (blue) and two measurements for t_{on}, due to the power spike (P_1) followed by the normal power curve (P_2). The switch energy was then determined.

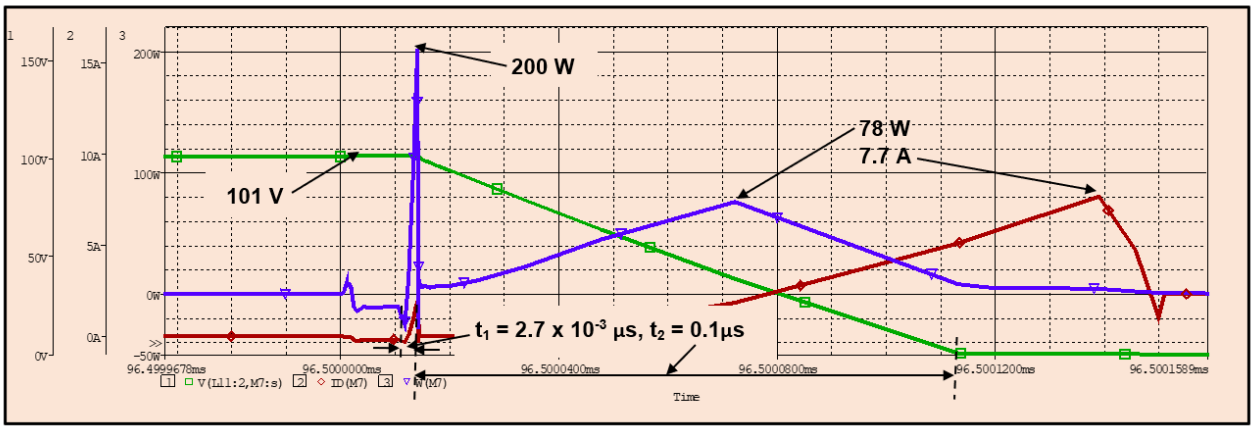

Figure 4-16 Simulation Result of the Trial-and-Error Method

In Figure 4-16, the switch t_{on} is,

$$t_{on} = (t_1 + t_2) = 0.1027\mu s$$

Calculation of the switch energy $E_{SW,}$

$$E_{SW} = \sum (E_1 + E_2)\, Joules$$

$$= \left(\frac{200\text{W} \times 2.7 \times 10^{-3}\mu\text{ns}}{2}\right) + \left(\frac{78\text{W} \times 0.1\mu\text{s}}{2}\right)$$

$$= (0.27 + 3.9)\mu\text{J}$$

$$E_{SW} = 4.17\mu\text{J}$$

In this Method 2: By Trial and Error, the values for L = 1μH and R = 0.19Ω for the Turn-On SC. The switch energy E_{SW} = 4.17 μJ.

In section 4.2.4, the turn-on switch energy E_{SW} without snubber circuit was 37.63 μJ. The reduction in switch energy due to the SC is: -

$$\%\ \text{Reduction}, E_{SW} = \frac{(37.63 - 4.17)\mu J}{37.63} \times 100\% = 89.6\%$$

4.3.3 Method 3- Graphical Optimisation to find Ls and R_S for the Turn-On SC.

This method used equation (4.8) i.e.

$$L_S = V_S \frac{t_{on}}{I_S} H$$

The schematic used is the same as Figure 4-6 and simulation results in Figure 4-13, from which the choice of the variables' limits are given in Table 4-3. Although the procedure is based on iterations and graph plotting, the nomenclature used are the same as in optimisation applications. Hence the reference to, decision variables, constraint, and objective function.

Table 4-3 Initial values of Variables to determine Ls in Turn-On SC

Decision Variable	Initial value	Increment	Iterations
I_s - Amps	24	-1	20
t_{on} - μs	0.091	+0.0001	20
L_s - μH	0.23	+0.05	20
Constraint	$\boldsymbol{V_{LS} = V_S = 100\ volts}$		
Objective Function	$\boldsymbol{V_{LS} = L_S \times \frac{I_S}{t_{on}}}$		

From Table 4-3, calculations were made for the three variables using the respective increments and the objective function shown in Table 4-4 , with the initial values in Row 1. The values in the Objective Function V_{LS} column were compared to V_S Constraint. In rows 6 and 15 identify when V_{LS} is approximately equal to V_S. At these two rows, Ls = 0.48 μH and 0.93 μH. However, these values need fine tuning, so that V_{LS} equates exactly to the set constraint of 100volts. To achieve the fine tuning, a graph was plotted from Table 4-4 as shown in Figure 4-17. It identifies two intersection points, where ((V_{LS} (blue) ≈ Vs (orange)) with corresponding exact values for Ls = 0.5μH and 0.92μH.

Table 4-4 Decision Variables,
Constraint and Objective Function values

Row	Decision Variables				Constraint	Objective Function
	Is – amps	t_{on} - µs	I_s/t_{on}	Ls - µH	Vs – volts	V_{LS} – volts
1	24.00	0.0910	571	0.230	100	60.66
2	23.00	0.0911	250	0.280	100	70.69
3	22.00	0.0912	239	0.330	100	79.61
4	21.00	0.0913	228	0.380	100	87.40
5	20.00	0.0914	217	0.430	100	94.09
6	**19.00**	**0.0915**	**206**	**0.480**	**100**	**99.69**
7	18.00	0.0916	195	0.530	100	104.15
8	17.00	0.0917	184	0.580	100	107.52
9	16.00	0.0918	173	0.630	100	109.80
10	15.00	0.0919	162	0.680	100	110.99
11	14.00	0.0920	151	0.730	100	111.09
12	13.00	0.0921	140	0.780	100	110.10
13	12.00	0.0922	129	0.830	100	108.03
14	11.00	0.0923	118	0.880	100	104.88
15	**10.00**	**0.0924**	**107**	**0.930**	**100**	**100.65**
16	9.00	0.0925	96	0.980	100	95.35
17	8.00	0.0926	86	1.030	100	88.98
18	7.00	0.0927	75	1.080	100	81.55
19	6.00	0.0928	64	1.130	100	73.06
20	5.00	0.0929	53	1.180	100	63.51

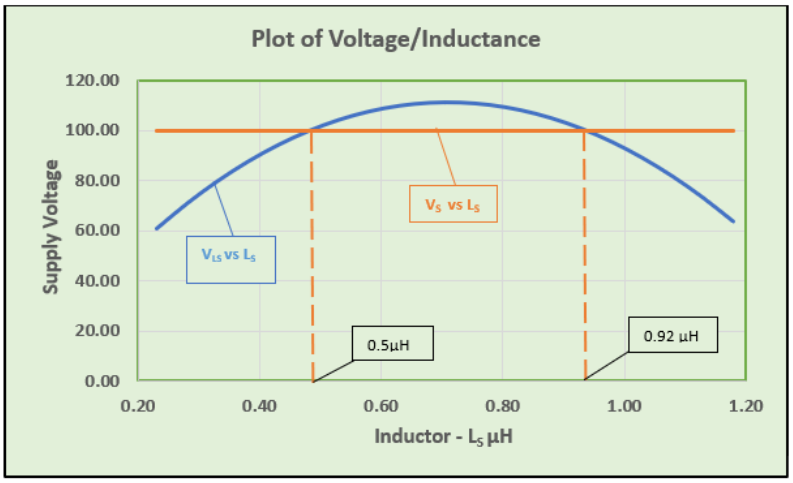

Figure 4-17 Plot to determine exact
values for the Turn-On snubber Inductance LS

In Figure 4-17, the values for L_S = 0.5µH and 0.92µH, closely compares to the values in Table 4-4 for L_S = 0.48µH and 0.93µH. To select Ls, the switch energy due to each Ls has to be determined which requires the Turn-On SC to include the discharge series resistor Rs for each Ls. The calculation for Rs follows.

Let the time constant,

$$\frac{L}{R} = \frac{T}{2} = 50\ \mu s$$

For,

$$L_S = 0.5\mu H,\ R_S = \frac{0.5\ \mu H}{50\ \mu s} = 0.1\Omega$$

For,

$$L_S = 0.92\mu H,\ R_S = \frac{0.92\ \mu H}{50\ \mu s} = 0.0184\Omega$$

The calculation of the IGBT switching loss follows, using in the above Ls and Rs components in the Turn-On SC in Figure 4-14.

4.3.3.1 Calculation of Switch Energy E_{sw} for L_s = 0.5 µH and R_s = 0.01Ω

In Figure 4-14 the Turn-On SC L_S and R_S values were changed to 0.5 µH and 0.01 Ω, respectively. The circuit was simulated with the results shown in Figure 4-18.

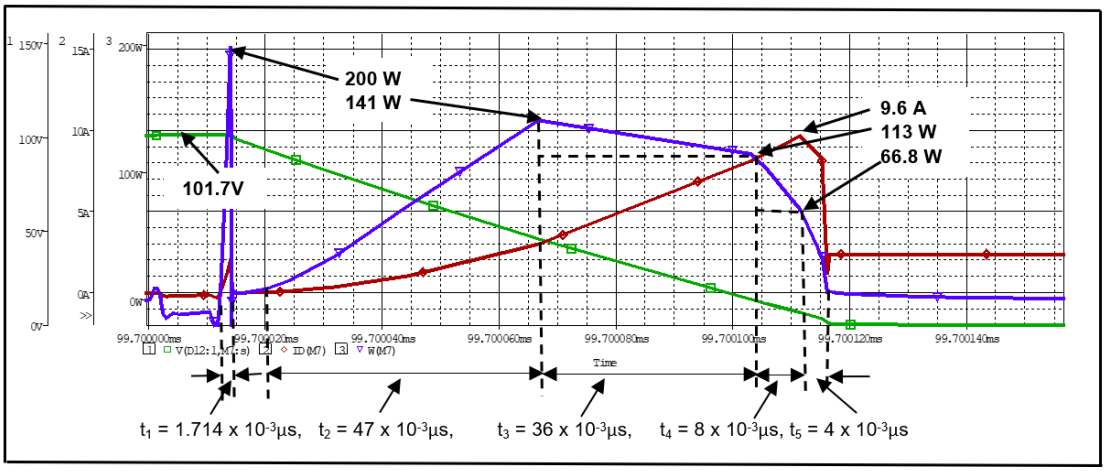

Figure 4-18 V, I and P traces for Ls = 0.5 µH and Rs = 0.01 Ω

Switch turn-on Energy calculations, based on the three Power traces in Figure 4-18.

$$\text{Turn} - \text{On}\ \ E_{SW} = \sum_{k=1}^{n} E_k, \ldots . n = 1, 2, 3, 4, 5, 6, 7\ \ \text{Joules}$$

$$= \sum_{k=1}^{n} \left(P_k \times \frac{t_k}{2}\right)\ \text{Joules}$$

$$= \left((200\ \text{W}) \times \frac{1.714 \times 10^{-3}\ \mu s}{2}\right) + \left(141\ \text{W} \times \frac{47 \times 10^{-3}\ \mu s}{2}\right) + \left((141 - 113)\ \text{W} \times \frac{36\ \times 10^{-3}}{2}\right)$$

$$+ \left((113\ \text{W}\ \times 36\ \times 10^{-3})\right) + \left((113 - 66.8)\ \text{W} \times \frac{8\ \times 10^{-3}}{2}\right)$$

$$+ \left((66.8\ \text{W}\ \times 8\ \times 10^{-3})\right) + \left(66.8\ \text{W} \times \frac{4 \times 10^{-3}\ \mu s}{2}\right)\ \text{Joules}$$

$$= (0.1714 + 3.3125 + 0.504 + 4.068 + 0.1848 + 0.5344 + 0.1336)\mu J$$

Turn-On E_{SW} = 8.9 µJ

Total switch energy for Ls = 0.5 µH and Rs = 0.01 Ω = 8.9 µJ

In this Method 3 Part 1– Determination of Ls & Rs for the Turn-On SC by Graph Ls = 0.5 µH, Rs = 0.01Ω and the Switch Energy at turn-on = 8.9 µJ.

In section 4.2.4, the turn-on switch energy E_{SW} without snubber circuit was 37.63 µJ. The reduction in switch energy due to the SC is: -

$$\%\ \text{Reduction}, E_{SW} = \frac{(37.63 - 8.9)\mu J}{37.63} \times 100\% = 76.4\%$$

4.3.3.2 Calculation of Switch Energy E_{SW} for L_S = 0.92 µH and R_S = 0.0184Ω

Ls and Rs were changed in Figure 4-14 to the second pair of Ls = 0.92 µH and Rs = 0.0184 Ω, respectively. The simulation result is shown in Figure 4-19 with traces for V, I and P.

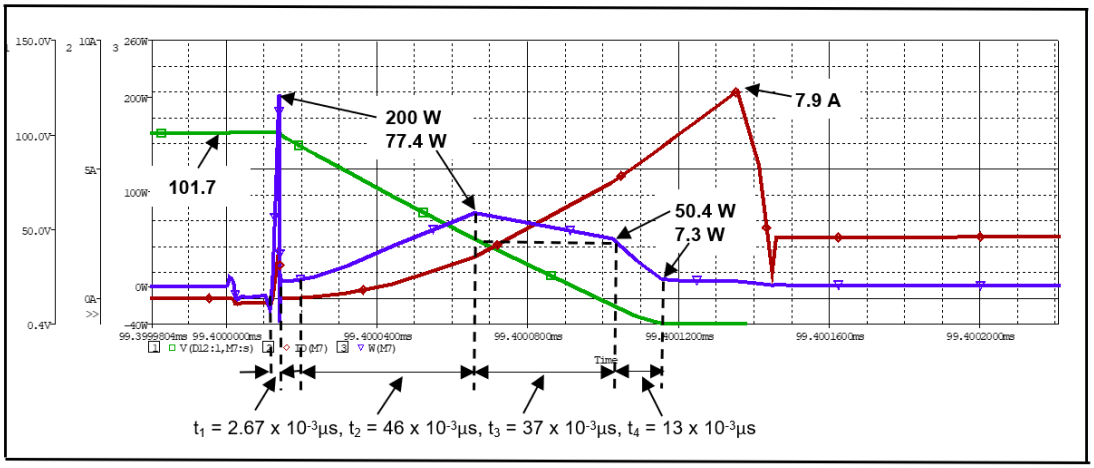

Figure 4-19 V, I and P traces for Ls = 0.92 µH and Rs = 0.0184 Ω

Switch turn-on Energy calculations, based on the three Power traces in Figure 4-19.

$$\text{Turn} - \text{On}\ \ E_{SW} = \sum_{k=1}^{n} E_k, \ldots . n = 1, 2\ 3, 4, 5\ \ \text{Joules}$$

$$= \sum_{k=1}^{n} \left(P_k \times \frac{t_k}{2} \right)\ \text{Joules}$$

$$= \left(200\ \text{W} \times \frac{2.67 \times 10^{-3}\mu s}{2} \right) + \left(77.4\ \text{W} \times \frac{46 \times 10^{-3}\mu s}{2} \right) + \left((77.4 - 50.4)\text{W} \times \frac{37 \times 10^{-3}\mu s}{2} \right)$$

$$+ \left((50.4\ \text{W} \times 37 \times 10^{-3}\mu s) \right) + \left((50.4\ -7.3\ )\text{W} \times \frac{13 \times 10^{-3}\mu s}{2} \right) \text{Joules}$$

$$= (0.267 + 1.7802 + 0.4995 + 1.8648 + 0.28015)\ \mu\text{J}$$

$$= 4.69\ \mu\text{J}$$

Total switch energy for Ls = 0.92µH and Rs = 0.018Ω = 4.69 µJ

In section 4.2.4, the turn-on switch energy E_{SW} without snubber circuit was 37.63 µJ. The reduction in switch energy due to the SC is: -

$$\%\ \text{Reduction}, E_{SW} = \frac{(37.63 - 4.69)\mu J}{37.63} \times 100\% = 87.5\%$$

From the two simulations, the essential parameters are presented in Table 4-5.

Table 4-5 – Area method - Parameters of the two Turn-On SCs

Result of simulation	Ls - µH	Rs - Ω	Turn-On E_{SW} µJ	% Reduction E_{SW}
1	0.50	0.010	8.9	76.4
2	0.92	0.0184	4.69	87.5

In Method 3 Part 2 - The results clearly show that in the second simulation with L = 0.92µH and R = 0.0184 Ω, obtained the minimum switching energy and a reduction of 87.9% switching energy of compared to the 76.4 % with L = 0.5 µH and R = 0.01Ω. The plotting of the graph achieved a fine tuning of L with the subsequent selection of the effective inductance value via the simulation process.

4.3.4 Method 4- GRG Solver to determine Ls & Rs for Turn-On Snubber Circuit.

GRG is the Generalised Reduction Gradient Solver.

The objective function (Fn) for the Solver is based on the voltage equation (4.6) developed across the Inductor, i.e.

$$V_S = V_L = L \times \frac{di}{dt}\ \text{volts}$$

Where, V_L must equal Vs as the constraint for the solver [68]. The data in Table 4-6, was entered in a spread sheet to execute the Solver procedure.

Table 4-6 GRG Solver Initial values for Variables, Constraints and Result

Excel Solver Parameters								
Cell Reference		C	D	E	F	G	H	I
	6	Variable 1	Variable 2	Variable 3	Constraint 1	Constraint 2	Constraint 3	Objective
	7	I - Amps	t - µs	L - µH	E - Volts	< I	> t	E
Solver Result	8	2	0.1	5.0	100	2.0	0.1	100
Initial values	9	10	0.09	1.2	100	2.0	0.1	

The Objective Function was entered in column 'I' as,

$$\textbf{Objective Fn} = \text{Sum}\left[(\$E\$8) * \left(\frac{\$C\$8}{\$D\$8}\right)\right]$$

The solver result is shown in row 8 with the initial values in row 9. Figure 4-20, shows the entry data table from which the solver window reads the data via the cell references. When a result

is found, the Solver Result window appears, from which, three reports can be selected as shown in the Figure 4-20.

.

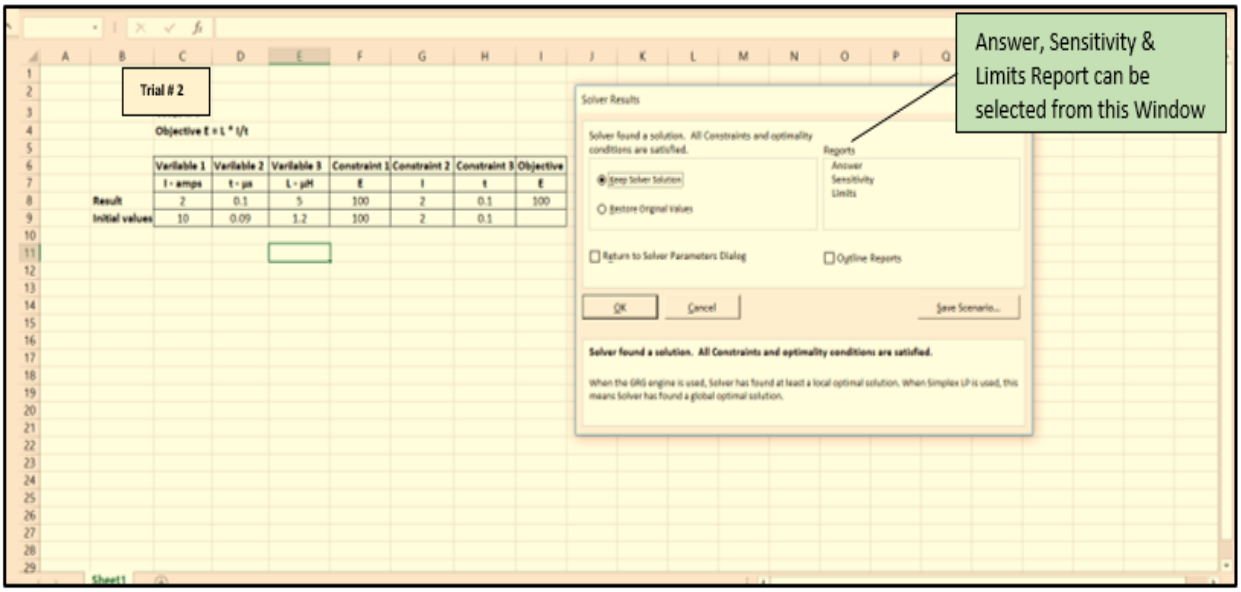

Figure 4-20 Solver data entry for Initial Values and the GRG Results Window

For this solution, the Answer Report was selected as shown in Table 4-7.

Table 4-7 Summary of data inputs and Results from Solver Answer Report

Worksheet: [Book1] Sheet 1
Report Created: 13/12/2018 21:23:08

Result: Solver found a solution. All Constraints and optimality conditions are satisfied.

SOLVER ENGINE

Engine: GRG Nonlinear

Solution Time: 0.031 Seconds.

Iterations: 2 Subproblems: 0

SOLVER OPTIONS

Max Time Unlimited, Iterations Unlimited, Precision 0.000001, Use Automatic Scaling

Convergence 0.0001, Population Size 100, Random Seed 0, Derivatives Forward, Require Bounds

Max Subproblems Unlimited, Max Integer Sols Unlimited, Integer Tolerance 0%, Assume Non-Negative

OBJECTIVE CELL (VALUE OF)

Cell	Name	Original Value	Final Value
I8	Result E	133.3333333	100

VARIABLE CELLS

Cell	Name	Original Value	Final Value	Integer
C8	Result I - amps	10	2	Contin
D8	Result t - µs	0.09	0.1	Contin
E8	**Result L - µH**	**1.2**	**5**	Contin

CONSTRAINTS

Cell	Name	Cell Value	Formula	Status	Slack
F8	Result E	100	F8=100	Binding	0
I8	Result E	100	I8=100	Binding	0
C8	Result I - amps	2	C8<=2	Binding	0
D8	**Result t - µs**	**0.1**	D8>=0.1	Binding	0

In Table 4-7 under VARIABLE CELLS, show the Final Value for L = 5 µH

Simulation using Figure 4-14, with L_S changed to 5 µH follows, to check on the effect it has on the minimisation of the switch turn-on energy.

4.3.4.1 Calculation of Rs and Validation by PSpice of Ls = 5µH

The Turn-On SC discharges Ls during the turn-off period of 50 µs and the discharge resistor Rs is,

$$\text{Time Constant } \frac{L_S}{R_S} = 50\ \mu$$

and,

$$R_S = \frac{5\ \mu H}{50\ \mu s} = 0.1\ \Omega$$

With Rs in the SC changed to 0.1 Ω, the circuit was simulated, with the result shown in Figure 4-21.

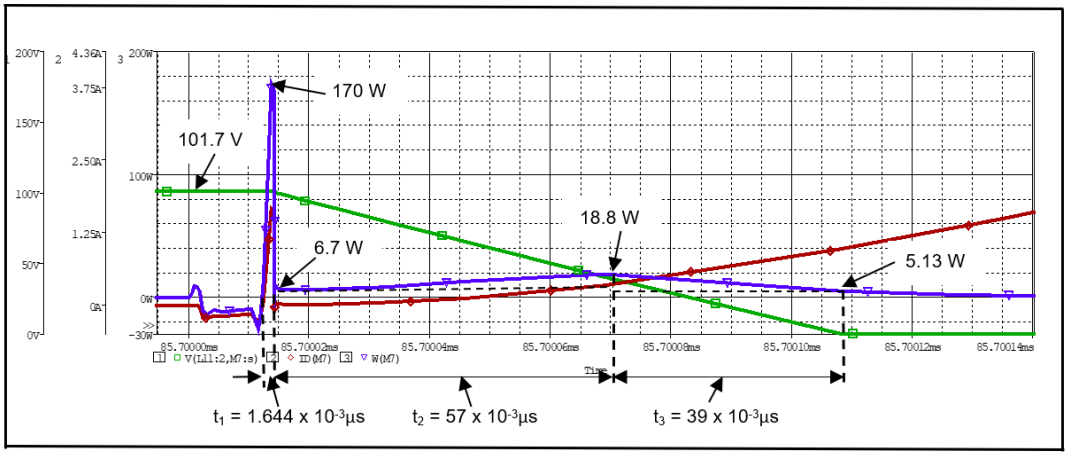

Figure 4-21 V, I and P Traces for L = 5 µH and R = 0.1 Ω

4.3.4.2 Calculation of Switch Energy for L = 5µH and R = 0.1Ω

$$\text{Turn} - \text{On}\ \ E_{SW} = \sum_{k=1}^{n} E_k, \ldots . n = 1, 2, 3\ \ \text{Joules}$$

$$= \sum_{k=1}^{n} \left(P_k \times \frac{t_k}{2} \right) \text{Joules}$$

$$= \left(\left((170\ \text{W}) \times \frac{1.644 \times 10^{-3}\mu s}{2} \right) + \left((18.8 - 6.7)\ \text{W} \times \frac{57 \times 10^{-3}\mu s}{2} \right) \right.$$

$$+ \ (6.7\ W \times\ 57 \times 10^{-3}\mu s) + \left((18.8 - 5.13)\ \text{W} \times \frac{39 \times 10^{-3}\mu s}{2} \right)$$

$$\left. + (5.13\ W \times\ 39 \times 10^{-3}\mu s) \right) \text{Joules}$$

$$= (0.13974 + 0.34485 + 0.3819 + 0.2666 + 0.20007)\mu J$$

$$= 1.33\ \mu\text{J}$$

Total switch turn-on energy at L = 5µH and R = 0.1Ω = **1.33** µJ

Method 4 –Determination of Ls & Rs for the Turn-On SC by GRG Solver, Ls = 5 µH and Rs = 0.1 Ω and the Switch Energy at turn-on = 1.33 µJ.

In section 4.2.4, the turn-on switch energy E_{SW} without snubber circuit was 37.63 µJ. The reduction in switch energy due to the SC is: -

$$\%\ \text{Reduction}, E_{SW} = \frac{(37.63 - 1.33)\mu J}{37.63} \times 100\% = 96.5\%$$

4.4 Summary of Methods to determine Ls & Rs for the Turn-On SC

Table 4-8 summarises the various methods used to determine the Inductance and Resistance for the Turn-On SC.

Table 4-8 Comparison of methods to find Ls & Rs for the Turn-On SC

No	Method	Title	L-µH	R-Ω	E_{SW} µJ	% reduction
0	N/A	Turn-On switch energy without SC	0	0	37.63	N/A
1	Vs = L di/dt	Equating Inductor voltage to the supply voltage	0.055	3	20.45	45.7
2	Manual	Manual (Trial and Error)	1	0.19	4.17	89.6
3	Graphical – Part 1	Graphical Optimisation based on the equation (3)	0.5	0.01	8.9	76.4
3	Graphical –Part 2	Graphical Optimisation based on the equation (3)	0.92	0.018	4.69	87.5
4	GRG Solver	Solver Optimisation based on the equation (3)	5	0.1	1.33	96.5

From Table 4-8, a plot of Esw versus Ls is shown in Figure 4-22. It compares the switch turn-on transition energy level by different methods to the level without any snubber circuit.

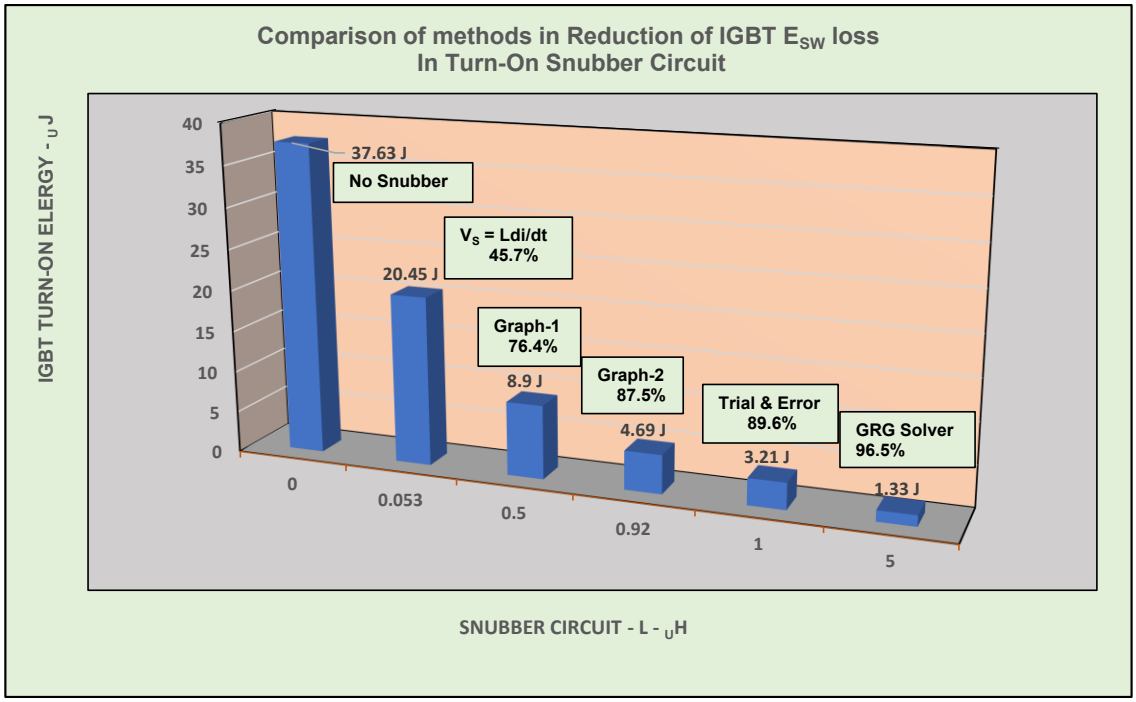

Figure 4-22 Comparison of different methods in the Reduction of IGBT- E_{SW}

Figure 4-22 shows that although the Graphical and Trial & Error methods resulted in acceptable reduced levels, the minimum reduction was clearly achieved by the GRG Solver

method. The reduction in IGBTs turn-on switching levels and corresponding increase in percentage efficiency reduction was due to the progressive increase in the snubber circuit inductance value, for which the GRG Solver/Optimiser was most efficient.

Having completed the various methods to determine the Inductance value for the Turn-On snubber circuit, the next chapter will consider various methods to determine the capacitor and discharge resistor values for the Turn-Off snubber circuit.

Chapter 5 Solvers to determine R & C in Turn-Off SC

5.1 Methods and Description.

Popular methods are described, followed by their application to determine the optimum values for the R and C components of the Turn-Off snubber circuit.

5.1.1 PSpice Parametrisation

The Parametric analysis is not an optimisation procedure. It determines a minimum value of a component from a range based on a constraint of an objective function. In the case for a Turn-Off snubber circuit a capacitor is selected which reduces the switching energy to a minimum at turn-off. This capacitor is then connected in the snubber circuit to validate the minimum energy of the switch at turn-off. Compared to optimised methods, where the optimum component is found it is then validated by simulation.

In PSpice the snubber capacitor C, is renamed {Cval} as a global parameter with a minimum and maximum range. The simulations, result in a number of traces due to the increments in the parameter range [69].

5.1.2 Generalized Reduced Gradient (GRG)

Method for non-linear optimization. GRG was recently established as one of the most effective optimization algorithms [70]. It was developed especially for optimization of complex engineering systems. The algorithm solves nonlinear problems with inequalities, using derivatives of the objective function as the variables change and finds the optimum solution when the partial derivatives equal zero.

5.1.3 Evolutionary Solving Algorithm (EA)

Method for non-smooth systems and uses a variety of genetic algorithm (GA) and local search methods. EAs have high-global search capability and is a population-based search technique inspired by natural phenomenon. Modern automation of these procedures can also include heuristics, swarm-intelligence approaches, multi-objective optimisations and Genetic Algorithms (GAs) [71].

5.1.4 Simplex Linear programming (LP)

Method for Linear Programming. The Simplex method can be considered as the standard algorithm for solving LP problems and is widely used in practice [72]. The efficiency of the simplex algorithm for

practical problems have been proven in many applications. Results are accurate and is a well-studied algorithm in optimization theory [73].

5.1.5 Particle Swarm Optimisation (PSO)

PSO is a swarm intelligence or higher-level procedure, to find an acceptable solution to an optimisation problem, without complete data/information. It is inspired by the group behaviour of animals, e.g., bird flocks or fish schools. Similarly, to GA, it is a population-based method, as it represents the algorithm by a population, which is iteratively modified until a termination criterion is satisfied. In PSO, the population of the feasible solution is called particles. It views the set of feasible solutions as a "two-dimensional space" where the particles "move". For solving practical problems, depending on the sensitivity of the resolution required, the number of particles is usually chosen between 10 and 50 [74]. From the above methods, PSpice Parametrisation, Generalized Reduced Gradient (GRG) and Particle Swarm Optimisation (PSO) will be demonstrated.

5.2 Parametrisation Analysis to determine R & C in Turn-Off Snubber Circuit

The PSpice schematic in Figure 4-10 is used in the analysis. The Parametrisation analysis is not an optimisation procedure. It determines a minimum value of a component from a range based on a constraint of an objective function. In the case for a Turn-Off snubber circuit a capacitor is selected which reduces the switching energy to a minimum at turn-off. This capacitor is then connected in the snubber circuit to validate the minimum energy of the switch at turn-off. Compared to Optimised methods, when the optimum component is found it is then also validated by simulation.

In PSpice, the simulations result in a number of traces due to the increments in the parameter range [69]. The resistor value was fixed at 0.272Ω. In the PSpice schematic, C was swept from 0.2 µf to 0.4 µf, with 0.05 µf increments, resulting in five iterations.

Figure 5-1 shows five overlapping traces of V, I and P. The current traces are overlapped with the power traces at the positive edge of the switch voltage at turn-off and at zero point at t_2 where most of the voltage traces were also at zero value. There are five 't_3' periods one for each power trace, only one is shown for the blue trace.

Figure 5-1 is a magnified view of the current traces and the power traces at P_1 with high (*di/dt)* gradients reducing the currents to zero at t_2. The switch power was not completely reduced

between t_1 and t_2 as it continued to zero at t_3, due to the product of voltage rise *(dv/dt)* and turn off leakage current along the time axis, giving rise to the power traces between t_2 and t_3. The t_1, t_2, and t_3 are shown for the (blue) minimum power trace only. The peak power P_2 between t_2 and t_3 is measured for energy calculation. All measurements were made using the PSpice cursor function.

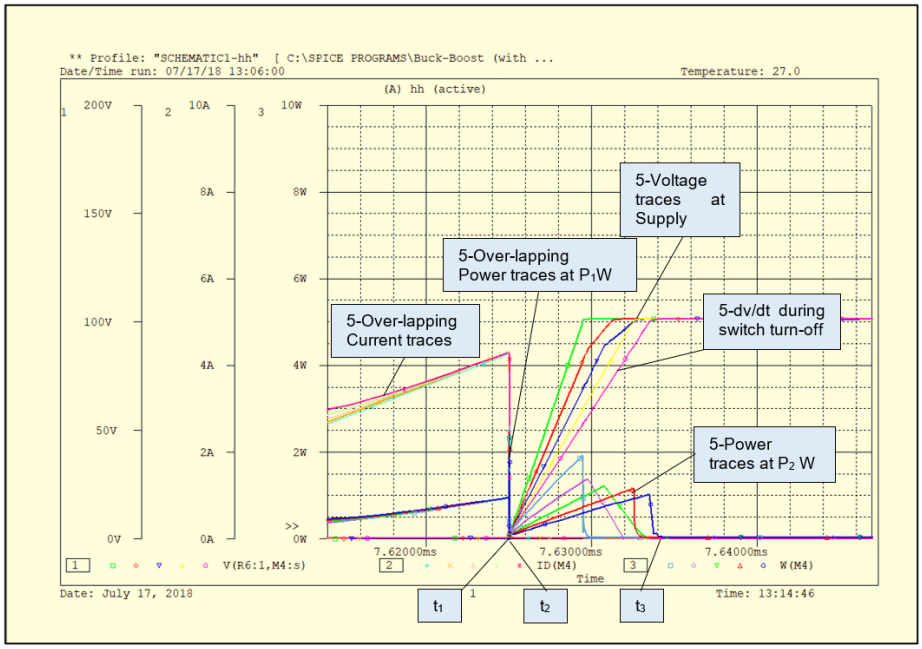

Figure 5-1 V, I and P Traces Snubber
Capacitor Range 0.2µf to 0.4µf, R = 0.272Ω

In Figure 5-1, PSpice uses distinct colours to identify the traces. Also, each trace is further marked with symbols of the same colour and are printed below the time axis. The order of the simulation starts with the square **(□)** symbol and ends with a circle **(○)** symbol as shown in Table 5-1.

Table 5-1 PSpice Trace Symbols, colour, and capacitor range

Simulation order	#1	#2	#3	#4	#5
Capacitor range - µf	0.2	0.25	0.3	0.35	0.4
Power trace Symbols	□	◊	∇	Δ	○
Colour	Light blue	Violet	Green	Red	Dark blue
Voltage trace symbols	□	◊	∇	Δ	○
Colour	Green	Red	Dark blue	Yellow	Violet

In Figure 5-2, shows a magnified view of the traces in Figure 5-1 between t_1 and t_2, which reveals an oscillation of all traces in that period.

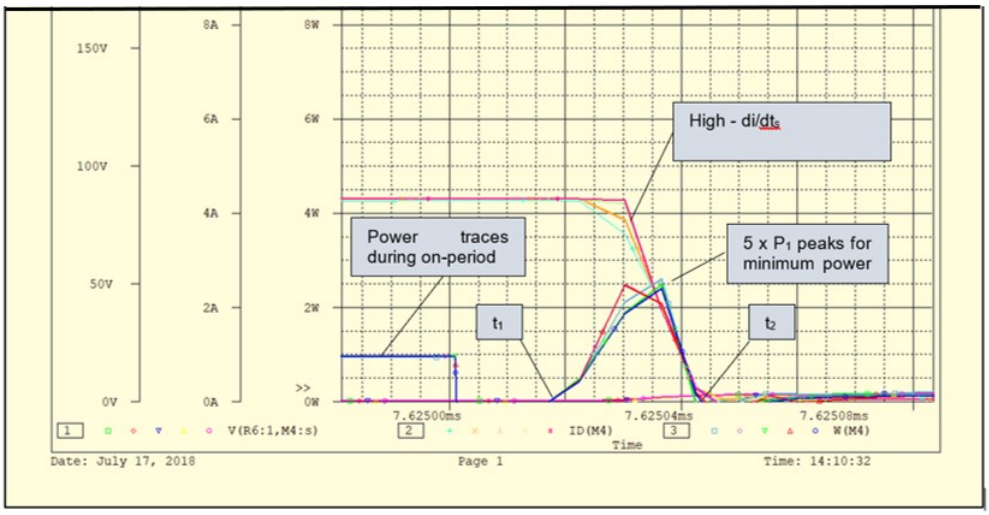

Figure 5-2 Magnified view of minimum power traces between t_1 and t_2

5.2.1 Result of Parametrisation simulation

Table 5-2, shows the simulation results for each capacitor value with R fixed at 0.272Ω.

Table 5-2 Results of simulation for the range of C values

RUN	C µF	t_1 ms	t_2 ms	t_3 ms	(t_3-t_1) ms	P_1 W	P_2 W	V	*dv/dt* = (V/(t_3-t_1))
1	0.2	7.62501	7.625041	7.6295	0.0045	2.6	1.8□	100.8□	0.0224kV/µs
2	0.25	7.62501	7.625041	7.6298	0.0047	2.4	1.4◊	89.94◊	0.01892kV/µs
3	0.3	7.62501	7.625041	7.6305	0.0055	2.5	1.2▽	89.94▽	0.01635kV/µs
4	0.35	7.62501	7.625041	7.6330	0.0079	2.4	1.1Δ	100.5Δ	0.01272kV/µs
5	0.4	7.62501	7.625041	7.6340	0.0089	2.3	1.0○	100.0○	0.01123kV/µs = **minimum dv/dt**

At simulation RUN-5, C = 0.4 µF and the switch is at the lowest *dv/dt* stress level of 0.01123 kV/µs (11.23 kV/ms), which slows down the rate of voltage rise across the switch. Calculation of the switch energy for each simulation follows. It is possible with a capacitor range extending beyond 0.4 µF to 1 µF, a lower dv/dt is possible, however there will be a congested cluster of traces to analysed.

5.2.2 Reduction of switch energy by Parametrisation method

To select the most effective RC for minimum switch energy, the area under each power trace was calculated. The total energy of each power trace is the sum of the energies (E_1 + E_2) J.

Assuming linearity in all power traces the switch energy 'E_{SW}' is,

$$E_{SW} = \left(\sum_{k=1}^{m} E_k = \sum_{k=1}^{n} P_k \times \frac{t_{k+1} - t_k}{2} \right) \text{Joules}, \quad \begin{matrix} m = 1, 2 \\ n = 1, 2, 3, 4, 5 \end{matrix} \qquad (5.1)$$

From Table 5-2 and equation (5.1), the total energy for each power trace is calculated and entered in Table 5-3. The colours for RUN #1 to RUN #5 are in the same colour as for the power traces in Figure 5-1.

Table 5-3 Calculation of total Energy for each Power trace

RUN	Symbol	C µf	P1	P1/2 W	t1 ms	t2 ms	(t2 - t1) µs	t3 ms	E1 µJ	P2	P2/2 W	(t3 – t2) µs	E2 µJ	(E1 + E2) µJ
1	□	0.2	2.6	1.3	7.62501	7.625041	0.031	7.6295	0.0403	1.8	0.90	4.459	4.01	4.05
2	◊	0.25	2.4	1.2	7.62501	7.625041	0.031	7.6320	0.0372	1.4	0.70	6.959	4.87	4.91
3	∇	0.3	2.5	1.25	7.62501	7.625041	0.031	7.6330	0.0387	1.2	0.60	7.959	4.77	4.81
4	Δ	0.35	2.4	1.2	7.62501	7.625041	0.031	7.6330	0.0372	1.1	0.55	7.959	4.38	4.42
5	○	0.4	2.3	1.15	7.62501	7.625041	0.031	7.6340	0.0356	1.0	0.50	8.959	4.48	4.52

5.2.3 Comparison of switch energy with and without Snubber Circuit.

In Section 4.2.1.1 with no SC connected, the E_{SW} = 62.16 µJ. In Table 5-3, for RUN #1, with C = 0.2 µF and R = 0.272 Ω, (Parametrisation simulation), the total minimum switch energy was 4.05 µJ

Therefore, the % reduction in E_{SW},

$$\%\ \text{Reduction in } E_{SW} = \frac{(62.16 - 4.05)\mu J}{62.16\ \mu J} \times 100$$

$$\text{Reduction in } E_{SW} = \ 93.5\ \%$$

5.2.4 Summary- PSpice Parametrisation

In the Parametrisation analysis, a range of capacitor values resulted in power traces corresponding to increments in the capacitor range. Using Energy calculations, the optimum capacitor was found. This resulted in a minimum switch energy of 4.05 µJ a reduction of 93.5% with C = 0.2µf and R = 0.272Ω.

5.3 Optimisation by GRG-Solver - to determine R & C in Turn-Off Snubber Circuit.

A description follows of the objective function, Constraints, and variables, which are the three main parameters in any solvers. If Excel formulas are used to execute the calculations, each parameter is entered in different cell in a spreadsheet. The location of these cells may be organised to permit logical analysis.

5.3.1 Objective cell

The task of solver is to find a maximum, minimum or a fixed value for a formula, called the Model placed in this cell.

5.3.2 Decision Variables and Constraints

The variables are used in computing the formulas in the objective and constraint cells. Constraints of lower and upper limits for variables in the formula are entered in other cells in the spreadsheet. Solver adjusts the values in the decision variable cells to satisfy the limits in the constraint cells and produce the result in the objective cell [75] [70].

5.4 Derivation of the Switch Energy Equation during t_{off}

The minimum switch energy E is discussed in [4], without the derivation, which is now presented. Figure 5-3 shows the decay of switch current i_s and corresponding rise of the snubber capacitor current i_c at t_f the time taken for I to fall to zero current.

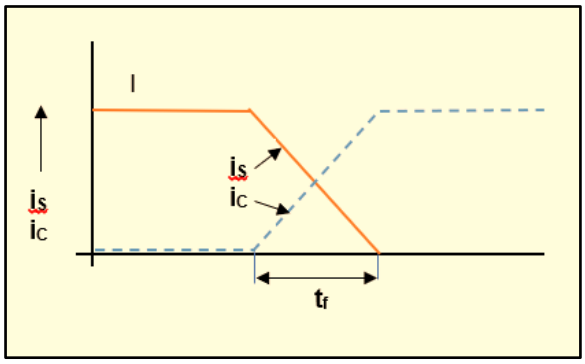

Figure 5-3 Currents in Switch at Turn-Off

The currents i_s and i_c are assumed to be linear and takes the form,

$$i = \frac{di}{dt}t + k, \text{ where 'k' is the value of 'i' at t = 0} \qquad (5.1)$$

From (5.1) the switch current,

$$i_s = \frac{di_s}{dt}t + I, \qquad \text{since it is seen in Figure 5.3 at } t = 0, i_s = I \qquad (5.2)$$

and from the Figure, $\frac{di_s}{dt} = -\frac{I}{t_f}$, then, $$i_s = -\frac{I}{t_f}t + I \qquad (5.3)$$

Rearranging (5.3), $$i_s = I - \frac{I}{t_f}t = I\left(1 - \frac{t}{t_f}\right) \qquad (5.4)$$

In Figure 5-3 the capacitor current,

$$i_c = \frac{I}{t_f}t \qquad \text{since at } t_{f(0)}, I = 0 \qquad (5.5)$$

The capacitor voltage is given by,

$$v_c(t) = \frac{1}{C}\int_0^t i_c\,dt + v_C(0) \tag{5.6}$$

Substituting (5.5) in (5.6) $$v_c(t) = \frac{1}{C}\int_0^t \frac{I}{t_f}\,t\,dt + v_C(0)$$

and $$v_c(t) = \frac{It^2}{2Ct_f}, \quad \text{at } t_0, v_c = 0 \tag{5.7}$$

At switch turn-off the capacitor is connected across the switch, with $V_{SW} = V_C$, (providing there is no voltage drop across R) and the switch energy is given by,

$$E_{SW} = \int_0^{t_f} (v_c(t) \times i_s)dt, \qquad \text{Joules} \tag{5.8}$$

Substituting (5.4) and (5.7) in (5.8), $$E_{SW} = \int_0^{t_f} \left(\left(\frac{It^2}{2Ct_f}\right) \times I\left(1 - \frac{t}{t_f}\right)\right)dt \tag{5.9}$$

Integrating (5.9), $$E_{SW} = \frac{I^2}{2Ct_f}\int_0^{t_f} t^2 \times \left(1 - \frac{t}{t_f}\right)dt$$

$$= \frac{I^2}{2Ct_f}\int_0^{t_f}\left(t^2 - \frac{t^3}{t_f}\right)dt$$

Inserting the limits of integration $$= \frac{I^2}{2Ct_f}\left[\frac{t^3}{3} - \frac{t^4}{4t_f}\right]_0^{t_f}$$

$$= \frac{I^2}{2Ct_f}\left[\frac{t_f^3}{3} - \frac{t_f^3}{4}\right]$$

Simplifying, $$= \frac{I^2 t_f^2}{2C}\left[\frac{4-3}{12}\right]$$

and finally, during t_{off} the Switch Energy is, $$E_{SW} = \left[\frac{I^2 \times t_f^2}{24 \times C}\right] \text{ Joules} \tag{5.10}$$

5.4.1 GRG Solver Analysis

GRG Solver is used since the equation and objective function to be optimised is non-linear and given in equation (5.10). The data entry required to determine the minimum energy level E_{SW}, is shown in Table 5-4, where the variables were entered in (green) block D13 to H15, with the Objective equation,

$$E = \frac{(D15^2 \times E15^2)}{F15 \times G15}$$

entered in cells H13 and H15.

Table 5-4 Data entry for Solver Sheet 1

In the spreadsheet, the equation for E is entered in cell H15 as, **Objective,**				$E = \frac{(D15^2 \times E15^2)}{F15 \times G15}$		
Trial #1		**Find 'C' for minimum E**				
Columns		D	E	F	G	H
Row		**Variable 1**	**Variable 2**	**Variable 3**		**Objective**
		I - Amps	**t_f - µs**	**C - µF**	**Constant**	**E_{SW} - µJ**
13	**Start Values**	**19.00**	**0.09**	**0.85**	**24.00**	$\frac{I^2 \times t_f^2}{24 \times C}$
14	**Constraints**					**0**
15	**Result**	17.79	0.01	1.06	24.00	0.001000

5.4.2 GRG procedure

In the data entry, only one constraint is given for E = 0 Joules. The sensitivity setting for acceptable difference was set to 0.001 in Solver settings.

Solver requires start values for the variables to initialise the calculation process. These are replaced by solver solutions. To avoid deletion of the start values and to allow comparison with the result, they were also entered in row 13. When Solver is initiated, an interface window appears in which the data in Table 5-4 is required to be entered in specific cells which are read by Solver to determine the solution for minimum E_{SW} having met the constraint. The solution is shown in row 15. The Solver Report for the above optimisation is shown in Table 5-5 and Table 5-6.

Table 5-5 Solver Report and Settings with Input and output data

Worksheet: [Excel Solver -Find the value of capacitor 'C' for minimum E-06-01-19.xlsx] Sheet 1. Report Created: 11/01/2019 17:58:19.					
Result: Solver found a solution. All Constraints and optimality conditions are satisfied.					
Solver Engine					
Engine: GRG Nonlinear					
Solution Time: 0.015 Seconds. Iterations: 1 Subproblems: 0					
Solver Options					
Max Time Unlimited, Iterations Unlimited, Precision 0.0001, Use Automatic Scaling					
Convergence 0.0001, Population Size 100, Random Seed 0, Derivatives Central					
Max Subproblems Unlimited, Max Integer Sols Unlimited, Integer Tolerance 1%, Assume Non-Negative					
Objective Cell (Value Of)					
Cell	**Name**	**Original Value**	**Final Value**		
H15	Result E	0.000990	0.001000		
Variable Cells					
Cell	**Name**	**Original Value**	**Final Value**	**Integer**	
D15	Result I	19	17.79	Contin	
E15	Result t_f	0.09	0.01	Contin	
F15	Result C	0.85	1.06	Contin	
Constraints					
Cell	Name	Cell Value	Formula	Status	Slack
H15	Result E	0.001000	H15<=0.001	Binding	0
H15	Result E	0.001000	H15=0.001	Binding	0

Table 5-6 The Solver Report, presented in eight sections.

1	Worksheet	**Gives the title and date the report was created**
2	Result	**Comments on solution and compliance to the Constraints**
3	Solver Engine	**Type of (Algorithm) used**
4	Solution Time	**The time taken to execute the algorithm and number of Iterations**
5	Solver Options	Time to run the program, the number of iterations, the precision of convergence, total variables, type of derivatives and percentage tolerance of non-negative whole numbers.
6	Objective cell	**Location, original and final value.**
7	Variable cells	**Locations, original and final values.**
8	Constraints	**Locations of the cells and their operators (<=, >=, =) to control the gradients of the respective increments.**

5.4.3 Validation of GRG results by PSpice Simulation

From the above GRG results, the switch t_{off} ($t_{off} = t_f$) period = 0.01μs and C = 1.06μF,

For minimum E_{SW}, let RC = 0.01μs, then R is given by,

$$R = \frac{T\ \mu s}{C\ \mu F}\ \Omega$$

$$R = \frac{0.01\ \mu s}{1.06\ \mu F} = 0.0094\ \Omega$$

The C and R values were entered in the PSpice schematic of Figure 4-8 with the simulation result shown in Figure 5-4.

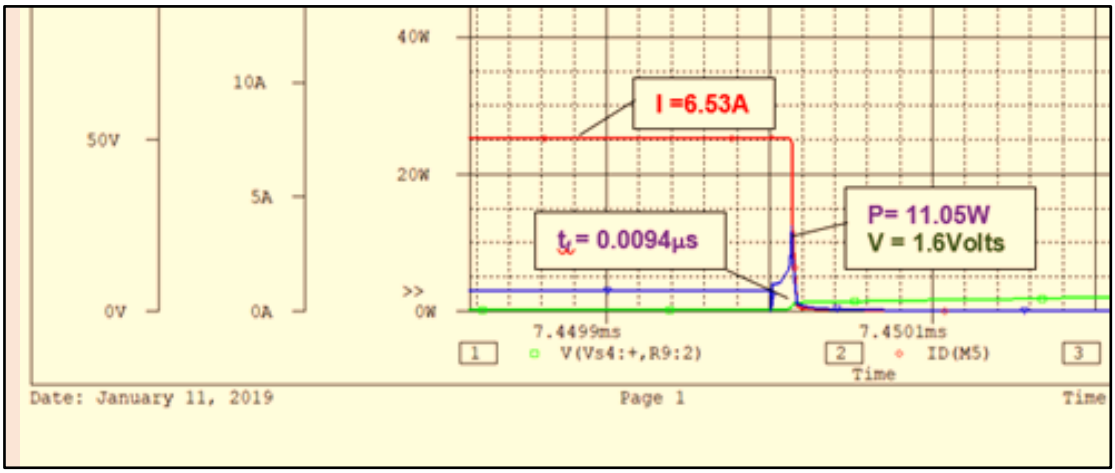

Figure 5-4 Simulation Results for C = 1.06 μF & R = 0.0094 Ω by GRG Solver

5.4.4 Reduction in Energy Level

From Figure 5-4, Switch Energy, $E_{SW} = \frac{P\ W \times t_{f\ \mu s}}{2}$ Joules

$$E_{SW} = \frac{11.05W\ \times 0.0094\mu s}{2}\ \text{Joules}$$

and $E_{SW} = 0.0519\ \mu J$

In Section 4.2.1.2 with no SC connected, the E_{SW} = 30.7 μJ

Energy in switching device with SC = 0.0519 μJ

Reduction in switching energy,

$$\text{Reduction in } E_{SW} = \frac{(30.7 - 0.0519)\mu J}{30.7\ \mu J} \times 100\% = 99.83\%$$

5.4.5 Summary - GRG Solver

The GRG Solver optimisation process, resulted in finding the optimum C = 1.06 μF and R = 0.0094**Ω**. The impact of these components resulted in a high reduction by 99.83% of switch energy. Also, the simulation turn-off period t_{off} (t_f) of 0.0094μs compares closely to the optimised time found by solver of 0.01μs. The solver method is an uncomplicated process which produced effective results. However, the main criteria is to ensure that initial start values and constraints are selected to avoid premature local minimum solutions. These local minimum solutions are due to discontinuities in the plot of the objective function. Hence the solver returns a local minimum solution since it cannot proceed along the plot due to the interruption.

5.5 PSO Method to Determine R and C for the Turn-Off Snubber Circuit

The switching device energy equation (5.10) is also the PSO Objective Function.

In (5.10), as in the GRG solver method, the variables, I, t and C have limits as in Table 5-7 to minimise the energy level during the turn-off transition period of the switching device.

Table 5-7 Lower and Upper limits for Variables, I, t_f and C

Variables limits,	$0 \leq I \leq 19\ Amps$	$0.09\ \mu s\ \geq\ t_f\ \geq 0.05\ \mu s$	$0.8\ \mu F \leq C \leq\ 1.5\ \mu F$

5.5.1 The PSO Equations

There are three PSO equations required to execute the method [74].

The 1st is a velocity equation, given by:

$$v_i^{k+1} = \{w_k \times v_i^k\} + \{c_1 \times r_1 \times (P_{best} - x_i^k)\} + \{c_2 \times r_2 \times (g_{best} - x_i^k)\} \quad (5.11)$$

The explanation of equation (5.11) parameters is given in Table 5-8.

Table 5-8 Inertia, P_{best} and g_{best} Parameters of PSO Equation

Parameters	Description
$w_k \times v_i^k$	is called the inertia part.
w_k	is the Inertia Weight (IW) of the particle at the k^{th} iteration
v_i^k	Is the velocity of the i^{th} particle at the k^{th} iteration
$c_1 \times r_1 \times (P_{best} - x_i^k)$	is called particle "Memory influence" or "Cognition part".
$c_2 \times r_2 \times (g_{best} - x_i^k)$	is called "Swarm influence" or the "Social part".
g_{best}	is the *Global best* and is the minimum particle value from the closest cluster group of minimum particles values from the result of iterations of the Objective Function.
P_{best}	is the *Personal best* and is the minimum particle from the remaining particles (i.e., excluding g_{best}) of the cluster group
c_1, c_2	are Positive low values of (acceleration) coefficients having values between [0, 2.5]. c_1 pulls particle towards P_{best} and c_2 pulls particle towards g_{best}. Large values can force particles to miss the target region. Typical value given is 2. [74]
r_1, r_2	Randomly generated numbers between [0, 1]

The 2nd PSO equation relates to the Inertia Weight w_k is calculated using the equation (5.12), [76] [77] [78], that defines the Linear Decreasing Inertia Weight (LDIW), as it forces the particles in the direction of convergence.

$$w_k = (w_{start} - w_{end}) \times \left(\frac{k_{max} - k}{k_{max}}\right) + w_{end} \quad (5.12)$$

where:

w_{start} = 0.9 and w_{end} = 0.4.

k = the current iteration number and k_{max} = the maximum iteration number.

The 3rd PSO equation, is the Position equation, given by:

$$x_i^{k+1} = x_i^k + v_i^{k+1} \quad (5.13)$$

The explanation of equation (5.13) parameters is given in Table 5-9.

Table 5-9 Velocity & Position Parameters of PSO Equation

Parameters	Description
v_i^{k+1}	is the velocity of i^{th} particle at $(k+I)^{th}$ iteration.
x_i^k	Is the position of i^{th} particle at k^{th} iteration.
x_i^{k+1}	Is the position of i^{th} particle at $(k+1)^{th}$ iteration.

5.5.2 Execution of PSO

The first step is to the determine the Particles by solving equation (5.10) (Objection Function) for minimum switch loss. 30 iterations were performed in an Excel spread sheet and presented in Table 5-10. The values for all variables were randomly generated within the limits given in Table 5-7.

Table 5-10 Iterations to determine Energy Particles from the Objective Fn

Spread sheet Row No.		D	E	F	G	H	I	J	K	L	
	Step No.	I A	I^2	t x 100	t µs	t^2	Constant	C x 10	C µF	Objective Fn E-µJ	Particle
15	1	14	196	5	0.05	0.0025	24	13	1.3	0.015705128	P_{best}
16	2	14	196	7	0.07	0.0049	24	8	0.8	0.050020833	P_{best}
17	3	9	81	5	0.05	0.0025	24	8	0.8	0.010546875	P_{best}
18	4	2	4	7	0.07	0.0049	24	10	1	0.000816667	P_{best}
19	5	4	16	7	0.07	0.0049	24	10	1	0.003266667	P_{best}
20	6	1	1	7	0.07	0.0049	24	8	0.8	0.000255208	P_{best}
21	7	11	121	7	0.07	0.0049	24	13	1.3	0.019003205	P_{best}
22	8	16	256	6	0.06	0.0036	24	14	1.4	0.027428571	P_{best}
23	9	11	121	6	0.06	0.0036	24	12	1.2	0.015125000	P_{best}
24	10	13	169	7	0.07	0.0049	24	14	1.4	0.024645833	P_{best}
25	11	4	16	6	0.06	0.0036	24	15	1.5	0.001600000	P_{best}
26	12	18	24	9	0.09	0.0081	24	15	1.5	0.072900000	P_{best}
27	13	11	121	7	0.07	0.0049	24	11	1.1	0.022458333	P_{best}
28	14	1	1	6	0.06	0.0036	24	13	1.3	0.000115385	P_{best}
29	15	14	196	7	0.07	0.0049	24	15	1.5	0.026677778	P_{best}
30	16	8	64	9	0.09	0.0081	24	8	0.8	0.027000000	P_{best}
31	17	16	256	5	0.05	0.0025	24	10	1	0.026666667	P_{best}
32	18	7	49	9	0.09	0.0081	24	9	0.9	0.018375000	P_{best}
33	19	11	121	7	0.07	0.0049	24	9	0.9	0.027449074	P_{best}
34	20	2	4	7	0.07	0.0049	24	12	1.2	0.000680556	P_{best}
35	21	1	1	8	0.08	0.0064	24	12	1.2	0.000222222	P_{best}
36	22	15	225	8	0.08	0.0064	24	8	0.8	0.075000000	P_{best}
37	23	15	225	5	0.05	0.0025	24	13	1.3	0.018028846	P_{best}
38	24	2	4	8	0.08	0.0064	24	11	1.1	0.000969697	P_{best}
39	25	5	25	9	0.09	0.0081	24	11	1.1	0.007670455	P_{best}
40	26	6	36	8	0.08	0.0064	24	14	1.4	0.006857143	P_{best}
41	27	1	1	5	0.05	0.0025	24	11	1.1	0.000094697	g_{best}
42	28	1	1	8	0.08	0.0064	24	12	1.2	0.000222222	P_{best}
43	29	4	16	8	0.08	0.0064	24	11	1.1	0.003878788	P_{best}
44	30	13	169	7	0.07	0.0049	24	9	0.9	0.038337963	P_{best}

From Table 5-10, the following actions were taken: -

1- The minimum particle under column 'L' was located and assign as g_{best}. All other particles were assigned as P_{best}.

2- A choice of twelve minimum value Particles, including g_{best} were selected to form a local cluster. Excluding g_{best}, the minimum particle from the remaining eleven particles was located and assigned as $\mathbf{P_{best}}$. The row with g_{best} was placed in the first row, followed by $\mathbf{P_{best}}$ in the second row. The remaining ten minimum values were selected and placed in random order in rows below $\mathbf{P_{best}}$. All twelve particles were presented in Table 5-11.

Table 5-11 Local Cluster of 12 Minimum particles in Random Order

Row	Step No.	I	I^2	t x 100	t	t^2	Constant	C x 10	C	Objective Fn E-UJ - Particle	
41	27	1	1	5	0.05	0.0025	24	11	1.1	0.000094697	g_{best}
28	14	1	1	6	0.06	0.0036	24	13	1.3	0.000115385	P_{best}
35	21	1	1	8	0.08	0.0064	24	12	1.2	0.000222222	P_{best}
39	25	5	25	9	0.09	0.0081	24	11	1.1	0.007670455	P_{best}
20	6	1	1	7	0.07	0.0049	24	8	0.8	0.000255208	P_{best}
34	20	2	4	7	0.07	0.0049	24	12	1.2	0.000680556	P_{best}
18	4	2	4	7	0.07	0.0049	24	10	1	0.000816667	P_{best}
38	24	2	4	8	0.08	0.0064	24	11	1.1	0.000969697	P_{best}
25	11	4	16	6	0.06	0.0036	24	15	1.5	0.001600000	P_{best}
19	5	4	16	7	0.07	0.0049	24	10	1	0.003266667	P_{best}
43	29	4	16	8	0.08	0.0064	24	11	1.1	0.003878788	P_{best}
40	26	6	36	8	0.08	0.0064	24	14	1.4	0.006857143	P_{best}

In Table 5-11, the P_{best} variables for each particle (i.e., I^2, t^2 and C) were subtracted from the corresponding variables for P_{best} and g_{best} as shown in (5.14), (5.15) and (5.16). Since there are three variables for each particle, each particle will generate three new velocity equations. Hence, the ten particles, will generate a total of thirty new particles to optimise the variables for minimum switch energy.

5.5.3 Velocity equations for I^2, t^2 and C.

Velocity equation for I^2:

$$v_i^{k+1} = (w_k \times v_i^{k}) + ((c1 \times r1) \times (\mathbf{I^2P_b} - \mathbf{I^2P})) + ((c2 \times r2) \times (\mathbf{I^2g_b} - \mathbf{I^2P})) \quad (5.14)$$

Velocity equation for t^2:

$$v_i^{k+1} = (w_k \times v_i^{k}) + ((c1 \times r1) \times (\mathbf{t^2P_b} - \mathbf{t^2P})) + ((c2 \times r2) \times (\mathbf{t^2g_b} - \mathbf{t^2P})) \quad (5.15)$$

Velocity equation for C:

$$v_i^{k+1} = (w_k \times v_i^{k}) + ((c1 \times r1) \times (\mathbf{CP_b} - \mathbf{CP})) + ((c2 \times r2) \times (\mathbf{Cg_b} - \mathbf{CP})) \quad (5.16)$$

Where, $w_k = (0.5 \times (30-k)/30) + 0.4$, derived from equation (5.12).

5.5.4 Calculation of the PSO variables (I^2, t^2 and C) equations

From Table 5-11, the essential local cluster data was sorted and presented in Table 5-12, for execution of the PSO procedure. The subsequent tables contain the calculation for the parts of the respective equations which were used as input to the Objection function.

Table 5-12 Local cluster data for analysis

Rows in spreadsheet	D	E	F	G	H
	Rows in Table 5-11	I^2	t^2	C	Particle
10	18	4	0.0049	1	P
11	19	16	0.0049	1	P
12	20	1	0.0049	0.8	P
13	25	16	0.0036	1.5	P
14	28	1	0.0036	1.3	P
15	34	4	0.0049	1.2	P
16	35	1	0.0064	1.2	P
17	38	4	0.0064	1.1	P
18	39	25	0.0081	1.1	P
19	40	36	0.0064	1.4	P
20	41	1	0.0025	1.1	gb
21	43	16	0.0064	1.1	Pb

The parameter values for the three velocity equations for I^2 in (5.14), t^2 in (5.15) and C in (5.16), were taken from Table 5 12. Due to the volume of the data, it was entered in Appendix A -Table A1 in columns 'E', 'F' and 'G' respectively.

The PSO analysis continued in Appendix A until the optimised parameters were determined. These were: -

$$\text{Optimised Current, I Amps} = \sqrt{I^2} = \sqrt{5.168121} = 2.27 \text{ Amps}$$

$$\text{Optimised Switching period, t } \mu\text{s} = \sqrt{t^2} = \sqrt{0.004265} = 0.065 \ \mu\text{s}$$

$$\text{Optimised Capacitor, C } \mu\text{F} = 1.2924 \text{ Mf}$$

5.5.5 Validating the PSO result by PSpice simulation.

Reduction of IGBT energy.

Calculation of Snubber resistor R:

Let CR = t = 0.065μs,

and

$$R = \frac{0.065\mu s}{1.292\mu F} = 0.051\Omega$$

PSpice simulation was carried out for the turn-off snubber with values for C = 1.29μF and R = 0.05Ω. Figure 5-5, shows, the voltage, current and power traces from the simulation result.

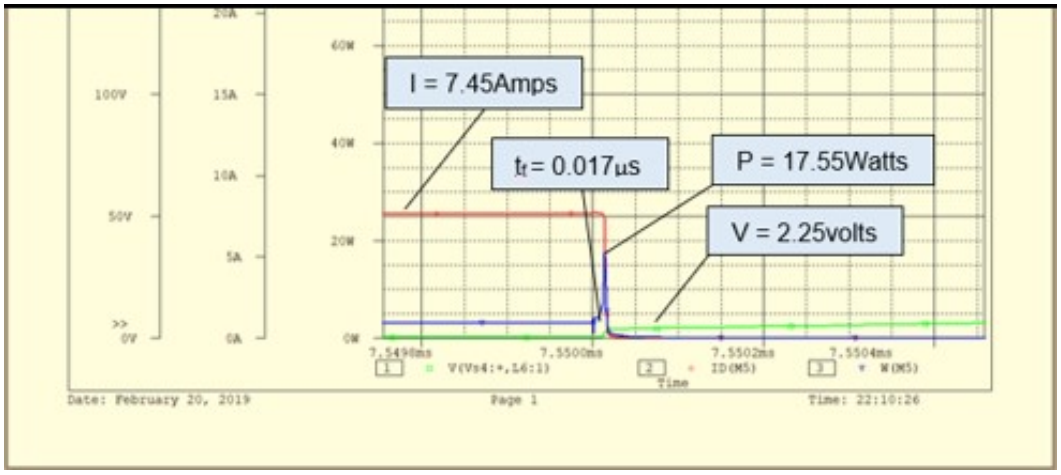

Figure 5-5 PSO Simulation Result showing V, I and P Traces

Reduction in Energy Level:

In Section 4.2.1.2, energy in switching device without E_{sw} = 30.7 µJ

Energy in switching device, with SC, $$E_{SW} = \frac{17.55W \times 0.017\mu s}{2} = 0.149\ \mu J$$

% Reduction in switch energy, $$E_{SW} = \frac{(30.7 - 0.149)}{30.7} \times 100\% = 99.51\%$$

5.5.6 Summary of PSO method

The PSO method resulted in the compilation of large data tables to provide 'visibility' to the procedure., Compared to the high reduction of 99.83% obtained by the GRG solver, in spite of the lengthy PSO method a reduction of 99.51% was obtained.

The spreadsheet calculations were initiated on the selection of a Local Cluster Particle Group resulting in a length of 30 iterations, and execution of the Velocity, Position and Momentum equations. These resulted in the selection of the optimised variables which were then subjected to the same process as the initial values which converged to a minimisation of the Objective Function in units of Joules. At this energy level, the final value of switching current I, snubber capacitor 'C' and turn-off time (t_f) were extracted and used for the components in a Turn-Off snubber circuit which was validated by PSpice simulation. The resulting reduction in energy level obtained was 99.76%.

MATLAB programme exists for other objective functions, but in this analysis higher energy reduction is possible, with MATLAB programming, with a larger iteration number of (>100). This method eliminates large tables but at a cost of program design and debugging.

However, use of the Spread Sheet PSO method provided an understanding of the updating process in the relationship between the parameters of the velocity and the 'particle position'.

5.6 Summary- Methods to Optimise Turn-Off Snubber Components for $E_{SW\text{-}Min}$.

Three methods were described to determine the optimum component values and minimum energy at switch turn-off transition period (t_{off}) in a switching device. Table 5-13, lists the methods, the corresponding (t_{off}), the reduction in the switch energy and the respective efficiencies. From this table a column plot is presented in Figure 5-6 to compare the energy levels and the switching efficiencies.

Table 5-13 Data for Switch Energy-EμJ, Efficiency and t_{off}-

Clause No.	Method (to determine RC)	t_{off} - μs	E - μJ	% Efficiency
4.2.1.2	No SC	0.074	30.7	-
5.1	PSpice Parametric	0.031	4.05	93.5
5.5	PSO	0.017	0.149	99.51
5.3	GRG-Solver	0.01	0.052	99.83

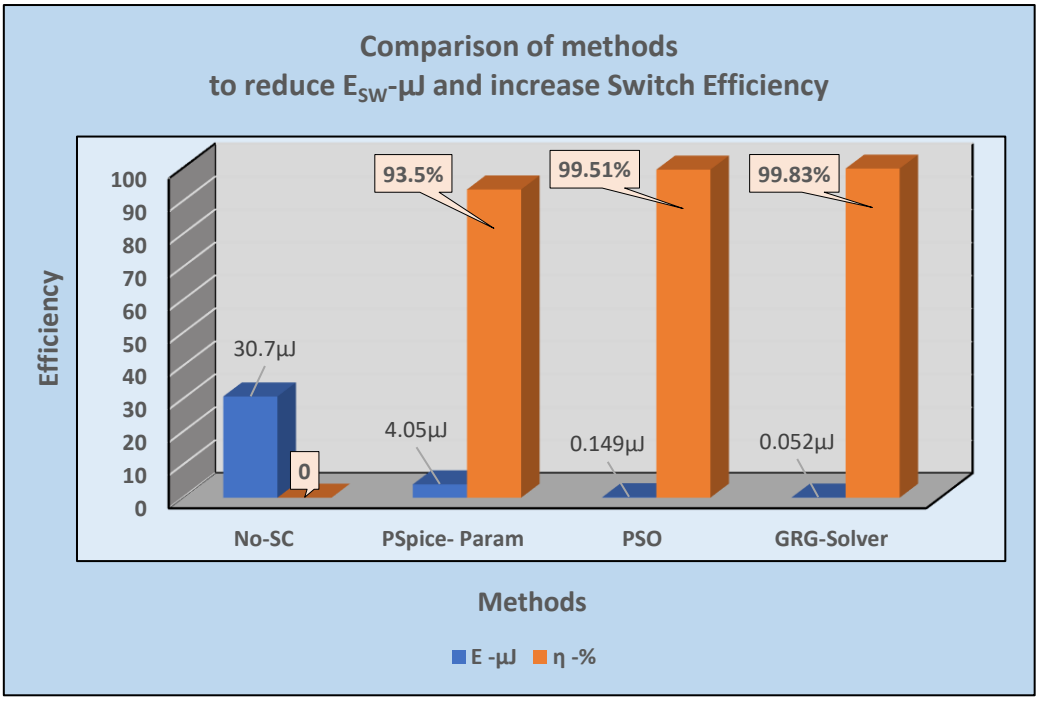

Figure 5-6 Comparison of Methods to reduce E_{SW}-μJ and Increase Switching Efficiencies

In Figure 5-6, the PSpice PARAM method, although not an optimisation technique, resulted in a close comparison to the results of the PSO and GRG Solver methods, especially in the reduction in switching efficiency of the IGBT at 93.5%. However, as expected, the two

Optimisers, PSO and GRG-Solver, achieved much lower switching energies and higher switching efficiency of 99.51% and 99.83% respectively.

The PSO method took a longer time to execute but made visible the various stages to solve the variable (I^2, t^2 and C) PSO equations. These stages can be applied to structure a MATLAB program as an efficient, effective, and fast alternative tool, which will compete closely to the fast GRG Solver method. For a fast and efficient optimisation procedure, Figure 5-6 validates the GRG solver's superior execution.

This chapter ends the analysis on snubber circuit used on a low power Buck-Boost Converter. The next chapter discusses thermal simulation on the Power IGBT to establish its Power (W) vs Junction Temperature (T_J ^{0}C) (W/T_J) characteristic, prior to its application in the case study of Energy Efficient SC used on a basic high power CHBMLC in HVDC Transmission Stations.

Chapter 6 COMSOL Thermal Simulation on Power IGBT

6.1 Safe Operating Area (SOA) determined from Thermal Simulation

For reliable and safe operation of the IGBT, it is important to ensure that subsequent to the reduction in switching loss, the Junction temperature T_J of the IGBT is less than the Maximum Junction Temperature, 'T_{Jmax}'. Since the snubber circuit when connected to the IGBT cannot be analysed by thermal simulation, it will be replaced by a heat sink to determine the IGBT SOA. The reduction of dissipated energy by the heat sink will be set as the target for the snubber circuit.

Thermal simulations with and without a heat sink fitted to the model of the IGBT, will determine the module case junction temperature T_J. Without heatsink fitted, the elevated and dangerous temperatures of T_J within the IGBT will be measured. These measurements will be compared to those with a heat sink fitted, to determine the safe T_J.

With the minimum and maximum power range given in the data sheet, the power dissipation in the IGBT at Turn-Off will be carried out. For the dissipation test, a heatsink will be designed which will be attached to the module. The results obtained will be used as a target reference for the snubber circuit connected to the IGBT. The difference between the case T_J and the data sheet T_{Jmax} will establish the limits for SOA.

For the thermal simulation, COMSOL Multiphysics software was used [79]. Detail requirements for the thermal simulation is given in [80], from which a brief input data for the simulation is given, such as:

Creation of Geometric Objects
- Model of IGBT (L, W, D)
- Design of Heatsink

Specification of material properties
- Heat capacity at constant pressure (Cp),
- Thermal conductivity (k)
- Density (rho)
- Specification of aluminium properties for heatsink

Given the above requirements, the Simulation was performed, followed by processing of the results. The power switch chosen for this study, is the 'Littelfuse IGBT Power Module-1200V, 600A (720kW), MG 12600WB-BRRMM' [15]. Maximum Junction Temperature 'T_{Jmax}' = 175^0C. This power switch was selected, since in PSpice the switch used in the low power analysis of the research has similar parameters which can be updated with the data sheet parameters of the selected switch, instead of importing the entire data into PSpice to create a new component.

6.2 Power IGBT case model design for Thermal simulation

The IGBT is encapsulated in a silicon carbide case (SiC) shown in Figure 6-1.

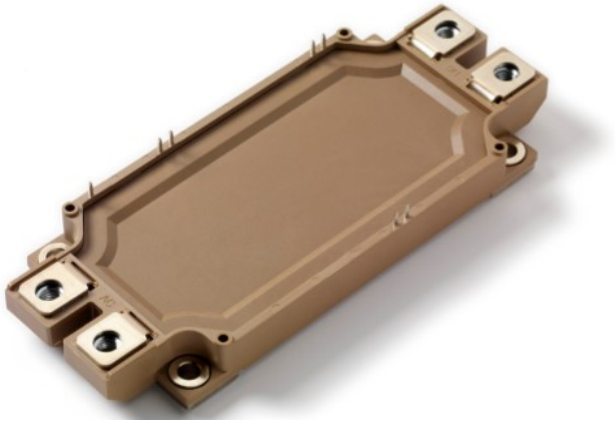

Figure 6-1 The Silicon Carbide (Sic) case for the IGBT [81]

The data sheet dimensions of the IGBT case is given in Figure 6-2.

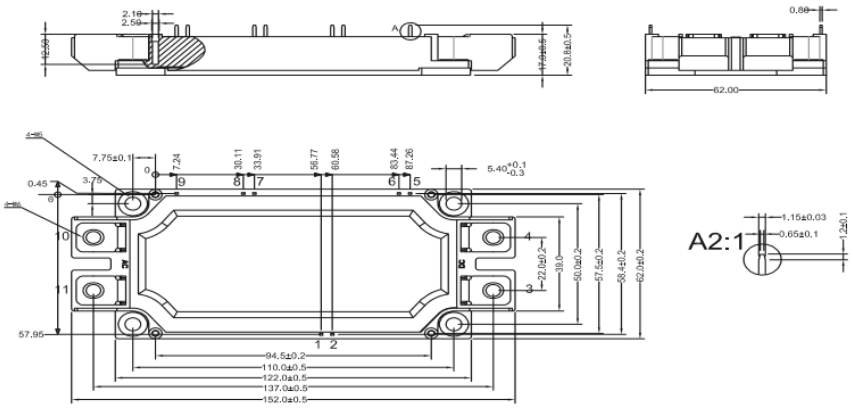

Figure 6-2 Physical parameter of the IGBT [81]

A model of the case was produced for the thermal simulation is shown in Figure 6-3.

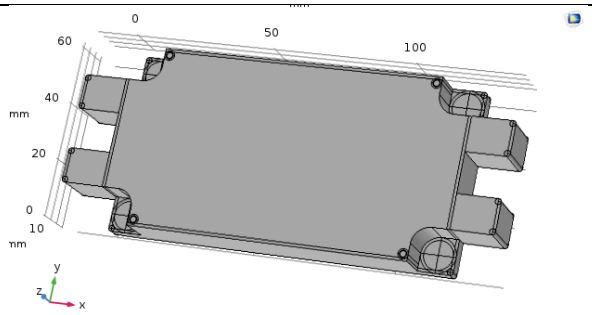

Length (L) = 100mm
Width (W) = 60mm
Depth (d) = 10mm

Figure 6-3 IGBT Model for Thermal Simulation

The case model is used in the next section for thermal simulation tests.

6.3 Input Power (Watts) vs T_J (^{0}C) for IGBT case model without heatsink

The power range used for the thermal simulation is shown in Table 6-1.

Table 6-1 Power Range for Thermal Simulation without Heatsink

INPUT POWER Q - W										
50	300	550	800	1050	1300	1550	1800	2050	2300	2550
5000	80000	155000	230000	305000	380000	455000	530000	605000	680000	Max-755000

From Table 6-1, twenty-two thermal simulations were carried out. A sample of five thermal images at input powers of, 50W, 5 kW, 230 kW, 380 kW and 755 kW (Red in Table 6-1) were selected as shown in Figure 6-4, Figure 6-5, Figure 6-6, Figure 6-7, and Figure 6-8. In these figures, change from dark red colours to lighter red, to yellow and finally to white colours indicate the range from high to higher temperatures, with Figure 6-8 showing the hottest temperature with White Heat.

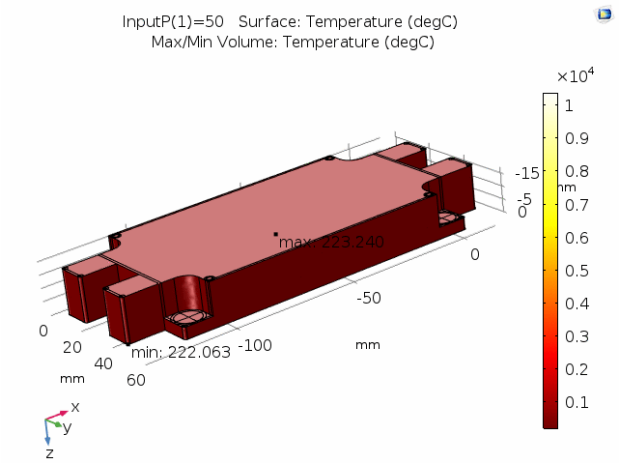

Figure 6-4 Thermal image of model - input 50 Watts, T_{min} = 222 ^{0}C, T_{max} = 223 ^{0}C

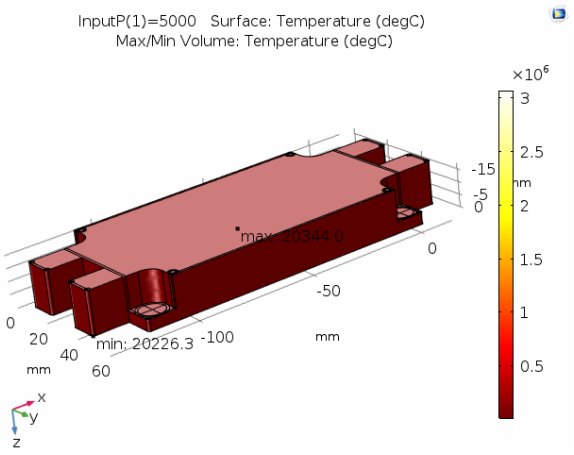

Figure 6-5 Thermal image of model - input 5 kW, T_{min} = 20226 ^{0}C, T_{max} = 20344 ^{0}C

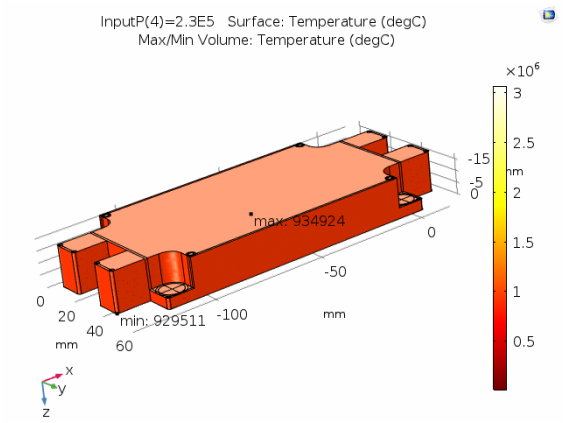

Figure 6-6 Thermal image of model - input 230 kW, T_{min} = 929511 ^{0}C, T_{max} = 934924 ^{0}C

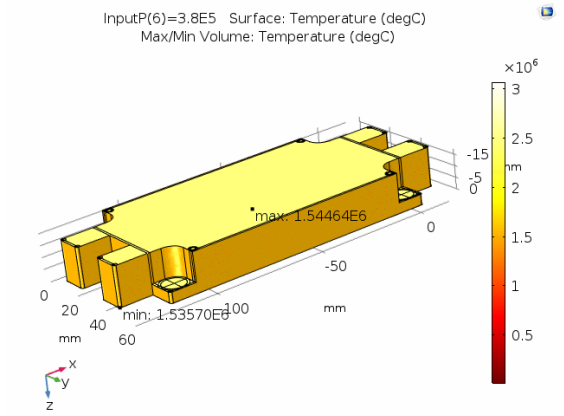

Figure 6-7 Thermal image of model - input 380 kW, T_{min} = 1.53E6 ^{0}C, T_{max} = 1.54E6 ^{0}C

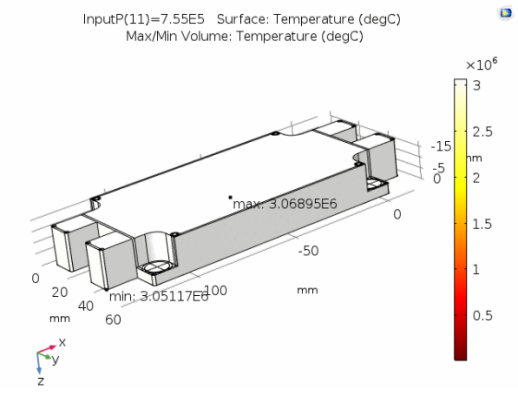

Figure 6-8 Thermal image of model input 755 kW, T_{min} = 3.05E6 ^{0}C, T_{max} = 3.06E6 ^{0}C

6.3.1 Thermal Simulations Results

The thermal conduction equation [82], for the package of a semiconductor is given by,

$$Q = \frac{KA\,(T_J - T_C)}{d} \quad \text{Watt} \tag{6.1}$$

Where:

Q = Conduction heat transfer or the switch loss (W)

K = Silicon carbide (Sic) module material thermal conductivity. K = 170 W/mK

A = Cross sectional area (m²)

T_J = Chip junction temperature (°C)

T_C = Module case temperature (°C)

d = Material thickness (m)

From (6.1), the Junction Temperature is,

$$T_J = \frac{Q\,d}{K\,A} + T_C \quad {}^0C \tag{6.2}$$

In (6.2) let, $\frac{d}{KA} = C$ as d, K and A are fixed values.

and

$$T_J = QC + T_C \quad {}^0C \tag{6.3}$$

6.3.1.1 Calculation of constant 'C'

From Figure 6-2, Plan Elevation, W = 62 mm = 0.062 m, L = 137 mm = 0.137 m. Area is,

$$A = (W \times L)m^2 = (0.062 \times 0.137)m^2$$
$$= 8.494 \times 10^{-3} m^2$$

and from Figure 6-2 side elevation d = 12.5 mm, and constant 'C' is,

$$C = \frac{d}{K \times A}$$

$$C = \frac{0.0125\ m}{170\frac{W}{mK} \times 8.494 \times 10^{-3}\ m^2} = 0.00866 \cong 0.01$$

For the range of power values (Q-Watts) in Table 6-1, the measured values of module case temperature (T_C ^{0}C), the Junction temperatures (T_J ^{0}C) were calculated and presented in Table 6-2 and Table 6-3.

Table 6-2 Thermal simulation results without Heatsink-from low to high Power

Q (W)	50	300	550	800	1050	1300	1550	1800	2050	2300	2550
C	0.01	0.01	0.01	0.01	0.01	0.01	0.01	0.01	0.01	0.01	0.01
Tc ^{0}C	223	1239	2256	3272	4288	5304	6320	7337	8353	9369	10385
T_J ^{0}C	224	1242	2261	3280	4299	5317	6336	7355	8373	9392	10411

Table 6-3 Thermal results without Heatsink-from high to very high Power

Q	5000	80000	15500	23000	305000	380000	455000	530000	605000	680000	755000
C	0.01	0.01	0.01	0.01	0.01	0.01	0.01	0.01	0.01	0.01	0.01
Tc	2034	32520	63006	934,92	1,239,78	1,544,64	1,849,51	2,154,37	2,459,23	276409	306895
T_J	2039	32600	63161	93722	1242838	1548449	1854060	2159671	2465282	277089	307650

From Table 6-2 and Table 6-3, Figure 6-9 and Figure 6-10 were plotted.

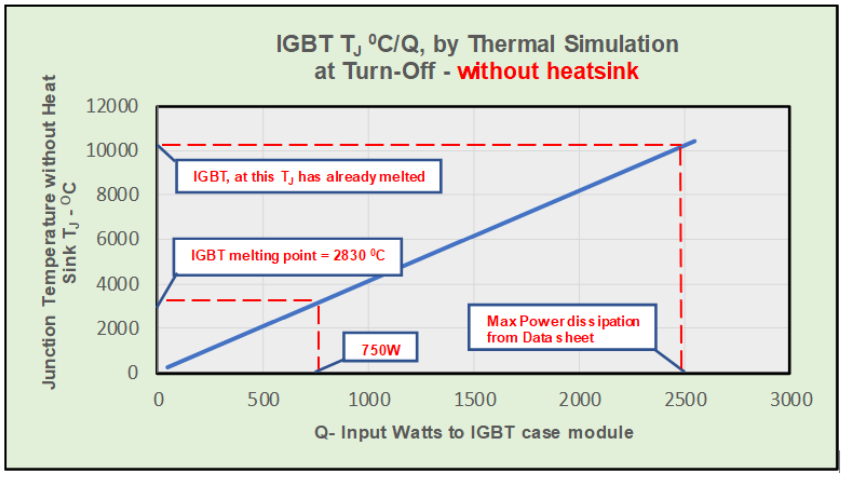

Figure 6-9 Shows the IGBT melting point at low power of 750 Watts

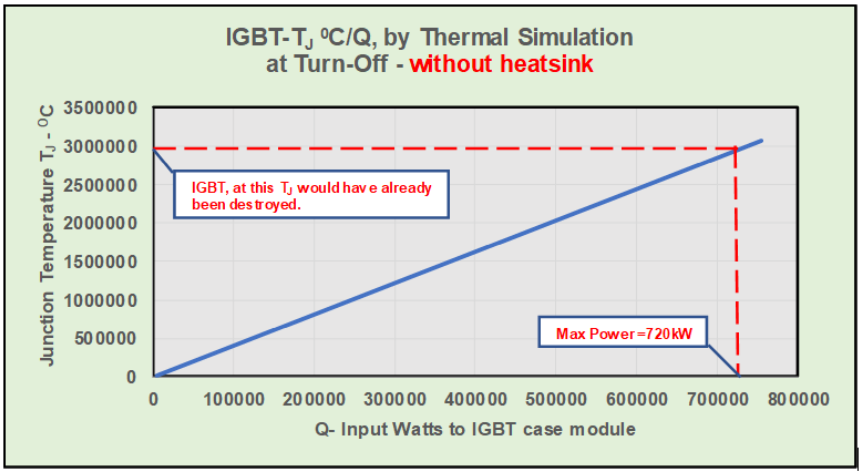

Figure 6-10 Destruction of IGBT without protection at higher power ranges

The above results have shown, that without any type of cooling for heat dissipation from the IGBT or switching energy reduction by use of snubber circuit, the IGBT would not be capable of switching power at a level 750W. To prevent damage to the IGBT and possibly to associated components, thermal simulations from low power to a maximum power with heatsink fitted follows.

6.4 T_J (^{0}C) vs IGBT dissipation loss at t_{off} – 20 W to 2.5 kW_{max}, with heatsink.

For the above IGBT, the total power dissipation given in the data sheet = 2500 W

100 cm ² of aluminium dissipates 10 W [82].

Therefore, to dissipate 2500 W, total heatsink area,

$$A = \frac{2500}{10} \times 100\ \text{cm}^2 = 25000\ \text{cm}^2$$

For a square base, dimension of the sides would be,

$$\text{Side dimension} = \sqrt{25000}$$

$$\approx 158 \text{ cm}$$

The area (25000 cm^2) must be shared with fins to reduce the large flat metal if such a heat sink was used. Therefore, the area must be divided between a base and several fins. The calculation carried out to determine the dimensions of the base and fins are shown in Table 6-4, from which the dimensions in red were chosen to design the heatsink as it produced a smaller footprint.

Table 6-4 Calculation of heatsink base and fins

Total Area	Heatsink base -cm		Area		Suggested FIN dimensions		Area	Number of Fins = (A-A1)/A2
A -cm^2	L	W	A1 = L x W cm^2	A - A1	l-cm	w-cm	A2 = l x w cm^2	
25000	30	20	600	24400	30	20	600	40
				24400	35	25	875	27
25000	30	30	900	24100	30	20	600	40
				24100	35	25	875	27
Note: Thickness of fins and base plate = 5 mm								

6.4.1 Heatsink Model for Thermal simulation

Figure 6-11, shows the COMSOL heatsink model

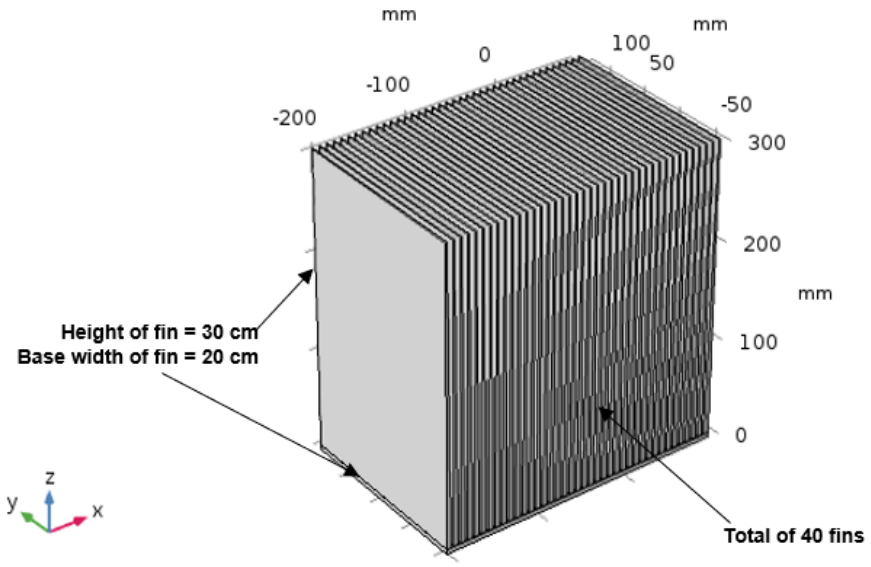

Figure 6-11 COMSOL model of the heatsink with 40 FINS

6.4.2 COMSOL Thermal Simulations with Heatsink fitted to module

Thermal simulations were carried out for the input range of Q watts shown in Table 6-5.

Table 6-5 Input watts for Heatsink dissipation.

Q Watts – (5 to 15) W and (20 to 2520) W - Dissipation in module										
5	6	7	8	9	10	11	12	13	14	15
20	270	520	770	1020	1270	1520	1770	2020	2270	2520

Thermal simulation results at 20 W and 2520 W (2500 W = Module Maximum dissipation) are shown in Figure 6-12 and Figure 6-13

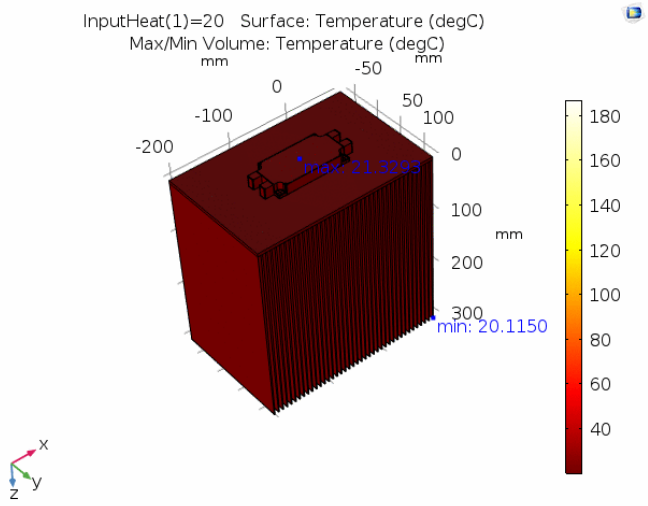

Figure 6-12 Heat dissipation in module and heatsink for Q = 20 Watts with Tc = 21.329^{0}C

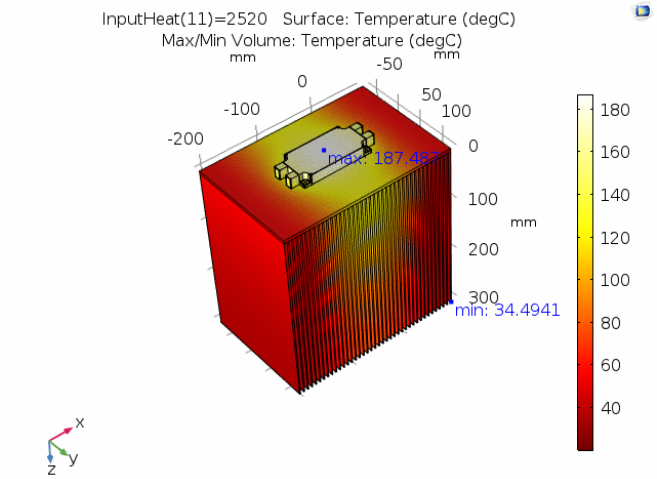

Figure 6-13 Heat dissipation in module and heatsink for Q = 2.52 kW with Tc = 187.49 ^{0}C

6.4.3 COMSOL Thermal Simulation Results of Heatsink Fitted to Module

From Section 6.3.1.1 constant 'C' was calculated to be 0.01. The module junction temperatures T_J ^{0}C was calculated for the twenty-two input power dissipation range (Q-Watts). The values of T_J, 'C', and T_C were entered for the range of Q from 5 Watts to 2520 Watts to establish the SOA (and not to 720 kW) in Table 6-6.

Table 6-6 Calculation of IGBT T_J
for lower input power range, with Heatsink

Q Watts	C	Q*C	T_C (^{0}C)	T_J(^{0}C)
5	0.01	0.05	20.332	20.382
6	0.01	0.06	20.398	20.458
7	0.01	0.07	20.465	20.535
8	0.01	0.08	20.531	20.611
9	0.01	0.09	20.598	20.688
10	0.01	0.1	20.664	20.764
11	0.01	0.11	20.731	20.841
12	0.01	0.12	20.797	20.917
13	0.01	0.13	20.864	20.994
14	0.01	0.14	20.93	21.07
15	0.01	0.15	20.997	21.147
20	0.01	0.2	21.329	21.53
270	0.01	2.7	37.945	40.59
520	0.01	5.2	54.561	59.66
770	0.01	7.7	71.177	78.73
1020	0.01	10.2	87.794	97.79
1270	0.01	12.7	104.41	116.86
1520	0.01	15.2	121.03	135.93
1770	0.01	17.7	137.64	154.99
2020	0.01	20.2	154.26	174.06
2270	0.01	22.7	170.87	193.12
2520	0.01	25.2	187.49	212.19

From Table 6-6 a plot of T_J ^{0}C vs Q watts (5 W to 15 W) is shown in Figure 6-14.

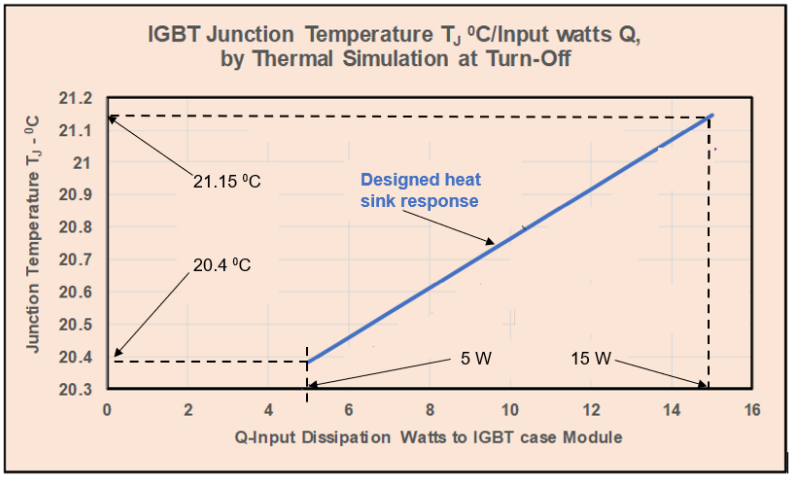

Figure 6-14 Plot of IGBT T_J
against a Lower Power Dissipation Range

In Figure 6-14, the blue trace shows that the power module with the designed heatsink have an input power range from 5 W to 15 W, operating at a low T_J range of 20.4 ^{0}C to 21.15 ^{0}C. In Figure 6-15, a plot for the complete range of T_J ^{0}C vs Q watts (5 W to 2520 W) is presented.

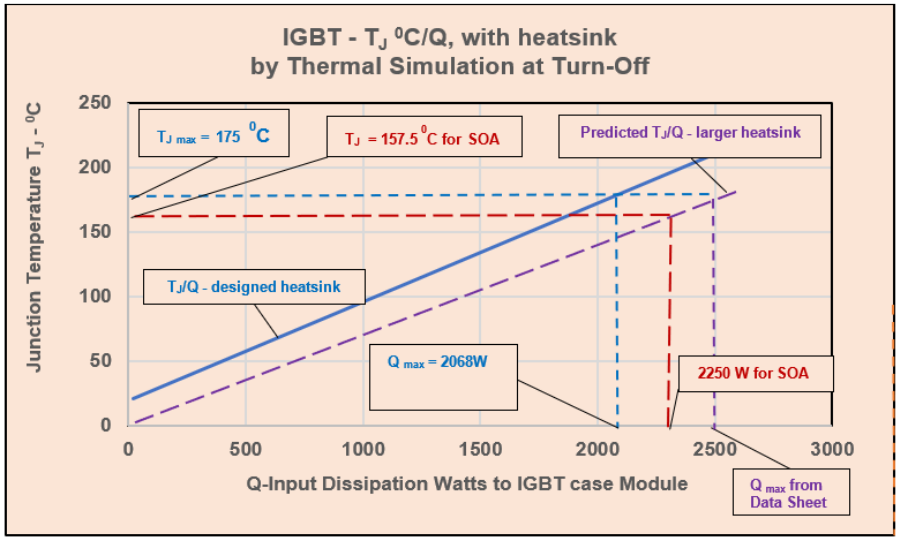

Figure 6-15 Plot of IGBT Junction Temperature
Against a Higher Power Dissipation

The solid blue trace in Figure 6-15 predicts a maximum input of 2068 watts at the data sheet T_J of 175 ^{0}C, compared to the 2500 Watts maximum for the IGBT. Shifting the vertical dotted blue line to meet the 2500 Watts, intersects with the horizontal dotted blue line which corresponds to the $T_{J\,max}$ of 175 ^{0}C. The change from 2068 Watts to 2500 Watts is an increase of 17 %. Hence, an increase of 17% in the heatsink size (shown by the dotted violet line) would comply with the required data sheet IGBT dissipation. Extracted data from Figure 6-15 is entered in Table 6-7.

Table 6-7 Results from linear response of T_J vs Dissipated power in Watts

Solid and dashed Traces	Q_{max} Dissipated I/P Watts in IGBT	IGBT Junction Temperature-$T_{J\,max}$
Designed heatsink (solid **blue** line) – based on 10W/100cm^2	2068 reduced from 2500 (17% reduction from data sheet value)	175^{0}C (data sheet)
Resized heatsink (dashed **violet** line) - an increase of 17%, larger area to dissipate more heat.	2500 (data sheet)	175^{0}C (data sheet)
For SOA-Resized heatsink (dashed **red** line)	Operate at 90% Q_{max} = 2250W - SOA	157.5^{0}C for a SOA = 90% $T_{J\,max}$

From Table 6-7, the operating conditions with the designed heatsink. The use of the heatsink in the thermal simulation enabled the design of the SOA in the case study for the power IGBT-MG 12600WB-BRRMM is shown in Table 6-8.

Table 6-8 Operating conditions (SOA) for IGBT- with heatsink

IGBT- Data Sheet Parameters		IGBT-Safe Operating Area -SOA
Max. Power	720 kW	648 kW
Max. Dissipation	2500 Watts	2250 Watts
Max Jun Temp -$T_{J\,max}$	175 ^{0}C	157.5 ^{0}C
Supply voltage	1200 Volts	1200 Volts
Load current	600 A	540 A

6.5 Summary of COMSOL Thermal Simulation Results

The thermal simulation have shown that the Power IGBT without any means of cooling or reduction of switching loss by a snubber circuit, will be destroyed at a low input power of 750 Watts, as at this power it reaches its melting point of 2830 ^{0}C. To avoid irreparable damage, the input power must be maintained below 750 Watts, which degrades its power rating below the complete range to 720 kW.

The designed heatsink was employed as a replacement for the snubber circuit, since the latter could not be tested under Thermal simulation. The heatsink was effective in dissipating the heat from the IGBT, which resulted in an SOA within the maximum data sheet ratings, which justifies the heatsink design. In the next chapter, this SOA will be validated by PSpice simulation of the snubber circuit with the same input power range to a maximum load of 648 kW. At this load, the snubber circuit is expected to reduce the IGBT switching loss to 2250 Watts.

The thermal simulation was effective as an additional tool to measure the IGBT dissipation loss which can greatly improve the reliability, safe operation, and design of switching circuits. In this case it provided a kW vs T_J reference chart for snubber circuits. The next Chapter will investigate Energy Efficient snubber circuits used in a CHBMLC and applying where necessary the results obtained in the above Thermal simulation, especially to the SOA for the IGBT in Power Inverter.

Chapter 7 Design of EESCs In High Power Converter

7.1 Introduction

The previous chapters discussed snubber circuit at low power providing experience in their design. Followed by Chapter 6 which applied COMSOL multi-physics thermal simulation and resulted in the design of an SOA for high power IGBT. This chapter will apply those ideas and results to the analysis of (EESCs) in high power CHBMLC.

Review of articles on CHBMLC, have shown that the dissipated energies in the bridges during the switching cycle were wasted or used in (non-electrical) heating applications, e.g., for the heating of onsite buildings of the HVDC converter stations. Furthermore, the review lacked any reference to the protection of the IGBTs in CHBMLC, except that water cooling or other refrigeration methods were used to avoid thermal damage to the switches. Figure 7-1 is a simple schematic of an CHBMLC circuit with fly back diodes connected across the power switches [4].

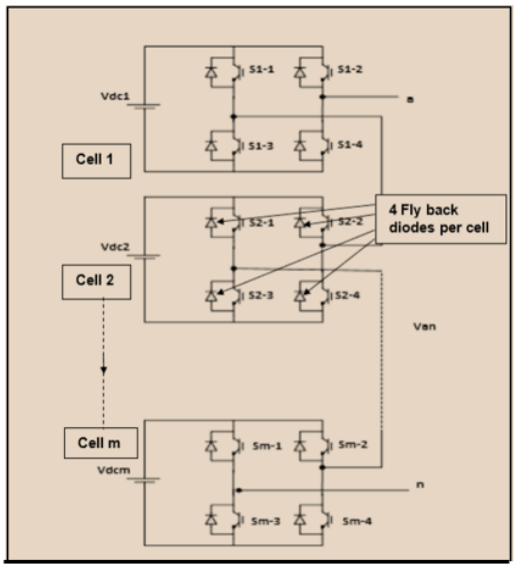

Figure 7-1 CHBMLC with '1 to m' cells with
4-IGBTs and diodes per bridge [4]

Figure 7-2, shows a schematic of a 3-Ph Converter Station A and B for a bipolar HVDC Transmission Line [83]. This case study analysed the effectiveness of the EESCs when connected to the inverter section of the HVDC lines.

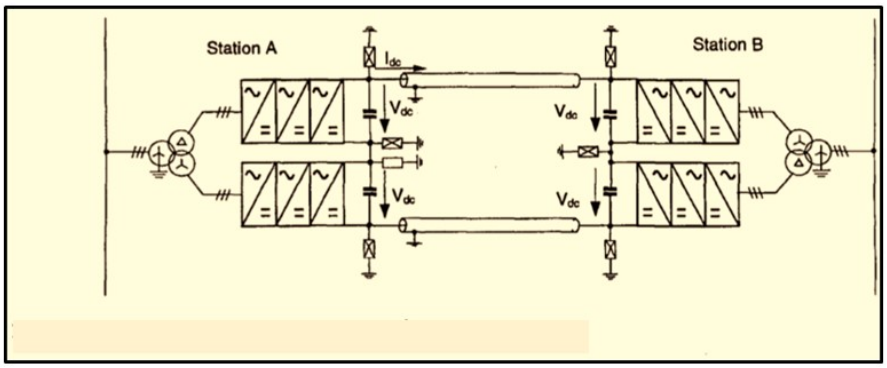

Figure 7-2 Schematic Example of a HVDC Transmission System [83]

The proposed EESC provided protection to the IGBTs and recovered the switching energies, consequently reducing the dependence on the present method of liquid refrigerants and forced water or air-cooling methods to reduce the radiated heat from the power semiconductor during the switching transitions. Figure 7-3, shows two examples of expensive cooling methods for IGBTs [3]. Appendix D presents a recent research into improving the cooling of HVDC converter by changing the medium from water to a fatty acid ester-based fluid with a viscosity of 100 times that of water, but the pumping power was 17% higher than for water [3]. However, the cooling of HVDC Converters continue to be a circulatory water pumping circuit, similar to that of pumping water via a radiator to cool a car engine.

Application of current Industrial kWh unit tariffs was used to estimate the cost of wasted heat due to the present methods of cooling the ‘assemblies of large stacks’ of switching devices used in HVDC converter stations. The findings are presented under section 7.6.4.1 and section 7.6.5.

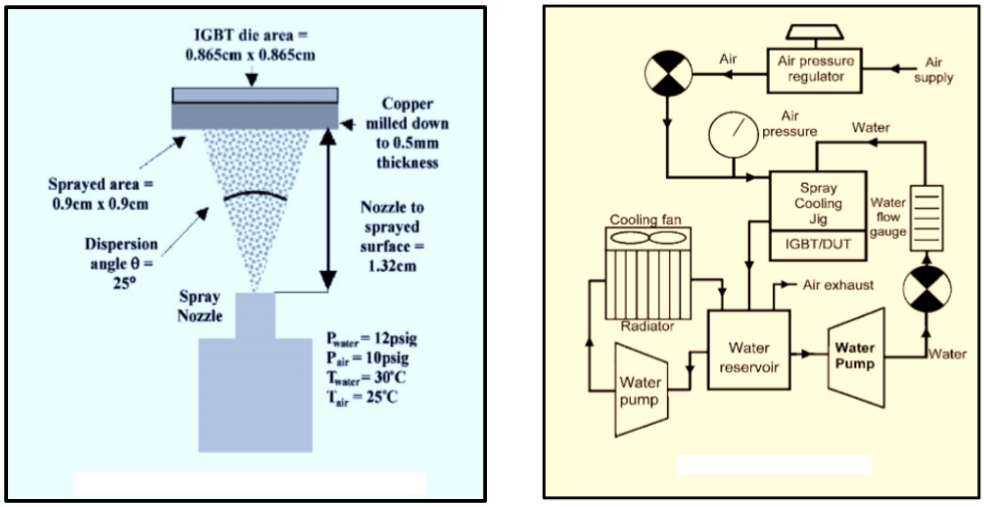

Figure 7-3 Spray and Air-Water cooling methods for Power Switching devices [3]

7.2 Requirements for the 3-Bridge 7-level Cascaded Inverter

Before the PSpice schematic can be designed, the DC voltage for the CHBMLI voltage level had to be selected. This voltage is dependent on the ratings of the chosen IGBT, the 'Littelfuse Power Module-1200 V, 600 A (720 kW), MG12600WB-BRRMM', which was subjected to COMSOL multi-physics thermal simulation in Chapter 6. After updating the PSpice IGBT component library module (IRF840) with the parameters of the Littlefuse Power IGBT and with simulation test runs, the schematic (Figure 7-4) was finalised with the level of DC supply of 550 volts that allowed successful simulations.

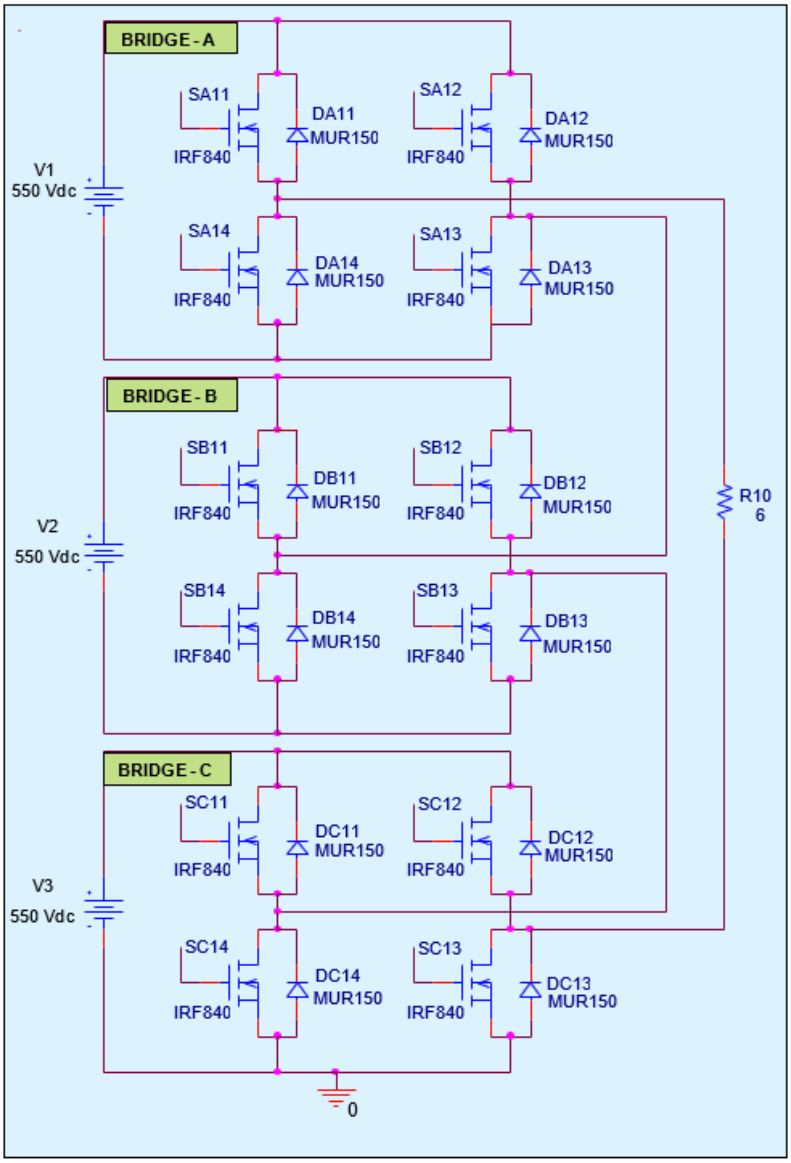

Figure 7-4 Basic schematic with Bridges A, B & C in series with a resistive load

7.2.1 IGBTs switching periods for the Positive and Negative Output voltages.

Figure 7-5 shows the pulse widths (PW) for the voltage levels to generate the symmetrical inverter output voltage and Figure 7-6 shows the series circuits for switching the 550 volts per bridge to increase the positive and negative half cycles of the output inverter voltage.

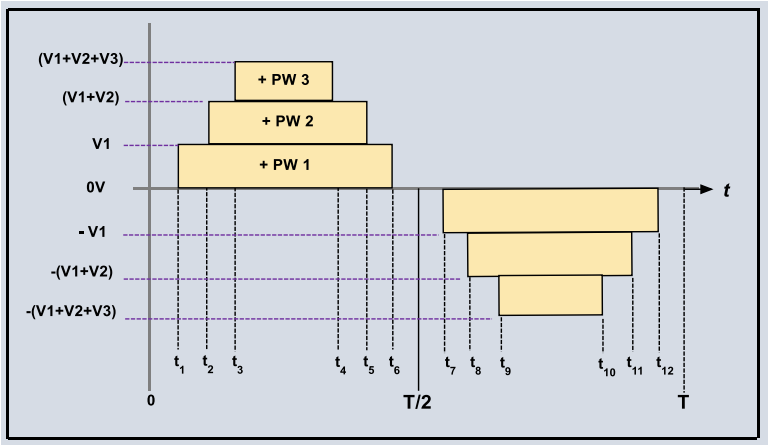

Figure 7-5 Switching sequence for Positive and Negative Inverter voltage with 7-levels

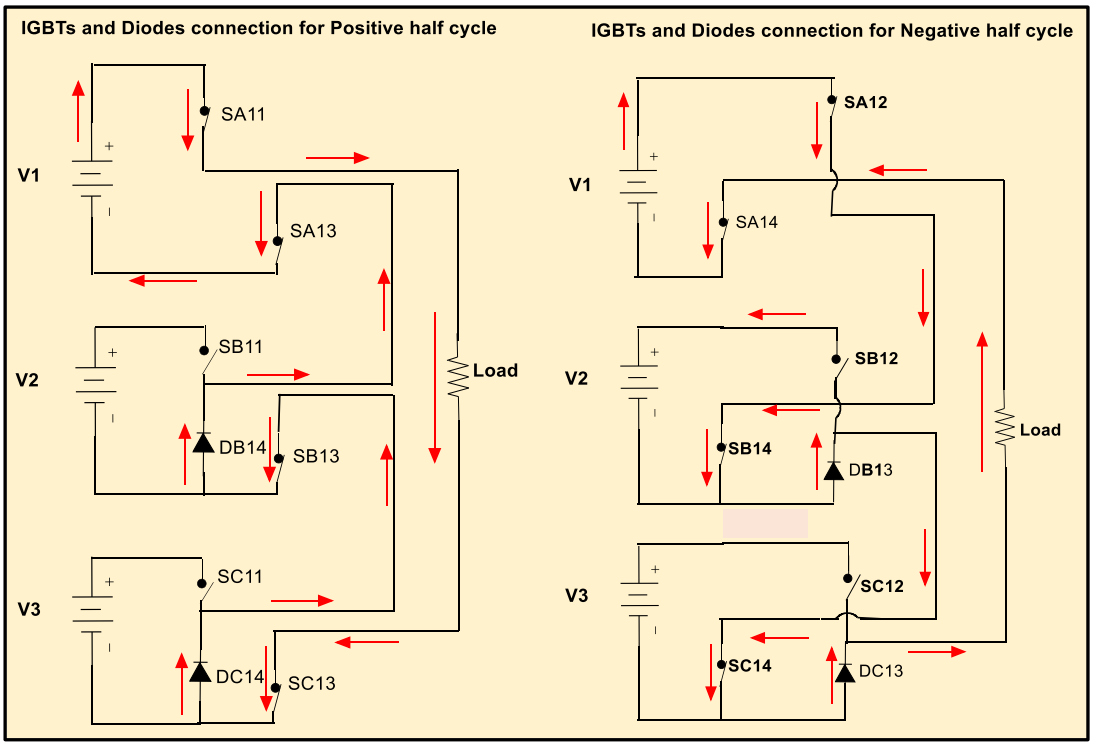

Figure 7-6 Circuit for the Inverter Positive and Negative Half Cycles Output Voltage

In Figure 7-6, the switching circuits for the positive and negative inverter output voltage have been separated to illustrate how the direction of current in the load is reversed.

7.2.1.1 Circuit components to Generate PW-1

For the positive output voltage, IGBTs, SA11, SC13, SB13, SA13 are closed with DC14 and DB14 conducting with IGBT-SB11 and SC11, open to produce PW-1 in Figure 7-5. Hence, IGBTs, SA11, SC13, SB13 and SA13 are switching in phase with the same On-Off drive signals.

7.2.1.2 Circuit components to Generate PW-2

To produce PW-2, on the top of PW1, IGBT- SB11 closes and DB14 is reversed biased due to V 2 now in circuit.

7.2.1.3 Circuit components to Generate PW-3

To produce PW-3, IGBT-SC11 closes and DC14 is reversed biased due to V 3 now in circuit. These IGBTs are switching with shorter periods as shown in Figure 7-5.

Similarly, for the negative output voltage, the complementary IGBTs and Diodes will generate the corresponding PW-1, PW-2, and PW-3.

7.2.2 Switching angles Θ_1, Θ_2 and Θ_3 for at Level 1, Level 2 and Level 3 voltages

For an H-Bridge 7-level Inverter, a comparative study [84] was carried out to determine the switching angles Θ_1, Θ_2 and Θ_3, corresponding to t_1, t_2 and t_3 in Figure 7-5. The calculation of these angles included the reduction of the 5th and 7th harmonics. An extract from the table is shown in Table 7-1, for Modulation Index (Mi), 0.75 to 1 together with the values for the three angles and %THD being the same for PSO and GA. Hence, to determine the switching times (t_1 to t_{12}) in Figure 7-5, the values for the chosen angles are, $\Theta_1 = 5.4^0$, $\Theta_2 = 16.4^0$ and $\Theta_3 = 34.8^0$.

Table 7-1 Calculation of switching angles and THD by different Methods [84]

Mi	Θ1			Θ2			Θ3			% THD		
	NR	PSO	GA	NR	PSO	GA	NR	PSO	GA	NR	PSO	GA
0.7	18.3	5.3	5.3	44.1	16.6	16.6	35.0	35.0	35.0	11.4	5.2	5.2
0.75	13.5	5.4	5.4	36.6	16.5	16.5	34.9	34.9	35.0	7.8	5.2	5.2
0.8	11.5	5.4	5.4	28.7	16.5	16.5	34.8	34.8	34.8	8.0	5.2	5.2
0.85	**	5.4	5.4	**	16.4	16.4	34.8	34.8	34.8	**	5.2	5.2
0.9	11.2	5.4	5.4	13.4	16.4	16.4	34.8	34.8	34.8	9.2	5.2	5.2
0.95	**	5.4	5.4	**	16.4	16.4	34.8	34.8	34.8	**	5.2	5.2
1	**	5.4	5.4	**	16.4	16.4	34.8	34.8	34.8	**	5.2	5.2

7.2.3 Calculation of the IGBTs Switching periods

The t_1, t_2 and t_3 switching times corresponds to $\Theta_1 = 5.4^0$, $\Theta_2 = 16.4^0$ and $\Theta_3 = 34.8^0$ The half cycle of the output voltage is 180^0 which corresponds to 10 ms. Hence, the simple equation (7.1) is presented which was used to convert Θ_1, Θ_2 and Θ_3. The result of the calculations is shown in Table 7-2.

$$\sum_{k=1}^{\theta} t_k = 10\text{ms} \times \sum_{k=1}^{\theta} \theta_k \times \frac{1}{180^0}\ \text{ms} \ldots\ldots \theta_1 = 5.40^0, \theta_2 = 16.40^0 \text{ and } \theta_3 = 34.80^0 \quad (7.1)$$

Table 7-2 IGBTs in the CHB7-LI switching times (ms)

Positive half cycle								Negative half cycle						
t_0	t_1	t_2	t_3	t_4	t_5	t_6	T/2	t_7	t_8	t_9	t_{10}	t_{11}	t_{12}	T
0	0.3	0.91	1.93	8.1	9.1	9.7	10	10.3	10.91	11.93	18.1	19.1	19.7	20

7.2.4 Identification of IGBTs to generate the Inverter output voltage.

From Figure 7-5, Figure 7-6, and Table 7-2, the IGBTs and their switching pulse widths (PW) have been determined and presented in Table 7-3. This identifies the IGBTs with common drive signals, and those IGBTs which require separate drives.

Table 7-3 Identification of IGBTs and Switching Periods for CHB-7LC Output Voltage

BRIDGE	Inverter output voltage – Period (PER) = 20ms													
	IGBT & Diodes Switching Periods – ms	Positive – T/2 = 10ms						Negative – T/2 = 10ms						
		V1		V1+V2		V1+V2+V3		-V1		-(V1+V2)		-		
		On (t_1)	Off (t_6)	On (t_2)	Off (t_5)	On (t_3)	Off (t_4)	On (t_7)	Off (t_{12})	On (t_8)	Off (t_{11})	On (t_9)	Off (t_{10})	
		0.3	9.7	0.91	9.1	1.93	8.1	10.3	19.7	10.91	19.1	11.93	18.1	
	PW - ms	9.4		8.19		6.17		9.4		8.19		6.17		
A	SA11	1	0											
	SA12							1	0					
	SA13	1	0											
	SA14							1	0					
	DA11													
	DA12													
	DA13													
	DA14													
B	SB11			1	0									
	SB12									1	0			
	SB13	1	0											
	SB14							1	0					
	DB11													
	DB12													
	DB13							1	0					
	DB14	1	0											
C	SC11					1	0							
	SC12											1	0	
	SC13	1	0											
	SC14							1	0					
	DC11													
	DC12													
	DC13							1	0					
	DC14	1	0											

In Table 7-3, for the output voltage of V1 with period of (0.3ms to 9.7ms), IGBTs, SA11, SA13, SB13 and SC13 are connected to drive generators with ON time at 0.3ms and OFF time at

9.7ms. For the output voltage of (V1+V2) with period of (0.91ms to 9.1ms), IGBT SB11 is connected to a drive generator with ON time at 0.91ms and OFF time at 9.1ms.

For the output voltage of (V1+V2+V3) with period of (1.93ms to 8.1ms) IGBT SC11 is connected to a drive generator with ON time at 1.93ms and OFF time at 8.1ms. Similarly, the Negative output voltage is generated in the same way as for the Positive output voltage, except the drive generators timings are increased by 10ms, to place the negative output voltage in the second half of the 20ms period.

7.2.5 Setting the IGBT Drive Signal Generator in PSpice.

From Table 7-3, the IGBTs' were identified for each output voltage level and the gate drive signals were defined and shown in Figure 7-7.

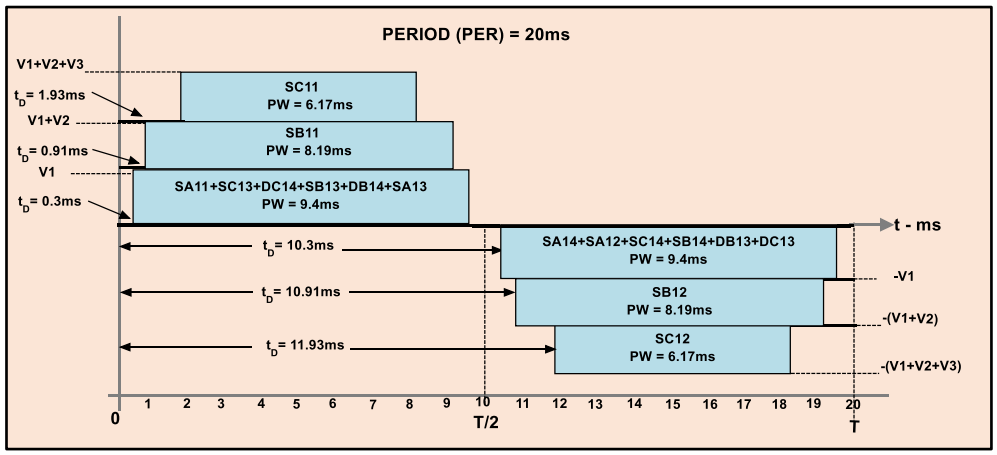

Figure 7-7 CHB7-Level Inverter IGBTs, PWs and switching delays t_D

The parameters t_D, PW and PER defined in Figure 7-7, were used to modify the PSpice V-Pulse generator to drive the IGBTs. The IGBT used in PSpice simulation was the IRF840. It was modified via the model editor with the parameters shown in Table 7-4 for the IGBT Power module 1200V, 600A, MG12600WB-BR2MM [75]. This procedure avoided importing into PSpice Component Library the entire data sheet for the power module.

Table 7-4 Essential Parameters of the IGBT Power module

Parameters for Power module 1200V, 600A, MG12600WB-BR2MM		
Parameter	**Description**	**Value**
T_{Jmax}	Max. Junction Temp.	175^0C
V_{CES}	Collector Emitter Voltage	1200V @ $T_J = 25^0$C
V_{GES}	Gate Emitter Voltage	± 20V
I_C	DC Collector Current	750A @ $T_C = 25^0$C, 600A @ $T_C = 80^0$C
P_{tot}	Power dissipation	2500W
t_r	Rise Time	220ns @ $T_J = 25^0$C, 240ns @ $T_J = 125^0$C
t_f	Fall Time	170ns @ $T_J = 25^0$C, 190ns @ $T_J = 125^0$C
E_{on}	Turn-on energy	20mJ @ $T_J = 25^0$C, 35mJ @ $T_J = 125^0$C
E_{off}	Turn-off energy	105mJ @ $T_J = 25^0$C
R_{thJC}	Junction-to-Case Thermal Resistance	0.06K/W
Note: For IGBT turn-on Resistance is given by the dv/di gradient at Figure 2 in the data sheet. I_C = 150A and V_{CE} = 275V		

7.2.6 PSpice schematic with IGBT Drive Generators connected

Having established the parameters for the IGBTs Drive generators and updated the IGBT with the ratings for the Power module, the PSpice schematic (without snubber circuits) was designed and shown in Figure 7-8.

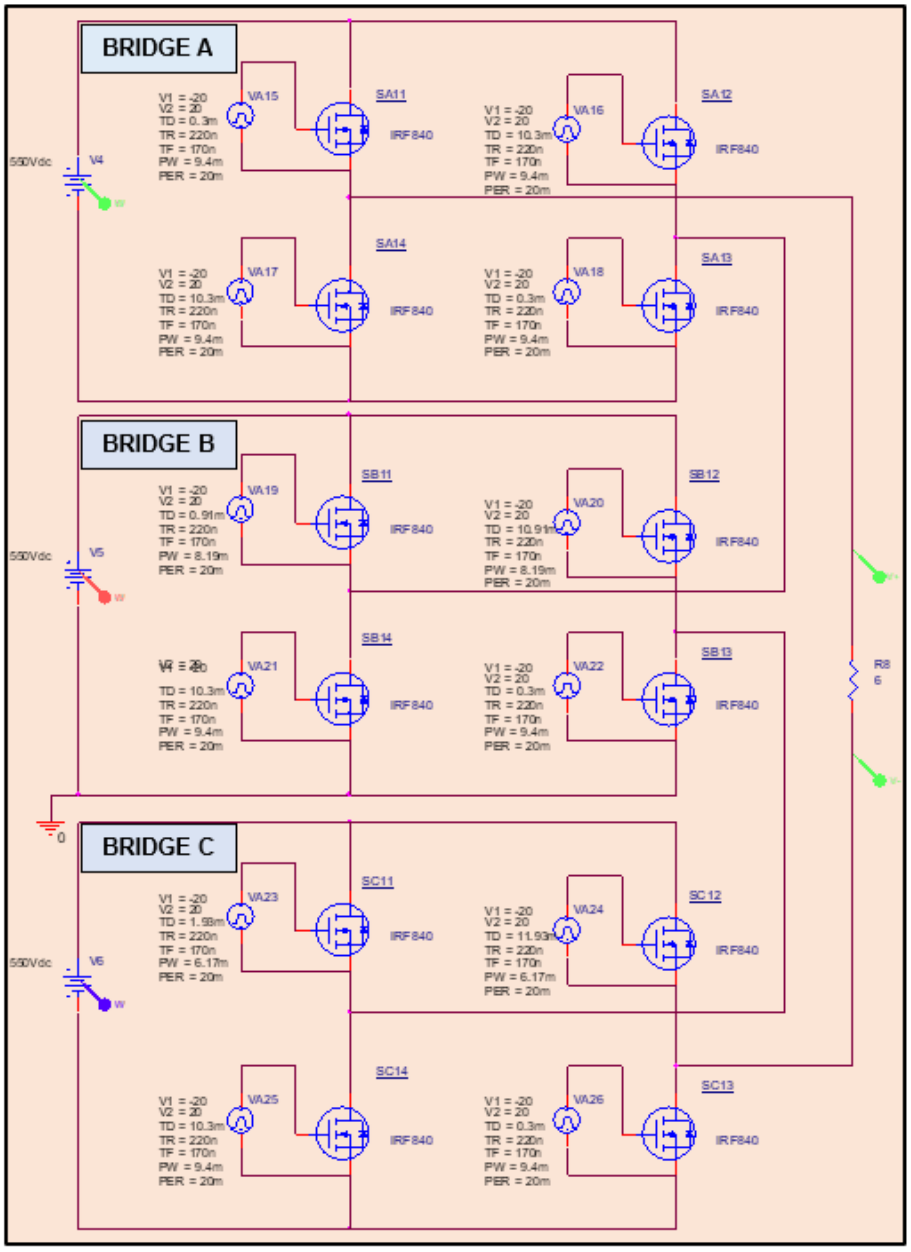

Figure 7-8 PSpice schematic with IGBTs Drive generators connected

7.2.7 Measurement of CHB7LC Switching and Dissipated Energy

The difference between the measured energy (by simulation) delivered by the supply batteries and the measured load energy gives the switching and dissipated energy. An annual cost figure of the wasted dissipated energy can be calculated when standard National Industrial kWh tariffs are applied. Later in this chapter, analysis will show that the EESCs can decrease dissipated energy and impact in the reduction of annual cost.

7.2.7.1 Measurement and Calculation of Battery Energies without Snubber Circuit

Measuring probes are shown in Figure 7-8 and the result of simulation is shown in Figure 7-9.

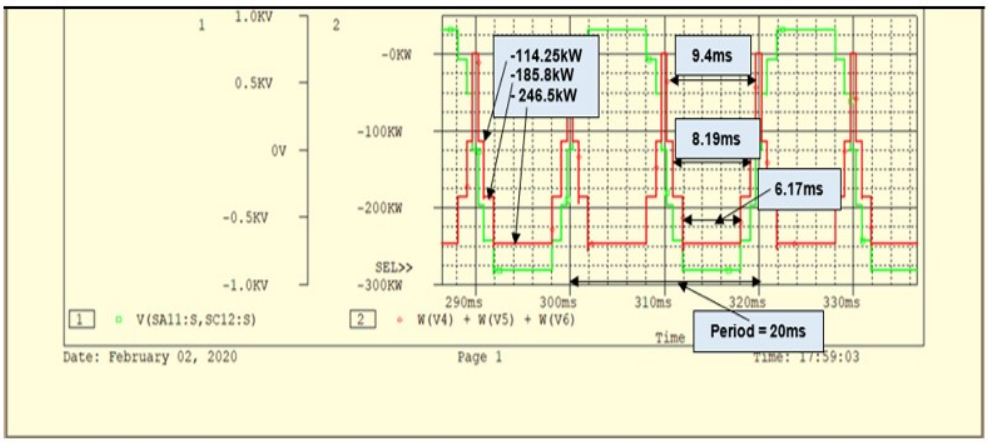

Figure 7-9 Traces, Green - Output voltage, Red - Total Power (W_{V1} + W_{V2} + W_{V3})

In Figure 7-9,

- The basic CHB7-Level Inverter generated a symmetrical output voltage (green trace), which would imply correct switching periods of the IGBTs.
- the Pulse Widths (PW) shown were, PW1 = 9.4ms, PW2 = 8.19ms and PW3 = 6.17ms.

The Energy due to 1st half cycle (10ms) is given by,

$$E_{1st\ half\ cycle} = \sum_{k=1}^{n} (P \times PW)_k \ \text{Joules}, \qquad n = 1, 2, 3$$

$$= \big((-114.25\text{kW} \times 9.4\text{ms}) + ((185.8\text{kW} - 114.25\text{kW}) \times 8.19\text{ms}) + ((246.5\text{kW} - 185.8\text{kW}) \times 6.17\text{ms})\big) \text{ Joules}$$

$$= (1073.95 + 585.99 + 374.52)$$

$$E_{1st\ half\ cycle} = 2034.46 \text{ Joules}$$

The 1st half cycle energy is .2034.46 Joules delivered by the batteries.

Due to Symmetry, the 2nd half cycle energy is also 2034.46 Joules.

The total battery energy delivered in the complete cycle = 2034.46 x 2 = 4068.92 Joules

7.2.7.2 Calculation of Load Energy

Simulation using the schematic in Figure 7-8, the load voltage V_{R8} was measured.

The forward (IGBT-SA11) and reverse (IGBT-SA12) currents through the load were measured.

The output power measured is given by,

$$WR_8 = \left((VR_8 \times I_{SA11}) + (VR_8 \times I_{SA12})\right) \text{Watts}$$

The result of these measurements are shown in the Red and Green Traces in Figure 7-10

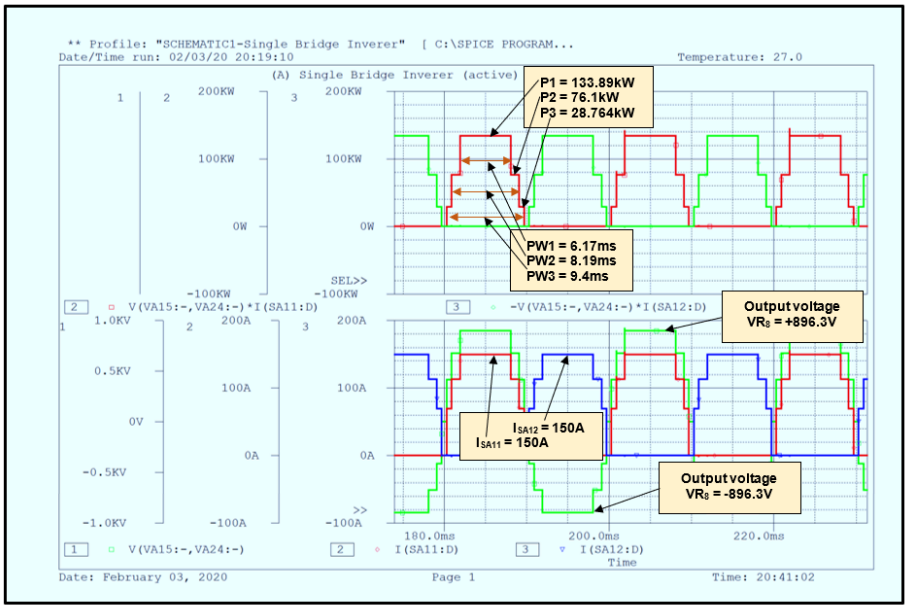

Figure 7-10 Top - R & G = Output power, Bottom - G = V_{Load}, R & B = I_{SA11} & I_{SA12}

The load energy for the 1st half cycle is given by the area enclosed by the Top red trace in Figure 7-10, which is calculated as follows,

$$E_{Load,+ve\ cycle} = \sum_{k=1}^{n} (P \times PW)_k \text{ Joules}, \qquad n = 1, 2, 3$$

$$= \Big((28.76\ \text{kW} \times 9.4\ \text{ms}) + \big((76.1\ \text{kW} - 28.76\ \text{kW}) \times 8.19\ \text{ms}\big) + \big((133.89\ \text{kW} - 76.1\ \text{kW}) \times 6.17\ \text{ms}\big)\Big)\ \text{Joules}$$

$$= (270.344 + 387.72 + 356.56)\ \text{Joules}$$

$$E_{Load,+ve\ cycle} = 1014.62\ \text{Joules}$$

Due to Symmetry, the 2nd half cycle energy = 1014.62 Joules

Total Load energy,

$$E_{R8} = 1014.62 \times 2\ \text{Joules/cycle}$$

$$\text{Total Load Energy } E_{R8}/\text{cycle} = 2029.24 \text{ Joules}$$

Load in kW, (kJ/S),

$$\text{Load}_{kW} = \frac{2029.24}{0.02} = 101462 \text{ J/S}$$

$$\text{Load}_{kW} \cong 101.5 \text{ kW}$$

In Section 7.2.7.1, the input energy = 4069 Joules

The Load energy = 2029 Joules.

Hence, the switching and dissipated energy during the Turn-On period is,

$$E_{(SW+ \text{ Dissipated})} = \text{Input energy} - \text{Load energy}$$

Without snubber circuit, Turn-On $E_{(SW+ \text{ Dissipated})} = 4069 - 2029 = 2040$ Joules/cycle

7.2.7.3 Alternative Method to Determine CHB7LC Turn-On dissipation without SC

The CHB7LC without any snubber circuit, total dissipated energy of 2040 Joules, is the sum of the dissipated IGBTs energy in both the positive and negative circuits. This dissipated energy is confirmed by the summation of the dissipated energy measured at each IGBT. The Simulation and calculation is presented in Appendix C – Determination of CHB7LC dissipative Energy. The result obtained was 2039.6 Joules which compares closely to the above 2040 Joules and validates the method used in 7.2.7.2.

7.2.7.4 Plot of Energy distribution - without Snubber Circuit

From the above calculations, Figure 7-11, display the CHB7LC energy distribution.

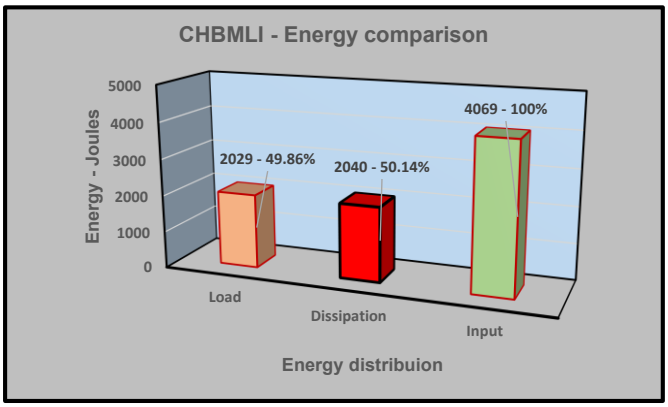

Figure 7-11 No SC - Distribution of E_{input} between Load and Dissipation

In Figure 7-11, the Load and Dissipation energies are approximately equal. The CHB7LC is a basic design with the standard PSpice gate drive circuit (No PWM control) connected at each IGBT. With further investigation it is possible to reduce the high dissipation losses. Several articles have discussed switching losses in IGBTs mainly due to parasitic drain source capacitances (Coss) which are significant at low power applications [20] [23]. At high power

applications, these switching losses can be ignored especially when energy efficient snubber circuit are employed to reduce the Turn-On and Turn-Off switching losses. In the latter case, dissipation losses are during the turn-on and turn-off periods which can be calculated by simulation measurements in the formula,

$$\begin{aligned}&\text{CHBMLC } E_{\text{Dissipation/Bridge}}\\&= \text{IGBT}\sum_{k=1}^{n}\left(((V_{RMS}\times I_{RMS})_k)\ \text{turn}-\text{on}\right)\\&+\left(((V_{RMS}\times I_{RMS})_k)\ \text{turn}-\text{off}\right),\ \ \text{for n}=1,2,3,4\ \text{IGBTS/Bridge}\end{aligned}\tag{7.2}$$

Since at turn-off period, the current is zero or at a low leakage value, the $E_{Dissipation}$ during turn-off can be ignored with the Dissipation occurring mainly during the turn-on period. In Figure 7-14, during the turn-on period, the turn-on voltage is not zero but steps-up to a maximum of 125 volts with a corresponding step-up maximum current of 150 Amps. The product (V*I) generates a turn-on dissipated power, which in this case resulted in a dissipated energy of 2039.6 Joules as shown in Appendix C. This procedure was similarly analysed for a CHB7LC in cited article [85]. However, the main focus in this concluding chapter was the investigation into the performance of Energy Efficient Snubber Circuits and its effect on the dissipation losses impacted by recovered energy.

7.2.7.5 Energy per IGBT in one cycle – without Snubber Circuit

The switching and dissipation energy covered the cycle period of 20ms. Therefore, the switching and dissipation energy in 1s is,

$$\begin{aligned}E_{(SW+Dissipated)} &= \frac{2040}{0.02}\times 1\ \text{Joules}\\&= 102000\ \text{Joules/sec}\\&= 102\ \text{kW}\end{aligned}$$

In one hour, the kW dissipated is,

$$\begin{aligned}&102\ \times 1\text{Hr}\\&\mathbf{E_{(SW+Dissipated)}} = \mathbf{1}02\ \text{kWh}\end{aligned}$$

The bridge consists of 12 IGBTs and 4 conducting diodes, each device and will dissipate,

$$\text{Device dissipation} = \frac{102\text{kW}}{16} = 6.4\ \text{kW}$$

6.4kW exceeds the maximum dissipation of 2.5 kW/IGBT at 175 ^{0}C given in the data sheet and also the safe SOA of 2.25 kW at 157.5^{0}C resulted from the COMSOL Thermal simulation investigation (Table 6-7 and Table 6-9). The result would be permanent and irreparable damage to expensive IGBTs. It is therefore necessary to ensure adequate cooling to remove

the conduction energy and also provide energy efficient feedback circuits to remove or reduce the switching energies and improve the system efficiency.

7.2.7.6 Cost of Dissipated (wasted) Energy

In the UK, the unit cost/kWh [86] for a group of Business sizes is given in Table 7-5.

Table 7-5 Electricity rates based on Business size

Business Size	Usage/Year	Unit Price/KWH	Standing Charge	Cost/Year
Micro Business	8,000 kWh	14.42p	27.40p	£1,254
Small Business	20,000 kWh	13.98p	26.83p	£2,894
Medium Business	40,000 kWh	13.79p	26.41p	£5,612
Large Business	80,000 kWh	13.24p	26.20p	£10,688

From Table 7-5, a line plot is shown in Figure 7-12, to enable comparison between electricity charges for kWh usage per year for the different business sizes.

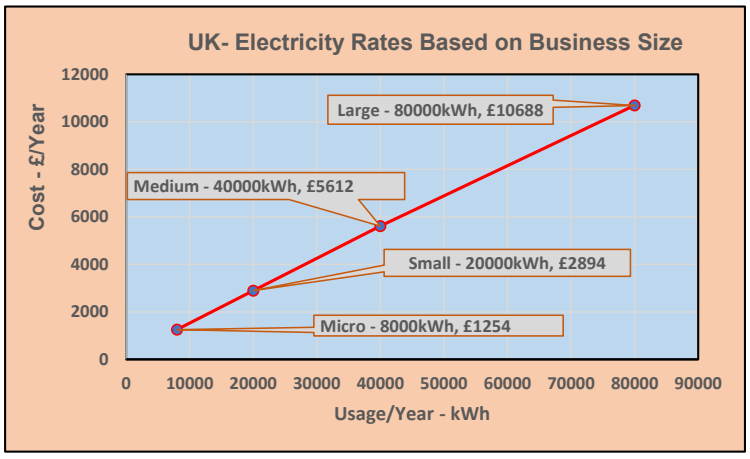

Figure 7-12 Comparative Electricity cost based on Business size.

The values in Table 7-5 are used to provide an estimate of the cost of the dissipated energy in the CHB7LC. The average Unit Price is 14p/kWh, is used to calculate the cost of dissipated energy kWh over one year. The CHB7LC without any protection for the IGBTs, the cost of total (Switching and Dissipated) energy/hour is,

$$102\ \text{kWh} \times £0.14$$
$$= £\ 14.28/\text{Hr}$$

Annual cost,

$$= 8760\ \text{Hr/year} \times £14.28$$
$$\boldsymbol{C}\text{ost of E}_{(\text{SW+Dissipated})} \approx £125{,}000/\text{year}$$

The cost appears to be excessive and exceeds the Usage/year scale in Figure 7-12. Instead of reducing the losses, complex charges, and energy efficiency schemes (White Certificate) are used to reduce energy costs agreed by the countries at both ends of HVDC Transmission

Converter Stations. To compensate for the losses, loads connected to the supply by industries and end users are based on the types of loads shown in Figure 7-13 [87].

However, the switching losses can be reduced, by the connection of energy efficient snubber circuits to the switching devices. The snubber circuits are designed to capture the switching energies and return them to the load or supply. The effect would be to reduce the total dissipation losses, resulting in cheaper electricity for businesses and end users, and also reduce or eliminate the costs in providing water pumps, piping networks, cooling towers etc and other refrigeration ambient cooling methods for the safe operation of the power IGBTs in converter stations.

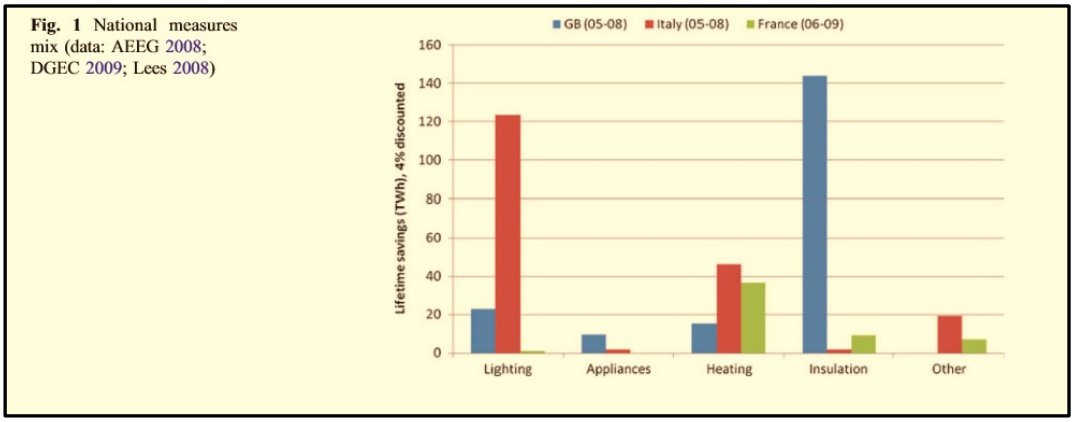

Figure 7-13 Load distribution scheme to impact on energy saving [87]

7.3 IGBT turn-on and turn-off switching energies without Snubber Circuit.

From data in Figure 7-7, Table 7-6 identified the groups of IGBTs switching at the ± level 1, ± level 2 and ± level 3.

Table 7-6 Identification of IGBTs switching at the three voltage levels

Voltage level	PW-ms	IGBT(s)	IGBT- t_{on}	IGBT-t_{off}
± V1	9.4	SA11, SC13, SB13, SA13	4	4
	9.4	SA14, SA12, SC14, SB14,	4	4
± (V1 + V2)	8.19	SB11	1	1
	8.19	SB12	1	1
± (V1 + V2 + V3)	6.17	SC11	1	1
	6.17	SC12	1	1
		Total	12	12

The grouping of the IGBTs ensured that the measurement of the turn-on and turn-off IGBT switching is at the correct level at which *di/dt* and *dv/dt* intersects. The turn-on switching energy measurement followed using the schematic in Figure 7-8.

7.3.1 Level 1 – Turn-on Switching Energy at IGBT-SA11

Simulation result for the measurement of the voltage, current and power, is shown in Figure 7-14, where V and I intersection is at level 1.

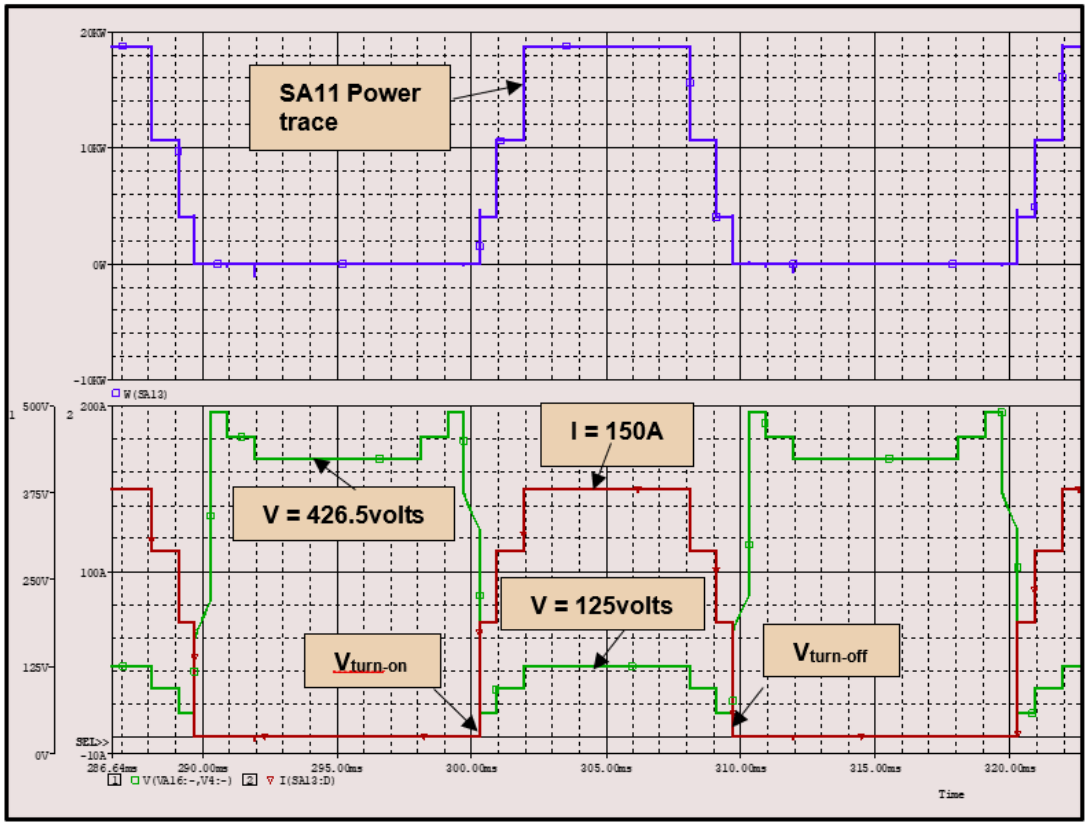

Figure 7-14 IGBT-SA11, V, I & P traces showing $V_{turn\text{-}on}$ and $V_{turn\text{-}off}$ overlap of V and I

The turn-on overlap in Figure 7-14 is enlarged to show the intersection of *+di/dt* and *-dv/dt*. The traces of V, I, and the power due to the intersection is shown in Figure 7-15.

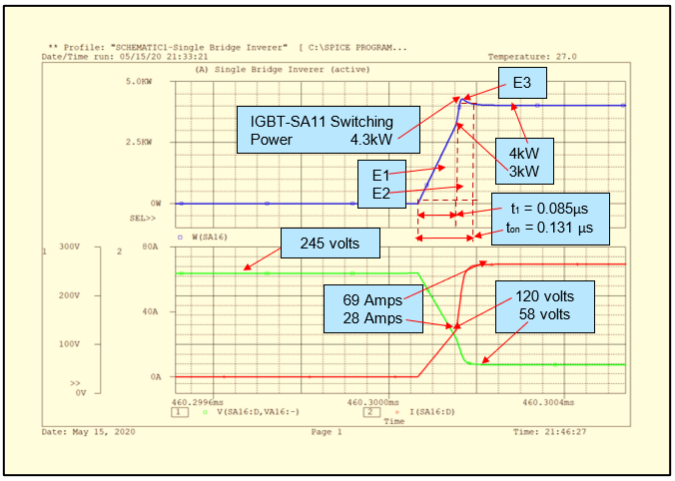

Figure 7-15 Enlarged view of turn-on switching at IGBT- SA11

The turn-on power is divided into three sections, E1, E2 and E3 and the switching energy is,

$$E_{\text{turn-on switching}} = \sum_{k=1}^{n} \left(P \times \frac{t}{2}\right)_k, \text{for } n = 1, 2, 3$$

$$= \sum (E_1 + E_2 + E_3) \text{ Joules}$$

$$= \left(\left(3\text{kW} \times \frac{0.085\mu\text{s}}{2}\right) + (4\text{kW} \times 0.046\mu\text{s}) + \left((4.3\text{kW} - 4\text{kW}) \times \frac{0.046\mu\text{s}}{2}\right)\right) \text{ Joules}$$

$$= (0.1275 + 0.184 + 0.0039)\text{ mJ}$$

$$\text{Level } 1 - E_{\text{turn-on switching}} = 0.3154\text{mJ}$$

7.3.2 Level 2 – Turn-on switching Energy at IGBT-SB11

Simulation result for the measurement of the voltage, current and power, is shown in Figure 7-16, where V and I intersection is at level 2.

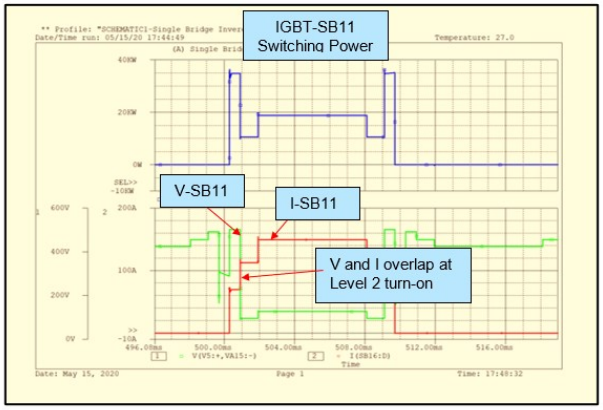

Figure 7-16 Turn-on switching at IGBT- SB11

The turn-on overlap in Figure 7-16 is enlarged to show the intersection of *+di/dt* and *-dv/dt*. The traces of V, I, and the power due to the intersection is shown in Figure 7-17.

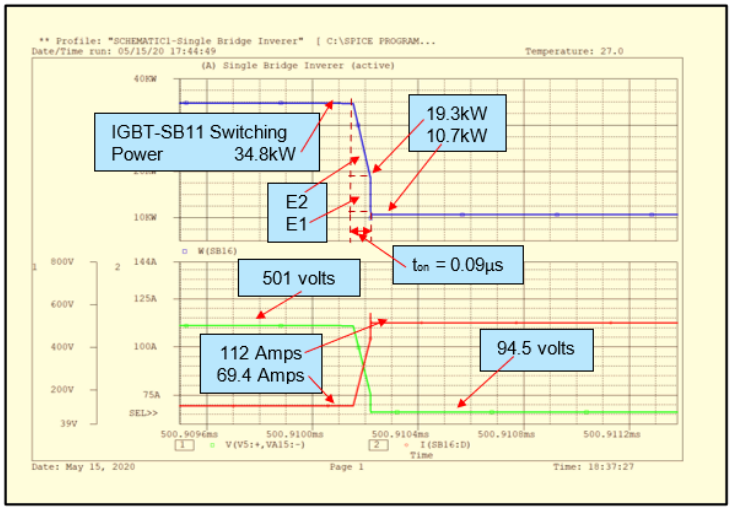

Figure 7-17 Enlarged view of Turn-on switching at IGBT- SB11

The turn-on power is divided into two sections, E1 and E2 and the switching energy is,

$$E_{\text{turn-on switching}} = \sum_{k=1}^{n} \left(P \times \frac{t}{2}\right)_k, \text{for } n = 1, 2$$

$$= \sum (E_1 + E_2) \text{ Joules}$$

$$= \left((19.3\text{kW} - 10.7\text{kW}) \times 0.09\mu\text{s} + \left((34.8\text{kW} - 19.3\text{kW}) \times \frac{0.09\mu\text{s}}{2} \right) \right) \text{Joules}$$

$$= ((774 + 0.697)\text{mJ}$$

$$\text{Level 2} - E_{\text{turn-on switching}} = 1.5\text{mJ}$$

7.3.3 Level 3 – Turn-on switching Energy at IGBT-SC11

Simulation result for the measurement of the voltage, current and power, is shown in Figure 7-16 where V and I intersection is at level 3.

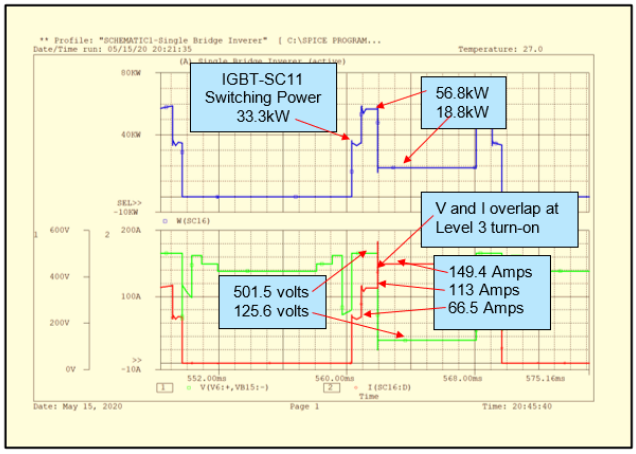

Figure 7-18 Turn-on switching at IGBT- SC11

The turn-on overlap in Figure 7-18 is enlarged to show the intersection of *+di/dt* and *-dv/dt*. The traces of V, I, and the power due to the intersection is shown in Figure 7-19.

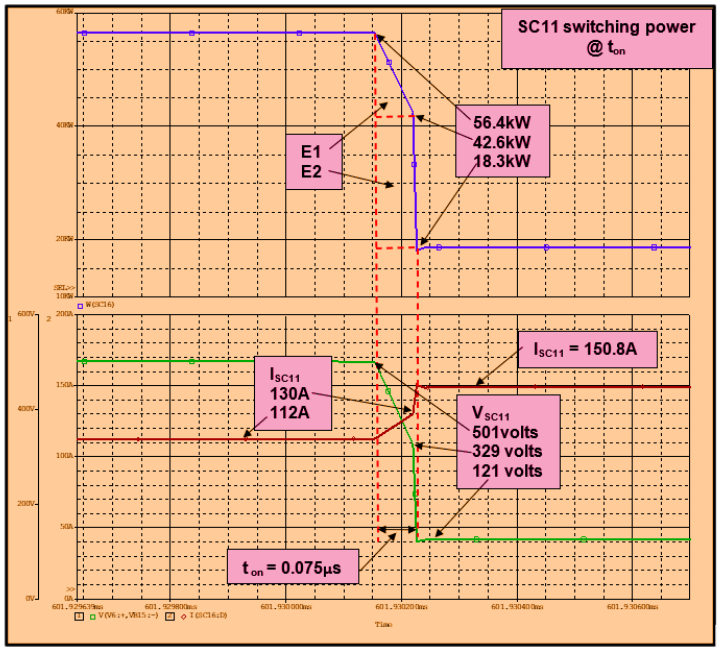

Figure 7-19 Enlarged view of Turn-on switching at IGBT- SC11

In Figure 7-19, the turn-on power is divided into two sections, E1 and E2 and the switching energy is,

$$E_{\text{turn-on switching}} = \sum_{k=1}^{n} \left(P \times \frac{t}{2}\right)_k, \text{for } n = 1, 2$$

$$= \sum (E_1 + E_2) \text{ Joules}$$

$$= \left(\left((56.4 - 42.6)kW \times \frac{0.075\mu s}{2} \right) + \left((42.6 - 18.3)kW \times 0.075\mu s \right) \right) \text{ Joules}$$

$$= ((0.052 \times 10-3) + (1.823 \times 10-3))\text{Joules}$$

$$= (1.875 \times 10^{-3})\text{Joules}$$

$$\text{Level 3} - \text{E}_{\text{turn-on switching}} = 1.875\text{mJ}$$

7.3.4 Total turn-on Switching Energy per cycle, without SC

A compilation of the turn-on switching energies for voltage levels 1, 2 and 3 are presented in Table 7-7.

Table 7-7 Compilation of turn-on switching energies - without SC

Clause No.	Level	IGBTs in +ve circuits	$E_{turn-on}$ mJ	Total $E_{turn-on}$ mJ	t-on - µs	I-Range - Amps	V-Range-Volts	Power Range-kW
7.3.1	1	SA11, SA13,SC13,SB13	0.315 x 4	1.26	0.131	28 ≤ I ≤ 69	245 ≥ V ≥ 120 V ≥ 58	0 ≤ P ≤ 3 ≤ P ≤ 4.3
7.3.2	2	SB11	1.5 x 1	1.5	0.09	69.4 ≤ I ≤ 112	501 ≥ V ≥ 94.5	34.8 ≥ P ≥ 10.7
7.3.3	3	SC11	1.875 x 1	1.875	0.075	112 ≤ I ≤ 150.8	501 ≥ V ≥ 121	56.4 ≥ P ≥ 18.3
Total Positive cycle – $E_{turn-on}$				4.635				
Due to symmetry, the Total Negative cycle – $E_{turn-on}$				4.636				
Total $E_{turn-on}$ per cycle for Bridges (A, B and C)				**9.27**				

In Table 7-7, the total turn-on switching energies for the CHB7-level Inverter for levels, 1, 2 and 3 is 9.27 mJ. The following section repeated above procedure for the turn-off switching energies.

7.3.5 Level 1 – Turn-off switching Energy at IGBT-SA11

In Figure 7-14, for level 1, the V and I overlap area at the IGBT turn-off is shown at the $V_{turn-off}$ arrow. For the other levels 2 and 3 the turn-off region is at the opposite side of the V and I turn-on overlap area. Figure 7-20 shows the magnified view of the voltage, current and power at the $V_{SA11-turn-off}$.

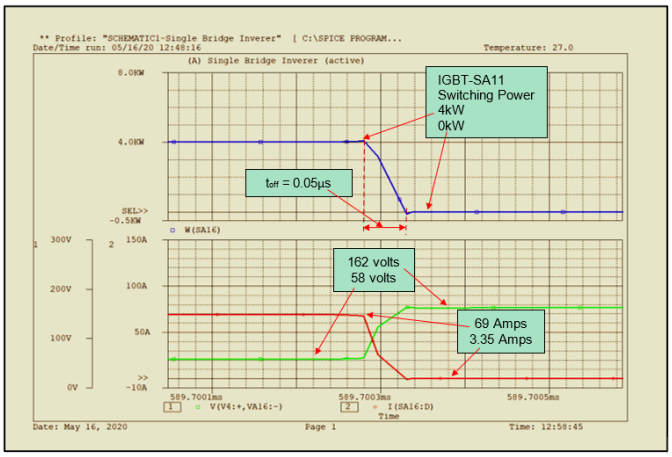

Figure 7-20 Enlarged view of Turn-off switching at IGBT- SA11

In Figure 7-20 the turn-off switching energy is,

$$E_{\text{turn-off switching}} = 4\text{kW} \times \frac{0.05\mu s}{2}$$

$$= 0.1\text{mJ}$$

$$\text{Level } 1 - E_{\text{turn-off switching}} = 0.1\text{mJ}$$

7.3.6 Level 2 – Turn-off switching Energy at IGBT-SB11

Figure 7-21 shows the magnified view of the voltage, current and power at the $V_{SB11\text{-turn-off}}$.

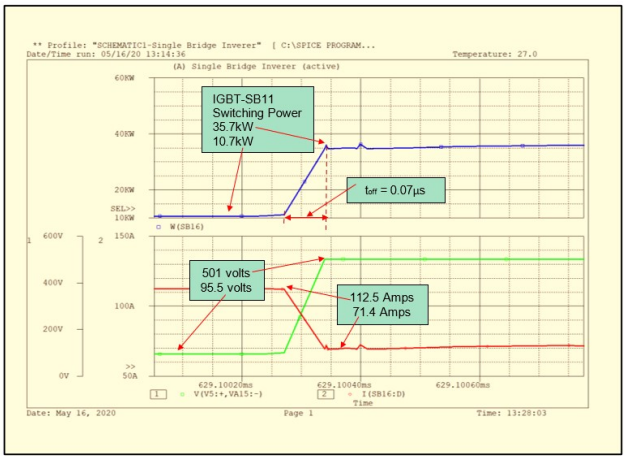

Figure 7-21 Enlarged view of Turn-off switching at IGBT- SB11

In Figure 7-21 the turn-off switching energy is,

$$E_{\text{turn-off switching}} = (37.54\text{ kW} - 10.7\text{ kW}) \times \frac{0.07\ \mu s}{2}$$

$$= 0.875\text{ mJ}$$

$$\text{Level } 2 - E_{\text{turn-off switching}} = 0.875\text{ mJ}$$

7.3.7 Level 3 – Turn-off switching Energy at IGBT-SC11

Figure 7-22 shows the magnified view of the voltage, current and power at the $V_{SC11\text{-}turn\text{-}off}$.

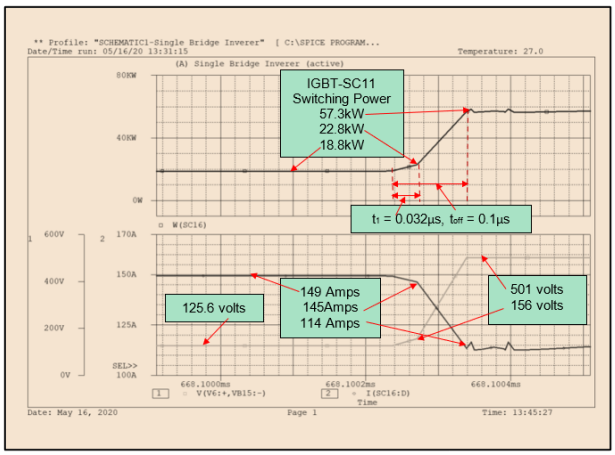

Figure 7-22 Enlarged view of Turn-off switching at IGBT- SC11

The turn-off switching power trace is divided into three sections and the energy is calculated as follows,

$$E_{\text{turn-off switching}} = \sum_{k=1}^{n} \left(P \times \frac{t}{2}\right)_k \text{ Joules}, \qquad \text{for } n = 1, 2, 3$$

$$= \left(\left((22.8\ \text{kW} - 18.8\ \text{kW}) \times \frac{0.032\ \mu\text{s}}{2} \right) + \left((57.3\ \text{kW} - 22.8\ \text{kW}) \times \frac{0.1\ \mu\text{s} - 0.032\ \mu\text{s}}{2} \right) + \left((22.8\ \text{kW} - 18.8\ \text{kW}) \times (0.1\ \mu\text{s} - 0.032\ \mu\text{s}) \right) \right) \text{ Joules}$$

$$= \left((0.064\ \text{mJ}) + (1.173\ \text{mJ}) + (0.272\ \text{mJ}) \right)$$

$$\text{Level 3} - E_{\text{turn-off switching}} = 1.51\ \text{mJ}$$

7.3.8 Total turn-off Switching Energy per cycle, without SC.

A compilation of the turn-off switching energies for Levels 1, 2, and 3 are presented in Table 7-8.

Table 7-8 Compilation of turn-off switching energies - without SC

Clause No.	Level	IGBTs in +ve circuits	$E_{turn-off}$ mJ	Total $E_{turn-off}$ mJ	t-off µs	I-Range -Amps	V-Range-Volts	Power Range-kW
7.3.5	1	SA11, SA13, SC13, SB13	0.1 x 4	0.4	0.05	69 ≥ I ≥ 3.35	58 ≤ V ≤ 162	4 ≥ P ≥ 0
7.3.6	2	SB11	0.875 x 1	0.875	0.07	112.5 ≥ I ≥ 71.4	95.5 ≤ V ≤ 501	10.7≤ P ≤ 35.7
7.3.7	3	SC11	1.51 x 1	1.51	0.1	149 ≥ I ≥ 145 ≥ I ≥ 114	125.6 ≥ V ≥ 156 ≤ V ≤ 501	18.8 ≤ P ≤ 22.8 ≤ P ≤ 57.3
Total Positive circuit - $E_{turn-off}$				2.785				
Due to symmetry, the Total Negative circuit – $E_{turn-off}$				2.785				
Total $E_{turn-off}$ per cycle for Bridges (A,B and C)				5.57				

7.3.9 Total CHB7-Level I switching energies ($E_{turn-on}$ + $E_{turn-off}$)

From Table 7-7 and Table 7-8, the total CHB7-LI switching energy is,

$$\text{Total Bridge } E_{switching} = \sum (E_{turn-on} + E_{turn-off}) \text{ mJ}$$

$$= (9.27 + 5.57) \text{ mJ}$$

$$\text{Total CHB7-LC } E_{switching} = 14.84 \text{ mJ}$$

From the energy calculations a column plot the total turn-on and turn-off switching is shown in Figure 7-23.

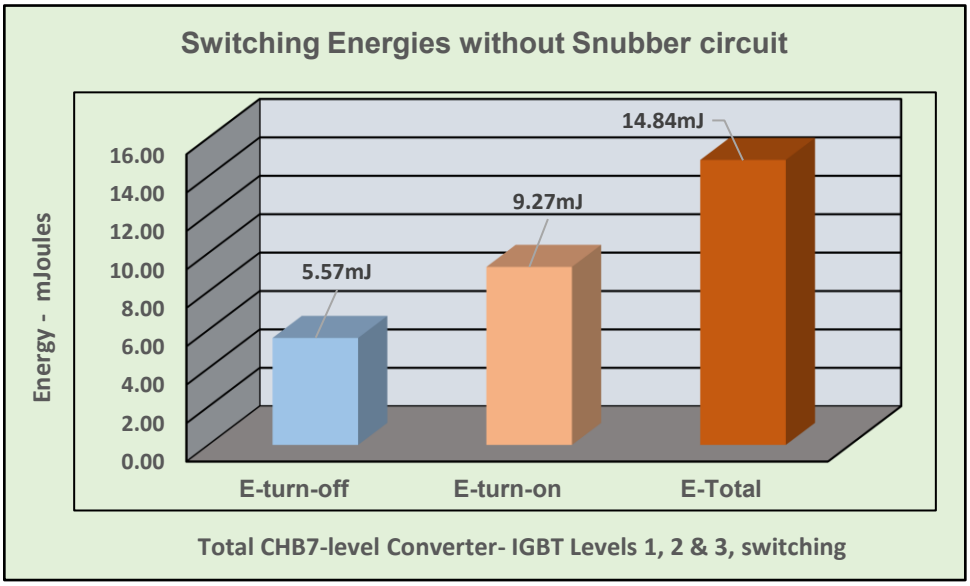

Figure 7-23 Comparison of the total turn-on and turn-off IGBTs' switching energies

Figure 7-23 show that the turn-on and turn-off switching losses contributes 62% and 38% respectively of the total switching losses. Hence, reduction in the turn-on switching losses will impact more in reducing the total switching losses.

7.4 Switching of V2 and V3 for Output Voltage Stepped wave shape.

In Figure 7-24, circuits 1, 2 and 3 simplify the connection of the IGBTs for the positive output voltage.

Circuit 1, shows four IGBTs, SA11, SC13, SB13 and SC13 (and two diodes, DC14 and DB14) with a common PW (9.4ms) connected in series with V1 and the load. The drive generators turn these IGBTs on for 9.4ms.

Circuit 2, shows Circuit 1 in series with V2 which is switched in circuit when IGBT-SB11 closes and reverse biases DB14, and Level 2 voltage is (V1 + V2). IGBT-SB11 conducts for 8.19ms

Circuit 3, shows Circuit 1 and Circuit 2 in series with V3 which is switched in circuit when SC11 opens and reverse biases DC14, and Level 3 voltage is (V1 + V2 + V3). This IGBT conducts for 6.17ms.

The switching of V2 and V3 in series with V1 achieves the positive output voltage of (V1+V2+V3).

Similarly, the negative output voltage is generated when the complimentary pairs of IGBTs are used (circuits not shown).

Figure 7-24, shows the connection point for the Turn-On inductors LA, LB and LC in circuits 1, 2 and 3, respectively. Each inductor needs to generate a voltage of – *L*di/dt* to reduce the turn-on voltage and in rush current of the respective IGBT. However, in an ideal case, assuming no voltage drops, the value of each inductor is,

$$\mathrm{LA} = \left(\mathrm{V1} \times \frac{\mathrm{t_1}}{\mathrm{i_1}}\right) < \mathrm{LB} = \left((\mathrm{V1} + \mathrm{V2}) \times \frac{\mathrm{t_2}}{\mathrm{i_2}}\right) = \mathrm{LC} = \left((\mathrm{V1} + \mathrm{V3} - \mathrm{V2}) \times \frac{\mathrm{t_3}}{\mathrm{i_3}}\right) \qquad (7.3)$$

Equation (7.3) shows that LB and LC are equal but greater than LA. With these unequal inductors in circuit, the inverter voltage can become unsymmetrical due to unequal current delays at turn-on. To avoid any output voltage imbalance, a common Inductor is essential for the three connection points shown in Figure 7-24. To determine this common inductor, a linear current equation by the method of 'Least Square' to approximation the 'step rise' current wave shape during turn-on is presented in the next section.

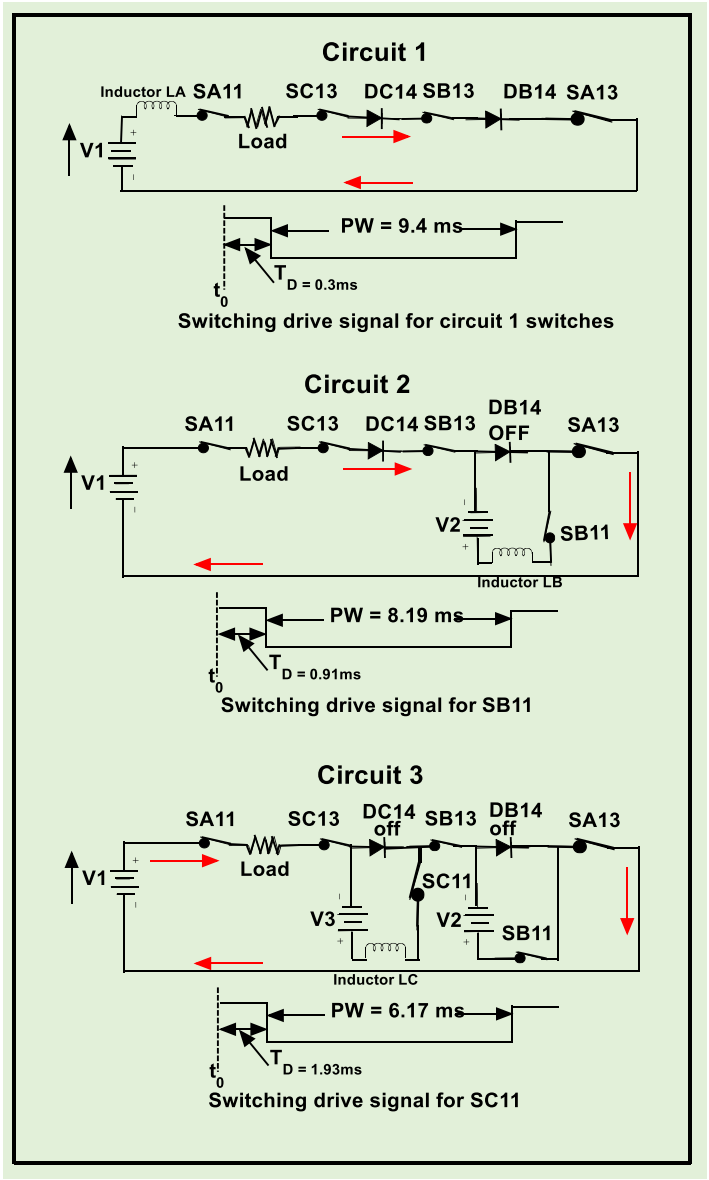

Figure 7-24 Simplified Switching
Circuits showing location of Bridge Inductance

7.4.1 Linearisation of IGBT current during 't_{on}', by method of Least Square.

In section 7.3.1, Figure 7-14, the current and voltage switching waveforms are both 'stepped shape' with a defined t_{on} period. Hence, in the equation for L_S, ($L\_S = V\_S \times t\_on/I\_s \ \ H$), the stepped waveform for $I_{S,}$ is approximated by a linear equation which was determined by the method of Least Square [88] [89] [90]. In general notation, the method of Least Square states that, to fit a straight line,

$$y = mx + b \tag{7.4}$$

given a set of data points,

$$(x_1, y_1), (x_2, y_2) \ldots \ldots (x_n, y_n),$$

two equations are necessary to determine the coefficients 'm' and intersect 'b', these are,

$$m = \frac{(n\sum_{i=1}^{n} x_i y_i) - (\sum_{i=1}^{n} x_i \sum_{i=1}^{n} y_i)}{(n\sum_{i=1}^{n} x_i{}^2) - (\sum_{i=1}^{n} x_i)^2} \quad (7.5)$$

Where, 'i' is the number identification of a measured value of y and x.

and

$$b = \frac{(\sum_{i=1}^{n} y_i - m\sum_{i=1}^{n} x_i)}{n} \quad (7.6)$$

Where, 'n' is the number of 'i' measurements or iterations

To represent each pair of values (i, t), given in Figure 7-14, let 'x_i' be replaced by 't_i' and 'y_i' be replaced by 'i_i' in equations (7.5) and (7.6). The above equations can be rewritten as,

$$m = \frac{(n\sum_{i=1}^{n} t_i i_i) - (\sum_{i=1}^{n} t_i \sum_{i=1}^{n} i_i)}{(n\sum_{i=1}^{n} t_i{}^2) - (\sum_{i=1}^{n} t_i)^2} \quad (7.7)$$

and

$$b = \frac{(\sum_{i=1}^{n} i_i - m\sum_{i=1}^{n} t_i)}{n} \quad (7.8)$$

From Figure 7-14, 'i' and 't' data values were tabulated in Table 7-9, to populate equations (7.7) and (7.8) to determine the values for 'm' and 'b'.

Table 7-9 Current measurements during turn-on period (t_{on})

i	1	2	3	4	5	6	7
t -ms	0	0.5	0.5	1.105	1.105	2.115	2.115
i-Amps	0	0	68.8	68.8	112.8	112.8	150
For (5), n = 7							

Data from Table 7-9, were entered in Excel (Table 7-10) to calculate the elements of the equations (7.7) and (7.8) for 'm' and the intercept 'b' on the 'y' axis.

Table 7-10 Calculated values for elements of equations (7.7) and (7.8)

i	t_i - ms	i_i -Amps	$(t_i)^2$	$t_i * i_i$
1	0	0	0.000	0
2	0.5	0	0.250	0
3	0.5	68.8	0.250	34.4
4	1.105	68.8	1.221	76.024
5	1.105	112.8	1.221	124.644
6	2.115	112.8	4.473	238.572
7	2.115	150	4.473	317.25
Σ	7.44	513.2	11.889	790.89
n=7	Σt_i = 7.44	Σi_i = 513.2	$\Sigma(t_i)^2$ =1 1.889	$\Sigma(t_i * i_i)$ = 790.89

The repeated values of 'i' ensures the stepped shape for i' with respect to 't'. The gradient 'm' and intercept 'b' were calculated separately, as shown in Table 7-11, with the summation 'Σ' values in Table 7-10 as input to (7.7) and (7.8).

Table 7-11 Calculations for 'm' and 'b'

n	n Σ (x y)	Σ x Σ y	n Σ (x y) -Σ x Σ y	n Σ(x^2)	(Σ x)^2	n Σ(x^2) -Σ(x)^2	m	b
7	5536.23	3818.21	1718.022	83.220	55.3536	27.866	61.7	7.8

From calculations presented in Table 7-10 and Table 7-11, the linear equation to approximate the stepped current wave form was,

$$\mathrm{I} = 61.7\mathrm{t} + 7.8, \text{ Amps} \tag{7.9}$$

Before applying the equation for 'I' in the calculation for the components in the Turn-On EESC, it is necessary to show that the derived equation (7.9) is a 'close fit' line with minimum 'error' to the plotted pairs of (i, t) points. The minimum 'error' can be measured by the Residual Squared (R^2) formula,

$$\mathrm{R}^2 = \frac{\sum_{\mathrm{i}=1}^{\mathrm{n}} \mathrm{r}_\mathrm{i}^2}{\sum_{\mathrm{i}=1}^{\mathrm{n}} (\mathrm{y}_\mathrm{i} - \bar{\mathrm{y}})^2} \tag{7.10}$$

Where, 'r' is the distance between a point in the data (i, t) and a point on the line.

r = (i, t) – (61.7t + 7.8).

y_i is a value of each data point,

$\bar{y}$ is the mean of the data.

For a 'close fit' line, $R^2 \leq 1$

Table 7-12, shows the calculations for R^2 given in equation (7.10).

Table 7-12- Calculation for the determination of R^2

t_i- ms	i_i -Amps	I	r^2	$(y - \bar{y})^2$	R^2
0	0	7.8	60.84	5374.98	**0.8**
0.5	0	38.7	1493.82	5374.98	
0.5	68.8	38.7	909.02	20.38	
1.105	68.8	76.0	51.53	20.38	
1.105	112.8	76.0	1355.82	1559.12	
2.115	112.8	138.3	650.02	1559.12	
2.115	150	138.3	137.00	5880.70	
7.44	**513.2**		**4658.05**	**19789.7**	
Σt_i	Σi_i		Σr^2	$\Sigma (y - \bar{y})^2$	
n = 7	$\Sigma i_i/n = 73.31$				
Key	I = 61.7t + 7.8 Amps				
	$r^2 = (i_i - I)^2$				
	$(y - \bar{y})^2 = (i_i - \Sigma i_i/n)^2$				

The result of the calculations in Table 7-12, gives R^2 a value of 0.8 (i.e., 80% fitness value). It shows that the linear equation (7.9), is a close-fit-line to the IGBT-SA11 step current and corresponding time points. The IGBT step current trace and its linear approximation is shown in Figure 7-25. Having determined a linear current equation to approximate the current step rise during IGBT-SA11 turn-on, the calculation for Turn-On SC inductor can proceed.

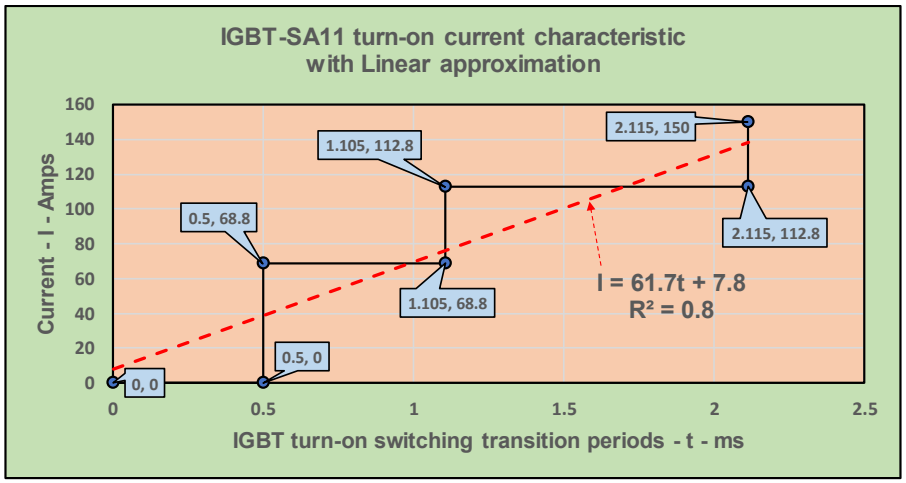

Figure 7-25 IGBT-SA11 current step rise (black) and a linear approximate equation (red)

7.5 Determination of Lp and Ls for the Turn-On EESC

In equation (7.9) the linear equation was determined where *di/dt* = 61.7amp/s. In Figure 7-14, V_{ton} = 125 volts. The primary inductor Lp in the Turn-on EESC is given by,

$$L_P = V_{ton} \times \frac{1}{di/dt}$$

$$L_P = 125 \text{ volts} \times \frac{1}{61.7 \text{amp/s}} \cong 2 \text{ mH}$$

To ensure an efficient transfer of recovered energy to the supply, let the turns ratio n = 1.5,

$$L_s = n^2 \times L_P$$

$$L_s = 1.5^2 \times 2 \text{ mH} = 4.5 \text{ mH}$$

With values of L_P (L1) and Ls (L2) the Turn-On EESC was designed and connected to the top two IGBTs in the CHB7-Level Inverter shown in Figure 7-26, where L_P = L1 and L_S = L2.

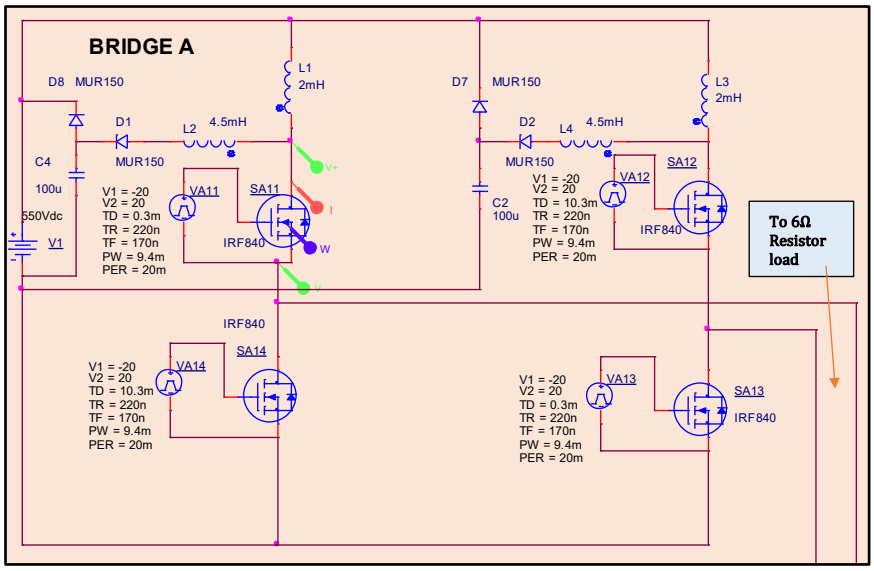

Figure 7-26 Schematic of Bridge A with
Turn-On EESC connected to SA11 and SA12

The turn-on switching power is measured at IGBT-SA11 with probes shown placed at the IGBT. The simulation result is shown in Figure 7-27.

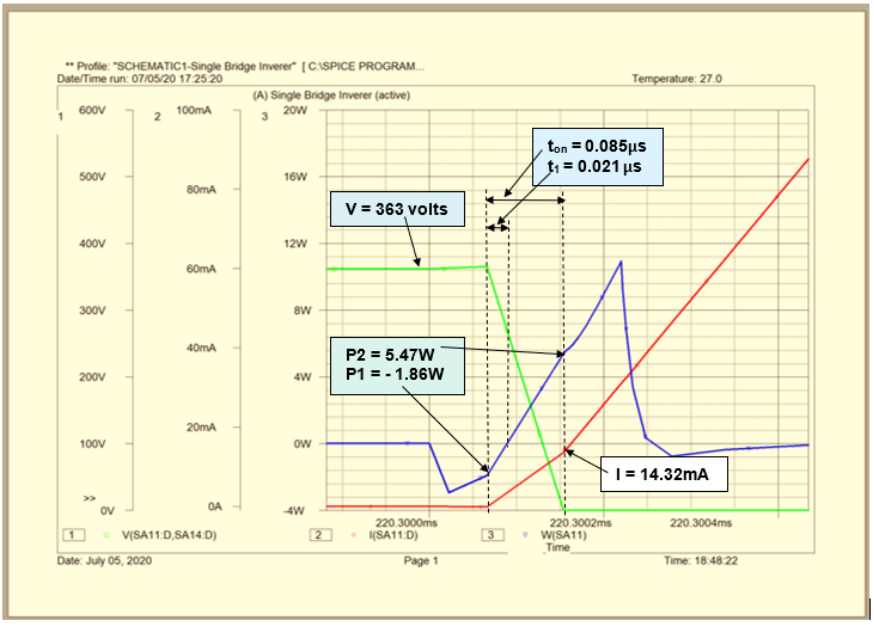

Figure 7-27 IGBT-SA11 Switching Power at t_{on}

7.5.1 Calculation of the turn-on switching energy at Level 1- IGBT-SA11.

$$E_{ton} = \sum_{k=1}^{n} \left(P \times \frac{t}{2}\right)_k, \text{for } n = 1, 2$$

$$= \sum (E_1 + E_2) \text{ Joules}$$

$$= \left((-1.86\ \text{W}) \times \frac{0.021\ \mu\text{s}}{2} + \left((5.47\ \text{W}) \times \frac{(0.085 - 0.021)\ \mu\text{s}}{2} \right) \right) \text{Joules}$$

$$= (-0.0195 + 0.175)\ \mu\text{J}$$

$$SA11 - E_{ton} = 0.1555\ \mu\text{J}$$

Since the positive and negative Inverter circuits are the same, then IGBT-SA12 E_{ton} will be the equal to E_{ton} IGBT-SA11. Hence the total E_{ton} for level 1 is,

$$\text{Total Level 1 } E_{ton} = 0.1555\ \mu\text{J} \times 2 = 0.311\ \mu\text{J}$$

7.5.1.1 Calculation of the Efficiency of the turn-on switching energy at IGBT-SA11

In Table 7-7, the total Level 1 t_{on} without SC = (1.26 x 2 = 2.52) mJ, therefore the reduction in switching energy with the Turn-On EESC was,

$$\text{Turn} - \text{On EESC } E_{\text{Reduction}} \text{ Level}_1 = \frac{2.52\ \text{mJ} - 0.000311\ \text{mJ}}{2.52\ \text{mJ}} \times 100\% = 99.98\%$$

The Inductor value was determined using the *di/dt* gradient from the linear approximate equation (7.9) resulted in a 99.98% reduction of turn-on switching energy at Level 1 of the CHB7-Level Inverter.

7.5.2 Calculation of the turn-on switching energy at Level 2- IGBT-SB11

Similarly, as in Figure 7-26, the turn-on switching power is measured at IGBT-SB11. The simulation result is shown in Figure 7-28.

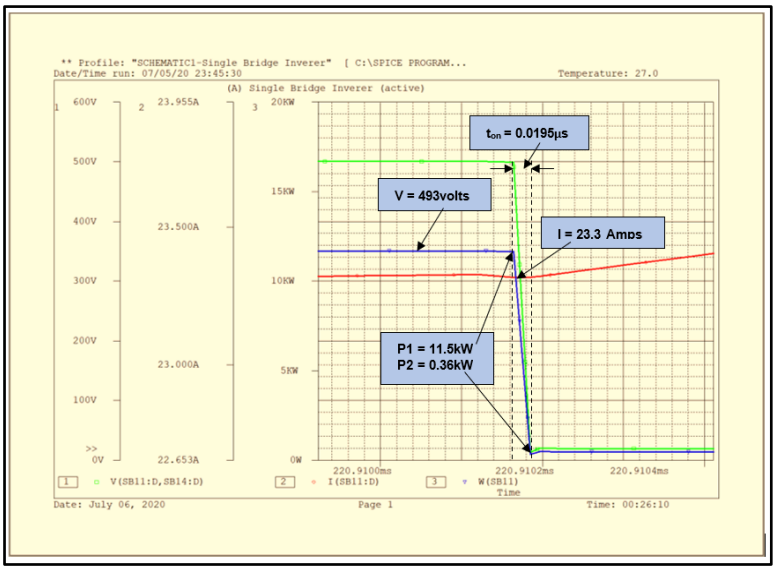

Figure 7-28 IGBT-SB11 Switching Energy at t_{on}

Calculation of IGBT-SB11 Et_{on},

$$E_{ton} = \sum \left((P_1 - P_2) \times \frac{t_{on}}{2} \right) \text{J}$$

$$= \left((11.5\ \text{kW} - 0.336\ \text{kW}) \times \frac{0.0195\ \mu\text{s}}{2} \right) \text{J}$$

$$= 0.1088 \times 10^{-3}\ \text{J}$$

$$= 0.1088\ \text{mJ}$$

The total t_{on} switching energy for IGBT-SB11 and IGBT-SB12 = 0.1088 mJ x 2 = 0.217 mJ

7.5.2.1 Calculation of the Efficiency of the turn-on switching energy at - IGBT-SB11

In Table 7-7, the total level-2-t_{on} energy for IGBT-SB11 and IGBT-SB12 without SC = 3 mJ. Therefore, the reduction in switching energy with the Turn-On EESC was,

$$\text{Turn} - \text{On EESC } E_{\text{Reduction}}\ \text{Level}_2 = \frac{3\ \text{mJ} - 0.217\ \text{mJ}}{3\ \text{mJ}} \times 100\% = 92.8\%$$

The Turn-On EESC with the calculated inductor values at level 2 continues to produce a high-level of percentage reduction at 92.8% in switching energy.

7.5.3 Calculation of the turn-on switching energy at Level 3- IGBT-SC11

Similarly, as in Figure 7-26, the turn-on switching power is measured at IGBT-SC11. The simulation result is shown in Figure 7-29.

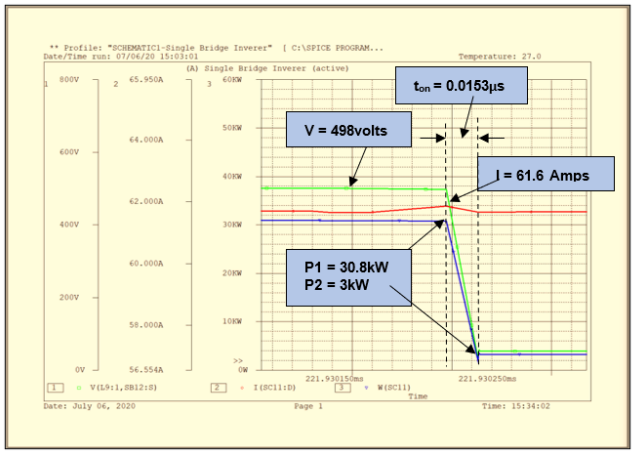

Figure 7-29 IGBT-SC11 Switching Energy at t_{on}

Calculation of IGBT-SC11 Et_{on},

$$E_{ton} = \sum \left((P_1 - P_2) \times \frac{t_{on}}{2} \right) J$$

$$= \left((30.8\,\text{kW} - 3\,\text{kW}) \times \frac{0.0153\,\mu\text{s}}{2} \right) J$$

$$= 0.2126 \times 10^{-3}\,J$$

$$= 0.2126\,\text{mJ}$$

The total t_{on} switching energy for IGBT-SC11 and IGBT-SC12 = 0.0.2126mJ x 2 = 0.425 mJ.

7.5.3.1 Calculation of the Efficiency of the turn-on switching energy at - IGBT-SC11

In Table 7-7, the total energy level-3-t_{on} for IGBT-SC11 and IGBT-SC12 without SC = 3.75 mJ. Therefore, the reduction in switching energy with the Turn-On EESC was,

$$\text{Turn} - \text{On EESC } E_{\text{Reduction}}\ \text{Level}_3 = \frac{3.75\text{mJ} - 0.425\text{mJ}}{3.75\text{mJ}} \times 100\% = 88.7\%$$

To maintain a symmetrical output wave shape, the Inductor used at SC11 and SC12 in level 3 was the same as in level 1 and level 2. The progressive percentage reduction of switching energies of 99.87% at level 1, 92.8% at level 2 and 88.7% at level 3, was due to the higher levels of (step rise) current at the respective levels. A higher and possibly constant percentage reduction is possible by determining a different valued inductor for each stage without using the *di/dt* method in equation (7.9).

7.5.4 Comparison of Switching Energy per cycle, with Turn-On-EESC

A compilation of the turn-on switching energies for Levels 1, 2 and 3 was presented in Table 7-13.

Table 7-13 Compilation of switching energies – with Turn-On EESC

Clause No.	Level	IGBTs in +ve circuit	$E_{turn\text{-}on}$ mJ	Total $E_{turn\text{-}on}$ mJ	Efficiency %	t-on -µs
7.5.1	1	SA11, SA13, SC13, SB13	0.00016x 4	0.00064	99.87	0.085
7.5.2	2	SB11	0.1088 x 1	0.109	92.8	0.0195
7.5.3	3	SC11	0.2126 x 1	0.213	88.7	0.0153
			Total Positive circuit- $E_{turn\text{-}on}$	0.323		
			Due to symmetry, the Total Negative circuit – $E_{turn\text{-}on}$	0.323		
			Total $E_{turn\text{-}on}$ per cycle for Bridges (A, B and C)	0.645		

Total percentage reduction in turn-on switching energy (0.645 mJ) by the Turn-On EESC compared to turn-on switching energy without SC (5.57 mJ) was,

$$\text{Total Turn} - \text{On EESC E}_{\text{Reduction}} = \frac{5.57\ \text{mJ} - 0.645\ \text{mJ}}{5.57\ \text{mJ}} \times 100\% = 88.4\%$$

From Table 7-13, a column plot in Figure 7-30 gave a visual comparison of the switching energies at levels 1, 2 and 3.

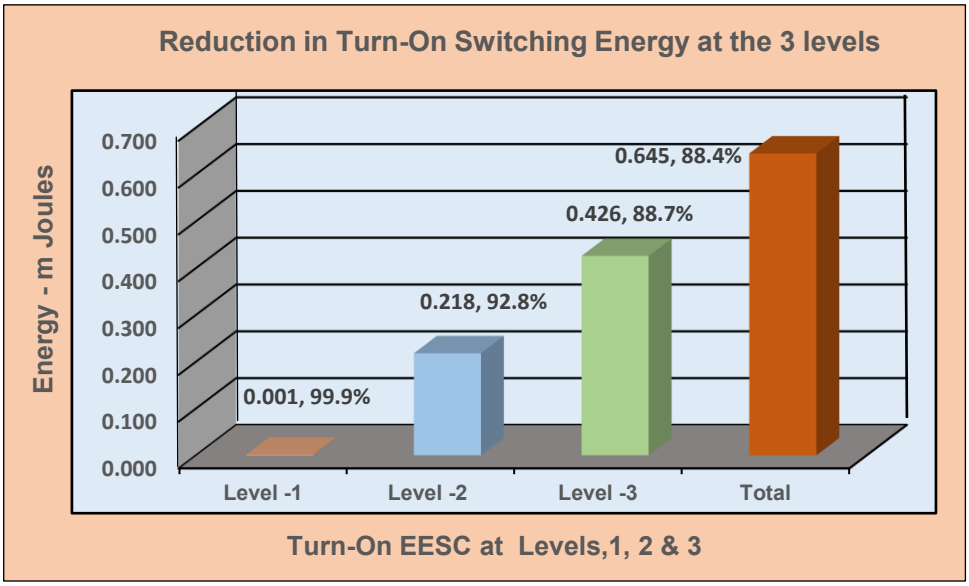

Figure 7-30 Reduction in turn-on E_{SW} by Turn-On EESC compared to E_{SW} without SC.

In Figure 7-30, the highest reduction (99.9%) was shown to be at Level – 1, with eight IGBTs in the switching circuits, at a supply voltage of V1, followed by level - 2 (92.8%) at a supply voltage of (V1 + V2) and Level - 3 (88.7%) at a supply voltage of (V1 + V2 + V3). The progressive decrease in the percentage reduction is a result of:

5.7.4.1 Comparison of Turn-On Inductor at level, 1, level 2, and level 3

At level 1, the Turn-On inductor voltage to minimise the IGBT inrush current was equal to V1 given by,

$$L \times \frac{di_{level\ 1}}{dt} = V_1$$

which resulted in the high switching energy reduction of 99.9%

At level 2, the Turn-On inductor voltage to minimise the IGBT inrush current was not equal to (V1 + V2) given by,

$$L \times \frac{di_{level\ 2}}{dt} \neq (V_1 + V_2)$$

and resulted in a lower switching energy reduction of 92.8%

Similarly, at level 3, the Turn-On inductor voltage to minimise the IGBT inrush current was not equal to (V1 + V2 + V3) given by

$$L \times \frac{di_{level\ 3}}{dt} \neq (V_1 + V_2 + V_3)$$

and hence resulted in a further switching energy reduction of 88.7%

Additionally,

$$\frac{di_{level\ 1}}{dt} < \frac{di_{level\ 2}}{dt} < \frac{di_{level\ 3}}{dt}$$

However, given the inequalities in the voltages and current gradients levels, the Turn-On inductor values determined by Linear approximation of the step current rise resulted in acceptable high reduction in switching energies. Hence, the Least Square method of linearising a step-current wave shape was an effective tool in simplifying the switching energy reduction analysis.

7.5.5 Determination of Turn-On EESC recovered energy.

The Turn-On EESC recovered energy $E_{Turn\text{-}On}$ is given by,

$$\text{EESC } E_{ton} = \sum (E(V1 + V2 + V3)_{No-sc}) - (E(V1 + V2 + V3)_{With-sc}) \tag{7.11}$$

In Section 7.2.7.1,

$$(E(V1 + V2 + V3)_{No-sc}) = 4069 \text{ Joules}$$

Determination of the second part of equation (7.11).

Simulated Power measurement were made for the batteries, V1, V2 and V3 and shown in Figure 7-31.

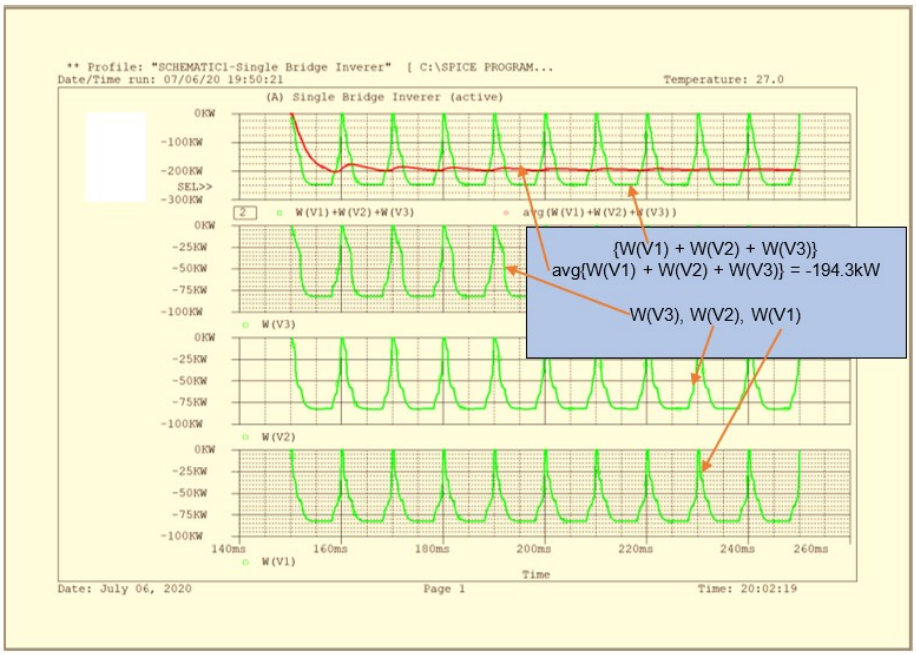

Figure 7-31 Power Traces of V1, V2, V3, their Sum and Average

From Figure 7-31,

$$E_{(V1+V2+V3)} = \sum_{k=1}^{n} (W_k \times T) \text{ Joules}$$

$$= \sum(\text{avg}(\text{W(V1)} + \text{W(V2)} + \text{W(V3)}) \times 0.02\text{s}, \text{Joules}$$

$$= (-194.3\text{kW} \times 0.02\text{s})\text{Joules}$$

$$\text{E}_{\text{Cycle}} = -3886\text{Joules}$$

Substituting in equation (7.11) and ignoring the negative sign, which is the notation used to indicate energy direction,

$$\text{EESC E}_{\text{ton}} = \sum(4069 - 3886)\,\text{joules}$$

$$\text{EESC E}_{\text{ton}} = 183\ \text{Joules}$$

Hence, the energy recovered by six Turn-On EESC was 183 Joules.

7.5.5.1 Annual cost saving from recovered energy by Turn-On EESCs.

The 183 Joules of energy was recovered in 20 ms (1- cycle)

Energy recovered in 1h,

$$\text{E}_{\text{per h}} = \frac{183\ \text{J}}{0.02\ \text{s}} \times 1\text{h} = \frac{9150\ \text{J}}{\text{s}} = 9.15\ \text{kWh}$$

Annual energy recovered,

$$\text{E}_{\text{Year}} = 9.15\ \text{kW} \times 24\ \text{h} \times 365\ \text{days} = 80154\ \text{kWh}$$

Annual cost of Electricity at £0.14/kWh,

$$\text{Cost}_{\text{Year}} = 80154\text{kWh} \times £0.14 = £11{,}221$$

In Section 7.2.7.5, the annual dissipation cost = £125,000.

$$\text{Reduction in Annual Dissipation Cost} \quad = £125{,}000 - £11221$$

$$= £113779$$

Hence, the impact of six Turn-On EESC was a reduction by £11,221 (9%) of the annual dissipation cost.

7.5.6 Design Strategy used and benefits of the Turn-On EESC.

This chapter introduced the CHBMLI to which the Energy Efficient Turn-On SC was connected to reduce the IGBTs switching energy. The PSpice schematic was designed for a 7-level bridge with the following main design requirements: -

- Define the IGBTs pulse widths (PWs) for the PSpice Drive generators.
- Identify the IGBTs which require the same PWs to generate the positive and negative Inverter output voltage.
- Update the PSpice Power IGBT with the high-power parameters of the chosen Power IGBT module.
- Choose a convenient battery voltage for each of the three bridges.

The completed schematic with a connection to a resistive load, successful simulations were made to measure the voltage, and current at each IGBT. To avoid different values of Inductors for the Turn-On Energy Efficient SC (EESC), the step rise of the current wave was linearised by the application of Least Square Linear approximation analysis. This resulted in a common inductor for the Turn-On EESC connected to each IGBT.

Six Turn-On EESC were connected, two to the upper IGBTs in each of the three bridges. With the connection of a secondary Inductor, the recovered energy by the primary inductor was returned to the supply. The IGBTs switching energy were measured with elevated levels of energy reduction in the 90% to 99% range when compared to the switching levels without any SC connected.

Applying an average National electricity kWh tariffs, to the reduction of switching energy values, the annual cost savings resulted in the reduction of dissipation costs from £125,000 to £113,779, a saving of £11221. These savings increased with the application of the Turn-Off EESC which is the topic for the next section.

7.6 Design of the Turn-Off EESC for connection to the CHB7LI.

The above section on the Turn-On EESC was successfully completed by achieving high reduction of the IGBTs turn-on switching energy. This section continues with similar switching tests during the IGBT's turn-off transitions.

7.6.1 Calculation of the capacitor and energy Inductor for the Turn-Off EESC

At the IGBT turn-off the maximum load current is diverted to the capacitor, whilst the IGBT current drops to zero *(-di/dt)* and the voltage rises *(+dv/dt)* to the measured supply voltage.. The snubber capacitor voltage, V_C is determined from equation (5.7), when t = t_{fall}, hence,

$$V_C = \frac{i_C \times t_{fall}}{2 \times C_s} \text{ volts} \tag{7.12}$$

The time difference from I_{max} to V_{max} is defined as t_{fall}. In Figure 7-14, I_{max} = 150A, V_{max} = 500Volts and t_{fall} ≈ 2ms. Substituting these values in (7.12) and equating for Cs returns the value of C_S,

$$C_s = \frac{i_C \times t_{fall}}{2 \times V_C} \text{ F}$$

$$C_s = \frac{150 \text{ A} \times 2 \text{ ms}}{2 \times 500} \text{ F}$$

$$C_s = 300 \text{ µF}$$

7.6.1.1 Calculation of the primary inductor Lp

The frequency of the PSpice IGBT gate drive generator is 50Hz. Let the transfer of the capacitor energy to the discharge series inductor Lp occur at a resonant frequency of 50Hz. Hence Lp can be calculated from the standard series circuit resonant frequency equation,

$$f_0 = \frac{1}{2\pi\sqrt{L_p \times C_S}}\ \text{Hz}$$

$$\sqrt{L_p \times C_S} = \frac{1}{2\pi \times 50} = \frac{1}{314.2}$$

$$L_P = \left(\left(\frac{1}{314.2}\right)^2 \times \frac{1}{300\mu F}\right)\ \text{H}$$

$$= \left(\frac{10^4}{314.2^2} \times \frac{1}{3}\right)\ \text{H}$$

$$\approx 34\ \text{mH}$$

7.6.1.2 Calculation of the Secondary inductor Ls

Ls is mutually coupled to L_P and discharges the recovered energy into the supply.
Choosing a turns ratio, n = 5,

$$L_s = n^2 \times L_P$$

$$L_s = 25 \times 34\ \text{mH} = 850\ \text{mH}$$

The main components for the Turn-Off EESC are,

Cs = 300 µF

Lp = 34 mH

Ls = 850 mH

Lp and Ls forms the primary and secondary inductors for the PSpice K_Linear transformer used in the Turn-Off EESC energy recovery.

Since the IGBTs current in both positive and negative circuits of the CHB7-Level Inverter are the same (and equal to the load current), each IGBT in the lower pair of the bridges will have the same Turn-Off EESC.

Figure 7-32, represents Bridge A section of the complete schematic shown in Appendix *B – Schematic for the CHB7LC with Turn-On and Turn-Off EESCs*. In subsequent simulations for IGBTs energy recovery measurements, Figure 7-32 will be used.

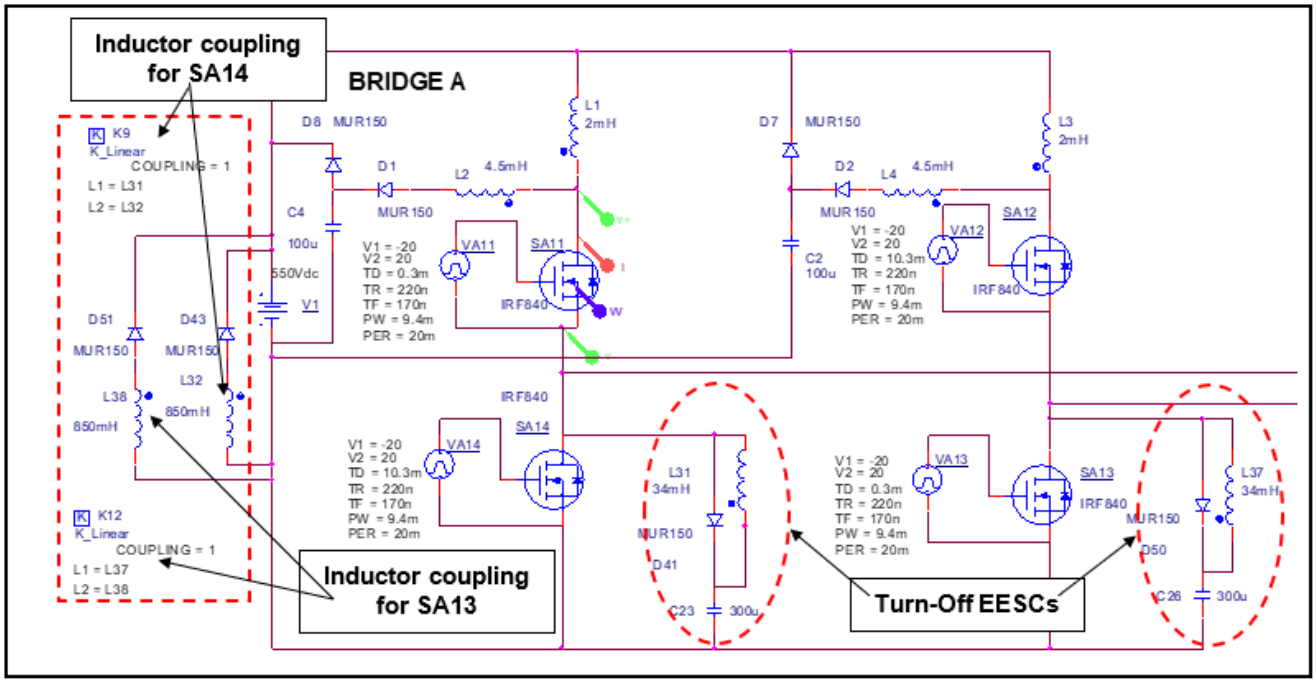

Figure 7-32 Bridge A showing the Turn-Off EESCs and its Energy Recovery Inductors

7.6.2 Circuit operation of the Turn-Off EESC

In Figure 7-32, the dotted red circle on the right shows the Turn-Off EESC connected to IGBT-SA13 and the other to the left connected to IGBT-SA14.

At turn-off, V_{SA13} rises and forward biases D50 and charges C26 to supply voltage. At turn-on, C26 discharges through L37 (D50 is blocked) which is coupled to L38. As the voltage (V_{L38} = L_{38}*di/dt) developed across L38 becomes greater than V1, the energy transferred from L37 to L38 is discharged into V1 less the energy dissipated in D51. The energy discharge into V1 stops when V_{L38} drops below V1 voltage.

Similarly, in the negative cycle the Turn-Off EESC across IGBT-SA14 energy stored in C23 is transferred to L31 and discharges the energy into V1 via L32.

To determine the total energy recovered by the six Turn-Off EESCs and fed-back to the three batteries, the reduction in turn-Off switching energy at the six IGBTs need to be measured. The energy removed/recovered from the IGBTs is delivered by the EESC to V1, V2 and V3. This recovered energy will be determined by taking the difference between the total battery energy without and with Turn-Off EESC connected.

Before calculating the total Turn-Off EESC recovered energy, one example of turn-Off switching energy and one of energy transfer in Bridge A by simulation measurements will follow in the next two sections.

Example 1

7.6.2.1 Measurement of Turn-Off switching energy at IGBT-SA13

Measurement by simulation of voltage, current, power and t_{off} is shown in Figure 7-33.

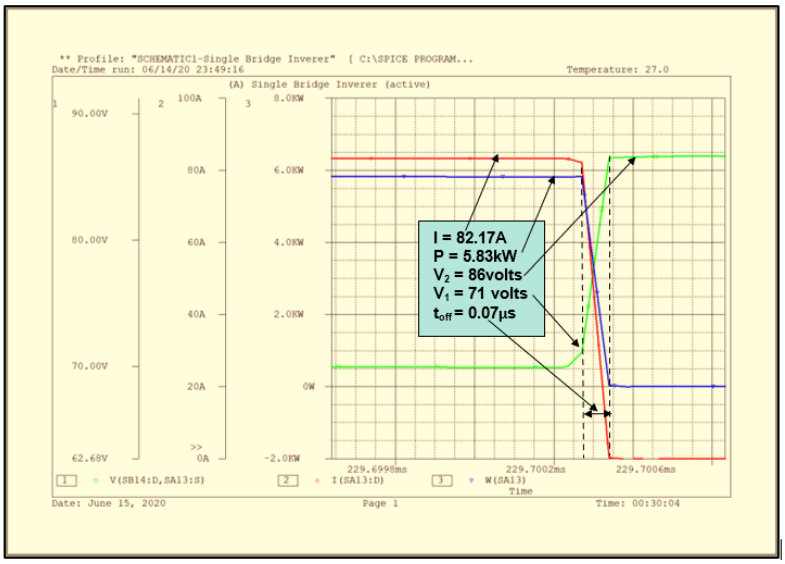

Figure 7-33 Traces of V, I and P at IGBT-SA13 for $E_{SW\text{-}Off}$

From Figure 7-33, the IGBT-SA13 turn-Off energy is,

$$E_{Sw-toff} = 5.83\text{kW} \times \frac{0.07\mu s}{2} \text{ Joules}$$

$$E_{Sw-toff} = 0.204 \times 10^{-3} \text{ Joules}$$

$$E_{Sw-toff} = 0.204 \text{ mJoules}$$

The IGBT-SA13 turn-Off switching energy is 0.204 mJ

7.6.2.2 Measurement of Turn-Off switching energy at IGBT-SA14

Measurement by simulation of voltage, current, power and t_{off} is shown in Figure 7-34.

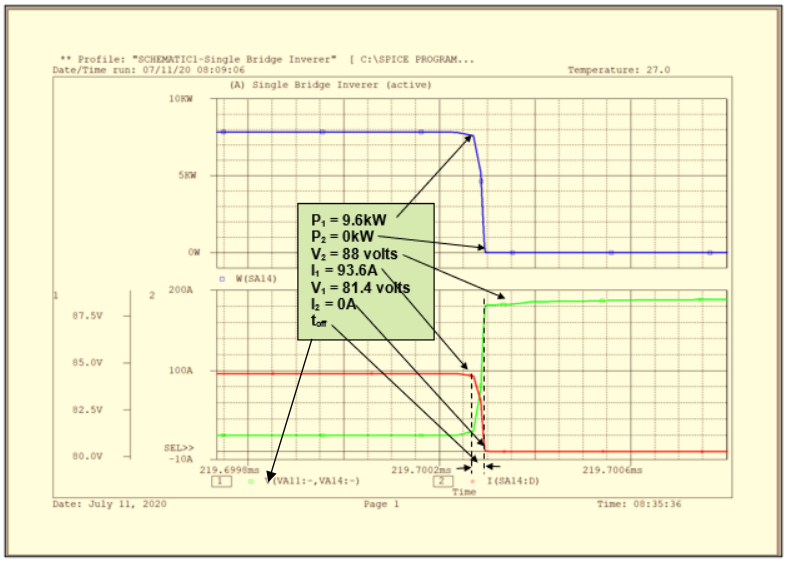

Figure 7-34 Traces of V, I and P at IGBT-SA14 for $E_{SW\text{-}Off}$ (t_{off} = 0.025μs)

From Figure 7-34, the IGBT-SA14 turn-off energy is,

$$E_{Sw-toff} = 9.6\ \text{kW} \times \frac{0.025\ \mu\text{s}}{2}\ \text{Joules}$$

$$E_{Sw-toff} = 0.12 \times 10^{-3}\ \text{Joules}$$

$$E_{Sw-toff} = 0.12\ \text{m Joules}$$

The IGBT-SA14 turn-Off switching energy is 0.12 mJ

7.6.2.3 Total turn-off switching energy for bridge A

$$E_{SW-\text{Bridge A}} = \sum (SA13E_{SW-toff}) + (SA14E_{SW-toff})\text{mJ}$$

$$E_{SW-\text{Bridge A}} = \sum (0.204 + 0.12)\text{mJ} = 0.324\ \text{mJ}$$

The total turn-off switching energy for Bridge A is 0.324 mJ

7.6.2.4 Measurement of Turn-Off switching energy at IGBT-SB13

Measurement by simulation of voltage, current, power and t_{off} in Figure 7-34, resulted in the IGBT-SB13 $E_{SW\text{-}toff}$ = 0.095mJ (same as for IGBT-SA14).

Hence, the total Bridge B, $E_{SW\text{-}toff,}$.

$$\text{Total Bridge B } E_{SW-toff} = \sum (SB13\ E_{SW-toff} \times 2)\ \text{mJ}$$

$$\text{Total Bridge B } E_{SW-toff} = 0.12\ \times 2\ \text{mJ} = 0.24\ \text{mJ}$$

The total turn-off switching energy for Bridge B is 0.24 mJ

7.6.2.5 Measurement of Turn-Off switching energy at IGBT-SC13

Measurement by simulation of voltage, current, power and t_{off} also resulted in traces as in Figure 7-34, resulting in the IGBT-SC13 $E_{SW\text{-}toff}$ = 0.0.12 mJ and the total Bridge C, $E_{SW\text{-}toff}$ = 0.24 mJ.

The total turn-off switching energy for Bridge C is 0.24 mJ

End of Example 1

Example 2

7.6.3 Transfer of recovered energy from IGBT-SA13 to V1

Measurement by simulation of V_{C26}, P_{L37}, V_{L38}, P_{L38} and the discharge current in D_{51} are shown in Figure 7-35.

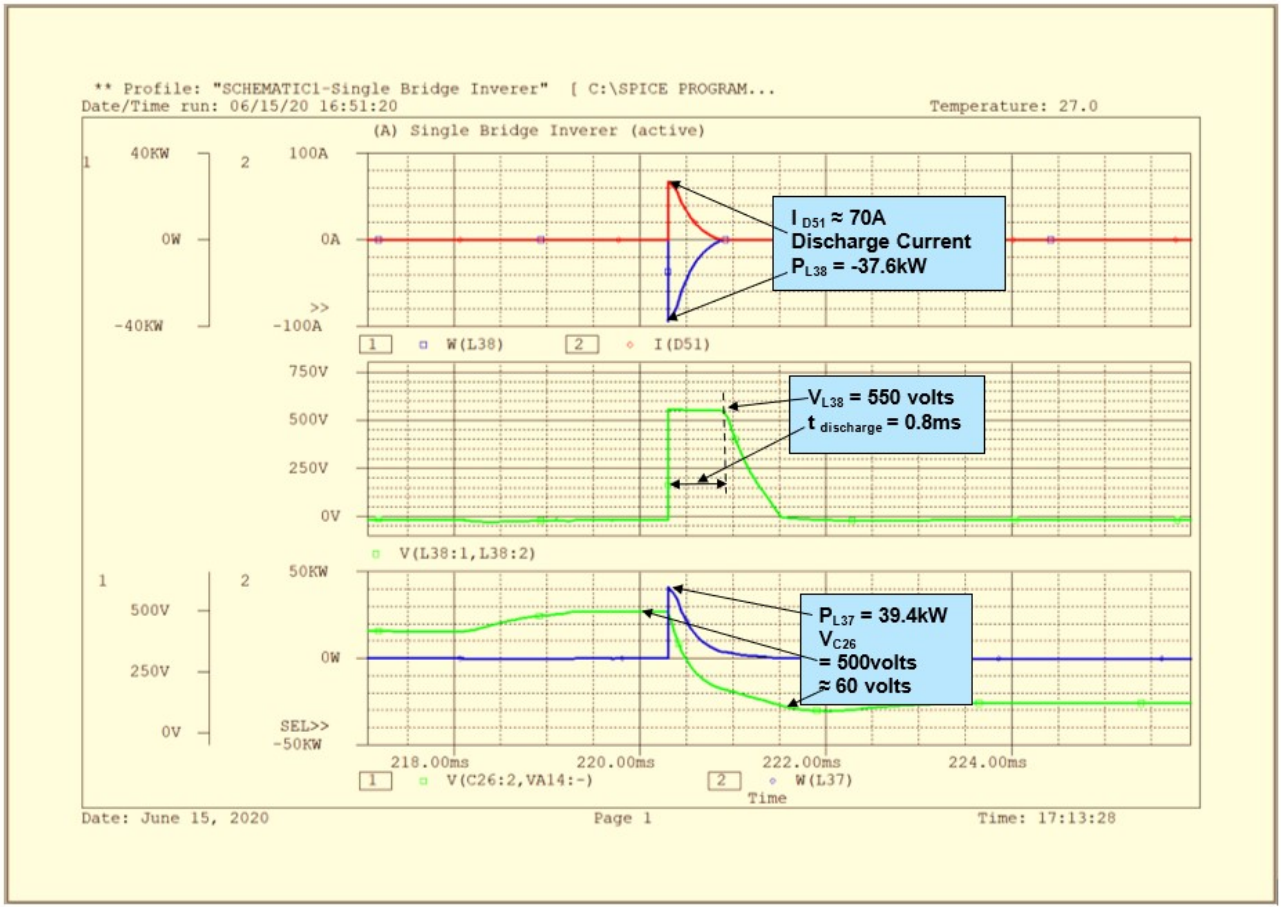

Figure 7-35 IGBT-SA13 Measurement of Recovered energy from L37 to L38 to V1

In Figure 7-35, the middle green trace of V_{L38} has an initial voltage greater than V1 (550 volts), which is clamped to 550 volts whilst it is discharging current via D_{51}. V_{L38} is greater than V1 for the period of 0.8ms, during which time the discharge energy continues, after which it reduces to zero. The energy discharged by L_{38} (referring to the top blue trace) is,

$$E_{L38} = 37.6\text{kW} \times \frac{0.8\text{ms}}{2} = 15.04 \text{ Joules}$$

Energy transferred from L_{37},

$$E_{L37} = 39.4\text{kW} \times \frac{0.8\text{ms}}{2} = 15.76 \text{ Joules}$$

The coupling between L_{37} and L_{38} was set to 1 at the K_Linear coupling parameter which assumes no losses. However, there is a loss (possibly due to measurements) in energy transfer between L37 and L38 of,

$$E_{\text{coupling loss}} = 15.76\text{ mJ} - 15.04\text{mJ} = 0.72\text{ mJ}$$

7.6.4 Transfer and measurement of recovered energy from IGBT-SA14 to V1

The simulation resulted in traces being the same as in Figure 7-35 for SA13. Hence, the energy transfer from SA14 to V1 is also 15.04Joules.

Total Recovered energy from Bridge A,

$$\text{Total Bridge A } E_{\text{Transfer}} = \sum (15.04 \times 2)\text{mJ} \approx 30.08\text{ mJ}$$

Total Transfer of Recovered energy from Bridge A is 30 mJ

End of Example 2

7.6.5 Supply energy with six (Turn-On & Turn-Off) EESCs connected

The result of simulated measurements is shown in Figure 7-36.

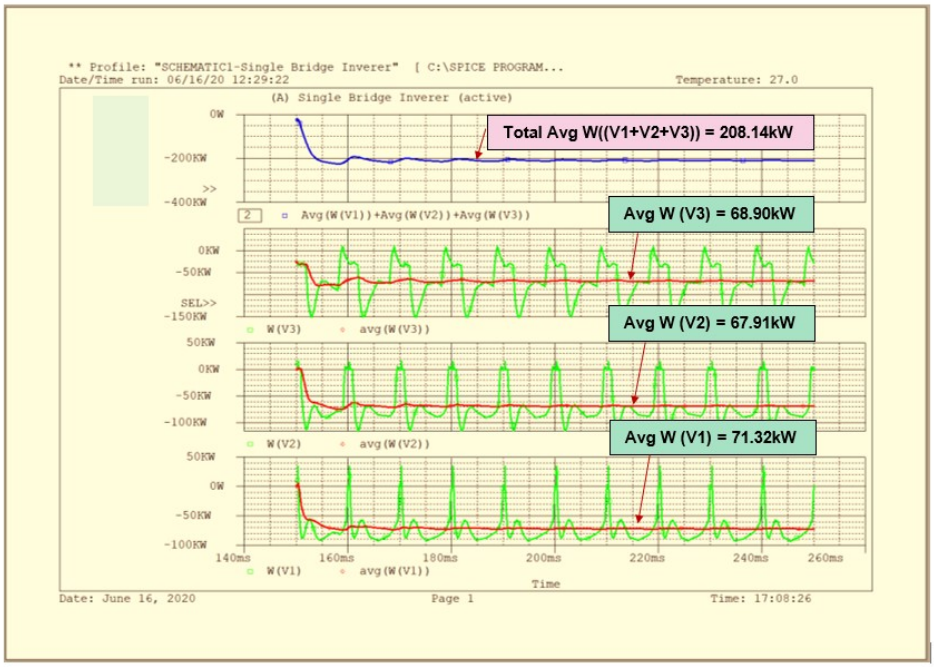

Figure 7-36 Average Supply Energy delivered by V1, V2 and V3 and sum (V1+V2+V3)

The Total average input battery energy after recovered energy per cycle by six Turn-On EESC and six Turn-Off EESC is,

Total $\mathrm{E_{Recovered}} = \big(\mathrm{AvgW}\big((\mathrm{V1}+\mathrm{V2}+\mathrm{V3})\big)\mathrm{kW} \times \mathrm{Tms}\big)\ \mathrm{J/cycle}$

$$(208.14\ \mathrm{kW} \times 20\ \mathrm{ms})\ \mathrm{J/cycle}$$

$$= 4162.8\ \mathrm{J/cycle}$$

In Section 7.5.5, the total average input battery energy measured after recovered energy per cycle by six Turn-On EESC = 3886 J/cycle. Therefore, the recovered energy by the six Turn-Off EESCs is,

$$\text{Energy recovered by 6 Turn} - \text{Off EESC, } \mathrm{E_{Recovered}} = (4162.8 - 3886)\ \mathrm{J/cycle}$$

$$= 276.8\ \mathrm{J/cycle}$$

7.6.5.1 Annual cost saving from six Turn-Off EESC

The 276.8 Joules of energy is recovered in 20ms

Energy recovered in 1s

$$\mathrm{E_{per\ s}} = \frac{276.8\ \mathrm{J}}{0.02\ \mathrm{s}} = 13840\ \mathrm{J/s} = 13.84\ \mathrm{kW}$$

Energy recovered in 1h,

$$\mathrm{E_{per\ h}} = 13.84\ \mathrm{kW} \times 1\mathrm{h} = 13.84\ \mathrm{kWh}$$

Annual energy recovered,

$$\text{Recovered } \mathrm{E_{Year}} = 13.84\ \mathrm{kWh} \times 365\ \mathrm{days} \times 24\mathrm{h} = 121238.4\ \mathrm{kW/annum}$$

$$\text{Recovered } \mathrm{E_{Year}} = 121.24\ \mathrm{MW}$$

Cost of Electricity at £0.14/kWh,

$$\mathrm{Cost_{per\ h}} = 13.84\mathrm{kWh} \times £0.14 = £1.94/\mathrm{h}$$

Annual cost of Electricity,

$$\mathrm{Cost_{Year}} = 121238.4\ \mathrm{kWh} \times £0.14 \approx £16{,}973$$

In Section 7.2.7.5, the annual Switch + Dissipation cost = £125,000.

$$\text{Reduction in Dissipation } \mathrm{Cost_{Year}} = £125{,}000 - £16{,}973$$

$$= £108{,}027$$

Hence, the impact of 6-Turn-Off EESC reduced the annual dissipation cost by £16973 (13.6%) from £125,000 to £108,027.

7.6.6 Total reduction of dissipation cost by six Turn-On and six Turn-Off EESC

In Section 7.5.5.1, the annual Dissipation cost saving by six Turn-On EESC = £11,221

In Section 7.6.4.1, the annual Dissipation cost saving by six Turn-Off EESC = £16,973. Since the current flowing in both positive and negative circuits is the same, it can be assumed, that if the Turn-On and Turn-Off EESCs were connected to the remaining twelve IGBTs, then an equivalent reduction of the switching energies, and annual cost savings will be doubled. Table 7-14, reflects this assumption and tabulates the energy reduction, annual cost savings, compared to the dissipation and corresponding cost made by the CHB-7LC without any SC connected.

Table 7-14 Annual Dissipation Cost saving by 24-Energy Efficient SC

Snubber Circuit	Clause	Recovered MWH/Annum	% Reduction	Clause	Annual cost £	Cost Reduction £ & %
12- Turn-On EESC	7.5.5.1	80 * 2 = 160	9%	7.5.5.1	11,221* 2 = 22442	102558, 18% (125000 – 22442)
12- Turn-Off EESC	7.6.4.1	121.24 * 2 = 242.48	13.6%	7.6.4.1	16,973 * 2 = 33946	91054, 27.2% (125000 – 33946)
(12*Turn-On + 12*Turn-Off) EESC		402.48	22.6%		56388	68612, 54.9% (125000 – 56388)
CHB-7LI (E_{SW} + $E_{Dissipation}$) and Cost (No SC)	7.2.7.1	4069 J/cycle = 1,782		7.2.7.5	125,000	

From Table 7-14, Figure 7-37 and Figure 7-38 gives a comparison of the annual cost savings and Energy reduction by the Turn-On and Turn-Off EESCs.

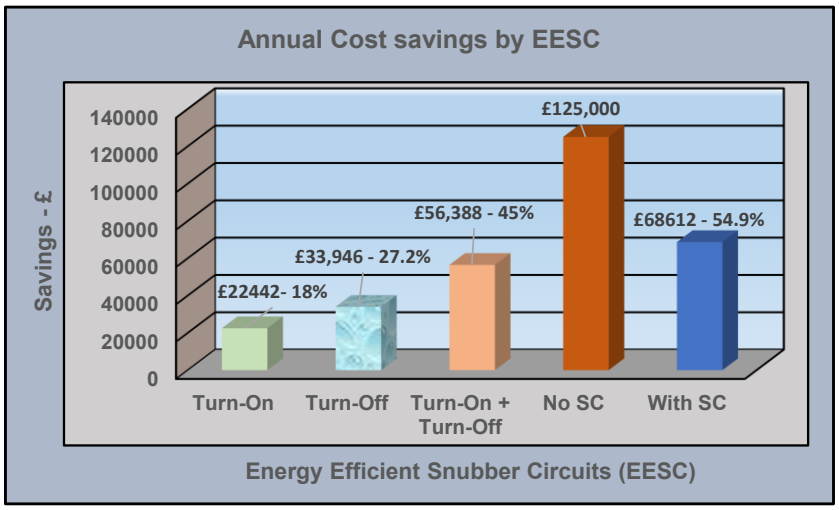

Figure 7-37 Comparison of Annual Cost Savings with & without EESCs to the CHB7LC

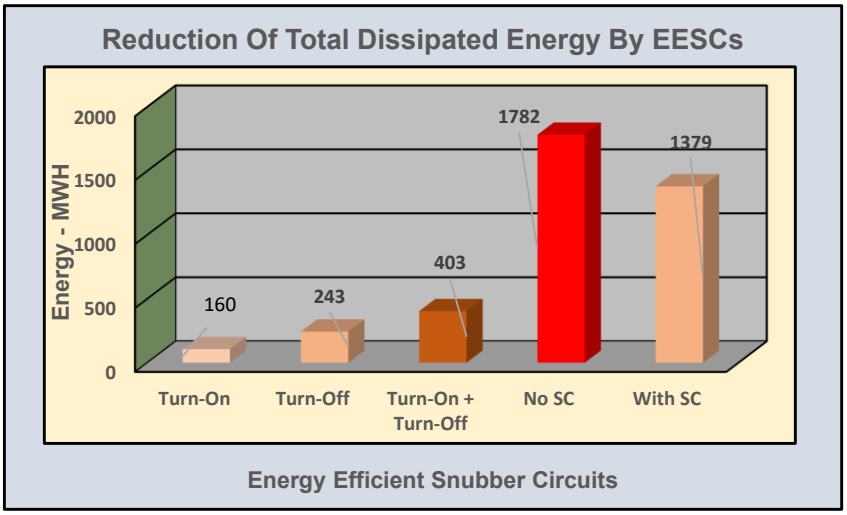

Figure 7-38 Annual Energy Reduction by EESCs compared to Losses without EESCs

In Figure 7-37, the annual savings in the reduction of dissipation cost is £56,388 a reduction of 45%, which reduced the total dissipation cost without snubber circuits from £125000 down to £68612 a reduction of 54.9%. This reduction is a direct result of the effective design of the EESCs.

In Figure 7-38, the impact of EESCs reduced the Total Dissipated Energy (1782 MWH) without EESCs down to (1379 MWH) 70%. This reduction translates to the annual power saving of 403MW, based on this case study load (98kW). This recovered energy can be significantly increased, if such EESCs were fitted to high power converters with switching devices and especially in HVDC Transmission Line Converter Stations.

7.6.7 Effect of EESCs on the power dissipation per IGBT.

In Section 7.6.4, the total input power with six Turn-On and six Turn-Off EESCs connected was 208.14kW. Assuming that with double the numbers of EESCs (i.e.,12), the recovered energy will half the input power, which will be 104.07kW. The Bridge dissipation is given by,

$$\mathrm{Bridge}_{\mathrm{Dissipaion}} = \left(\mathrm{P}_{\mathrm{input}} - \mathrm{P}_{\mathrm{Load}}\right) \text{ Watts} \tag{7.13}$$

To determine the Load Power, measurement at R10 by simulation results in Figure 7-39.

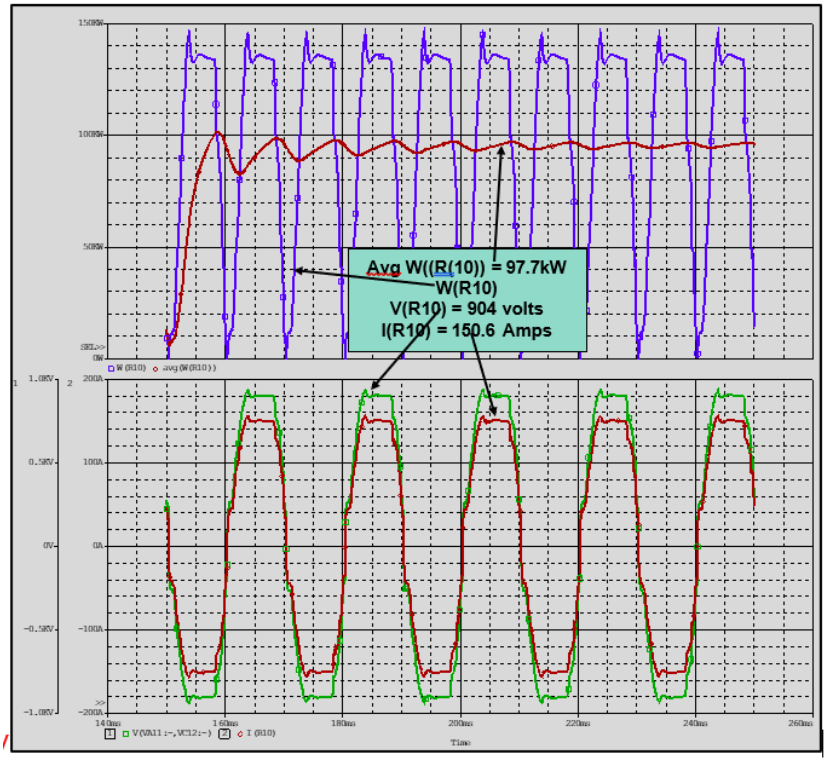

Figure 7-39 Measurement of V_{load}, I_{load} and P_{load}

From (7.13)

$$\text{Bridge}_{\text{Dissipaion}} = (104.07 - 97.7)\ \text{kW}$$

$$= 6.37\ \text{kW}$$

Assuming equal load distribution for the 12 IGBTs, each IGBT will dissipate,

$$\text{IGBT}_{\text{Dissipation}} = \frac{6370\ \text{W}}{12}$$

$$\text{IGBT}_{\text{Dissipation}} = 531\ \text{W}$$

If the four diodes in both positive and negative circuits are also included, the dissipation per device is,

$$\text{Device}_{\text{Dissipation}} = \frac{6370\ \text{W}}{16}$$

$$\text{Device}_{\text{Dissipation}} = 398\ \text{W} \approx 400\ \text{W}$$

From Figure 6-15, result of COMSOL Thermal simulation, the corresponding T_J for the IGBT dissipation at 531W and 400W are, 75^0C and 50^0C, respectively. These temperatures are less than the IGBT designed SOA T_J max of 157.5^0C and are operating at the lower region of the SOA. However, to maximise their power rating within the design SOA, the IGBTs power can increase to 2250W, an increase of (2250W – 531W) approximately 1.7 kW or by 1.8kW for

sixteen devices. Table 7-15 summarises the data for the IGBT dissipation versus its junction Temperature $T_J{}^0C$.

Table 7-15 Dissipation W_D - kW vs Junction Temperature - $T_J{}^0C$

IGBT (SW)	W_D - kW	T_J ^0C
SW - No SC	6.4	448
SW Data -Sheet SOA - No SC	2.5	175
SW COMSOL SOA – (with Heat sink)	2.25	157.5
SW - With SC	0.53	75

From Table 7-15, Figure 7-40 and Figure 7-41 presents a comparison of the Dissipation and Junction Temperature versus IGBTs with and without EESC connected.

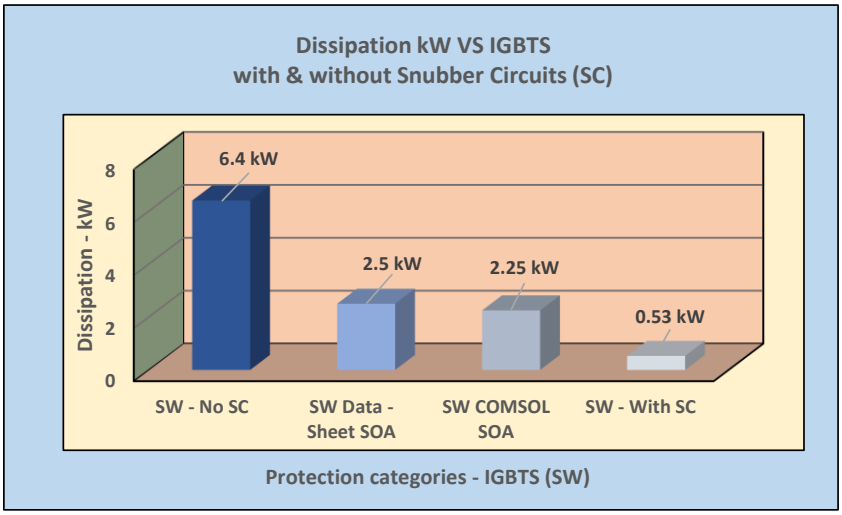

Figure 7-40 Comparison between IGBT SOA Dissipation with & without SC

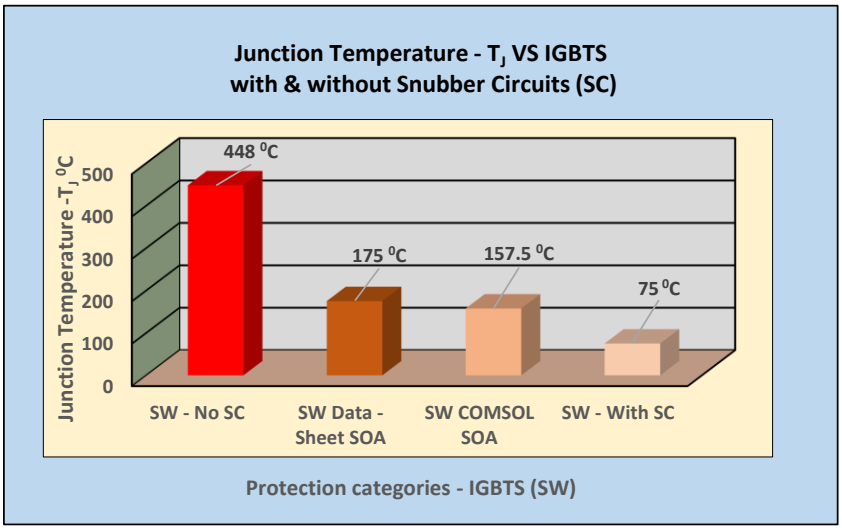

Figure 7-41 Comparison between IGBT T_J ^0C in SOA with and without SC

Figure 7-40 and Figure 7-41 visibly show that the application of the Turn-On and Turn-Off EESCs were very effective in reducing the IGBTs T_J well below the data sheet value of 175^0C, which was made possible by use of the COMSOL Thermal Simulation. Operation within the design SOA will extend the life of the IGBTs and Diodes which would require a minimum of cooling by heat sink or other cooling methods at a much-reduced cost.

The next section will examine the output voltage wave form as a result of the connection of the EESCs to the CHB7-LI.

7.6.8 Output voltage harmonics and THD with EESCs

The connection of V_1, V_2 and V_3 in series with the CHB7-LI without any SC connected, produced a stepped voltage and current wave shape at each IGBT. The connection of the Turn-On EESC to the IGBTs reduced both the inrush current and also its *di/dt*. To ascertain the change in the output wave shape made by the Turn-On and Turn-Off EESCs, additional test is made by Fourier frequency analysis on the harmonic levels and THD of the inverter output voltage and current. Simulation result is shown in Figure 7-42.

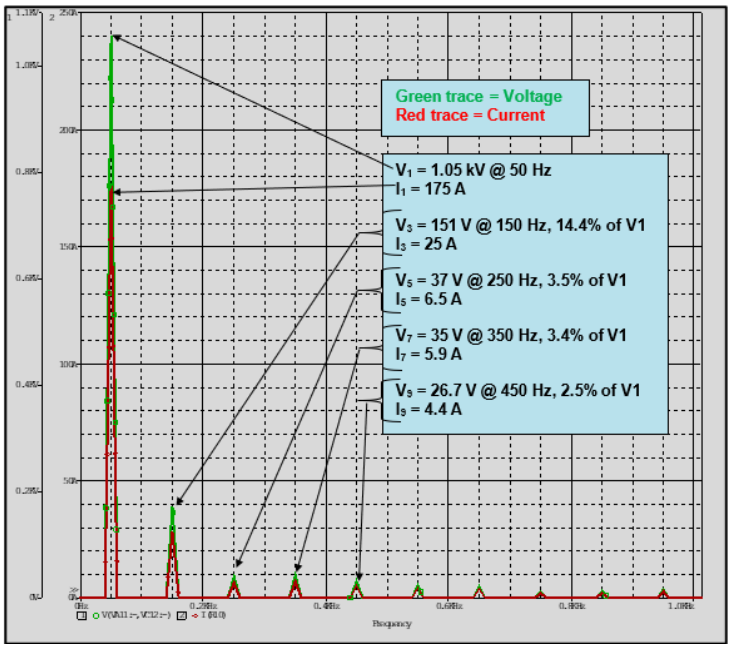

Figure 7-42 CHB7-LI Output Voltage and Current Harmonic Levels with EESCs

7.6.8.1 Determination of Total Harmonic Distortion (THD) with EESCs

THD is described as – The ratio of the sum of the RMS voltage or current of all harmonic components to the RMS voltage or current at the fundamental frequency. In Figure 7-42, the calculation of THD [4] of the voltage follows.

$$\mathrm{TDH} = \sum_{0}^{\infty} \frac{\mathrm{V_H}}{\mathrm{V_{1rms}}} \tag{7.14}$$

Where V_H is,

$$\mathrm{V_H} = \sqrt{(\mathrm{V_{T-RMS}})^2 - (\mathrm{V_{1-RMS}})^2} \tag{7.15}$$

7.6.8.2 Determination of $V_{T\text{-}RMS}$

In Figure 7-43 shows the output voltage green trace from which the RMS value was measured from the red trace to be 756.28 volts.

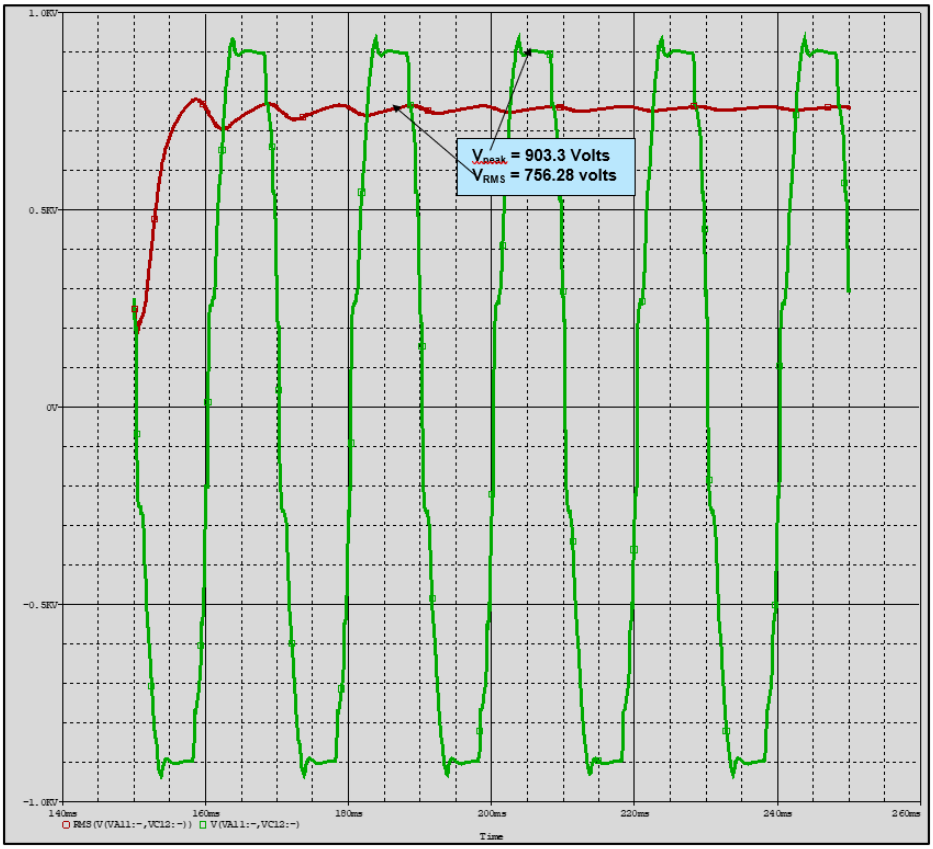

Figure 7-43 Measurement of RMS value of Inverter output Voltage

Where, $V_{T\text{-}RMS}$ is the total RMS harmonic voltage and $V_{1\text{-}RMS}$ is,

$$\mathrm{V_{1-RMS}} = \frac{\mathrm{V_{Peak}}}{\sqrt{2}}$$

From Figure 7-42, V_1 peak was measured to be 1050 volts, from which the $V_{1\ RMS}$ is,

$$\mathrm{V_{1-RMS}} = \frac{1050\ \text{volts}}{\sqrt{2}} = 742.6\ \text{volts}$$

and

$$(\mathrm{V_{1-RMS}})^2 = 742.6^2 = 551454.76$$

From (7.15),

$$V_H = \sqrt{756.28^2 - 742.6^2}$$

$$V_H = \sqrt{571959.43 - 551454.76}$$

$$V_H = \sqrt{20504.67} = 143.19 \text{ volts}$$

and from (7.14) the %THD is,

$$\%\text{THD} = \frac{143.19}{742.6} \times 100 = 19\%$$

To determine the effect the EESCs have on the harmonic and THD levels, the next section will measure these levels in the bridge with-out SC connected.

7.6.8.3 Determination of Total Harmonic Distortion (THD) without EESC

Harmonic voltage measurements by simulation is shown in Figure 7-44.

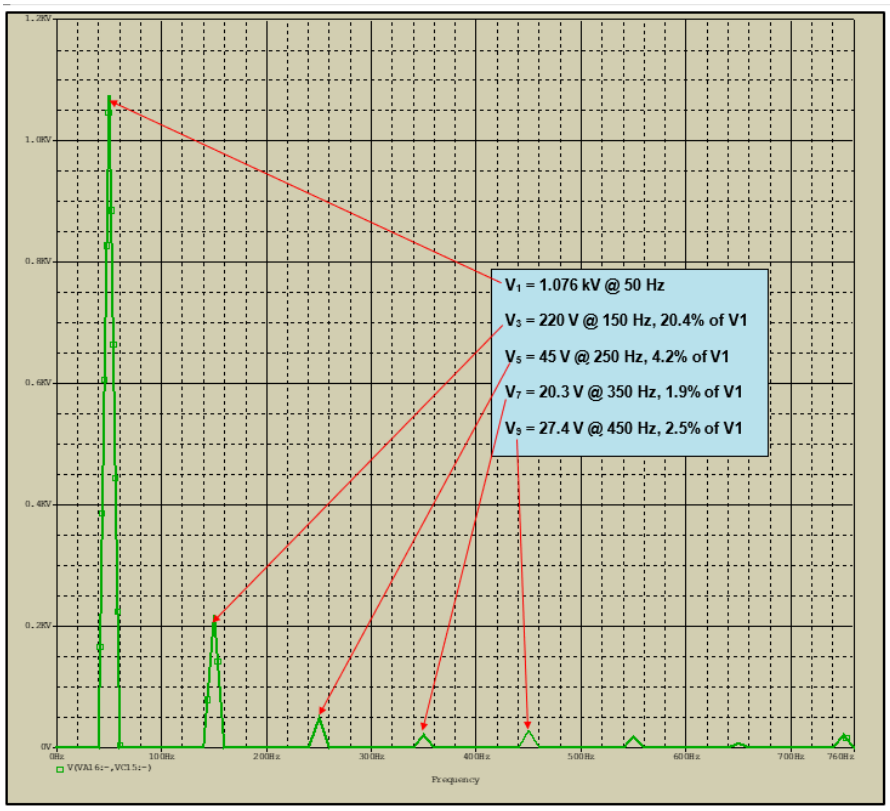

Figure 7-44 CHB7-LI Output Voltage Harmonic Levels without EESCs

To determine $V_{T\text{-}RMS}$ the output voltage was simulated, and the RMS value measured was 778.6 volts as shown in Figure 7-45.

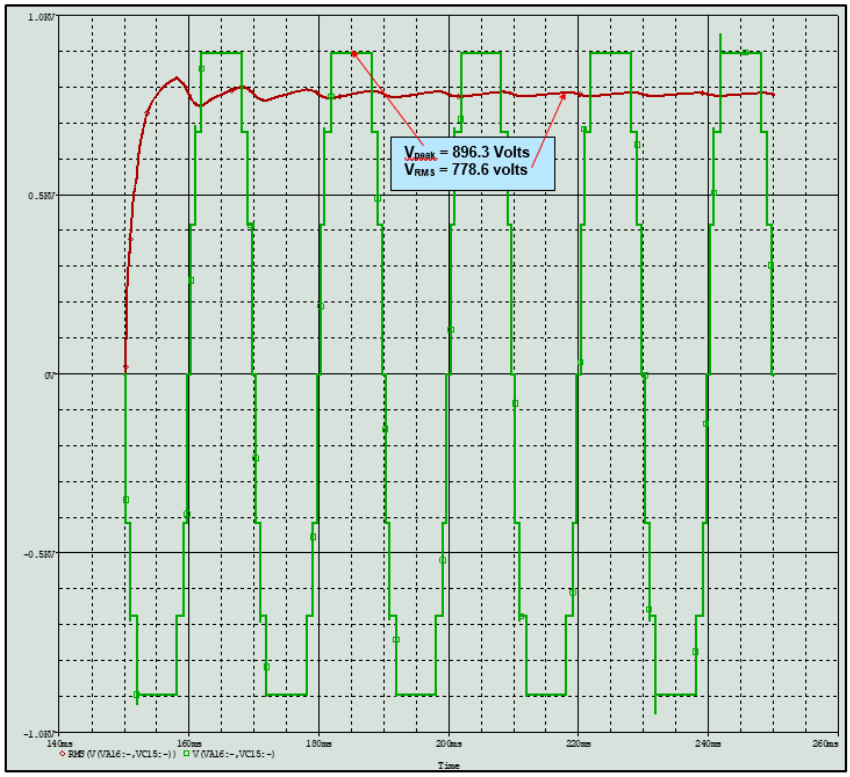

Figure 7-45 RMS value of Inverter output Voltage without SC

$$V_{1-RMS} = \frac{V_{Peak}}{\sqrt{2}}$$

From Figure 7-44 $$V_{1-RMS} = \frac{1076 \text{ volts}}{\sqrt{2}} = 760.96 \text{ volts}$$

and $$(V_{1-RMS})^2 = 760.96^2 = 579062.9$$

From (7.15), $$V_H = \sqrt{778.6^2 - 760.96^2}$$

$$V_H = \sqrt{606217.96 - 579060.12}$$

$$V_H = \sqrt{27157.84} = 164.8 \text{ volts}$$

and from (7.14) the %THD is, $$\%THD = \frac{164.8}{760.96} \times 100 = 21.7\%$$

7.6.8.4 Comparison of Harmonic V- levels & THD with & without SC

From the above measurements on harmonics voltage levels and percentage values compared to the fundamental at 50Hz, and calculation on the THD, Table 7-16 presented the data up to the 9th harmonic level. From this table, a visual comparison of the harmonic levels is presented in Figure 7-46.

Table 7-16 Harmonic Voltage levels and THD in CHB7LC

CHB7-LI	V1 Volts	V3 Volts	% V1	V5 Volts	% V1	V7 Volts	% V1	V9 Volts	% V1	% THD
Frequency -Hz	50	150		250		350		450		
With SC	1050	151	14.4	37	3.5	35	3.4	26.7	2.5	19
Without SC	1076	220	20.4	45	4.2	20.3	1.9	27.4	2.5	21.7

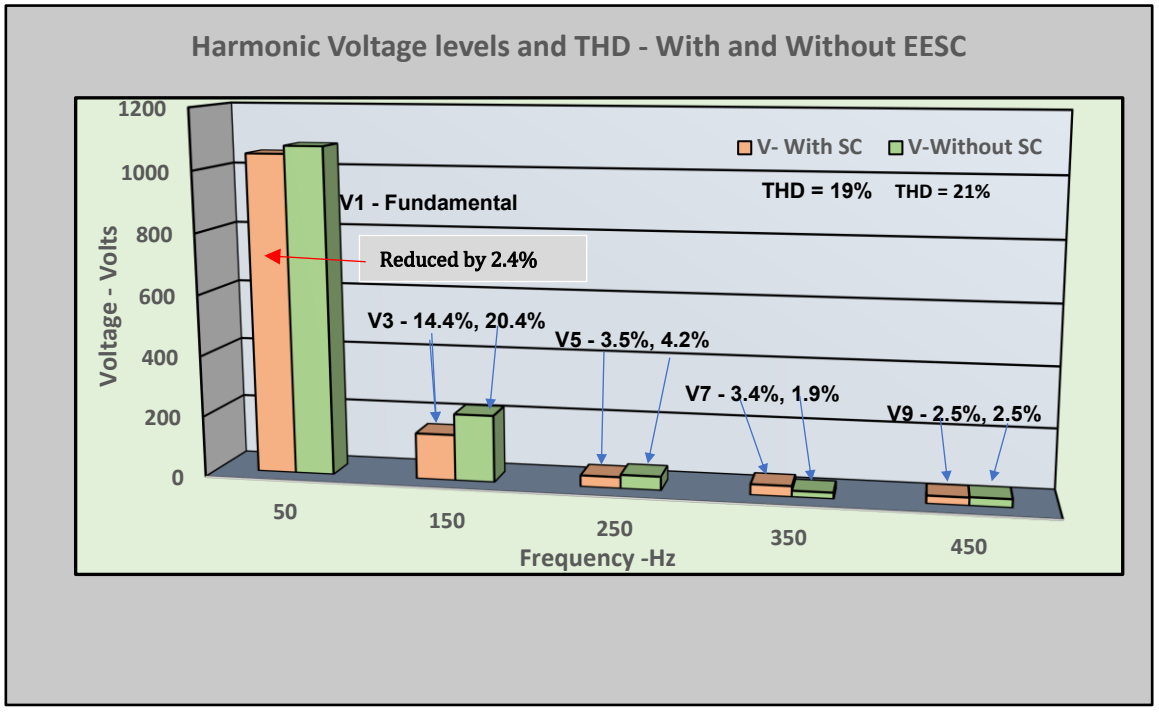

Figure 7-46 Comparison of Harmonic voltages and THD with & without EESCs

The harmonic levels obtained by the Turn-On and Turn-Off EESCs reduced the 3rd harmonic voltage level by 6% and the 5th by 0.7% compared to levels in the CHB7-LI with-out any SC. The levels were the same for the 9th harmonic, except for the 7th, the level increased by 1.5%. However, with reduced levels at the important harmonics of the 3rd and 5th, the output wave shape 'links' the connection of the EESC to the improved linearity of the Inverter output voltage.

At switch turn-off, the snubber capacitor diverts the load current which consists of harmonics. The reduction of switch energy during the turn-off period (t_{off}) is a product of V_{sw} and I_{load}, with I_{load} having components of odd harmonics. Hence, at the 7th harmonic which occurs at 350Hz, it is suggested that the Turn-Off EESC capacitor was not effective at the frequency of 350Hz. The IGBTs switching frequency was 50Hz (same as the inverter output frequency), at which the snubber capacitor value was determined and minimises the switching energy only at the fundamental frequency of 50Hz.

Hence, future investigation to optimise the Turn-Off EESC capacitor for application in CHBMLI, would be to calculate additional capacitors to minimise switching energies at the harmonic frequencies of 150Hz, 250Hz and 350Hz. With such 'tuned' capacitors, the energies can be recovered and returned to the supply, as compared to filters connected at the output stage where the harmonic energies are wasted in dissipated loss.

7.6.9 Design strategy used and benefits of the Turn-Off EESC

The Turn-Off Snubber capacitor was determined by measuring the overall voltage step rise and current step fall and the time difference between V_{max} and I_{min}. Due to the series circuit, each IGBT current was the same, hence, this method eliminated different EESC for each IGBT. Using the IGBTs switching frequency as the resonant frequency, the standard series resonant equation enabled calculation of the primary inductor to transfer energy from the capacitor to the energy recovery primary inductor (L_P).

The delivery of the recovered energy by (L_P) to the supply was enabled by a secondary inductor (L_S) whose value was determined by choosing a turns ratio to establish a large voltage gradient to force current into the supply. The PSpice K_Linear inductor symbol was used to provide the mutual transfer of the recovered energy from L_P to L_S irrespective of the location of the secondary inductor, which made it convenient to simplify circuit connection.
Two Turn-Off EESCs were connected to the lower IGBTs of each of the three cascaded bridges. Total recovered energy delivered by the six Turn-Off EESCs was determined by taking the difference between the total energy from the three batteries with and without SC connected.

With the use of an average UK electricity tariff of £0.14/ kWh, the total CHB7LC annual dissipation cost was £125,000. With the recovered energy from 12 x Turn-Off EESCs (6 for the positive circuit and 6 for the negative circuit), this amount was reduced to £91,054/annum, a reduction of 27.2%.

The standard application of the Turn-Off EESC to reduce the turn-off switching losses achieved major additional benefit in the reduction of dissipated energy and its impact in the reduction of annual costs. Together with the Turn-On EESCs, the total benefits when scaled up to the MW range of power corresponds to a substantial proportion of energy fed back to the supply. National and Global scaling of these benefits, in addition to the possibility of reduction in end-user's energy tariffs may significantly contribute to the current Global topic of environmental pollution in the reduction of Global Warming. Dr Bimal K Bose recognised the crucial role Power Electronics (PE) has to offer, when he commented in his article [6] in 2009:

> Increasing emphasis is now placed on saving energy with the help of power electronics. Saving energy gives the financial benefit directly; it is particularly important where the

energy cost is high. In addition, reduced consumption means reduced generation that helps to indirectly solve the global warming problem.

Before completing this chapter, a brief component costing for both the Turn-On and Turn-Off EESC follows. It permits a comparison between the cost invested to provide electronic protection for the switching devices and the recovery of switching losses, with the annual cost Saving in reducing dissipation losses.

7.7 Component Cost for the Turn-On and Turn-Off EESCs.

In this Chapter, the case study involved HVDC converter stations which are installed by contractual agreements between Governments, Energy Suppliers, and large Electrical/ Power Electronics Industrial Companies e.g., ABB, Siemens etc. Due to the power requirements, the components used are usually custom made and their costs are not available for public access. Furthermore, for competitive tenders such information are not available to the public.

After several failed attempts in finding costs for high power rating components for the snubber circuits, the PPM Power company that supplies Brunel stores, assisted in finding comparative component costs which would give an effective estimate for the cost of the snubber circuits. Component costs were based on Data sheets [91], [92], [93], which enabled the costing figures in Table 7-17. For simplicity, the cost for both the Turn-Off and Turn-On EESCs were made the same.

Table 7-17 Turn-On and Turn-Off EESC Component Costs

Citation No.	Component	Turn-On-EESC	Turn-Off-EESC	Cost - £ per component	Quantity	Total - £
[86]	Power Diodes	X 2	X 2	334	4	1336
[87]	Inductor - L_P	2 mH x1	34 mH x 1	237	2	474
	Inductor, L_S	4.5 mH x 1	850 mH x 1	237	2	474
[88]	Capacitor	100 µF x 1	300 µF x1	400	2	800
Cost for (1 x Turn-On EESC) + (1 x Turn-Off EESC) =						**£3084**
Cost for (6 x Turn-On EESCs) + (6 x Turn-Off EESCs) connected in the Inverter =						**£18,504**

From Table 7-17, the estimated component cost for both Turn-On and Turn-Off EESCs (to date November 2020) for the final schematic shown in Appendix B is: -

$$\text{Component Cost for 12 Snubber Circuits} = £18{,}504$$

In Section 7.5.5.1, the cost saving in dissipation reduction loss by the six Turn-On EESC was £11,221. In Section 7.6.4.1, the cost saving in the dissipation reduction loss by the six Turn-Off EESC was £16.973. Hence, the total cost savings in dissipation reduction loss, was: -

$$\text{Total dissipation reduction cost saving/annum by 12 the Snubber Circuits} = £11{,}221 + £16{,}973$$
$$= £28{,}194$$

From the total dissipation reduction saving of £28,194, the component cost for the 12 snubber circuits can be recovered in: -

$$\text{Component cost recovered} = \frac{£18504}{\left(\frac{£28194}{12}\right)} \text{ mths}$$
$$= 7.9 \approx 8 \text{ mths}$$

Hence, the twelve EESCs will recover the components cost in 8 MThs.

7.8 Summary

This chapter introduced the PSpice schematic for a CHB7LC comprised of three cascaded bridges each with its own HVDC supply. The Turn-On and Turn-Off EESC were connected to the CHB7LC to reduce the IGBTs switching energy. To avoid different values of Inductors for the Turn-On EESCs, the step-rise of the current wave was linearised by the application of Least Square Linear approximation analysis. This resulted in a common Primary Inductor for the Turn-On EESC, with a Secondary Inductor to transfer the discharged energy by the Primary Inductor back to the respective battery supply. Six Turn-On EESC were connected achieving levels of energy reduction in the 90% to 99% range when compared to the IGBTs switching levels without any snubber circuits. Applying an average UK electricity tariff of £0.14/kWh, the total CHB7LC annual dissipation cost without snubber circuits was £125,000. The impact of six Turn-On EESCs, reduced the annual dissipation cost by £11,221 (9%).
The Turn-Off snubber circuit capacitor was determined by measuring the waveforms of the overall voltage step-rise and current step-fall values and the time difference between V_{max} and I_{min}. Due to the CHB7LC series circuit, each IGBT current was the same, hence, this method avoided the use of different snubber circuits for each IGBT. Using the IGBTs switching frequency as the resonant frequency for the transfer of energy from the Turn-Off snubber circuit capacitor to the recovery primary inductor (L_P), the standard series resonant equation enabled calculation of L_P. PSpice K_Linear inductor symbol was used to provide the mutual transfer of the recovered energy from L_P to the secondary inductor (L_S) irrespective of the location of L_S, which made it convenient to simplify circuit layout and connection. The impact of six Turn-Off EESCs, reduced the annual dissipation cost by £16973 (13.6%). The combined Turn-On and Turn-Off annual Dissipation cost reduction was £28194 (£11221+£16973)

The reduction in annual cost can be doubled to a substantial amount of £56,388 (£28194 x 2), if all 12-IGBTs in the CHB7LC were protected by Turn-On and Turn-Off EESCs,. Hence the annual cost would be reduced from £125,000 to £68,612 (£12500 - £56388). This huge cut in cost corresponds to an annual decrease in dissipated energy from 1782 MWH to 1379 MWH,

a significant reduction of 403MWH, which is comparable to the output capacity per hour of a Power Station.

An estimate of £18504 for the total component cost of the snubber circuits was presented. It was shown that this cost could be recovered by the cost saving in reduction of dissipation losses in less than eight months. However, connections of snubber circuits to the bridge will include labour costs and possible cost of down time if the converter is required to be shut down.

The analysis of COMSOL Multiphysics Thermal Simulation, resulted in establishing a reference SOA of (kW vs T_J ^{0}C), against which the effectiveness of both the Turn-On and Turn-Off EESCs were measured. Measurements by simulation revealed that the IGBTs T_J was reduced by approximately 57% from the Data sheet T_J of (175 ^{0}C). This implied that at the test Load the IGBTs could operate without any heatsink. To maximise their power rating within the design SOA, the IGBTs power can increase to the Data sheet SOA dissipation of 2.5kW at T_J of 175 ^{0}C. Hence a long maintenance free life of the IGBTs in the CHB7LC, was possible due to the application of COMSOL Thermal analysis.

The efficient design and application of the Turn-On and Turn-Off EESC reduced the switching losses. However, it also revealed a major additional benefit in the reduction of dissipated energy and its impact in the reduction of annual costs, which was an observation made by Dr Bimal K Bose in 2009 [6]. The total benefits when scaled up to the MW range of power, corresponded to a substantial increase in energy fed back to the supply and major reduction in energy costs. With National and Global scaling, in addition to the reduction in end-user's energy tariffs, may contribute to the very important current National and Global topic of Environmental Pollution in the reduction of Global Warming.

Chapter 8 Conclusions and Future Work

8.1 Derivation of the Research Title

In this research it was necessary to establish a defined title for the thesis which presented question(s) to be answered. This process was started by the review of Articles (Chapter 2 and Chapter 3) on snubber circuits (SC), which were found to apply only to low power applications. There was no data found on high power and elevated temperature applications of SC on the protection of switching devices, which led to a gap in power application of SCs. This gap revealed that there was a need to develop SCs to protect expensive power switching devices at the higher power levels.

Where IGBTs were switching high currents in power converters e.g., CHBMLC, in HVDC Converter Stations, air cooling condensers and circulating water cooling pumping systems were installed to cool the IGBTs to remove the switching and the turn-on dissipated energies. It was concluded that in those early days (1930), Power Electronics (PE) was not as yet developed to protect switching devices in high power converters (**Error! Reference source not found.**). Appendix D, confirmed that to date the practice of water cooling for the complete bridge was still being developed and implemented using liquid coolants. Such cooling methods were without any Energy Efficient Recovery System with high dissipation losses impacting on wasted input energy and related costs.

This research therefore took the challenge to investigate the possibility to at least provide protection of the power IGBTs by minimising the IGBTs' switching loss and develop Efficient Energy Recovery System with the design of Snubber Circuits.

Hence, the Research Title:

Design of Energy Efficient Snubber Circuits for Protection of Switching Devices in High Power Applications.

8.2 Design Requirements in the Research Title

The Research Title identified three design requirements which were all implemented successfully: -

1 – Energy Efficient Snubber Circuits (EESCs), i.e., a Turn-On and a Turn-off EESCs with energy recovery were designed.

2 – Scale down model of a HVDC Transmission Line Station CHBMLC was used for the Power Application.

3 – EESCs were connected to the switching devices (IGBTs) in the Converter. These provided protection by reducing the switching energies.

8.2.1 Low Power Implementation of Requirements #1 - Reduction in E_{sw}.

In Chapter 4 component optimisation was determined for the Turn-On EESC which were connected to the IGBT in a low power Buck-Boost Converter. Methods used for the component optimisation were, Graphical, Trial & Error were compared with the Graduated Reduction Gradient (GRG) solver in the determination of the Inductor for the Turn-On snubber circuit. The reduction in the IGBT switching efficiency levels obtained were, Trial and Error 90.8%, Graphical 93.8% and GRG Solver 97.1 %.

In Chapter 5 component optimisation was determined for the Turn-Off EESC. These EESCs were also connected to the IGBT in a low power Buck-Boost Converter. PSpice PARAM simulation was used to determine the capacitor from a range of capacitor values for minimum energy at IGBT turn-off, was compared with PSO and the GRG Solver methods in the determination of optimum capacitor for minimum switch energy. The reduction in the IGBT switching efficiency levels obtained were, PSpice PARAM, 93.3%, PSO 99.75% and GRG Solver 99.92%. In both Chapters 4 and 5, the results obtained validated that the GRG Solver was a superior Optimiser as it achieved the highest percentage efficiency reduction in switching energy.

8.2.2 High Power Implementation of Requirements #2 & #3 - Design of CHB7LC

Three cascaded bridges were designed to form a CHB7LC. Use of PSpice simulation ensured that each bridge was functioning correctly before they were connected in cascade. Each bridge was supplied by a 550 Volt DC battery with a 150 Amp resistive load. The switching periods set at the gate drive for the selected IGBTs were predetermined, which generated the seven-level step current and step voltage waveforms. This schematic was used throughout the research with simulations made by PSpice.

8.3 Application of COMSOL Multiphysics Thermal Simulation.

The use of Thermal Simulation establishing a reference SOA of (Input power kW vs T_J ^{0}C), against which the effectiveness of the EESCs were measured. Measurements revealed that the IGBTs' T_J was reduced by approximately 57% from the Data sheet T_J of (175 ^{0}C). At this SOA, thermal fatigue is avoided in the IGBTs and will provide a long or minimum maintenance free lifetime. The application of COMSOL Thermal analysis was found to be a very useful tool to permit cool operation of the switching devices.

8.4 Application of Least Square Analysis.

Application of the GRG Solver was investigated in the Component optimisation for the EESCs. Since the case study involved cascaded bridges with series connected IGBTs, and step current and voltage waveforms, the use of the GRG Solver would have been complex and very time consuming. Hence, it was not used and instead a scheme of simplifying the analysis was investigated. It was decided to apply the Least Square Analysis to linearise the step rise current due to the three cascaded connected bridges. This approximation permitted the determination of one Turn-On inductor per IGBT per bridge for the Positive Inverter output voltage and one for the IGBT Negative Inverter output voltage. This design approach, avoided calculation of inductors for each current step rise and also prevented an unsymmetrical Inverter Output voltage at the quarter cycle point. It also reduced the components costs for the Turn-On EESCs. High reduction in switching energies were achieved in the 90% range. Hence, the Least Square method of linearising a step-current wave shape was an effective tool in simplifying the switching energy reduction analysis and also achieving the additional benefit of attaining a symmetrical output Inverter voltage and current.

8.5 Energy Recovery circuits by use of PSpice Inductors

For the Turn-On EESC, two PSpice inductors were connected as a transformer. This model allowed the stored energy in the primary Inductor during IGBT turn-on to be transferred to the secondary inductor during IGBT turn-Off. This recovered energy was used to feed a capacitor pump circuit which discharged a current into the 550 Volt battery when the capacitor voltage exceeded the Battery voltage. The capacitor was allowed to charge due to a reversed bias power diode connected between the capacitor and the battery. This energy recovery scheme was successful in reducing the energy supplied by the battery to the bridge.

The Turn-Off EESC also used two PSpice inductors, but these were coupled by the PSpice ‘K_Linear’ inductor label. The use of this symbol enabled a remote location of the second inductor to be closer to the battery, with the primary kept close to the IGBT and in series to the switching capacitor. At IGBT Turn-Off, the capacitor provided an alternative path for the load current, which is discharged into the series inductor at IGBT Turn-On. The K_Linear label allowed transfer of the primary inductor energy to the secondary inductor. The inductance value of the secondary inductor was chosen to generate a voltage much higher than the 550volts battery to maintain an appreciable period of discharge current into the battery. The combined Turn-On and Turn-Off energy recovered and discharged back to the battery significantly reduced the input energy supplied to the bridge.

8.6 Research Results

8.6.1 Energy Recovery - Impact on Annual Energy and Cost Reduction

The EESCs Recovery circuits significantly reduced the CHB7LC annual input energy from 1782 MW (without any EESCs connected) to a level of 1379 MW (78.4%), a reduction of 403MW (22.6%), analogous to the capacity of a Power Generating plant.

Use of energy tariffs (£/kWh), revealed cuts in annual cost from £125,000 to £68,612 (55%) in the reduction of wasted dissipated energy. This decrease can benefit both the Supply authorities and consumers.

8.6.2 EESCs Components cost

Components cost for the twelve snubber circuits used in the CHBMLC was £18,504. This cost can be recovered in less than eight months by the snubber circuits on the annual cost saving of £28,194 in the reduction of switching dissipation losses.

8.6.3 Reduced dependence on Liquid cooling methods

The switching energy minimisation and recovery process of the IGBTs, resulted in a cooler IGBT, and the liquid cooling method currently used need only to remove the remaining dissipated energy during turn-on cycle. However, the remaining dissipated energy is further addressed under Future Works.

8.7 Main Contributions

8.7.1 Design of Energy Efficient Recovery Snubber Circuits

The successful Design of Energy Efficient Recovery Snubber Circuits.

When connected in a High-Power Converter the EESCs significant cost benefits from £125,000 to £68,612 (55%) in the reduction of wasted dissipated energy

This reduction in switching energy can reduce the dependence on water cooling methods, and benefit both the Supply Authorities and Consumers. Furthermore, it has brought attention to a source of Energy dissipation which is wasted by water cooling methods, without any Energy Recovery system in place.

An additional benefit from the inductors in the EESCs, resulted in an output inverter voltage with reduced gradient (dv/dt & di/dt) in the voltage and current step rise at each of the three switching stages. Simulated harmonic measurements resulted in a reduction of approximately 6% at V_3 down to 1.5% at V_7 when compared to the harmonics levels of the output voltage without any EESCs connected to the IGBTs in three bridges.

8.8 Potential Future Work

8.8.1 Automatic Voltage Control (AVC) for varying loads

Active EESCs were not designed in this research to manage varying loads, as the focus was on the performance of the EESCs rather than engaging in the design of an Automatic Voltage Control (AVC) system. Hence, future research can investigate feedback circuits with applying PWM gate drive signals to maintain AVC for the inverter output voltage due to varying loads. An extension of the AVC System can include the design of digitally controlled switched capacitors in the Turn-Off EESC to maintain minimum switched energy in the IGBTs at varying loads

8.8.2 Application of EESCs in HVDC CHBMLC Stations

If the EESCs can be applied to current HVDC Transmission CHBMLC Stations, significant advantages are possible towards reduction in fuel costs, better management in Power demands, decrease in consumers tariffs and most importantly impact on the reduction of Environmental Temperature Rise, an observation made by Dr Bimal K Bose recognised the crucial role Power Electronics (PE) has to offer, when he commented in his article [6] in 2009:

> Increasing emphasis is now placed on saving energy with the help of power electronics. Saving energy gives the financial benefit directly; it is particularly important where the energy cost is high. In addition, reduced consumption means reduced generation that helps to indirectly solve the global warming problem.

8.8.3 Parallel Connection Of Turn-On and Turn-Off EESCs

In the case study to avoid overlap in the reduction of switching energies, the Turn-On EESCs were connected to the upper pairs of IGBTs in each Bridge, and the Turn-Off EESCs were connected to the lower pairs. This separation enabled switching energy reduction analysis without encountering conflict between the EESCs. To enable both Turn-On and Turn-Off EESCs to be connected to the same IGBT, combining the snubbers could be considered. Suggested implementation would be to enable the Turn-Off EESC discharge period to begin after the Turn-On EESC reduced the IGBT switching energy at the turn-on period. One solution would be to use The Turn-On EESC Inductor to delay the start of the Turn-Off EESC discharge, by connecting the Turn-Off EESC discharge connection to the input side of the Turn-On EESC Inductor.

8.8.4 Switching Energy Reduction at harmonic components of I_1

The Turn-Off EESC was designed for resonance at 50Hz. Reduction of switching energy at the third and fifth harmonic load currents were not considered. With additional tuned capacitors connected in the EESC, calculated at 150 Hz for the 3rd harmonic and 250 Hz for the 5th

harmonic, an additional 17.5% of the fundamental recovered energy is possible, based on the current harmonic levels of 14% and 3.5% at 150Hz and 250 Hz, respectively.

8.8.5 Harvest of Recovered Energy and Application of EESCs in EVs

Harvest recovered energy to produce a separate power supply for CHBMLC auxiliary control circuits with the use of Boost Converters. Storage of recovered energy for Charging Stations for EVs. Application of EESCs in EVs, power unit especially those designed for high performance, speed, and battery energy management.

To protect the expensive IGBTs with energy recovery to impact on increase in miles per kWh. To optimise recovered energy for instant demand in load current due to rapid acceleration at high speeds.

8.8.6 Recover Turn-On Dissipated Energy with Thermo-Electric Generators (TEG)

Investigate the application of Thermo-Electric Transducers in CHBMLC to convert the remaining dissipated turn-on energy in the IGBTs to optimise the efficiency of the complete CHBMLC. The immediate benefit would be the reduction or elimination the expensive and complex circulatory of liquid coolant system currently in use. The Electrical energy obtained from the conversion of the IGBTs Turn-On dissipated energy by the TEG can be returned to the CHBMLC input supply. Combined application of the EESCs and TEG in a CHBMLC will be the optimum energy feedback system.

8.9 Answered The Research Question

The contributions and results have confirmed that the three above design requirements were successfully achieved. The results contributed to huge economic benefits, energy reduction, and less dependence on water cooling methods, which can benefit both the Supply Authorities and Consumers. Furthermore, it has brought awareness to a source of Energy dissipation which when reduced can have significant impact on the reduction of Environmental Temperature and Global warming.

References

[1] P. C. Todd, “Snubber Circuits, Theory Design and Application,” Texas Instruments, May 1993. [Online]. Available: http://www.scribd.com/doc/288580639.

[2] A. Caraveo, R. Gonzalez, P. Sanchez and A. Soto, “Brief Review on Snubber Circuits,” in *2010 20th International Conference on Electronics Communications and Computers (CONIELECOMP)*, Choula Mexico, 2010.

[3] Q. Li, L. Fisher, G. Qiao, E. Mura, C. Li and Y. Ding, “High performance cooling of a HVDC converter using a fatty acid ester-based phase change dispersion in a heatsink with double-layer oblique-crossed ribs,” *Energy Research - Wiley, https://doi.org/10.1002/er.5347,* pp. 5819-5840, 28 February 2020.

[4] N. Mohan, T. M. Undeland and W. P. Robbins, Power Elctronics, Converters, Applications and Design, 2nd Edition,, Minneaplois, USA: John Wiley, 1995.

[5] T. Castagnet, “New Triac, is the Snubber Circuit Necessary?,” STMicroelectronics, 1999. [Online]. Available: http://www.st.com.

[6] B. K. Bose, “The Past, Present and Future of Power Electronics,” *IEEE Industrial Electronics Magazine,* pp. 1-14, June 2009.

[7] D. Garrido-Diez and I. Baraia, “Review of Wide Bandgap Materials and their Impact in New Power Devices,” in *Electronics, Control, Measurements, Signals and their Applications to Mechatronics (ECMSM), 2017 IEEE International Work shop*, Donostia San Sebastian, Spain, 2017.

[8] National Research Council. Combat Hybrid Power System Component Technologies., “High-Temperature, Wideband Gap Materials for High-Power Electric Power Conditioning,” National Academic Press doi, 10.17226/10595, Washington, DC, 2002.

[9] L. Bartolomo, L. Abbatelli, M. Macauda, F. D. Giovanni, G. Catalisano, M. Ryzek and D. Kohout, “Wideband Gap Materials: Revolution in Automotive Power Electronics,” in *EVTeC and APE Japan on May 26, 2016* , Japan, 2016.

[10] A. Huang, “New cost-effective silicon carbide high voltage switch created,” North Caroline State University, North Caroline , 2016.

[11] H. Dr. Stork, “ON Semiconductor - The Value and Supply Chain Impact of Wide BANdgap Substrate Materials,” 13 July 2016. [Online].

[12] D. o. E. USA, "Wide Bandgap Power Electronics - Technology Assessment," USA, Department of Energy, 13 February 2015. [Online]. Available: https://www.energy.gov/sites/prod/files/2015/02/f19/QTR ch8.

[13] J. Alnasseir, "Theoretical and Experimental Investigations on Snubber Circuits for High Valves of FACTS-Equipment for Over-Voltage Protection," Fredrich-Alexander University of Erlangen-Nuremberg, 26 March 2007. [Online]. Available: http://www.tf.fau.eu/index.shtml.

[14] "Switching Loss Reduction Networks -Snubber Circuits," PowerGuru-Semikron-Power Electronics Information Portal, 6 March 2013. [Online]. Available: Http://www.powerguru.org.

[15] "Snubber Circuit Design Calculators," Daycounter, Inc. Engineering Services, 2016. [Online]. Available: Http://www.daycounter.com/Contact.phtml.

[16] S. Dong, Q. Zhang and S. Cheng, "Analysis and Design of Snubber Circuit for Z-Source Inverter Applications," *IET Power Electronics,* vol. 9, no. 5, pp. 1083-1091, 2015.

[17] A. Brambilla and E. Dallago, "Snubber Circuits and losses of Voltage-Source GTO Inverters," *IEEE Transactions on Power Electronics, Vol. 7, No. 1,* pp. 231-239, January 1992.

[18] K. Bose, "Benefits in both Hard and Soft Switching Topologies," infineon, June 2016. [Online]. Available: http://www.infineon.com/coolmos.

[19] S. Mohanram, M. Darwish and C. Marouchos, "Power Switching Device Losses - Simulation and Non-Simulation Methods of Calculations," in *53rd International Universities Power Engineering Conference*, Glasgow, 2018.

[20] A. Smith, "Calculating Power Loss In Switching MOSFETS," Power Integrations, Inc, 8 January 2011. [Online]. Available: https://www.eetimes.com/document.asp?doc id=1278970.

[21] N. Rao and D. Chamund, "Power Losses in an IGBT Module -AN6156-1, LN31943," DYNEX Semiconductor Ltd, September 2014. [Online]. Available: www.dynexsemi.com.

[22] A. Laprade and R. H. Randall, "Numerical Method for Evaluating IGBT Losses-Application Note AN-7520," Fairchild Semiconductor Corporation, January 2000. [Online]. Available: www.onsemi.com.

[23] "Determination of switching losses in IGBTs by loss-summation-method," in *Industry Applications Conference, 1995. Thirtieth IAS Annual Meeting, IAS '95. Conference Record of the 1995 IEEE*, Florida, USA, 1995.

[24] D. Graovac, M. Purschel and A. Kiep, "MOSFET Power Losses Calculation Using the Data Sheet Parameters -Application Note, V1.1, July 2006," Infineon Technologies AG, Neubiberg, Germany, 2006.

[25] U. Nicolai and A. Wintrich, "Determining switching losses of SEMIKRON IGBT modules-Applcation Note AN 1403, 2014-08-19," SEMIKRON INTERNATIONAL GmbH, Nuremberg, 2014.

[26] F. Semiconductor, "Resistor-Capacitor (RC) Snubber Design for Power Switches," Digi-Key Electronics, 6 August 2014. [Online].

[27] J. Christoffersen, "Switch Bounce and how to deal with it," 3 September 2015. [Online]. Available: Https://www.allaboutcircuits.com/technical-articles/switch-bounce.

[28] R. Severns, "History of Soft Switching," 2006. [Online]. Available: http://www.SwitchingPowerMagazine.com.

[29] H. Mao, J. A, A. Qahouq, W. QIU, Y. Wen and I. Batarseh, "Lossless Snubber Circuits for Current Doubler Rectifiers to Reduce Reverse-Recovery Losses," *IEEE Transactions on Power Electronics Volume 26 No.1,* pp. 2639-2644, 2003.

[30] E. Lindell and L. Liljestrand, "Effect of Different Types of Overvoltage protection Devices Against Vacuum-Circuit-Breakers-Induced transients in Cable Systems," *IEEE Transactions on Power Delivery, Vol.31, No.4. August 2016,* vol. 31, no. 4, 2016.

[31] "The Structures Electronic Symbols Basic Operations and Several Charateristics Representations of Power Semiconductor Devices," Power Semiconductor Devices-Editorial Team, 13 June 2015. [Online]. Available: Https://www.allaboutcircuits.com.

[32] "AN-1012; Reverse Recovery Time (Trr) of the Super Barrier Rectifier," APD Semiconductor, February 2006. [Online]. Available: http://www.apdsemi.com.

[33] J. Hagerman, "Calculating Optimum Snubbers," Hagerman Technology, 24 July 1995. [Online].

[34] S. Finney, B. Williams and T. Green, "RCD Snubber Revisited," *IEEE Transaction on Industry Applications,* vol. 32, no. 1, pp. 155-160, January/February 1996.

[35] B. Williams, "An IGBT Turn-On Snubber Circuit with Passive Energy Recovery," *International Journal of Electronics,* vol. 89, no. 4, pp. 521-533, 1998.

[36] Integrated, Maxim;, "Snubber Circuits Suppress Voltage Transient Spikes in Multiple Output DC-DC Flyback Converter Power Supplies," 12 November 2001. [Online]. Available: Http://maximintegrated.com/an848.

[37] X. He, S. J. Finney, B. W. Williams and T. C. Green, "An Improved Passive Lossless Turn-On and Turn-Off Snubber," in *IEEE*, Edinburgh, 1993.

[38] R. T. Li, H. S.-H. Chung and A. K. Sung, "Passive Lossless Snubber For Boost PFC with Minimum Voltage and Current Stress," *IEEE Transactions On Power Electronics,* vol. 25, no. 3, pp. 602-613, March 2010.

[39] T. Taufik, "Undergraduate research in Power Electronics-Super Barrier Rectifier Diode Project," in *37th Asee/IEEE Frontiers in Electronics Conference T2-1*, Milwaukie W I, 2007.

[40] P. Haaf and J. Harper, "Understanding Diode Reverse Recovery and its Effect on Switching Losses," 2007. [Online]. Available: https://www.fairchildsemi.com/technical-articles/Understanding-Diode-Reverse-Recovery-and-Its-Effect-on-Switching-Losses.pdf.

[41] IEC, "IEC 60038 IEC standard voltages," The Internbational Electrotechnical Commission (IEC), Geneva, 2009.

[42] T. Platzer and P. Reiter, "Snubber Circuits for Inductive Loads-Application Note DE 0100, revision 0100," HIQUEL, Bad Gleichenberg, 2010.

[43] D. Penkov, C. Vollet, C. Durand and C. K. Edey, "IEC Standard High Voltage Circuit-Breakers: Practical Guidelines for Overvoltage Protection in Generator Applications," in *Petroleum and Chemical Industry Conference Europe Conference Proceedings*, Europe, 2012.

[44] B. W. Young, "Bala Consulting Engineers - IEEE Draft PC57.142/D1.7," 3 January 2009. [Online]. Available: http://www.csemag.com/search/search-single-display/snubbers-protecting-medium-voltage-transformers-from-electrical-transients/9593723fb6.html.

[45] D. Shipp, T. Dionise, V. Lorch and B. MacFarlane, "Transformer Failure Due to Circuit-Breaker-Induced Switching Transients," *IEEE Transactions on Industry Applications,* vol. 47, no. 2, pp. 707-718, March/April 2011.

[46] *Medium Voltage Application Guide,* Christchurch 8440: Aucom Electronics ltd, 2012.

[47] British Standards Institution, *BSEN 60831-1-1998: Shunt power capacitors of the self-healing type for a.c. systems having a rated voltage up to and including 1kV - Part 1: General - Performance, testing and rating - Safety requirements - guide for installation and operation,* London: Standards Board, 1998.

[48] "Capacitor For Power Electronics - Product Brief," IXYS-WESTCODE - Lampertheim, Germany, December 2012. [Online]. Available: Http://www.ixys.com.

[49] "Power Factor Correction (PFC) Handbook HBD853/D - ON Semiconductor," 5 April 2014. [Online]. Available: Http://www.onsemi.com.

[50] F. Cathell, "Increasing Low Power Converter Efficiency with Resonanat Snubbers - AND8296/D," ON Semiconductor, Denver, Colorado, USA, 2008.

[51] "High-Voltage Switcher for Medium Power Offline SMPS Featuring Low Standby Power - NCP1027," ON Semiconductor, Denver, Colorado, USA, 2015.

[52] R. T. Li, H. S.-H. Chung, W.-H. Lau and B. Zhou, "Use of Hybrid PWM and Passive Resonant Snubber for a Grid-Connected CSI," *IEEE Transactions On Power Electronics, Vol. 25, No. 2.,* pp. 298-309, February 2010.

[53] H. Yamamoto, M. Kaneda and M. Nakaoka, "Three-phase Soft-Switching Inverter Resonant with Unique Resonant Snubbers," in *IEEE 1999 International Conference on Power Electronics and Drive Systems, PEDS'99, July 1991*, Hong-Kong, 1999.

[54] J. S. Lai, "Resonant Snubber Based Soft-Switching Inverters for Electric Propulsion Drives," *IEEE Transactions on Industrial Electronics Vol: 44, Issue: 1, February 1997,* pp. 71-80, February 1997.

[55] T. Zhan, Y. Zhang, J. Nie, Y. Zhang and Z. Zhao, "A Novel Soft-Switching Boost Converter With Magnetically Coupled Resonant Snubber," *IEEE Transactions On Power Electronics, Vol. 29, No. 11, ,* pp. 5680-5687, November 2014.

[56] J. S. Lai, R. W. Young and G. W. Ott, "Efficiency Modelling and Evaluation of a Resonant Snubber Based Soft-Switching Inverter for Motor Drive Applications," in *Power Electronics Specialists Conference, 1995, PESC'95 Record, 26th Annual IEEE*, Atlanta, GA, 1995.

[57] N. Hoshi and K. Oguchi, "Control schemes for auxiliary switches of three-phase PWM resonant snubber inverters," *Electrical Engineering in Japan,* vol. 152, no. 4, pp. 57-67, 2005.

[58] S.-P. Mun, C.-R. Kim, J.-K. Lee, H.-S. Kim, S.-H. Jung and S.-K. Kwn, "Induction Heating PWM High Frequency Inverter using New Active Auxiliary Resonant Snubber," vol. 22, no. 3, pp. 40-51, 2008.

[59] H. Zhang, B. Kou, L. Zhang and Y. Jin, "Digital Controller Design Based on Active Damping Method of Capacitor Current Feedback for Auxiliary Resonant Snubber Inverter with LC Filter," *Applied Science, 2016, 6, 377,* vol. 6, no. 11, pp. 1-22, 2016.

[60] ABB, "RESIBLOC transformers Product presentation," ABB, Zurich, Switzerland, 2013.

[61] ABB, "Installation and Instruction manual Dry-Type Transformers 112.5-10,000kVA," ABB Inc. www.abb.com/transformers, Bland, VA 24315 US, 2014.

[62] *BSEN 61643-11:2012: Low-voltage surge protective devices - Part 11: Surge protective devices connected to low-voltage power systems - Requirements and test methods,* London: British Standards Institution, 2012.

[63] D. P. Hasse, Overvoltage protection of low voltage systems, Stevenage: Instutution of Electrical Engineers, 2000.

[64] C. S. Mardegan, D. D. Shipp and M. R. Santana, "The Experience Acquired Sizing Snubbers to Mitigate Switching Transients in Industrial Power Systems," *IEEE Transactions on Industry Applications, Vol. 52, No.5, ,* pp. 3644-3654, September/October 2016.

[65] IEC - International Electrotechnical Commision, *ISO/IEC Directivesa Part 2 - 16 Terms and definitions,* Geneva: IEC - International Electrotechnical Commision;, 2021.

[66] A. Isurin and A. Cook, "Passive Soft-Switching Snubber Circuit with energy recovery," in *Applied Power Electronics Conference and Exposition, 2008, APEC 2008, Twenty-Third Annual IEEE*, Austin, TX, USA, 2008.

[67] S. Mohanram, M. Darwish and C. Marouchos, "Optimisation and Simulation of RC Time Constants in Snubber Circuits," in *53rd International Universities Power Engineering Conference*, Glascow, 2018.

[68] M. Corporation, Excel User's Guide Ver 5, United States of America, 1993.

[69] *PSpice Advanced Analysis User Guide, Product Version 17.2-2016,* San Jose, CA 15134, USA: Cadence Design Systems, Inc., 2016.

[70] L. Chandrakantha, "Using Excel Solver in Optimization Problems," in *Electronic Proceedings of the 23rd Annual International Conference on Technology in Collegiate Mathematics (ICTCM)*, Denver, March 2011.

[71] K. Stoyka, N. Femia and G. D. Capua, "Optimizing Power Converters with Partially Saturated Inductors by Evolutionary Algorithms," Italy, 2017.

[72] F. Gensheimer, S. Ruzika, S. Scholl and N. Wehn, "A Simplex Algorithm for LP Decoding Hardware," in *IEEE 25th International Symposium on Personal, Indoor and Mobile Radio Communications*, 2014.

[73] D. Fylstra, L. Lasdon, J. Watson and A. Waren, "Design and Use of the Microsoft Excel Solver," *Interfaces, Vol. 28 No. 5,* pp. pp. 29-55, September -October 1998.

[74] A. Engelbrecht, "Particle Swarm Optimization: Velocity Initialization," in *WCCI 2012 IEEE World Congress on Computational Intelligence*, Brisbane, Australia, 2012.

[75] L. Stokes and J. Plummer, *Using spreadsheet solvers in sample design,* Austin, Texas: ELSEVIER, 2002.

[76] M. A. Arasomwan and A. O. Adewumi, "On the Performance of Linear Decreasing Inertia Weight Particle Swarm Optimization for Global Optimization," HindawiPublishingCorporation, Durban 4000, South Africa , 2013.

[77] P. Maca and P. Pech, "The Inertia Weight Updating Strategies in Particle Swarm Optimisation Based on the Beta Distribution," Hindawi Publishing Corporation, Praha, Czech Republic, 2014.

[78] M. Alrashidi and M. EL-Hawary, "A Survey of Particle Swarm Optimization Applications in Power System Operations," *Electric Power Components and Systems,* vol. 34, pp. 1349-1357, 2006.

[79] T. Azoui, S. Verdi, J. B. Sauveplane and P. Tounsi, "3D Electro-Thermal Study for Reliability of Automotive Power Vertical MOSFET Using COMSOL Multiphysics," in *COMSOL Proceedings*, Milan, 2009.

[80] C. Ltd., "COMSOL Multiphysics 5.3a - Electronic Chip Cooling," COMSOL Ltd. Park House, Castle Park, Cambridge UK, Cambridge, United Kingdom, 2017.

[81] *IGBT Power Module, 1200V 600A - MG 12600WB-BR2MM,* Chicago: Littelfuse, 2016.

[82] "ON Semiconductor Handbook HBD 856/D— Basic Thermal Properties of Semiconductors," ON Semiconductor -http://onsemi.com, June-2009.

[83] M. Grauer, G. Gruhn and L. Pollmer, "Optimization of a Complex Plant by a GRG Algorithm," *Computers & Chemical Engineering, Vol. 3,* pp. 597-602, January 1980.

[84] B. Alamri, A. Sallama and D. M. Darwish, *Optimum SHE for Cascaded H-Bridge Multilevel Inverters Using: NR-GA-PSO, Comparative Study,* London: IEEE, 2017.

[85] B. Alamri and D. M. Darwish, "Power Loss Investigation in HVDC for Cascaded HBridge Multilevel Inverters (CHB-MLI)," London, England, 2019.

[86] B. E. Prices.org.uk, "Unit kWh Prices - Business Electricity Rates -Advice Guides," Business Electicity Prices, London, 2020.

[87] L.-G. Giraudet, L. Bodineau and D. Finon, "The costs and benefits of white certificates schemes," Springer Science+Business Media B.V.2011, Paris, 2011.

[88] A. Jeffrey, Mathematics for Engineers and Scientists, Fifth Edition, Newcastle upon Tyne, England: Chaptman and Hall, 1996.

[89] E. Kreyszig, Advanced Engineering Mathematics - Fourth Edition, Columbus, Ohio: John Wiley & Sons, 1976.

[90] T. H. Cormen, C. E. Leiserson, R. L. Rivest and C. Stein, Inroduction To Algorithms - Third Edition, Cambridge, Massachusetts, London, England: The MIT Press, 2009.

[91] A. S. Ltd, "5SDF 03D4502 - Doc. No. 5SYA1117-Fast Recovery Diode," ABB Switzerland, Semiconductors Ltd, CH-5600 Lenzburg, Switzerland, 03 Nov. 2019 .

[92] H. Manufacturing, "195E100 & 195G10 - Heavy Current Chassis Mount Inductors (195-196 Series) - Hammond Mfg.," https://www.hammfg.com/electronics/transformers/choke/195-196 , Mansfield, Texas USA, 9 February 2020.

[93] B. Michael, "Power Ring Film Capacitors - Part #: 773D105," Advanced Conversion, 81 Parker Road • Barre, VT 05641 USA, 29 April 2020.

[94] *ANSI/IEEE C37.013: 1989, IEEE Standard for AC High Voltage Generator Circuit Breakers Rated on a Symmetrical Current Basis,* Washington, D.C.: ANSI, 1998.

[95] *BS EN 62271-100: 2009 +A1:2012, (IEC 62271-100:2008), High Voltage Switchgear and Control Gear-Part 100: Alternating Current Circuit Breakers,* London: British Standards Institution, 2009.

[96] *IEEE Std C37.011: 2005, IEEE Application Guide for Transient Recovery Voltage for AC High-Voltage Circuit Breakers (Revision of IEEE Std C37.011:1994),* Washington, D.C.: ANSI, 2005.

[97] *IEEE Draft PC57.142/D1.7:2009, Snubbers: Protecting medium-voltage transformers from electrical transients.,* Washington, D.C.: ANSI, 2009.

[98] D. D. Shipp, T. J. Dionise, V. Lorch and B. G. MacFarlane, "Transformer Failure Due to Circuit Breaker Induced Switching Transients," *IEEE Transactions On Industry Applications, Vol.47, NO.2,* vol. 47, no. 2, pp. 707-718, March/April 2011.

[99] *ANSI/IEEE C57.142: 2010, Draft, A Guide to Describe the Occurrence and Mitigation of Switching Transients Induced by Transformer and Switching Device Interaction.,* Washington, D.C.: ANSI, 2010.

[100] *IEEE C37.013-1997:1997, (R2008) Standard for AC High-Voltage Generator Circuit Breakers on a Symmetrical Current Basis,* Washington, D.C.: ANSI, 1997.

[101] *IEEE C62.45:1992, IEEE Guide on surge testing for equipment connected to low-voltage (1kV and less) AC power circuits,* Washington, D.C.: ANSI, 1992.

[102] *IEC 61000-3-2: 2014 (IEC 1000-2-2:1990): Electromagnetic compatibility (EMC), Part 3-2: Limits-Limits for harmonic current emissions (equipment input < or = 16 A per phase),* Geneva 20: International Electrotechnical Commission, 2014.

[103] *BS EN 61071:2007 (IEC 61071): Capacitors for power electronics applications,* London: British Standards Institution, 2007.

[104] *IEC 61881:2010 Railway App-Rolling stock equipment – capacitors for power electronics – Part 1: Paper/plastic film capacitors,* Geneva 20: International Electrotechnical Commission, 2010.

[105] *IEEE 1547:2003, (R2008) Standard for Interconnecting Distributed Resources with Electric Power Systems,* Washnington, D.C.: ANSI, 2003.

[106] *IEC 61312–1:1995, Protection against lightning electromagnetic impulse – Part 1: General principles,* Geneva 20: International Electrotechnical Commission, 1995.

[107] L. Loffin, "Zero-Crossing Detectors Circuits and Applications," 8 January 2011. [Online]. Available: http://www.bristolwatch.com/ele2/zero_crossing.htm.

[108] R. Elliott, "Zero-Crossing Detectors and Comparators - AN-005," 8 January 2011. [Online]. Available: Http://Sound.whsites.net/appnotes/an005.htm.

[109] J. Houdek, "Solving SCR Line Voltage Notching - Researchgate," 1 9 2000. [Online]. Available: https://www.researchgate.net/publications/291623956.

[110] A. Bradley, "Eliminating Voltage Notching on the Distribution System-Rockwell Automation," 2017. [Online]. Available: https://www.ab.com/Support/abdrives/documentation/index.html.

[111] *BS 4821 : Presentation of theses and dissertations,* London: British Standards Institution, 1990.

[112] Y. M. Chen, *Thesis on RC Snubber design using Root-Loci Approach for Synchronous Buck SMPS,* Ontario, Canada: University of Waterloo, 2005.

[113] C. K. Huing, H. H. Nien, S. K. Changchien, C. H. Chan and C. K. Chen, "An Optimal Designed RCD Snubber For DC-DC Converters," in *10th International Conference on Control, Automation, Robotics and Vision*, Hanoi, Vietnam, 2008.

[114] S. Ikeda and F. Kurokawa , "Isolated and Wide Input Ranged Boost Full Bridge DC-DC Converter with Low Loss Active Snubber," *IEEE,* no. 978-1-5090-2998-3/17, pp. 2213-2218, 2017.

[115] M. Jinno and K.-C. Lin , "An Efficient Active LC Snubber for Multi-Output Converters with Flyback Synchronous Rectifier," *IEEE,* no. 0-7803-7754-0/03, pp. 622-627, 2003.

[116] R. T.-H. Li and C. N.-M. Ho, "An Active Snubber Cell for N-Phase Interleaved DC–DC Converters," *IEEE Journal Of Emerging and Selected Topics in Power Electronics, Vol. 04, No. 2 June 2016,* pp. 344-351, June 2016.

[117] J.-W. Yang and H.-L. Do, "Soft-Switching Bidirectional DC-DC Converter Using a Lossless Active Snubber," *IEEE Transactions on Circuits and Syatems - I: regular papers, Vol. 61, No. 5, May 2014,* pp. 1588-1596, May 2014.

[118] M. Baei and G. Moschopoulos , "An Investigation into the use of Active Snubbers to Improve Light-Load Converter Efficiency," *IEEE,* no. 978-1-4577-1250-0111, 2011.

[119] B. Jacobson, "Developments in Multiterminal HVDC," in *IEEE EPEC - ABB Power Systems*, Manitoba, 2011.

[120] H. Huang, Christl and F. Schettler, HVDC Transmission Systems using Voltage Sourced Converters - Design and Applications, Erlangen, Germany: IEEE, 2000.

[121] R. G. Mertens, L. Chow and K. B. Sundaram, "Spray Cooling of IGBT Devices," *Transactions of the ASME -Vol.129,* pp. 316 - 323, September 2007.

Appendix A – PSO method to determine the optimum variables for $E_{SW\text{-}min}$ at t_{off}.

Calculation of the PSO variable velocity equations and their optimised values related to the minimum Objective Function. The calculations are presented in a table comprising of 29 columns from D to AF. Due to its size, it is divided into three tables, Tables A1, A2 and A3.

Table A1 - Columns D-M Spreadsheet

	D	E	F	G	H	I	J	K	L	M
		P = Particle position							w_k	Particle velocity v_i^k
Rows	Table 5-12 Reference	I^2 P	t^2 P	C P	k	30-k	30-k/30	0.5x(30-k)/30	K25+0.4	
25	18	4			1	29	0.9667	0.4833	0.8833	0
26	18		0.0049		2	28	0.9333	0.4667	0.8667	0
27	18			1	3	27	0.9000	0.4500	0.8500	0
28	19	16			4	26	0.8667	0.4333	0.8333	14.083787
29	19		0.0049		5	25	0.8333	0.4167	0.8167	-0.000547
30	19			1	6	24	0.8000	0.4000	0.8000	0.127578
31	20	1			7	23	0.7667	0.3833	0.7833	-11.736385
32	20		0.0049		8	22	0.7333	0.3667	0.7667	0.000079
33	20			0.8	9	21	0.7000	0.3500	0.7500	0.207592
34	25	16			10	20	0.6667	0.3333	0.7333	-6.308652
35	25		0.0036		11	19	0.6333	0.3167	0.7167	-0.002578
36	25			1.5	12	18	0.6000	0.3000	0.7000	0.610743
37	28	1			13	17	0.5667	0.2833	0.6833	-18.455734
38	28		0.0036		14	16	0.5333	0.2667	0.6667	-0.002900
39	28			1.3	15	15	0.5000	0.2500	0.6500	0.425900
40	34	4			16	14	0.4667	0.2333	0.6333	4.168121
41	34		0.0049		17	13	0.4333	0.2167	0.6167	0.000665
42	34			1.2	18	12	0.4000	0.2000	0.6000	-0.007594
43	35	1			19	11	0.3667	0.1833	0.5833	3.850270
44	35		0.0064		20	10	0.3333	0.1667	0.5667	-0.000535
45	35			1.2	21	9	0.3000	0.1500	0.5500	-0.152148
46	38	4			22	8	0.2667	0.1333	0.5333	20.030203
47	38		0.0064		23	7	0.2333	0.1167	0.5167	-0.002874
48	38			1.1	24	6	0.2000	0.1000	0.5000	-0.098762
49	39	25			25	5	0.1667	0.0833	0.4833	30.227013
50	39		0.0064		26	4	0.1333	0.0667	0.4667	-0.008798
51	39			1.1	27	3	0.1000	0.0500	0.4500	-0.049381
52	40	36			28	2	0.0667	0.0333	0.4333	-24.976194
53	40		0.0064		29	1	0.0333	0.0167	0.4167	-0.007477
54	40			1.4	30	0	0.0000	0.0000	0.4000	-0.022221

To move the particles forward, the values under column ‘M’ in Table A1 are updated by the corresponding (k-1) values under columns ’Z’, ‘AA’ and ‘AB’ in Table A3.

Table A2 - Columns D-X entries for part Velocity equations (5.5), (5.6) & (5.7)

	D	N	O	P	Q	R	S	T	U	V	W	X
Rows	**Table 5-12 Reference**	**c1**	**r1**	**c1 x r1**	**I^2Pb-I^2P**	**t^2Pb-t^2P**	**CPb-CP**	**c2**	**r2**	**c2 x r2**	**I^2gb-I^2P**	**t^2gb-t^2P**
25	18	2	0.619	1.2379	12			2	0.128	0.257	-3	
26	18	2	0.765	1.5317		0.0015		2	0.592	1.185		-0.0024
27	18	2	0.232	0.4649			0.1	2	0.637	1.275		
28	19	2	0.400	0.8010	0			2	0.782	1.564	-15	
29	19	2	0.549	1.0995		0.0015		2	0.234	0.468		-0.0024
30	19	2	0.665	1.3316			0.1	2	0.527	1.055		
31	20	2	0.096	0.1923	15			2	0.576	1.152	0	
32	20	2	0.679	1.3585		0.0015		2	0.974	1.948		-0.0024
33	20	2	0.167	0.3357			0.3	2	0.758	1.516		
34	25	2	0.556	1.1125	0			2	0.461	0.922	-15	
35	25	2	0.178	0.3578		0.0028		2	0.933	1.867		-0.0011
36	25	2	0.418	0.8361			-0.4	2	0.002	0.004		
37	28	2	0.559	1.1186	15			2	0.572	1.144	0	
38	28	2	0.806	1.6126		0.0028		2	0.871	1.742		-0.0011
39	28	2	0.404	0.8088			-0.2	2	0.711	1.422		
40	34	2	0.219	0.4385	12			2	0.675	1.350	-3	
41	34	2	0.774	1.5498		0.0015		2	0.681	1.362		-0.0024
42	34	2	0.712	1.4254			-0.1	2	0.738	1.475		
43	35	2	0.592	1.1856	15			2	0.858	1.717	0	
44	35	2	0.100	0.2005		0		2	0.329	0.659		-0.0039
45	35	2	0.923	1.8471			-0.1	2	0.075	0.150		
46	38	2	0.940	1.8818	12			2	0.506	1.012	-3	
47	38	2	0.840	1.6811		0		2	0.937	1.875		-0.0039
48	38	2	0.311	0.6238			0	2	0.946	1.892		
49	39	2	0.970	1.9411	-9			2	0.460	0.921	-24	
50	39	2	0.521	1.0430		0		2	0.432	0.864		-0.0039
51	39	2	0.324	0.6497			0	2	0.753	1.507		
52	40	2	0.851	1.7031	-20			2	0.920	1.840	-35	
53	40	2	0.797	1.5958		0		2	0.762	1.525		-0.0039
54	40	2	0.747	1.4940			-0.3	2	0.780	1.560		

In Table A3, the switch energy E, in 'AF' (Objective Function) is based on the Final Particle Positions, (New I^2, New t^2, and New C) in Column AC at Row 25, Column AD at Row 26 and Column AE at Row 27. The values are obtained by adding the corresponding particle in 'Z' to 'E', 'AA' to 'F' and 'AB' to 'G'. This is repeated for all 'k' iterations.

Table A3 - Columns D-AF entries for part Velocity equations (5.5), (5.6) & (5.7)

	D	Y	Z	AA	AB	AC	AD	AE	AF
						Final Particle Position.			
Rows	Table 5-12 Reference	Cgb-CP	v_i^{k+1} (I^2)	v_i^{k+1}(t^2)	v_i^{k+1}(C)	New I^2	New t^2	New C	E = Energy µJ
25	18		14.083787			18.083787			
26	18			-0.000547			0.004353		
27	18	0.1			0.1276			1.1276	0.002909
28	19		-11.736385			4.263615			
29	19			0.000079			0.004979		
30	19	0.1			0.2076			1.2076	0.000732
31	20		-6.308652			-5.308652			
32	20			-0.002578			0.002322		
33	20	0.3			0.6107			1.4107	-0.000364
34	25		-18.455734			-2.455734			
35	25			-0.002900			0.000700		
36	25	-0.4			0.4259			1.9259	-0.000037
37	28		4.168121			5.168121			
38	28			0.000665			0.004265		
39	28	-0.2			-0.0076			1.2924	0.000711
40	34		3.850270			7.850270			
41	34			-0.000535			0.004365		
42	34	-0.1			-0.1521			1.0479	0.001363
43	35		20.030203			21.030203			
44	35			-0.002874			0.003526		
45	35	-0.1			-0.0988			1.1012	0.002805
46	38		30.227013			34.227013			
47	38			-0.008798			-0.002398		
48	38	0			-0.0494			1.0506	-0.003255
49	39		-24.976194			0.023806			
50	39			-0.007477			-0.001077		
51	39	0			-0.0222			1.0778	-0.000001
52	40		-			-73.30352			
53	40			-0.009063			-0.002663		
54	40	-0.3			-0.4770			0.9230	0.008814

In Table A3, the positive minimum energy value of 0.000711 µJ is found in row 39. The corresponding optimised variables are,

Row 37 – Optimised Current, I Amps $= \sqrt{I^2} = \sqrt{5.168121} = 2.27$ Amps

Row 38 – Optimised Switching period, t_{off} µs $= \sqrt{t^2} = \sqrt{0.004265} = 0.065$ µs

Row 39 – Optimised Capacitor, C µF $= 1.2924$ µF

Appendix B –Schematic for the CHB7LC with Turn-On and Turn-Off EESCs

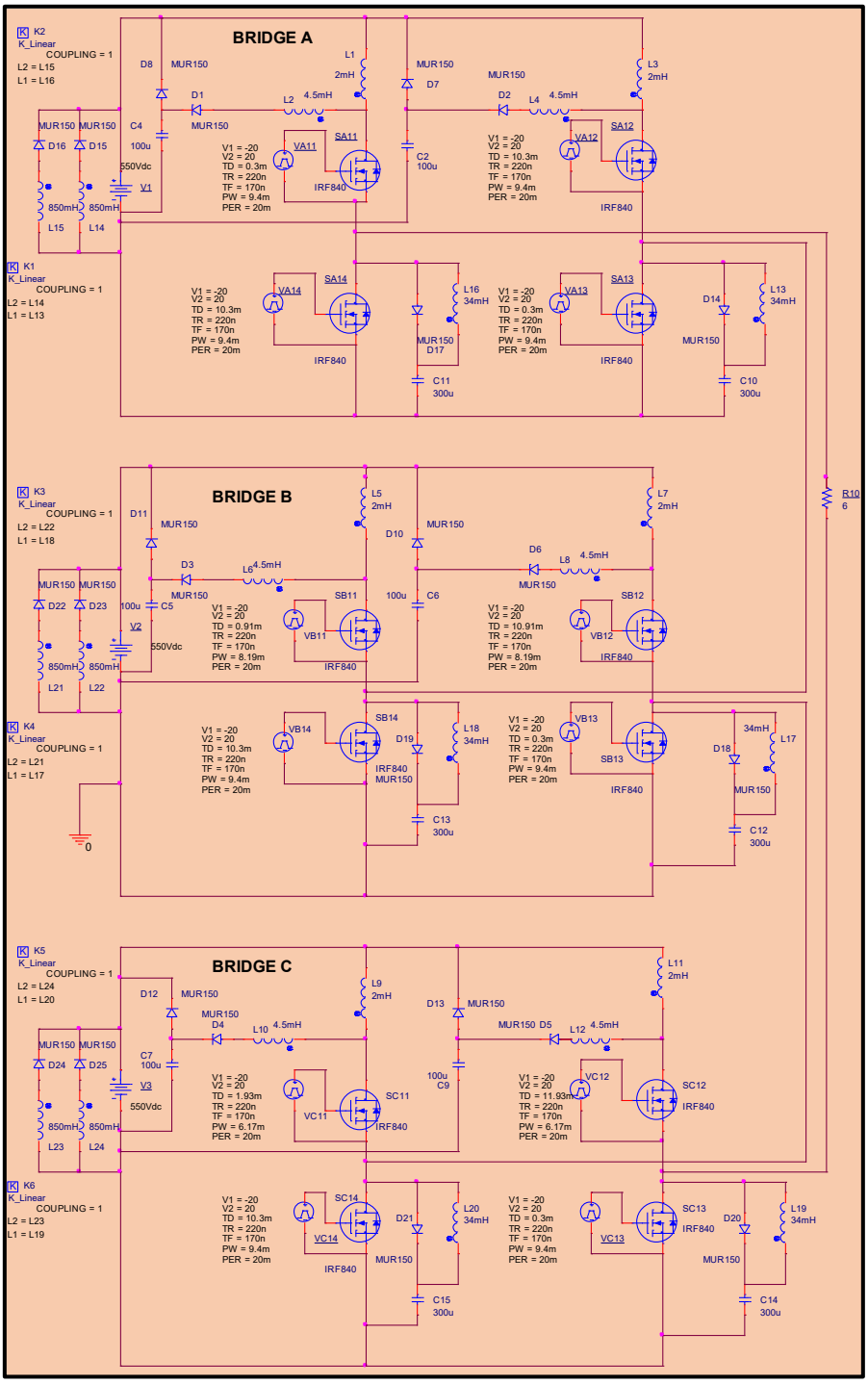

Figure B1-Turn-On & Turn-Off EESCs
connected to the upper & lower pairs of IGBTs

Appendix C – Determination of CHB7LC Dissipative Energy

This Appendix refers to section 7.2.7.3. The Power measurement during the Turn-On period for each IGBT is shown in Figure C1.

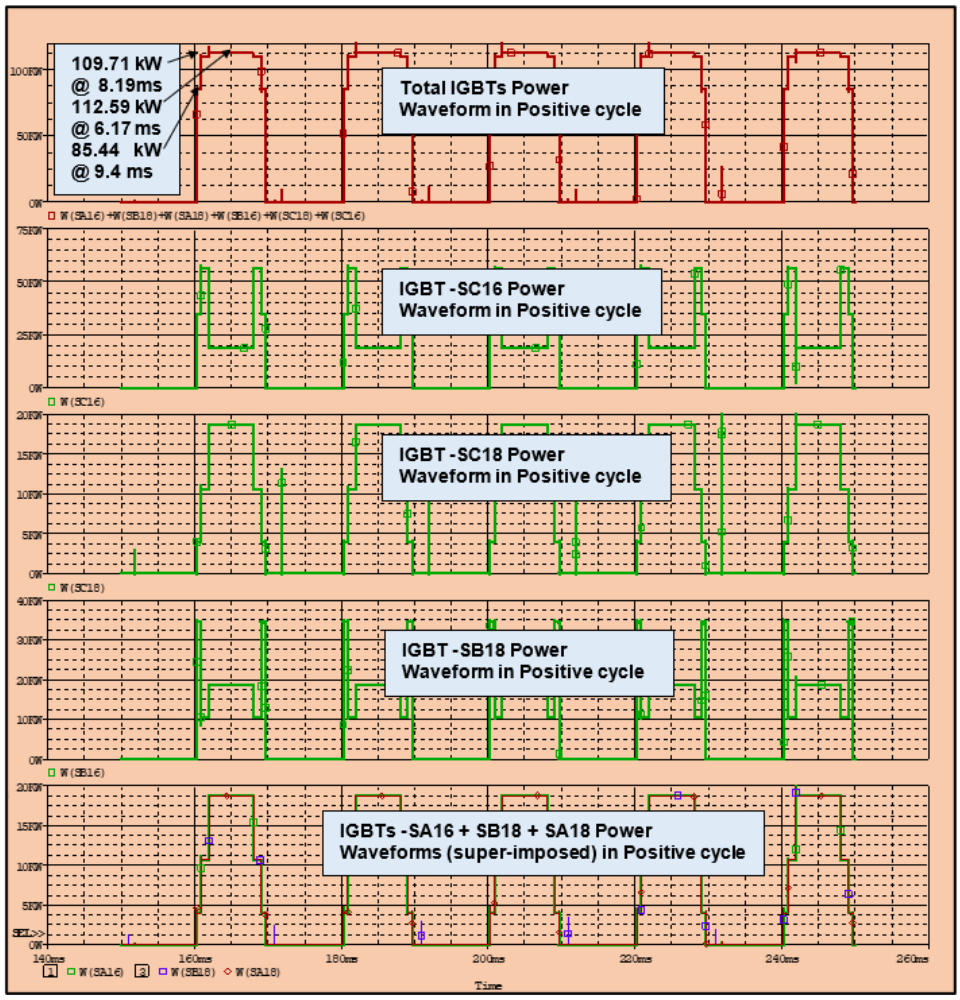

Figure C1 – Measurement of the Total
Turn-On Dissipated energy in the CHB7LC.

Calculation of the Turn-On Energy in the Total IGBTs Power waveform in the positive cycle is given by: -

$$Positive\ cycle\ dissipative\ E_{Turn-on} = \sum_{k=9.4ms}^{n} (P \times PW)_k\ , n = PW_{9.4ms}, PW_{8.19ms}, PW_{6.17ms}$$

$$\sum \big((85.44kW \times 9.4ms) + ((109.71kW - 85.44kW) \times 8.19ms)$$

$$+ (112.6kW - 109.71kW) \times 6.17ms\big)\ \text{Joules}$$

$$= (803.17 + 198.8 + 17.83)\text{Joules}$$

$$\text{Positive cycle dissipative} E_{Turn-on} = 1019 \text{ Joules}$$

Due to symmetry of the positive and negative circuit, the negative cycle dissipative Turn-On energy is also 1019.8 Joules. Hence, the total CHB7LC dissipative Energy is,

$$\boldsymbol{Total\ CHB7-LC\ dissipative\ E_{Turn-on} = 2 \times 1019.8 = 2039.6\ Joules}$$

This result validates the method used in section 7.2.7.3, as it compares closely to the value of 2040 Joules.

Appendix D – Diagram of the High-performance cooling of a HVDC converter

The cooling liquid used a fatty acid ester-based phase change dispersion in a heatsink with double-layer oblique-crossed ribs.

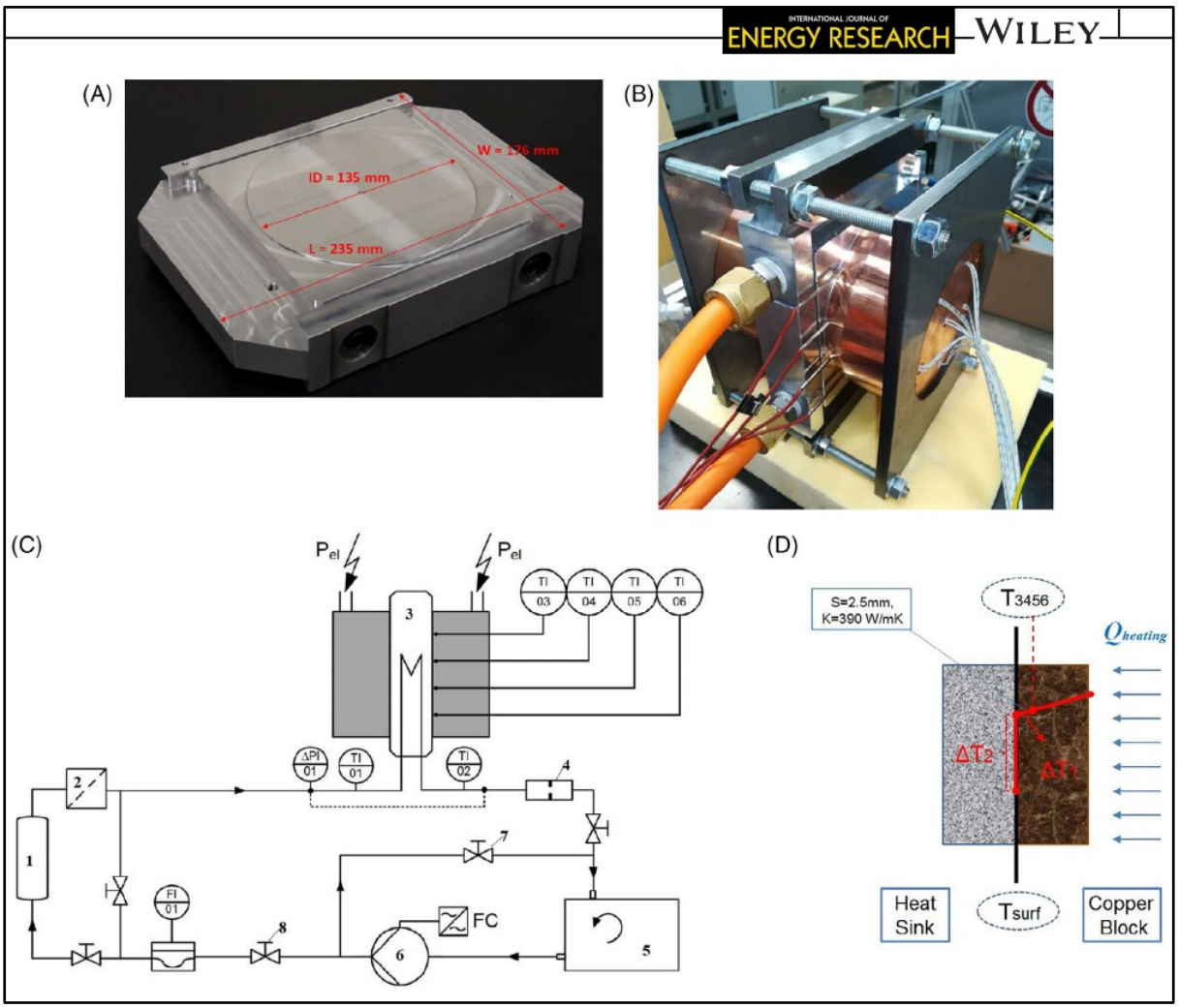

Figure D 1- A – Snapshot of Heatsink, B – Snapshot of heating section, C – Schematic diagram of the experimental rig., D – Schematic of the thermal resistance between heating surface and copper block.

Key for ©- Schematic diagram of the experimental rig.

1- Deionisation, 2 – Filter, 3 – Converter, 4 – Re-dispersion unit, 5 – Re-cooling unit, 6 – Pump, 7 – By-pass valve, 8 – Throttle valve,

Authors Publications

Conferences

Sat Mohanram, M. Darwish, CC Marouchos, "Optimisation and Simulation of RC Time Constants in Snubber Circuits", University Power Engineering Conference (UPEC), September 2018.

Sat Mohanram, M. Darwish, CC Marouchos, "Power Switching Device Losses – Simulation and Non-Simulation Methods of Calculations", University Power Engineering Conference (UPEC), September 2018.

Submitted for publication

Sat Mohanram, Maysam Abbod and M. Darwish, "Application of PSO in Calculating the Optimum Snubber Circuit Parameters for Minimum Switching Energy".